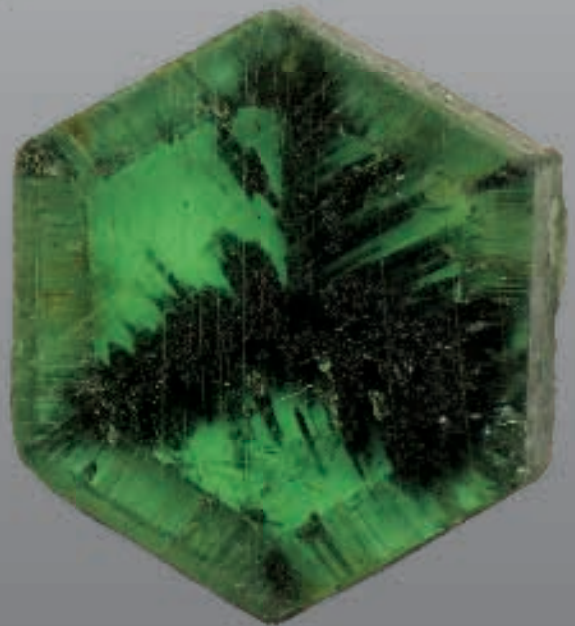
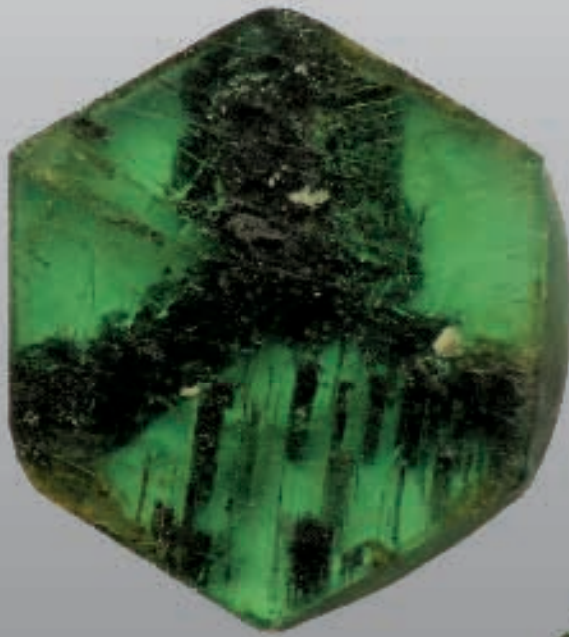




The Journal of
Gemmology

2011 / Volume 32 / Nos. 5/8



Trapiche tourmaline

The Gemmological Association of Great Britain

27 Greville Street, London EC1N 8TN, UK

T: +44 (0)20 7404 3334 **F:** +44 (0)20 7404 8843

E: information@gem-a.com **W:** www.gem-a.com

Registered Charity No. 1109555

Registered office: Palladium House, 1-4 Argyll Street, London W1F 7LD

President: Prof. A. H. Rankin

Vice-Presidents: N. W. Deeks, R. A. Howie, E. A. Jobbins, M. J. O'Donoghue

Honorary Fellows: R. A. Howie

Honorary Life Members: H. Bank, D. J. Callaghan, T. M. J. Davidson, J. S. Harris, J. A. W. Hodgkinson, E. A. Jobbins, J. I. Koivula, M. J. O'Donoghue, C. M. Ou Yang, E. Stern, I. Thomson, V. P. Watson, C. H. Winter

Chief Executive Officer: J. M. Ogden

Council: J. Riley – Chairman, S. Collins, B. Jackson, S. Jordan, C. J. E. Oldershaw, L. Palmer, R. M. Slater

Members' Audit Committee: A. J. Allnut, P. Dwyer-Hickey, E. Gleave, J. Greatwood, G. M. Green, K. Gregory, J. Kalischer

Branch Chairmen: Midlands – P. Phillips, North East – M. Houghton, North West – J. Riley, South East – V. Wetten, South West – R. M. Slater

The Journal of Gemmology

Editor: Dr R. R. Harding

Deputy Editor: E. A. Skaltwold

Assistant Editor: M. J. O'Donoghue

Associate Editors: Dr A. J. Allnut (Chislehurst), Dr C. E. S. Arps (Leiden), G. Bosshart (Horgen), Prof. A. T. Collins (London), J. Finlayson (Stoke on Trent), Dr J. W. Harris (Glasgow), Prof. R. A. Howie (Derbyshire), E. A. Jobbins (Caterham), Dr J. M. Ogden (London), Prof. A. H. Rankin (Kingston upon Thames), Dr K. Schmetzer (Petershausen), Dr J. E. Shigley (Carlsbad), Prof. D. C. Smith (Paris), E. Stern (London), Prof. I. Sunagawa (Tokyo), Dr M. Superchi (Milan)

Production Editor: M. A Burland

The Editor is glad to consider original articles shedding new light on subjects of gemmological interest for publication in *The Journal of Gemmology*. A guide to the preparation of typescripts for publication in *The Journal* is given on our website, or contact the Production Editor at the Gemmological Association of Great Britain.

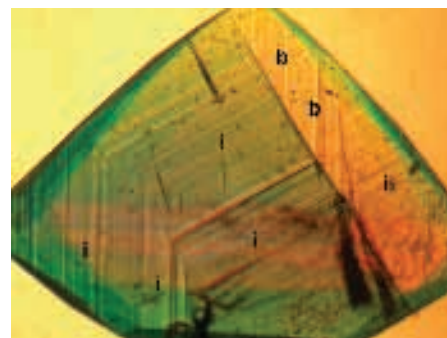
Any opinions expressed in *The Journal of Gemmology* are understood to be the views of the contributors and not necessarily of the publishers.

Measurement and interpretation of growth patterns in chrysoberyl, including alexandrite

Dr Karl Schmetzer

Abstract: Procedures for identifying growth planes, growth zones and twin planes in optical biaxial gemstones are described and the most commonly observed interfacial angles are tabulated, using chrysoberyl as an example. The strong pleochroism of the chromium-bearing chrysoberyl variety alexandrite was found to be a useful indicator for locating the positions of the crystallographic axes, and the optic axes are determined using interference figures under crossed polarizers. Examples of the typical features of growth zoning in natural alexandrites from Russia, Sri Lanka and Brazil are shown. Twinned chrysoberyls from Madagascar are described in detail.

Keywords: alexandrite, Brazil, chrysoberyl, crystal habit, Madagascar, optic properties, pleochroism, Russia, Sri Lanka, twinning



Introduction

Origin determination has become an increasingly important requirement in the gem trade during the last decade, especially for larger rubies, sapphires and emeralds. In addition to the 'traditional' examination of inclusions, trace element chemistry, e.g. by X-ray fluorescence or laser ablation inductively coupled plasma mass spectrometry (LA-ICP-MS), can provide the necessary data to determine the provenance of a gemstone.

However, with the increasing number of new sources of gem-quality stones on the international market such as blue sapphires from Madagascar or Tanzania, inclusion and chemical information may be insufficient — especially due to

overlapping trace element patterns — and the determination of the internal growth patterns of these uniaxial gemstones provides additional criteria to use for distinguishing between samples from different natural sources. With the exception of a few significant cases, growth patterns should be measured and assessed only in combination with a stone's other properties and not as a single technique.

The determination of the internal growth patterns of optically uniaxial gemstones, e.g. ruby, sapphire, emerald, amethyst and citrine, has been described in detail by Kiefert and Schmetzer (1991 a,b,c). The general technique was also comprehensively described by Smith (1996)

and applied to the distinction of natural and synthetic rubies. Further examples of characteristic growth patterns of optically uniaxial gemstones are also given in the literature, especially in connection with the description of new sources of ruby and sapphire and with the description of various synthetic quartz varieties.

In contrast, the description of characteristic growth patterns in optically

*Above: Growth structure and pleochroism in twinned alexandrite from Lake Manyara, Tanzania; the twin boundary separates a first individual with growth planes parallel to two **i** (011) faces and a second individual with growth faces parallel to **i** (011) and **b** (010). View parallel to the a-axis of both parts of the twin, immersion, 25 ×.*

Measurement and interpretation of growth patterns in chrysoberyl, including alexandrite

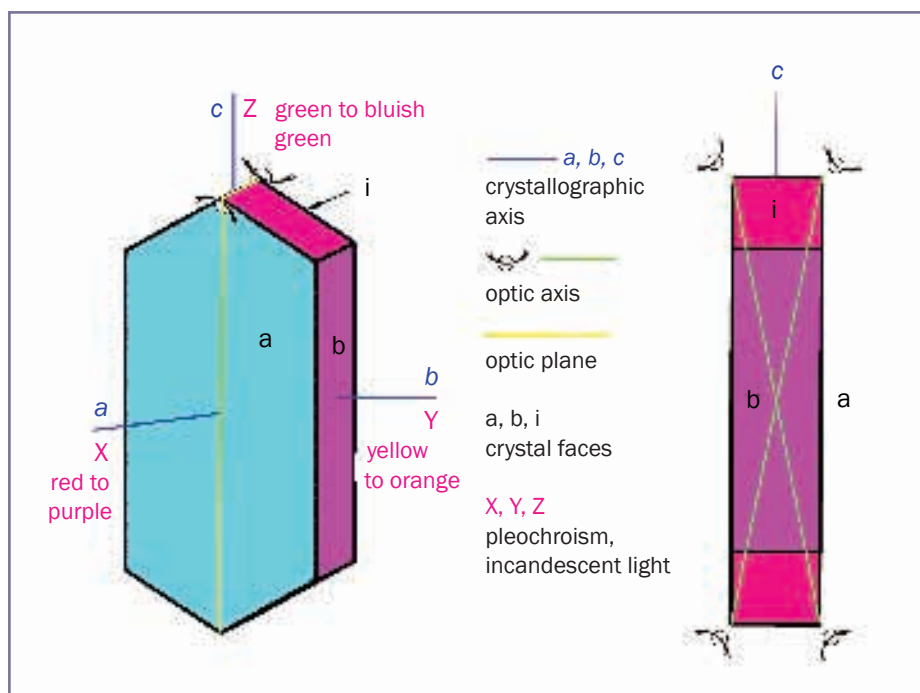


Figure 1: Orientation of the optic plane and the optic axes relative to the three crystallographic axes a, b and c in optically biaxial chrysoberyl; the optic plane is represented by the ac-plane of the crystal. Left: clinographic projection, view almost parallel to the a-axis; right: parallel projection, view parallel to the b-axis.

biaxial gemstones is limited. For flux-grown Russian synthetic alexandrites, the internal growth patterns were determined using immersion microscopy of rough and faceted samples (Schmetzer *et al.*, 1996). More recently, a detailed description of characteristic growth patterns in natural Russian alexandrites originating from the emerald mines in the Ural mountains has been published (Schmetzer, 2010) and includes practical guidance for the recognition of such characteristic patterns in Russian samples. However, a general overview of growth patterns in alexandrites from various natural sources and their determination is still missing.

General considerations

In optically uniaxial gemstones, the determination of the complete growth pattern is quite straightforward. Because the crystallographic c-axis is parallel to the optic axis, a growth plane can easily be determined by measurement of its inclination to the optic axis. The complete growth pattern can be seen by rotating the sample with the c-axis (coincident with the optic axis) as rotation axis of the sample holder.

In optically biaxial gemstones, on the other hand, neither optic axis can be expected to be parallel to any one of the three crystallographic axes (a-, b- and c-axes) and, therefore, the measurement of an angle of a growth plane relative to one of the optic axes or a rotation of the gemstone with one of the optic axes as rotation axis gives only limited information and doesn't show the complete growth pattern of a sample.

Consequently, the determination of growth patterns in optically biaxial gemstones can be considered as a trial and error process, which, depending upon the orientation of the table facet with respect to the crystallographic axes, may be very quick (comparable to the procedure for optically uniaxial gemstones) or somewhat more time consuming. For all biaxial gemstones it is necessary to rotate a faceted sample through an angle of 360° in a number of different orientations in the sample holder.

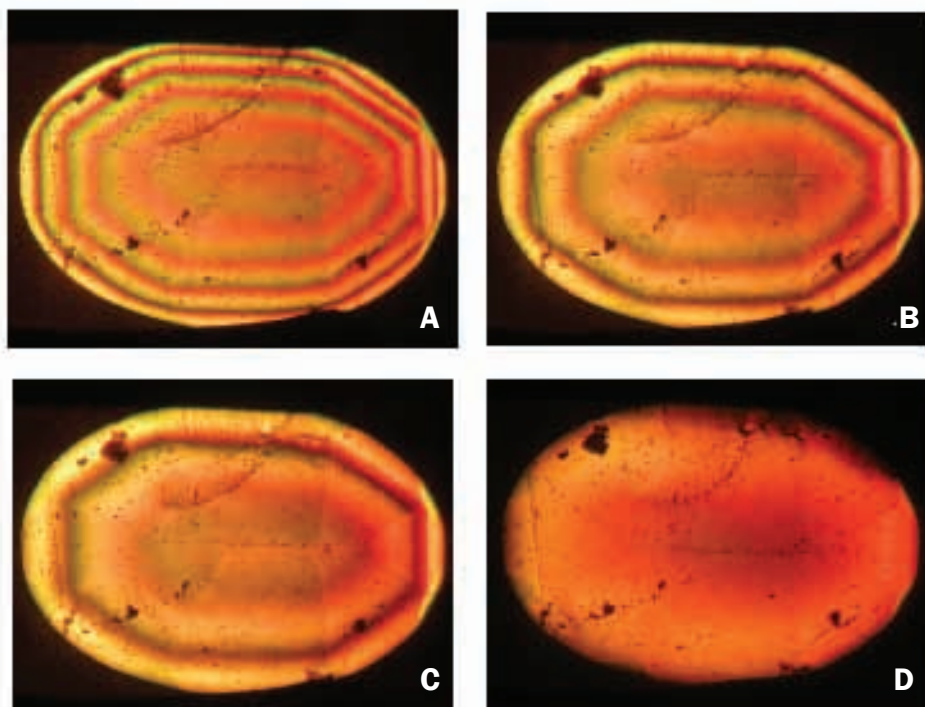


Figure 2: This series illustrates the variation of interference figures in alexandrite from Hematita, Brazil, during a slight rotation of the stone; tilting the alexandrite from a position, in which the optic axis is inclined to the direction of view (A) progressively towards positions in which the angle between the optic axis and the microscope axis is progressively diminished, moves the interference rings towards the centre (B and C); in (D) the optic axis is exactly parallel to the microscope axis. Consequently, this procedure is applied in a search for both optic axes and for the determination of crystal orientation in faceted samples by optical means. Immersion, crossed polarizers, 30x.

Measurement and interpretation of growth patterns in chrysoberyl, including alexandrite

The observed structural properties and their orientation within the gemstone, e.g. relative to the table facet, can then be noted. In subsequent steps, an orientation of the alexandrite in selected settings and subsequent rotations will give the basic information to determine the most characteristic structural properties. In other words, each setting and rotation of the gemstone in the sample holder yields information to solve part of a three-dimensional puzzle, i.e. part of the complete growth information.

Technical equipment

The facilities used for the determination of growth patterns in optically biaxial gemstones are identical with the tools used for optically uniaxial gems. Detailed descriptions are given by Schmetzer (1986), Kiefert and Schmetzer (1991a) and Smith (1996).

For the measurement of angles between structural features in the immersion microscope, a special sample holder with two rotation axes and a 360° dial attached to the vertical rotation axis is applied to determine the angle of rotation, i.e. the angle between two structural features observed in two angular positions of the sample holder. The second horizontal rotation axis of the sample holder, in general, is not used for the measurement of angles between structural properties, but this axis is essential for an orientation of a rough or faceted sample in a direction of view exactly parallel to the observed growth planes. Furthermore, an eyepiece with crossed hairs and a 360° dial attached to the eyepiece tube are used for the measurement of angles between two different structural features, e.g. between two differently orientated series of parallel growth planes.

Determination of optic and crystallographic axes using interference figures and pleochroism

The optic axial plane in chrysoberyl, including its colour-change variety alexandrite, is always located in the plane

formed by the crystallographic *a*- and *c*-axes (Figure 1). The position of an optic axis in this plane is found by placing the stone in the sample holder in different initial orientations and rotating the stone 360° in each position under crossed polarizers. This uses the vertical axis of the sample holder as rotation axis. A position with a view somewhat inclined to the optic axis is indicated by a typical pattern of interference rings (Figure 2A). Tilting the crystal continuously towards a position in which the optic axis is exactly parallel to the direction of view moves the interference rings continuously towards

the centre of the sample (Figure 2B to D).

If the geometry of the stone is such that it is possible to find both optic axes, its orientation relative to the three crystallographic axes can be determined. With a starting position in which the crystallographic *b*-axis is parallel or almost parallel to the rotation axis of the sample holder, it is possible to observe both optic axes within one single rotation of the gemstone. In this case, the optic axial angle of the chrysoberyl can be measured. In most gem chrysoberyls the optic axial angle lies in the range 65 to 70°, and exactly half way between both optic axes, a view

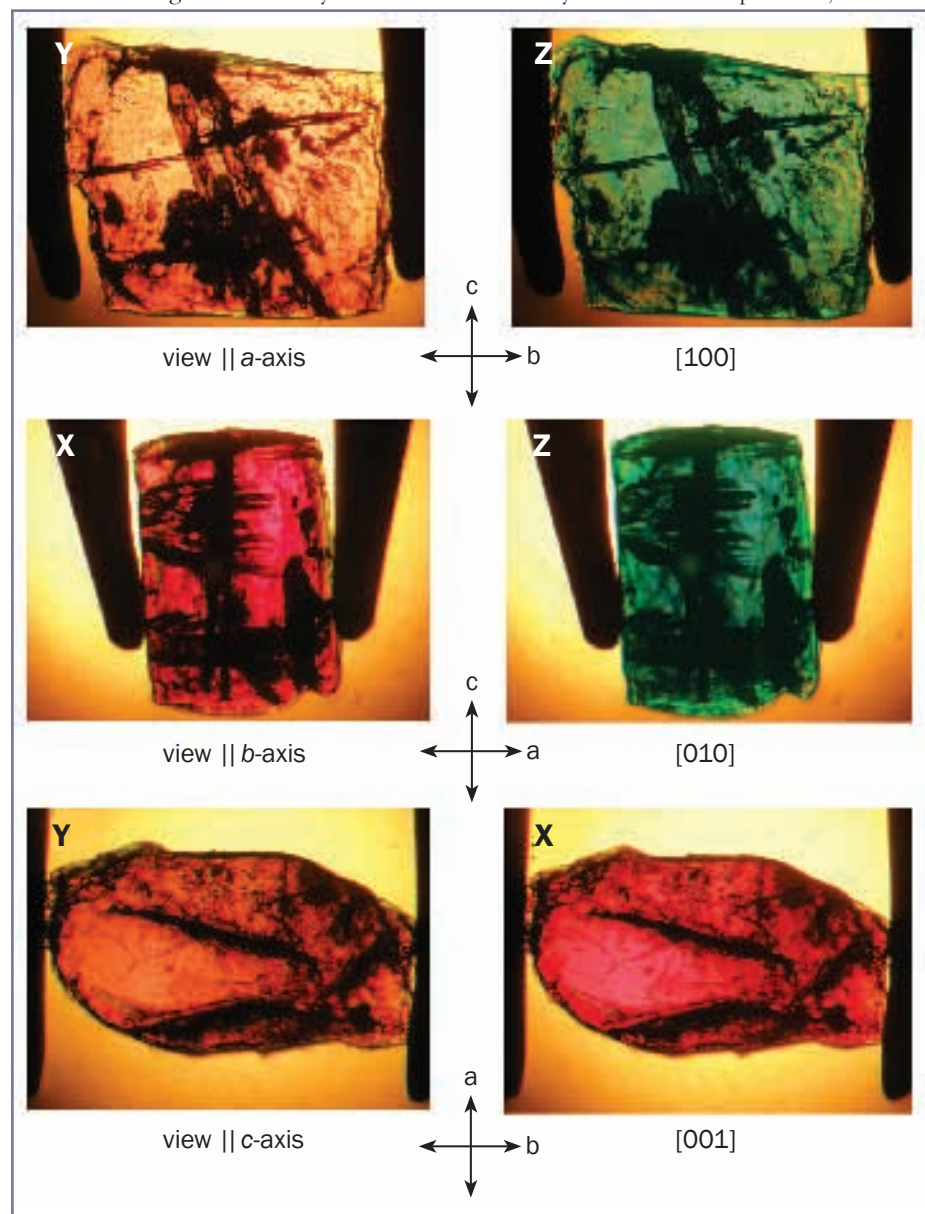


Figure 3: Pleochroism of an alexandrite crystal fragment from Hematita, Brazil, in immersion and incandescent light, view of the sample in directions parallel to the crystallographic *a*-, *b*- and *c*-axis in a cell with transmitted polarized light, with an orientation of $X||a$, $Y||b$ and $Z||c$. Size of the crystal fragment about 2.8 × 5.2 × 4.2 mm.

Measurement and interpretation of growth patterns in chrysoberyl, including alexandrite

parallel to the crystallographic *c*-axis can be obtained. After a rotation of 90° from this position with the *b*-axis chosen parallel to the rotation axis, the direction of view is exactly parallel to the *a*-axis.

This orientation in the sample holder, which enables determination of the position of both optic axes and — with that knowledge — the position of the three crystallographic axes, is ideal; to find it, the observation of pleochroism is helpful. For the chromium-bearing chrysoberyl variety alexandrite, the colours of X || *a*, Y || *b* and Z || *c* in incandescent light, as observed commonly in the immersion microscope, are always:

X red to purple, Y yellow to orange, and Z green to bluish green.

An example is given in *Figure 3*. Consequently, the observation of pleochroism is helpful to determine which

crystallographic axis (in the setting of the crystal examined) is more or less parallel to the rotation axis of the sample holder.

Pleochroism can also be used to control the search for optic axes. If one optic axis is parallel to the direction of view, no pleochroism is observed when the polarizer is rotated. In views parallel to the three different crystallographic axes, the following colours are observed (see again *Figure 3*):

Direction of view	Pleochroism
View to the <i>a</i> -axis [100]	Y yellow to orange Z green to bluish green
View to the <i>b</i> -axis [010]	X red to purple Z green to bluish green
View to the <i>c</i> -axis [001]	X red to purple Y yellow to orange

Table I: Morphological properties of chrysoberyls.

Crystal class 2/m 2/m 2/m = D_{2h}, single and repeated twinning on (031) and (0 $\bar{3}$ 1).

Crystal form	Designation	Miller indices (hkl)*	Number of faces
Pinacoid	a	(100)	2
	b	(010)	
	c	(001)	
Prism	i	(011)	4
	k	(021)	
	m	(110)	
	s	(120)	
	r	(130)	
	x	(101)	
Dipyramid	o	(111)	8
	n	(121)	
	w	(122)	
	v	(211)	

Zone axis [uvw]	Direction of view	Crystal faces, designation and Miller indices (hkl)
[001]	parallel to the <i>c</i> -axis	a (100), m (110), s (120), r (130), b (010)
[100]	parallel to the <i>a</i> -axis	b (010), k (021), i (011), c (001)
[010]	parallel to the <i>b</i> -axis	c (001), x (101), a (100)
[011]	between <i>b</i> - and <i>c</i> -axis	a (100), v (211), o (111), w (122), i (011)
[012]	between <i>b</i> - and <i>c</i> -axis	a (100), n (121), k (021)
[101]	between <i>a</i> - and <i>c</i> -axis, almost parallel to the optic axis	b (010), n (121), o (111), x (101)
[110]	between <i>a</i> - and <i>b</i> -axis	o (111), c (001)
[111]	oblique to all three axes	i (011), n (121), m (110)

*Based on a morphological cell with a 4.42, b 9.39, c 5.47

Observation of characteristic faces and growth zones

The determination of the presence of a single *growth plane* or a series of parallel growth planes — in general — is neither helpful for the characterization of a faceted alexandrite regarding its original crystal morphology nor for origin determination. What is needed is the recognition of one or several characteristic *growth zones*, each growth zone consisting of a group of crystal faces.

In crystallography, a *zone* is defined as a set of faces which are parallel to a line (the *zone axis*) and intersect in parallel edges (*Figure 4*). In general, two non-parallel crystal faces form a zone, but most characteristic zones in chrysoberyl consist of more than two crystal faces. A *crystal face* is indicated by Miller indices (hkl) in round brackets and a *zone axis* is indicated by the symbol [uvw] in square brackets.

To avoid confusion, the author will designate a part of a rough crystal or a faceted gemstone which shows parallel growth planes assigned to a single crystal face as a growth area. Consequently, several growth areas which are related to each other by a single zone axis form a growth zone.

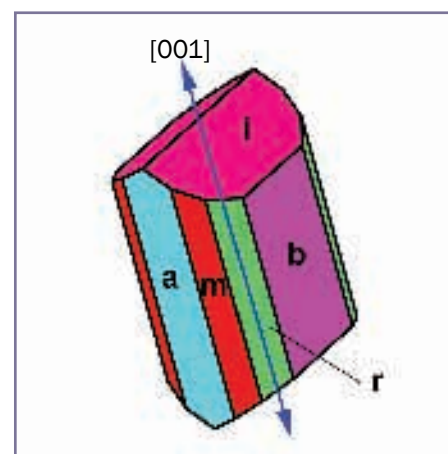


*Figure 4: Alexandrite crystal with simple morphology consisting of the faces **a** (100), **b** (010), **m** (110), **r** (130) and **i** (011); the intersection edges of the faces **a**, **b**, **m** and **r** are parallel to the zone axis [001]. In a view parallel to the zone axis, the growth planes equivalent to the faces **a**, **b**, **m** and **r** are visible in the immersion microscope as lines or bands.*

Measurement and interpretation of growth patterns in chrysoberyl, including alexandrite

In *Table I*, the major faces present in alexandrites from the most important sources are listed. The alexandrite crystals show the three pinacoids **a**, **b** and **c**, six prism faces **i**, **k**, **m**, **s**, **r** and **x**, and four dipyramids **o**, **n**, **w** and **v**. In *Figure 5*, a chrysoberyl crystal is drawn in different views, which show all 13 possible faces listed in *Table I*. In contrast to this theoretical crystal, natural alexandrite crystals from various sources reveal only a limited (smaller) number of crystal faces. In the simplest case, the

alexandrite crystals are formed of three different faces only, e.g. the pinacoids **a** and **b** in combination with the prism **i** (see again *Figure 1*). Thus, the habit of alexandrite crystals from different sources is formed by a limited number of faces, in most crystals between three and ten. The morphological differences between alexandrites from different sources are due to a selection of faces present and the relative sizes of these faces.

In *Table I*, the most important zones and the faces forming these zones

in natural alexandrites from different sources are also listed. In *Tables I* and *II*, the orientations of these zones, i.e. the directions of view in which the faces of these zones can be observed, are also given. These directions of view in the immersion microscope are identical with the zone axes. In *Table II*, the angles between different crystal faces of the most important zones are also listed.

In *Figure 6A*, the theoretical chrysoberyl crystal with all 13 crystal faces (*Figure 5*), is shown in different

Table II: Characteristic interfacial angles common in chrysoberyls, including twins and trillings.

Direction of view	Faces/ Interfacial angles(°)					
View parallel to the <i>c</i> -axis, faces (hk0), zone axis [001]	a b	90				
	a m	25.21	b r	35.30	m s	18.06
	a s	43.27	b s	46.73	s r	11.42
	a r	54.70	b m	64.79		
View parallel to the <i>a</i> -axis, faces (0kl), zone axis [100]	b c	90				
	b i	59.78	c i	30.22	i i' (adjacent)	60.44
	i k	19.14	k b	40.64	k k' (adjacent)	98.72
View parallel to the <i>b</i> -axis, faces (h0l), zone axis [010]	c a	90				
	a x	38.94	c x	51.06		
View perpendicular to a twin plane, between <i>b</i> - and <i>c</i> -axis, rotation 30.22° versus a view parallel <i>c</i> (001), faces (hkl k=l), zone axis [011]	a i	90				
	a v	25.06	v o	18.02	v v' (opposite)	129.88
	a o	43.08	i o	46.92	o o' (opposite)	93.84
	o w	18.79	i w	28.13	w w' (opposite)	56.26
View oblique to the three crystallographic axes, zone axis [111]	i n	42.64	n m	34.97	i m	77.62
View between <i>b</i> - and <i>c</i> -axis, rotation 40.64° versus a view parallel <i>b</i> (010), faces (hkl k=2l), zone axis [012]	a k	90				
	k n	38.87	n a	51.13		
View almost parallel to one optic axis, between <i>a</i> - and <i>c</i> -axis, rotation 38.94° versus a view parallel <i>a</i> (100), faces (hkl h=l), zone axis [101]	x b	90				
	x o	20.11	b o	69.89	o o' (adjacent)	40.22
	o n	16.10	b n	53.79	n n' (adjacent)	72.43
View between <i>a</i> - and <i>b</i> -axis, rotation 25.11° versus a view parallel <i>a</i> (100), faces o and c , zone axis [110]	o o' (diagonal)	107.66	o c	53.83		
Further important angles between dipyramids, views between <i>a</i> - and <i>c</i> -axis					w w' (adjacent)	52.70
					v v' (adjacent)	24.62

N.B.: The angles between growth planes visible in chrysoberyls in the immersion microscope can be obtained by subtracting the relevant interfacial angle from 180°.

Measurement and interpretation of growth patterns in chrysoberyl, including alexandrite

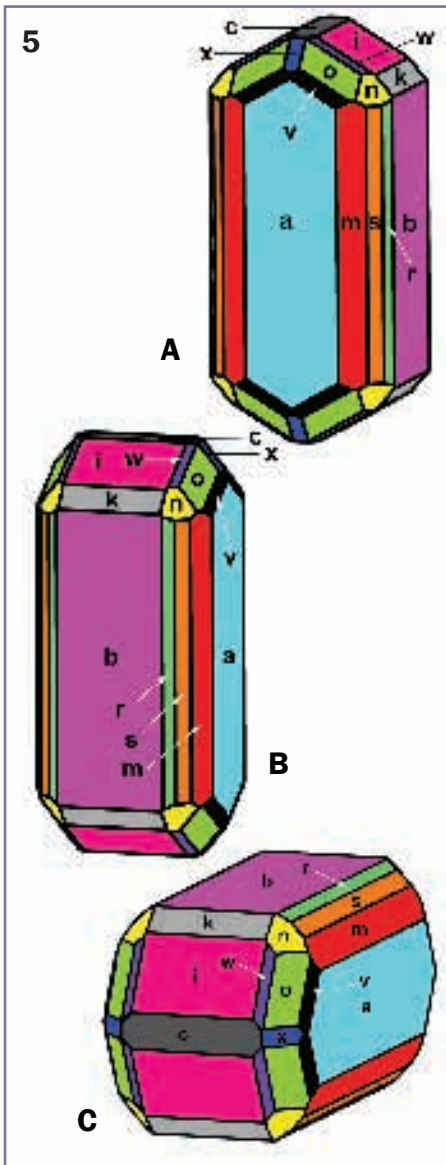
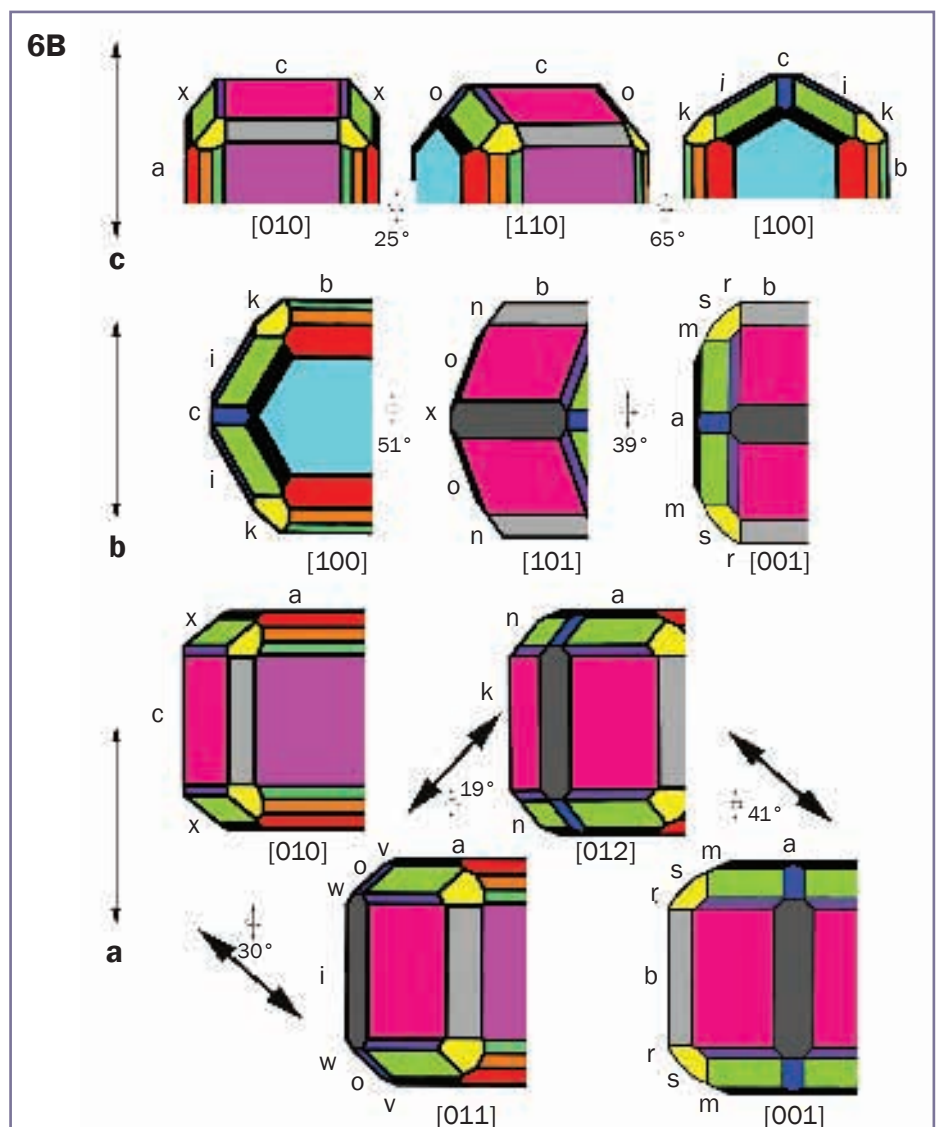
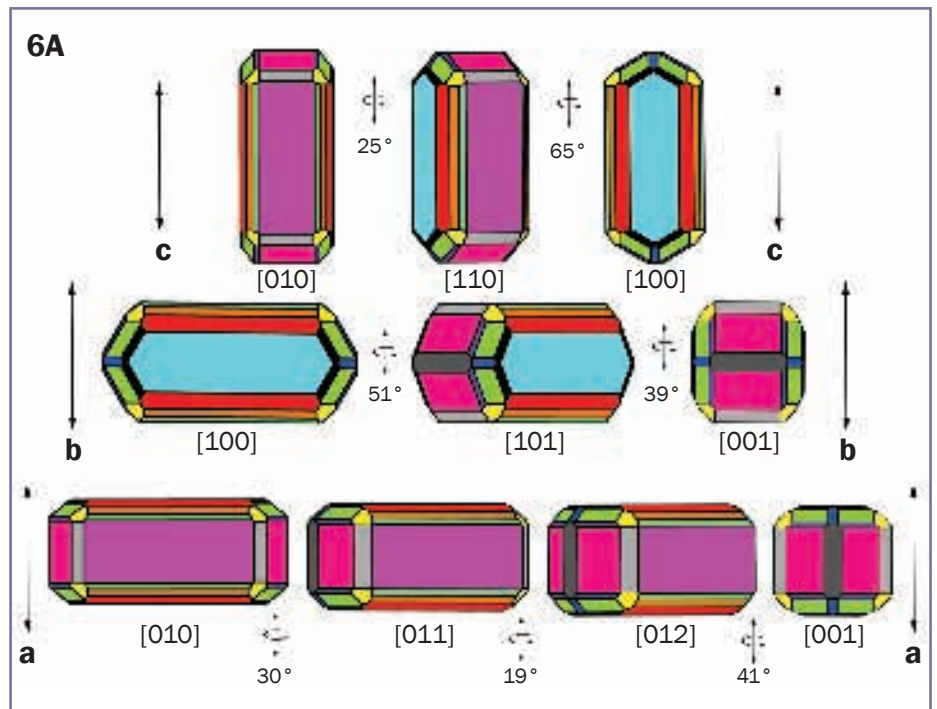


Figure 5: Diagrams showing the positions and labels (a, n, w, etc) of the 13 important faces that were seen in natural alexandrites from all major sources worldwide; A, B and C are clinographic projections to illustrate clearly where each face lies.

Figure 6A: Diagrams of the dominant morphological zones of chrysoberyl. The crystallographic axes c, b and a are indicated, and the zone axis in square brackets indicates the direction of view, e.g. [100] is the direction perpendicular to the blue face a, and [110] is perpendicular to the deep orange face m (Figure 5). The rotation angles between the different views with the crystallographic axes a, b and c as rotation axes are given.

Figure 6B: Enlarged parts of the crystal drawings of Figure 6A; the faces observable in the growth pattern of each view are indicated. Each crystal drawing represents a projection parallel to the respective zone axis (the number in square brackets); the rotation angles between the different viewings are also given.



Measurement and interpretation of growth patterns in chrysoberyl, including alexandrite

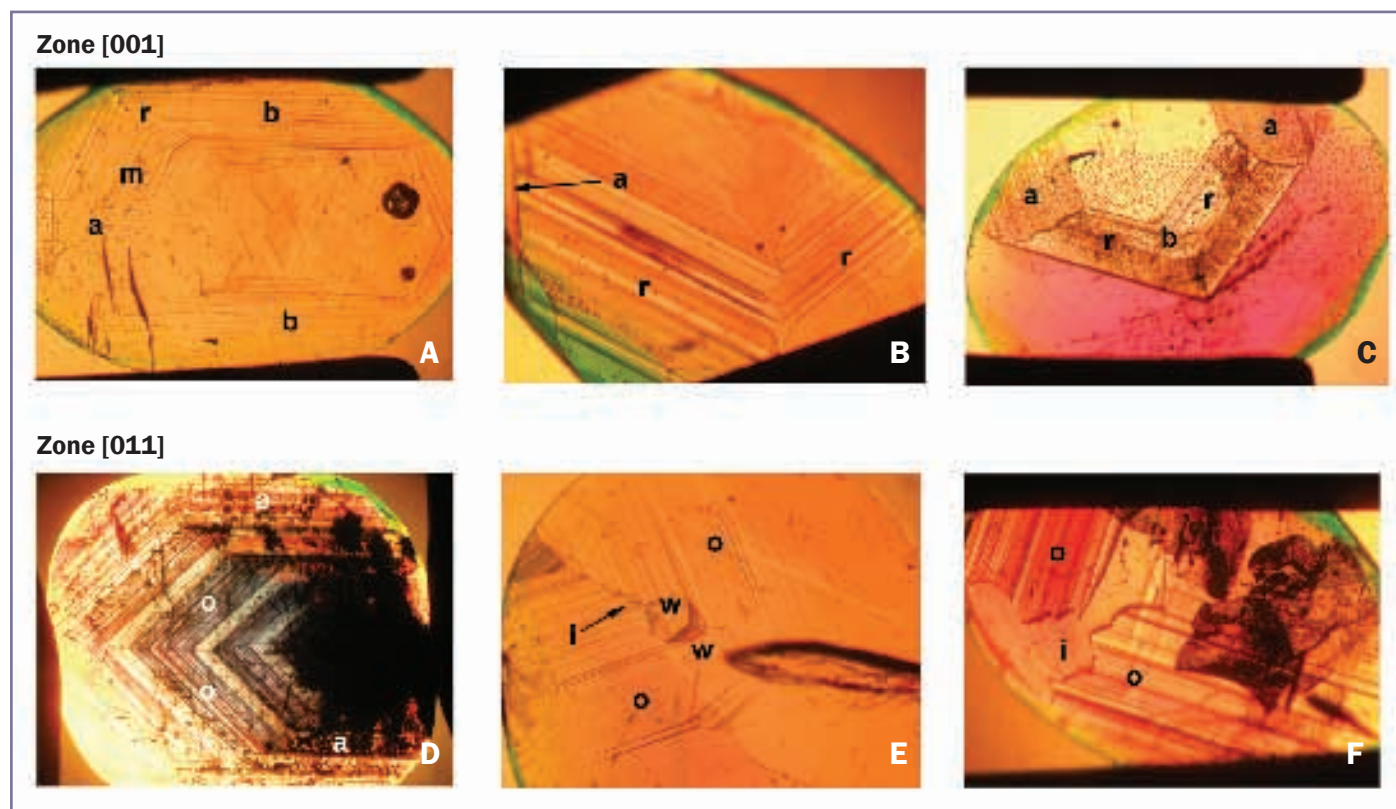


Figure 7: Examples of growth structures in alexandrites from three major natural sources (Urals, Russia; Hematita, Brazil; Sri Lanka). Top row, growth zone [001]: (A) Brazil, 50 ×; (B) Sri Lanka, 40 ×; (C) Sri Lanka, 30 ×; bottom row, growth zone [011]: (D) Russia, 30 ×; (E) Russia, 50 ×; (F) Sri Lanka, 35 ×. All photos in immersion.

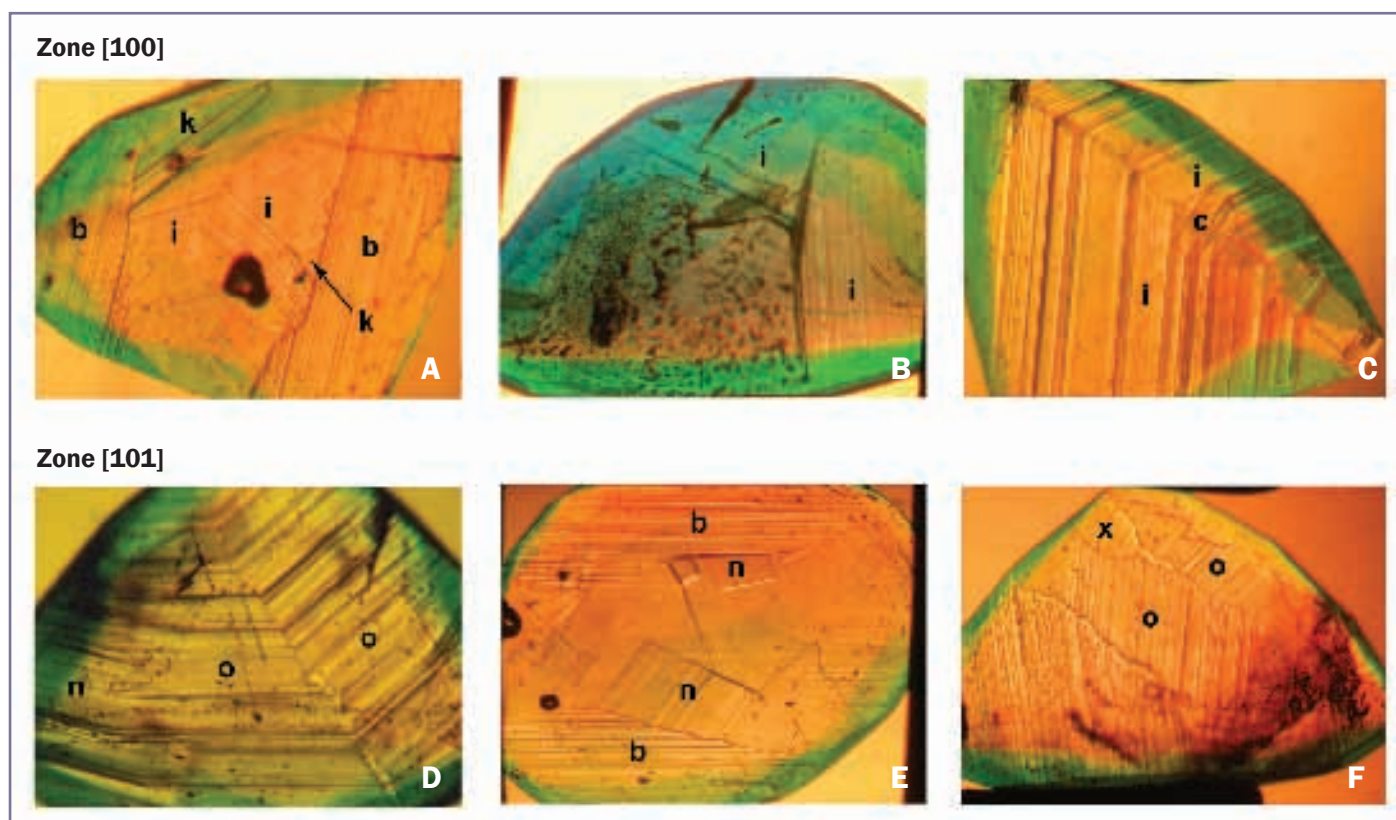


Figure 8: Examples of growth structures in alexandrites from three major natural sources (Urals, Russia; Hematita, Brazil; Sri Lanka). Top row, growth zone [100]: (A) Brazil, 50 ×; (B) Brazil, 40 ×; (C) Sri Lanka, 40 ×; bottom row, growth zone [101]: (D) Russia, 50 ×; (E) Brazil, 50 ×; (F) Sri Lanka, 35 ×. All photos in immersion.

Measurement and interpretation of growth patterns in chrysoberyl, including alexandrite

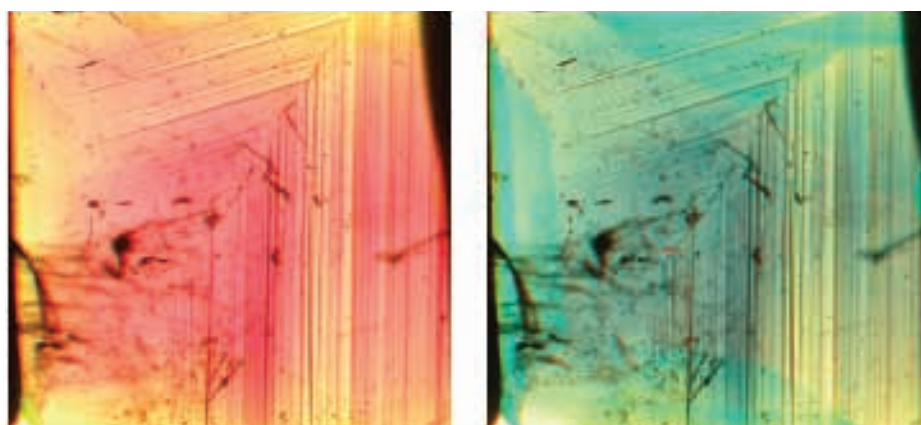


Figure 9: Growth structure and pleochroism in alexandrite from the Urals, Russia; growth zone [110] (i.e. looking perpendicular to the deep orange face *m* (110) in Figure 5), two *o* dipyramids (again see Figure 5) form an interfacial angle of 108° (the angle formed by the two faces is 180° - 108° = 72°). Immersion, 50 ×.

Table III: Structural pattern consisting of more than one growth plane.

Rotation axis of the sample holder parallel to one of the three crystallographic axes	Zone	Visible pattern of crystal growth planes (common examples)
<i>c</i> [001]	[010]	<i>a c a</i> or <i>a x c x' a'</i>
	[110]	<i>o c o'</i> or <i>o o'</i>
	[100]	<i>b i i' b'</i> or <i>b i c i' b'</i> or <i>b k i c i' k' b'</i>
<i>b</i> [010]	[100]	<i>b i i' b'</i> or <i>b i c i' b'</i> or <i>b k i c i' k' b'</i>
	[101]*	<i>b o o' b'</i> or <i>b o x o' b'</i> or <i>b n o x o' n' b'</i>
	[001]	<i>b a b'</i> or <i>b m a m' b'</i> or <i>b s a s' b'</i> or <i>b r a r' b'</i> or <i>b s m a m' s' b'</i> or <i>b r s a s' r' b'</i> or <i>b r m a m' r' b'</i> or <i>b r s m a m' s' r' b'</i>
<i>a</i> [100]	[010]	<i>a c a</i> or <i>a x c x' a'</i>
	[011]**	<i>a i a'</i> or <i>a o o' a'</i> or <i>a o i o' a'</i> or <i>a o w w' o' a'</i> or <i>a o w i w' o' a'</i> or <i>a v o o' v' a'</i> or <i>a v o i o' v' a'</i>
	[012]	<i>a n n' a'</i> or <i>a n k n' a'</i>
	[001]	<i>a b a'</i> or <i>a m b m' a'</i> or <i>a s b s' a'</i> or <i>a r b r' a'</i> or <i>a m s b s' m' a'</i> or <i>a s r b r' s' a'</i> or <i>a m r b r' m' a'</i> or <i>a m s r b r' s' m' a'</i>

Rotation axis of the sample holder perpendicular to a crystal face	Visible zones (examples)
Prism <i>i</i> (011)	[100], [111]***, [011]
Prism <i>x</i> (101)	[010], [101]
Dipyramid <i>o</i> (111)	[011], [101], [110]
Dipyramid <i>n</i> (121)	[101], [012], [111]***

* view almost parallel to one of the optic axes

** view perpendicular to a twin plane

*** faces *m, n, i*

projections. If one considers the three crystallographic axes *c*, *b* and *a*, each in turn parallel to the vertical rotation axis of the sample holder, it is apparent which zones can be visible in a single setting by rotation. In the upper part of Figure 6A, for example, the *c*-axis is selected as rotation axis. So, the different faces of each zone, [010], [110] and [100], can be seen after rotation of the crystal through angles of 25° and 65°, respectively.

In Figure 6B, only parts of the complete crystals shown in Figure 6A are drawn, and the crystal faces observable in different orientations are indicated. It needs to be mentioned that — in practice — only part of the crystal faces shown in Figures 6a and 6b are generally observable. The zone [100], for example, may show all four different faces, *b*, *k*, *i* and *c*, but some crystals only display two or three of these four faces. Examples of characteristic zone patterns which are common in natural alexandrites from different sources are listed in Table III. Photomicrographs of cut immersed alexandrites from three of the major natural sources, namely the Urals, Russia, Hematita, Brazil, and Sri Lanka, are given in Figures 7 and 8. Figure 9 shows an example of an additional growth pattern of zone [110] in a Russian alexandrite crystal and the pleochroism observed on rotation of the polarizer.

It should be emphasized that faceted gemstones normally represent only part of the original rough crystal, from which the gemstone was cut. This means that more or less included and impure parts of the original crystal might have been removed by the cutting process and, therefore, the pattern seen in the microscope might represent only part of a zone structure. It is the experience of the author that it is very helpful to have Figures 6a and 6b or a similar general overview and Tables I to III available beside the microscope for practical work with samples of unknown origin or morphology.

It is possible that during the microscope examination, only one of the optic axes is found. It is also possible that none of the pinacoids *a*, *b* or *c* is present

Measurement and interpretation of growth patterns in chrysoberyl, including alexandrite

or clearly recognizable, or that no growth zone with more than one face is visible. For such stones, it is recommended that a setting is selected with the most significant growth plane perpendicular to the rotation axis of the sample holder. In this setting, the strong growth plane is always visible and sharp in the microscope and any other faces forming a growth zone with this plane will appear during rotation. The measurement of angles in that particular zone together with a control by the observed pleochroism will determine this zone and the crystal planes present.

Examples of characteristic growth patterns which are common in alexandrites from Hematita, Brazil, are given. The first pattern consists of a distinct and jagged boundary between two growth areas (see, e.g., Bank *et al.*, 1987). In these areas the growth planes are rather weak (compared with the images in Figures 7–9) and are related by an interfacial angle of 43° (Figure 10A). In this orientation, the two growth zones show distinct pleochroism. Thus, although two dipyramidal o growth areas in growth zone [101] would abut at a similar angle of 40° , such a view is almost parallel to one of the optic axes and would show no pleochroism, so the pattern in Figure 10A cannot be assigned to this zone. Neither is this characteristic pattern visible when one of the *a*-, *b*- or *c*-axes is parallel to the rotation axis of the sample holder. However, because the prism *i* is a common growth face in alexandrites from Hematita, samples were oriented with these growth planes perpendicular to the rotation axis of the sample holder. With that particular orientation, growth planes of the prism *i* are always sharp in the microscope. Starting with a view of zone [011], after rotation of 21° (measured), a characteristic pattern was observed (Figure 10B), which consists of the prism *i* and the dipyramid *n* (Figure 11). In the same orientation, the dipyramid *n* abuts the prism *m*, again with a jagged boundary, forming an interfacial angle of 35° (Table II), and finally the growth zone is identified as [111]. The theoretical angle calculated for the rotation described is 22.13° .

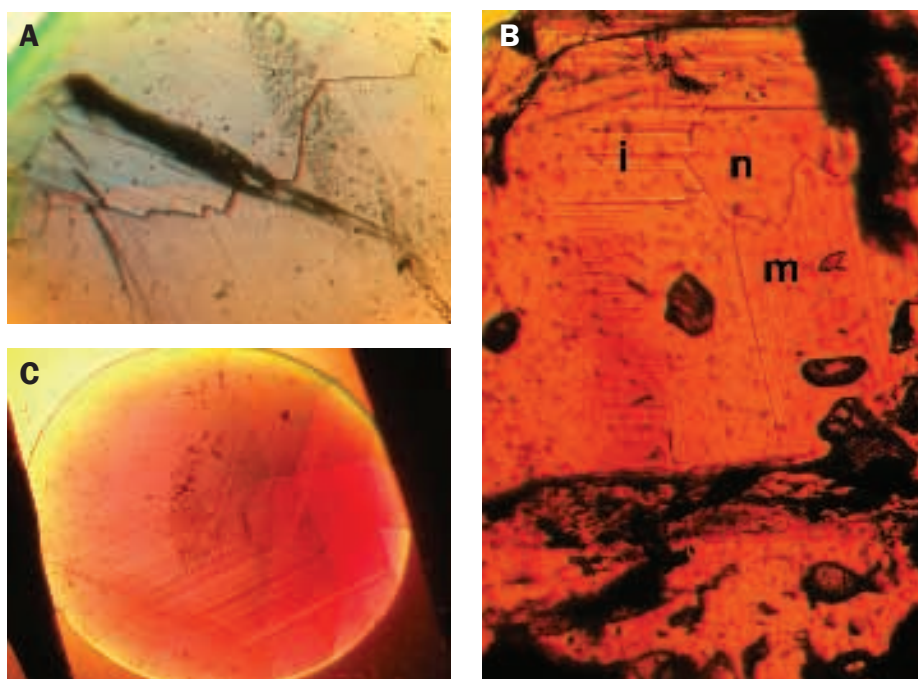


Figure 10A: Growth structure in alexandrite from Hematita, Minas Gerais, Brazil; growth zone [111], the crystal faces *i* (011) and *n* (121) form an interfacial angle of 43° (the angle formed by the two faces is $180^\circ - 43^\circ = 137^\circ$). Immersion, 50 \times .

Figure 10B: Growth structure in alexandrite from Hematita, Minas Gerais, Brazil; growth zone [111], the crystal faces *i* (011), *n* (121) and *m* (110) form interfacial angles of 43° and 35° . Immersion, 60 \times .

Figure 10C: Growth structure in alexandrite from Hematita, Minas Gerais, Brazil; growth zone [011], the crystal faces *i* (011) and *o* (121) form an interfacial angle of 47° (the angle formed by the two faces is $180^\circ - 47^\circ = 133^\circ$). Immersion, 20 \times .

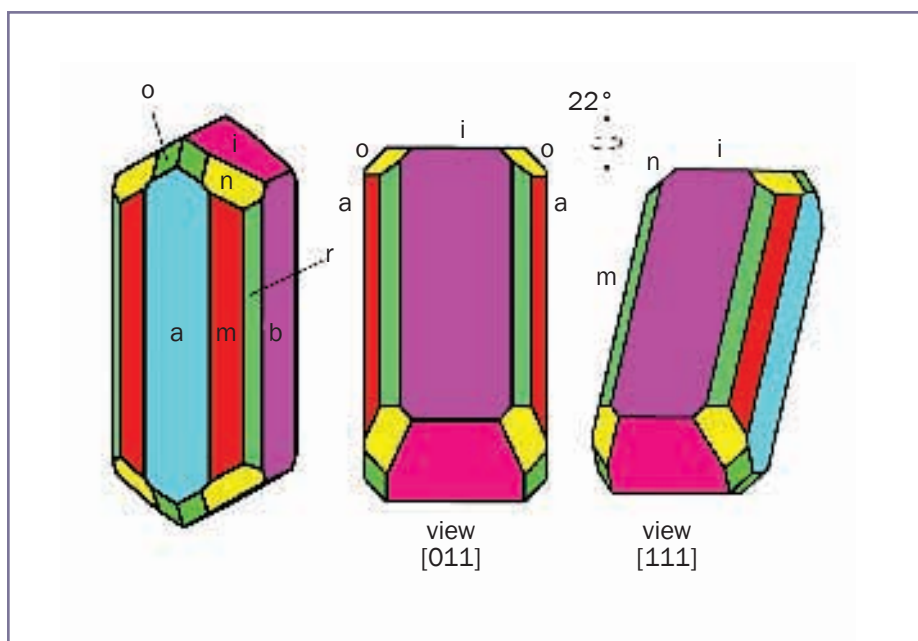


Figure 11: Diagrams of an alexandrite crystal from Hematita, Brazil. Left: clinographic projection; centre: parallel projection with [011] as zone axis; right: parallel projection with [111] as zone axis. When looking parallel to [011], growth structures parallel to the faces *a*, *o* and *i* are visible; upon rotation about an axis perpendicular to the *i* face through 22° , the growth faces *i*, *n* and *m* related to the zone [111] are visible.

Measurement and interpretation of growth patterns in chrysoberyl, including alexandrite

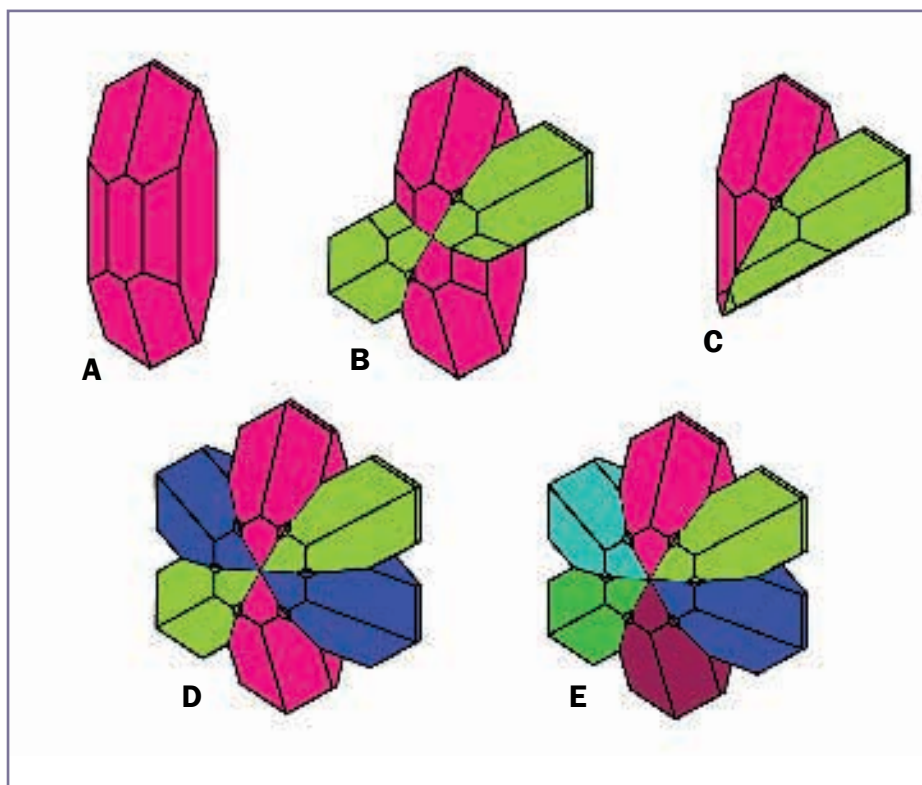


Figure 12: Diagrams of different types of twins in alexandrite: by reflection on the plane (031) a single crystal (A) forms penetration (B) or contact twins (C); a cyclic twin consists of three penetration twins (D) or six contact twins (E). According to the sizes of different faces of the single crystals, the twins may show distinct re-entrant angles (as shown here) or vanishingly small ones.

A second growth pattern commonly seen in alexandrites from Hematita which looks similar with planes forming an interfacial angle of 47° were identified as *i* and *o*, which are related to growth zone [011] (Figure 10C).

Twinning in chrysoberyl and alexandrite

Twinning in alexandrite was described by Rose (1839) in one of the first scientific papers mentioning the new gem material. Of the crystal twins shown in Figure 12, those which are common among the alexandrites recovered from the Uralian emerald mines in Russia are described as cyclic twins or trillings, which consist of three interpenetrant individuals (Figure 12D). However, such crystal twins may alternatively be interpreted as a contact twin of six independent individuals (Figure 12E). The governing twin law is reflection on (031) or (0 $\bar{3}$ 1). Both twin planes are also composition planes of the crystals. In alexandrites from several other occurrences, however, trillings are

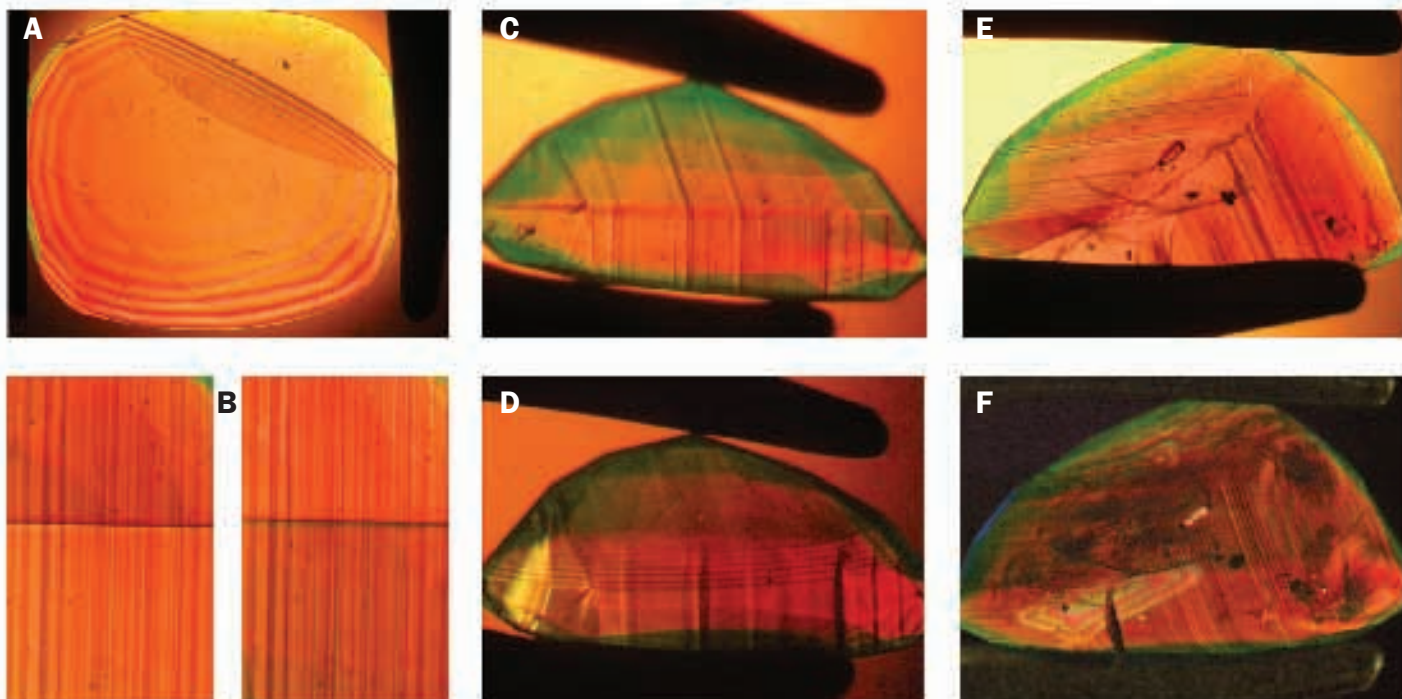


Figure 13: Interference patterns in twinned and untwinned alexandrites. (A) Alexandrite twin from Sri Lanka showing an interference pattern confined by the twin boundary; crossed polarizers; immersion, 25 x. (B) View parallel to a twin plane of alexandrite from Sri Lanka. Growth planes run perpendicular to the twin plane; upon rotation of the polarizer, the different parts of the twin show distinct pleochroism in deeper and paler shades of orange; immersion, 50 x. (C) Growth planes in alexandrite from Sri Lanka in plane polarized light, and showing interference patterns (D) under crossed polarizers; immersion, 30 x. (E) Growth planes in alexandrite from Hematita, Brazil, showing interference patterns (F) under crossed polarizers; immersion, 30 x.

Measurement and interpretation of growth patterns in chrysoberyl, including alexandrite

either rare or absent, although other kinds of twins are quite common. Such twins follow the same twin law as trillings and are developed as contact or penetration twins (*Figure 12 B,C*). In trillings and in contact twins or penetration twins on (031), the crystallographic *a*-axes of all parts of the twin are parallel to each other, and the *b*- and *c*-axes are inclined according to the twin law. For more details, the reader is referred to pp 62–67 in Schmetzer (2010).

In addition to reflection on (031), another twin law in chrysoberyl was described by Jeremejew in 1898 but this has not since been confirmed. Therefore, in this paper, studies are concentrated on twinning on (031).

Many faceted alexandrites show one simple twin boundary, but a few may show two or even three intersecting twin planes. The intersection line between different twin planes is always parallel to [100], i.e. parallel to the crystallographic *a*-axis. When rotating twinned crystals under crossed polarizers, the twin boundary shows a typical interference pattern (*Figure 13A*). Similar interference colours confined to different growth planes may also be present in alexandrites from Sri Lanka, Hematita, Brazil, or elsewhere. In twinned crystals, however, distinct pleochroism can be observed between different parts of a twin or trilling (*Figure 13B*), whereas such pleochroism is not present in crystals with interference colours related to simple growth planes (*Figure 13C to F*).

Growth patterns in twinned chrysoberyls

The best orientation for the examination of growth patterns in twinned chrysoberyls is a setting with the crystallographic *a*-axis (which is parallel for all parts of the twin) as rotation axis, i.e. with the *a*-axis parallel to the rotation axis of the sample holder. With this setting, it is possible to view the twinned sample parallel and perpendicular to the twin plane. Measuring the rotation angle between the visible twin plane and *a*



Figure 14: Slightly water-worn greenish yellow chrysoberyls from Ilakaka, Madagascar. The upper left sample is an untwinned single crystal, the crystal on the upper right is a trilling, all other samples are contact twins. The single crystal is about 8 × 15 mm.

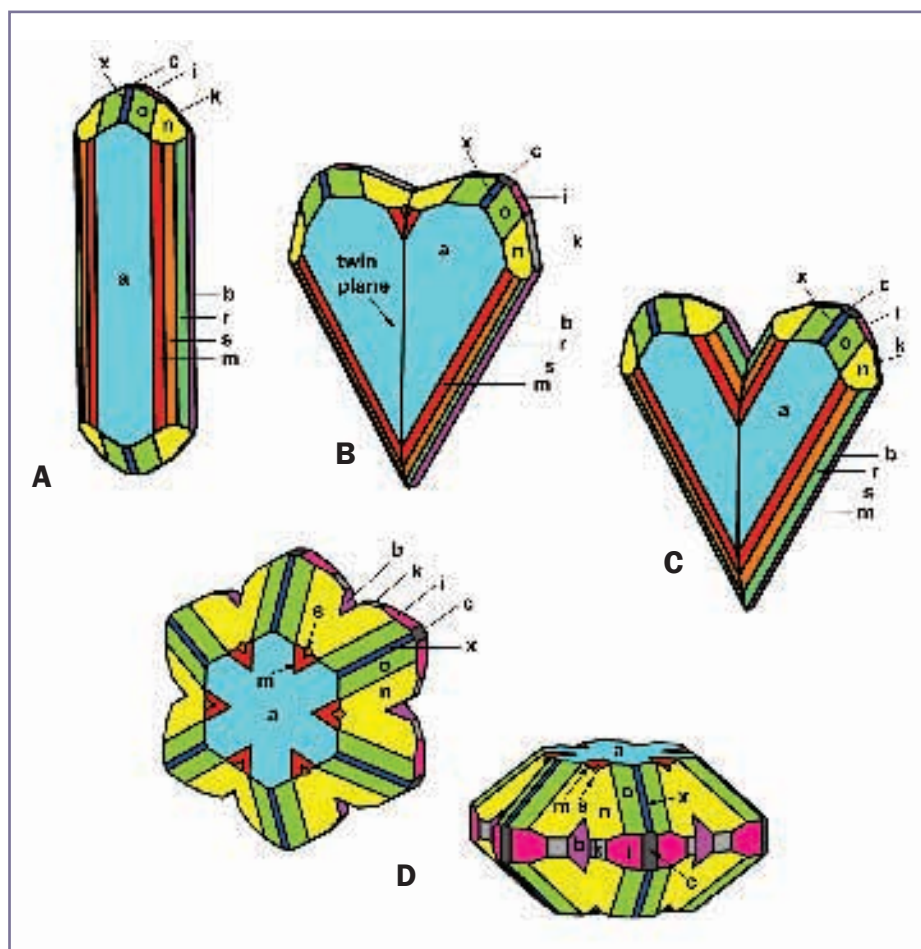


*Figure 15: Diagrams of chrysoberyl crystals from Ilakaka, Madagascar. (A) Single crystal, (B) contact twin with small re-entrant angle, (C) contact twin with a more distinct re-entrant angle, and (D) cyclic twin (trilling), viewed from two directions close to parallel and perpendicular to the *a*-axis.*

Measurement and interpretation of growth patterns in chrysoberyl, including alexandrite

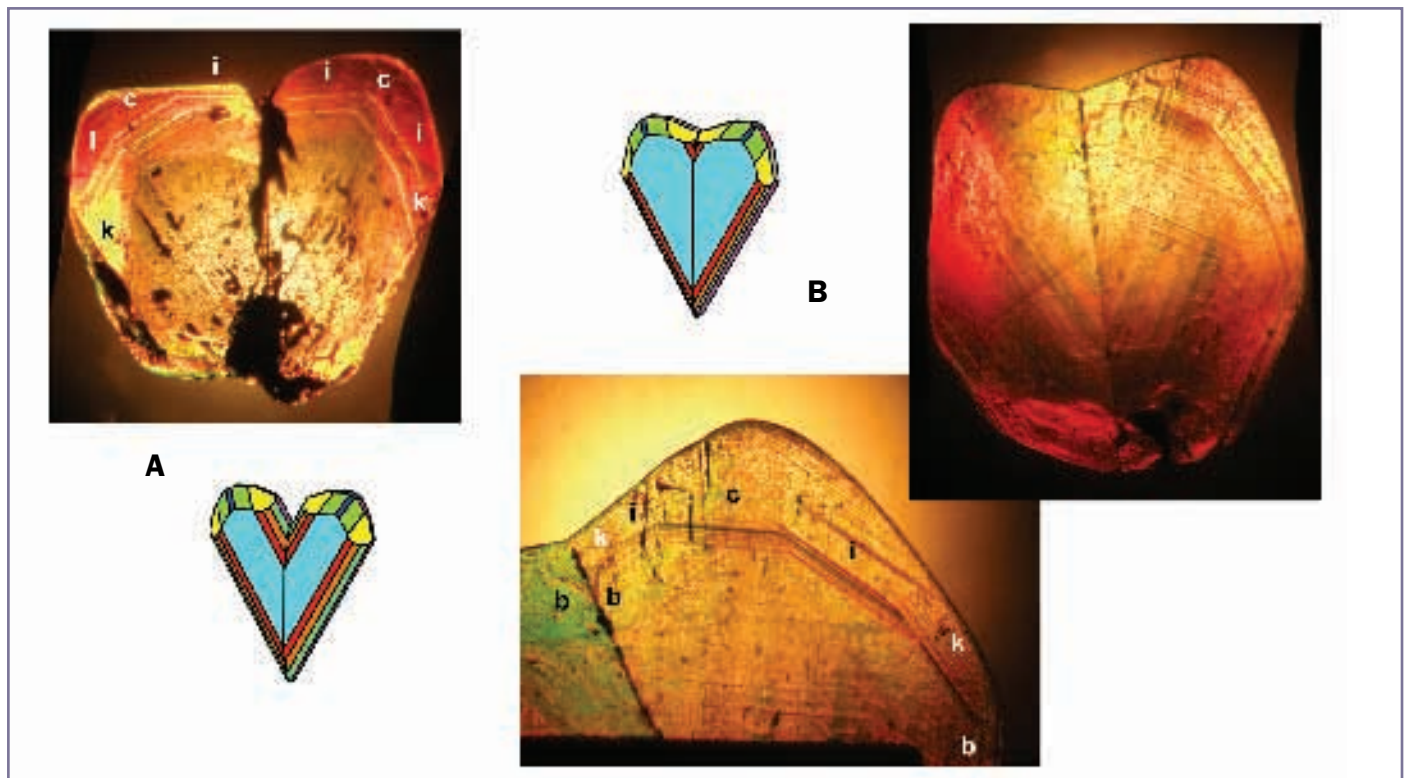


Figure 16 (above): Chrysoberyl twins from Ilakaka, Madagascar with more (A) or less (B) separation of the twin components. Views in the direction of the a-axis showing the [100] growth zones; the pinacoids **b** and **c** and the prism faces **i** and **k** of the waterworn twinned crystals are visible in immersion. Sample (A) measures about 11 × 11 mm, sample (B) measures about 9 × 10 mm.

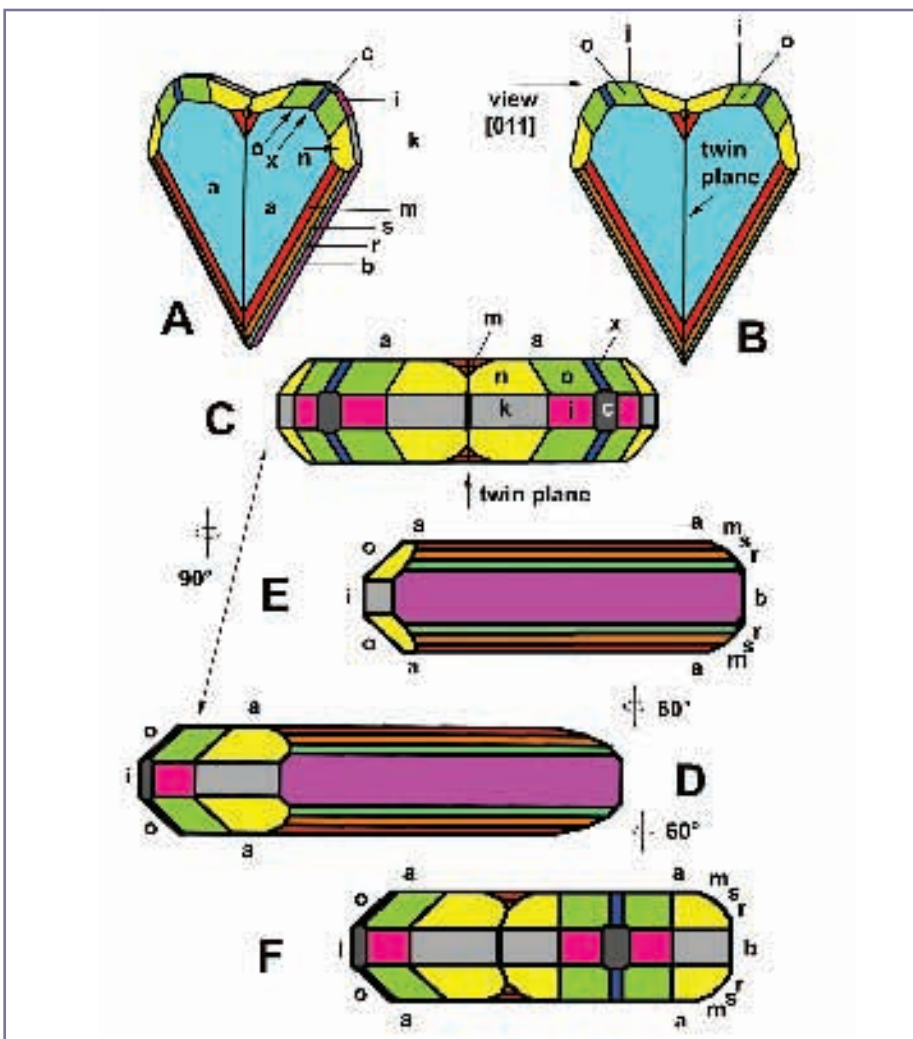


Figure 17 (left): Diagrams of a chrysoberyl twin from Madagascar in different orientations. (A) Clinographic projection, and (B) parallel projection with [100] as zone axis. If one looks parallel to the zone [011] the two **i** prism faces are near-parallel as are the four **o** dipyramids of the two individuals of the twin (only two are shown); this direction of view is indicated in drawing (B) and a parallel projection of the sample in this orientation is shown in drawing (C). Drawing (D) is connected to drawing (C) showing a view parallel to the twin plane by a rotation of 90° with the a-axis as rotation axis; starting from an orientation as shown in drawing (D), a rotation in both directions through 60° leads to orientations as shown in drawings (E) and (F), in which one part of the twin shows a view parallel to the zone [011] with crystal faces **i**, **o** and **a**, and the other part of the twin shows a view parallel to the zone [001] with crystal faces **b**, **r**, **s**, **m** and **a**.

Measurement and interpretation of growth patterns in chrysoberyl, including alexandrite

of a growth zone are visible, identifies the growth zone. In addition, determination of the angles between different growth planes within such a growth zone enables identification of the different growth faces.

For a better understanding of these investigations, the author selected some greenish yellow to yellowish green chrysoberyls from Ilakaka, Madagascar. The stones examined consisted of one single crystal, several contact twins and one trilling (Figure 14). Schematic crystal drawings are given in Figure 15. The crystal faces of 11 of the 13 crystal forms (Table I) are visible and, therefore, these Madagascan samples are useful to explain the sometimes really complex morphological properties and growth structures seen in twins. Due to the sizes of different crystal faces, twin crystals with deeper re-entrant angles are visible beside twins with vanishingly small re-entrant angles (Figure 16).

For the recognition of typical growth zones in faceted chrysoberyls, it can be helpful to orientate a twinned sample with the rotation axis of the sample holder perpendicular to the twin plane. During rotation, one position may be found where the [100] growth zones are symmetrically developed for both individuals of the twin with regard to the twin boundary (view parallel to the *a*-axes of both individuals). In this direction, the different faces of the [100] zone of both individuals are visible (Figure 16).

In simple contact twins, each part of the twin shows two [011] growth zones, i.e. for the complete twin four [011] growth zones are visible, each one with the faces *i*, *o* and *a* (Figures 16 and 17). Now, although the [011] axis is not exactly perpendicular to a twin plane on (031), it is sufficiently close (within 1°) so that in practice, the growth planes of the growth zone [011] are visible in a view perpendicular to a twin plane (see Figure 20 for the relevant twin plane and view). So, in that particular view (Figure 17D), two of these four [011] zones with faces *i*, *o* and *a* (one of each of the two individuals) are virtually parallel and visible together in the microscope. This

Table IV: Rotation of chrysoberyl and alexandrite twins and trillings with the *a*-axis [100] as rotation axis, view perpendicular to the rotation axis.

Chrysoberyl twin from Ilakaka, Madagascar; observed zones and faces

Rotation angle [°]	Zones and faces	
	Individual I	Individual II
-120	[-011] <i>a o i o' a'</i>	[-001] <i>a m s r b r' s' m' a'</i>
-101	[-012] <i>a n k n' a'</i>	
-90 view parallel to a twin plane		
-79		[-012] <i>a n k n' a'</i>
-60	[-001] <i>a m s r b r' s' m' a'</i>	[-011] <i>a o i o' a'</i>
-30		[010] <i>a x c x' a'</i>
0 view perpendicular to a twin plane	[011] <i>a o i o' a'</i>	[011] <i>a o i o' a'</i>
30	[010] <i>a x c x' a'</i>	
60	[011] <i>a o i o' a'</i>	[001] <i>a m s r b r' s' m' a'</i>
79	[012] <i>a n k n' a'</i>	
90 view parallel to a twin plane		
101		[012] <i>a n k n' a'</i>
120	[001] <i>a m s r b r' s' m' a'</i>	[011] <i>a o i o' a'</i>

Alexandrite trilling from Tokovaya, Urals, Russia; observed zones and faces

Rotation angle [°]	Zones and faces		
	Individual I	Individual II	Individual III
-60 view perpendicular to a twin plane	[011] <i>a o i o' a'</i>	[001] <i>a s b s' a'</i>	[011] <i>a o i o' a'</i>
-30 view parallel to a twin plane			
0 view perpendicular to a twin plane	[011] <i>a o i o' a'</i>	[011] <i>a o i o' a'</i>	[001] <i>a s b s' a'</i>
30 view parallel to a twin plane			
60 view perpendicular to a twin plane	[001] <i>a s b s' a'</i>	[011] <i>a o i o' a'</i>	[011] <i>a o i o' a'</i>
90 view parallel to a twin plane			
120 view perpendicular to a twin plane	[011] <i>a o i o' a'</i>	[001] <i>a s b s' a'</i>	[011] <i>a o i o' a'</i>

After rotation through 180°, the same sequence of faces is observable; this is indicated by identical background colours of the respective rows within the table.

means that after a rotation through 180° (viewing the sample from the opposite direction), the same growth pattern can be observed (Figure 17 and see Table IV). After a rotation of 60°, the remaining [011] growth zone of the first individual is parallel to the growth zone [001] of the second individual of the twin (Figure 17 E). This indicates that at one side of the sample, the faces belonging to the [011] zone of the first individual are seen, and at the other side the faces of the growth zone [001] of the second individual

are observed. This special feature is a geometric consequence of the twin law of chrysoberyl, which is also responsible for the pseudohexagonal nature of the cyclic twins. After a rotation of -60°, the remaining [011] growth zone of the second individual is parallel to the growth zone [001] of the first individual of the twin (Figure 17F).

In relatively small and clean chrysoberyls, growth zones of both individuals of such a twin are visible and careful measurements of the rotation

Measurement and interpretation of growth patterns in chrysoberyl, including alexandrite

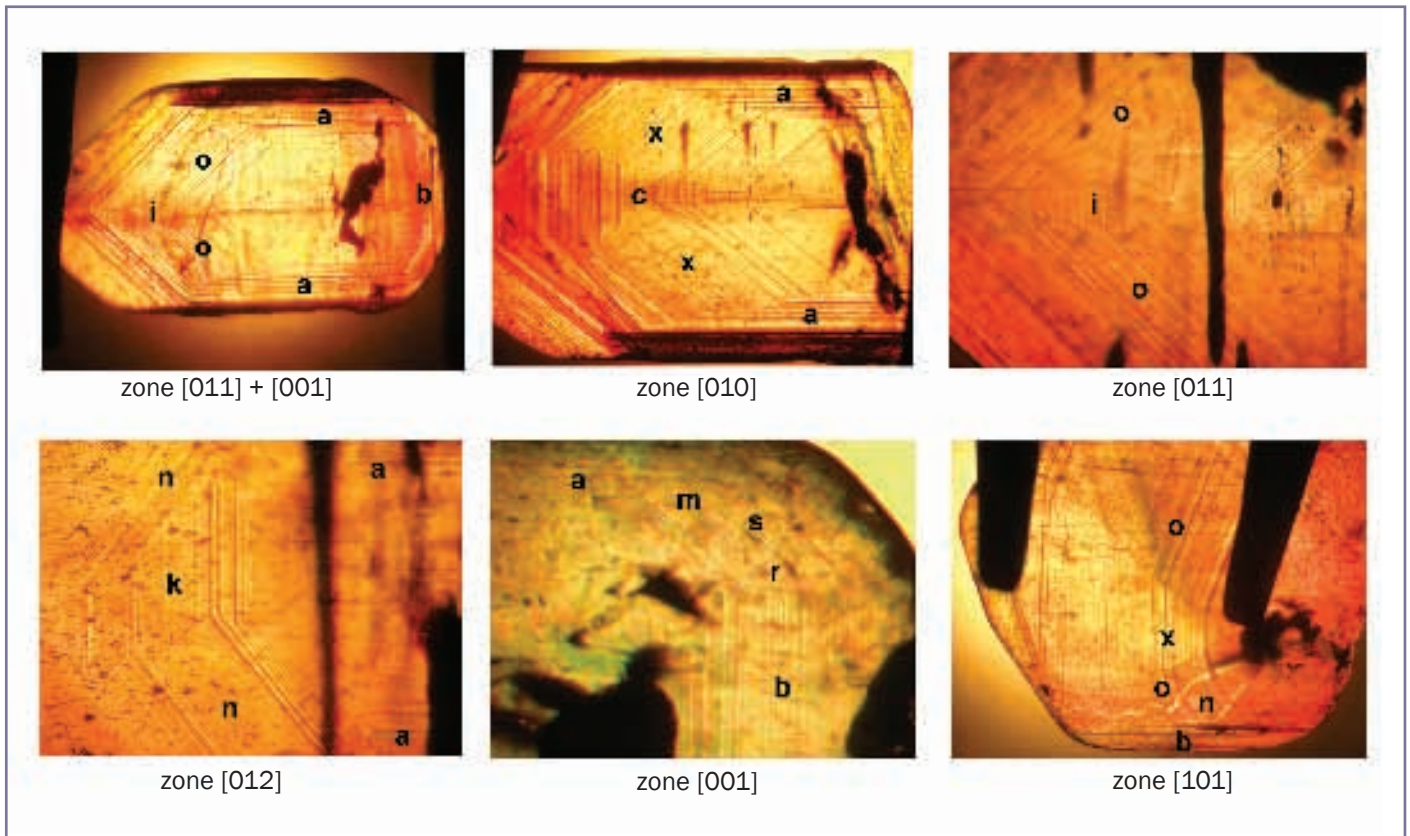


Figure 18: Different growth zones in chrysoberyl contact twins from Ilakaka, Madagascar. According to the orientation of the twin, the growth zones [011] and [001] of both parts of the crystal are shown together (upper left, see also Figure 17 E,F), in other parts of the twin, only one specific growth zone is visible. All photos in immersion, magnification from 15 to 40 ×.

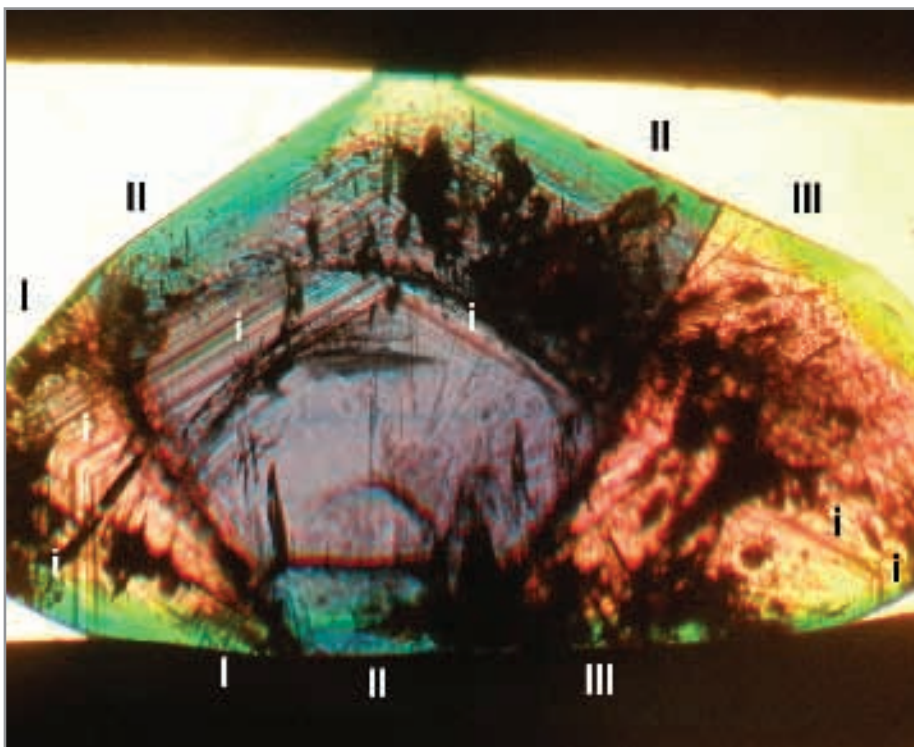


Figure 19: Alexandrite trilling from the Urals, Russia, looking parallel to the a-axis. The a-axes of all three components of the twin, I, II and III, are parallel. In this orientation, in each part of the trilling two *i* prism faces are observed; this sample has no re-entrant angles. Immersion, 40 ×.

angles versus the twin plane are necessary to assign the observed zones and faces to one of the two individuals (see Table IV). Using the *a*-axis of the twin as rotation axis of the sample holder, in addition to the various [011] and [001] growth zones mentioned above, the faces of the [010] and [012] growth zones can also be visible on rotation. An overview concerning rotation angles and growth zones is given in Table IV and examples are pictured in Figure 18. If a different setting is used with the *b*-axis of one individual of a twin as the rotation axis, the faces of the [101] growth zone can also be observed (Figure 18).

In trillings, the *a*-axes of all three components of the twin are parallel to each other (Figures 19 and 20). With the same orientation as mentioned above for twins, i.e. with the *a*-axes parallel to the rotation axis of the sample holder, similar observations are possible and can be interpreted with the help of the schematic drawing in Figure 20. In a view

Measurement and interpretation of growth patterns in chrysoberyl, including alexandrite

perpendicular to one of the three twin planes, the [011] zones of two individuals of the trilling are virtually parallel (*Table IV*) and are visible right and left of the centre of the alexandrite. In the same view, the [001] zone of the third individual of the trilling may be seen in the centre. Consequently, these different patterns are not related to the same part of the rough or faceted trilling and would be seen on opposite parts or ends of a sample (*Figure 21*). This pattern is repeated (for complete samples) after each rotation through an angle of 60°.

Conclusions

With a detailed knowledge of what patterns of internal growth structure are possible, the measurement and interpretation of characteristic growth zones in faceted optically biaxial gemstones such as chrysoberyl is achievable using immersion microscopy. Although not as straightforward as in optically uniaxial gemstones, patterns perhaps consisting of up to several growth areas can be assigned to various growth zones. The orientation of growth planes relative to the twin boundary may also assist understanding of the observed structural pattern. The observation of pleochroism and search for the positions of optic axes can also provide useful complementary information. Currently growth patterns in alexandrites from all major commercial sources, e.g. Russia, Brazil, Sri Lanka, Madagascar, Zimbabwe, India and Tanzania, are being compiled and, in combination with trace element contents, they will be a useful factor in origin determination of these gems.

Acknowledgements

The author is grateful to Dr D. Nyfeler and Mrs A.-K. Malsy, Gübelin Gem Lab, Lucerne, Switzerland, as well as Dr M. Krzemnicki, SSEF, Basel, Switzerland, for the loan of numerous chrysoberyl and alexandrite samples from the reference collections of the Gübelin Gemmological Laboratory and at the SSEF Swiss Gemmological Institute. Numerous samples were provided by the following

Figure 20: Diagram of alexandrite trilling with deep re-entrant angles, projection parallel to the a-axis. In this orientation, all i prism faces of the different parts of the trilling are visible. In views perpendicular to this projection (indicated by → and view), which is consequently perpendicular to the a-axis, the [011] zones of two individuals (I and II) of the trilling are virtually parallel, and parallel to the [001] zone of the third individual (III); the grey part of the trilling is absent in the crystal pictured in Figure 21.

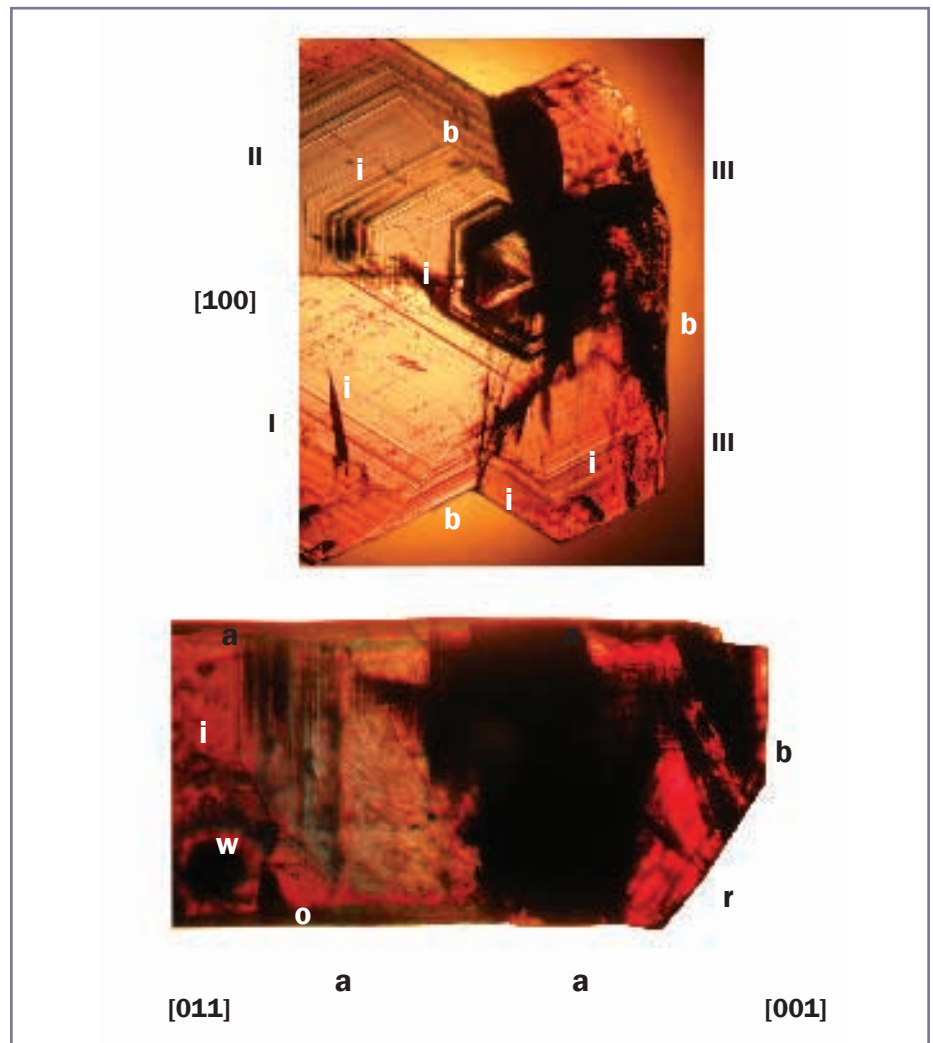
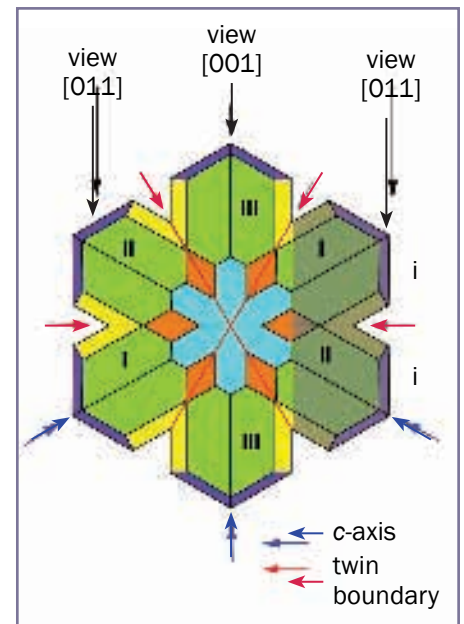


Figure 21: Alexandrite trilling from Lake Manyara, Tanzania. Top: view parallel to the a-axis; the three individuals I, II and III show growth planes parallel to the faces i and b. Below: view perpendicular to the a-axis; for two parts I and II of the trilling (left), the zone [011] is visible in which the growth planes a, o, w and i of both parts of the trilling are near-parallel; for the third part of the trilling III (right) the growth zone [001] with faces r and b is visible. Immersion, 20 ×.

Measurement and interpretation of growth patterns in chrysoberyl, including alexandrite

companies: Rolf Goerlitz and Gebrüder Henn Companies, both at Idar-Oberstein, Germany; Wild & Petsch and Paul Wild Companies, both at Kirschweiler, Germany; Mawingu Gems of Werner Radl, Niederwörresbach, Germany; and Rudolf Schupp Company, Pforzheim, Germany. They are all gratefully acknowledged.

References

- Bank, F.H., Bank, H., Gübelin, E., and Henn, U., 1987. Alexandrite von einem neuen Vorkommen bei Hematita in Minas Gerais, Brasilien. *Zeitschrift der Deutschen Gemmologischen Gesellschaft*, **36**(3/4), 121–31
- Jeremejew, P. Von, 1898. A new twin law for alexandrite. *Bulletin de l'Académie Impériale des Sciences de St.-Petersbourg, V^e Série*, **8**(5), LXIX–LXXI (in Russian). (See also abstract in German by Von Worobieff, V., 1900. Ein neues Zwillingsbildungsgesetz beim Alexandrit. *Zeitschrift für Krystallographie und Mineralogie*, **32**, 427)
- Kiefert, L., and Schmetzer, K., 1991a. The microscopic determination of structural properties for the characterization of optical uniaxial natural and synthetic gemstones. Part 1: General considerations and description of the methods. *Journal of Gemmology*, **22**(6), 344–54
- Kiefert, L., and Schmetzer, K., 1991b. The microscopic determination of structural properties for the characterization of optical uniaxial natural and synthetic gemstones. Part 2: Examples for the applicability of structural features for the distinction of natural emerald from flux-grown and hydrothermally-grown synthetic emerald. *Journal of Gemmology*, **22**(7), 427–38
- Kiefert, L., and Schmetzer, K., 1991c. The microscopic determination of structural properties for the characterization of optical uniaxial natural and synthetic gemstones. Part 3: Examples for the applicability of structural features for the distinction of natural and synthetic sapphire, ruby, amethyst and citrine. *Journal of Gemmology*, **22**(8), 471–82
- Rose, G., 1839. Ueber den Chrysoberyll vom Ural. *Annalen der Physik und Chemie*, **48**, 570–3
- Schmetzer, K., 1986. An improved sample holder and its use in the distinction of natural and synthetic ruby as well as natural and synthetic amethyst. *Journal of Gemmology*, **20**(1), 20–33
- Schmetzer, K., 2010. *Russian alexandrites*. Schweizerbart Science Publishers, Stuttgart, 141 pp.
- Schmetzer, K., Peretti, A., Medenbach, O., and Bernhardt, H.-J., 1996. Russian flux-grown synthetic alexandrite. *Gems & Gemology*, **32**(3), 186–202
- Smith, C.P., 1996. Introduction to analyzing internal growth structures: Identification of the negative d plane in natural ruby. *Gems & Gemology*, **32**(3), 170–84

All photos and crystal drawings by the author.

The Author

Dr Karl Schmetzer
 Taubenweg 16, 85238 Petershausen,
 Germany
 Email: SchmetzerKarl@hotmail.com

A Russian Maxixe beryl?

Lars Olov Andersson

Abstract: Maxixe beryl has a deep blue colour, which fades upon extended exposure of the crystal to daylight. In a 1976 publication a colourless Russian beryl was reported to contain a considerable amount of NO_2 . The published EPR spectrum of this beryl is similar to that of a bleached Maxixe beryl. Analysis of the colour centres of Maxixe beryl and the artificially created Maxixe-type beryl indicate that samples of this Russian beryl could display the blue colour of Maxixe beryl after irradiation.

Keywords: EPR, Maxixe beryl, NO_2 in beryl

Introduction

The observation of NO_2 impurities in a colourless Russian beryl by Electron Paramagnetic Resonance (EPR) spectroscopy (Sukharzhevskii, 1976) suggests that this Russian beryl may have had (and can again obtain) the features of the rare Maxixe beryl found around 1917 in Brazil. This possibility is based on a study of the creation and decay of the colour centre in the Maxixe beryl. Comparison of these processes is also made with the behaviour of the colour centre in the Maxixe-type beryl which appeared on the gemstone market around 1973.

A crystal of beryl ($\text{Be}_3\text{Al}_2\text{Si}_6\text{O}_{18}$) consists of silicate rings stacked upon each other, like stacks of doughnuts. The holes in the middle form channels stretching throughout the crystal structure. These channels are parallel to the *c*-axis of the beryl crystal and have a diameter which varies between 2.8 Å in the rings and 5.1 Å between the rings. Neighbouring stacks are held together by Be and Al ions. Impurity ions like Fe, Mn and Cr can replace Al or Be ions in natural beryl crystals. Relatively large

amounts (often more than one weight %) of other impurities, mainly alkali ions and water, but also CO_2 and CH_4 molecules, can be located in the channels.

Chemical bonds in molecules (such as CO_2), ions (such as CO_3^{2-}), and crystals usually contain paired electrons. NO_2 and NO_3 molecules are exceptions with unpaired electrons. Unpaired electrons are also a result from irradiation which can remove one electron (as in CO_3^-) or add one electron (as in CO_2^-). EPR spectrometers are used to detect such unpaired electrons and study their behaviour. They can also be used to study the unpaired electrons in paramagnetic ions (such as Fe^{3+} and Cr^{3+}). When a strong magnetic field is applied, the spin of the electrons will be oriented parallel or antiparallel to the magnetic field. These orientations have different energy levels and transitions between them occur in the microwave region. The EPR spectrometer registers the microwave absorption of the unpaired electrons. The spectrum is obtained by keeping the microwave frequency constant and changing the magnetic field.

Maxixe beryl and Maxixe-type beryl

Maxixe beryl was first described in the scientific literature by Wild (1933), who stated that the crystal had been found 15 years earlier in the Maxixe mine. This beryl had a deep blue colour, which faded when the crystal was kept for many days in daylight. It is strange that there are no earlier reports about this unusual beryl, after it had caused the gemstone dealers such disappointment. The samples investigated by Wild had been kept in the dark since about 1917 and had not lost their blue colour. More detailed investigations of this material were made by Schlossmacher and Klang (1935) and by Roebbling and Tromnau (1935). Schlossmacher and Klang (1935) describe the location of the Maxixe mine in Minas Gerais, Brazil, and state that the mine was closed when the loss of colour caused a lot of trouble. One other of Wild's samples has been described in detail by Schiffman (1977). No other beryl with the same properties as Maxixe beryl has since been reported.

In 1972–1973 more beryl crystals of an intense blue colour appeared on

A Russian Maxixe beryl?

the gemstone markets, but the initial enthusiasm for these beautiful stones changed to disappointment when it was found that their colour also faded upon extended exposure to daylight in shop window displays. Nassau *et al.* (1976) investigated these crystals and established that they have the opposite dichroism to that of aquamarine. The blue colour of the new beryl is carried by the ordinary ray, while that of aquamarine is carried by the extraordinary ray. Nassau *et al.* (1976) called these new beryls Maxixe-type beryls because their optical absorption spectra contained similar, but slightly different, absorption bands to those from the rare Maxixe beryl. They were also able to create similar blue crystals by irradiation of some other beryls. As will be seen below, this should be possible when the beryls contain enough carbonate ions.

Origin of the blue colour

The different colours of beryl are usually related to paramagnetic ions (iron, manganese, chromium, vanadium) substituting for aluminium in the octahedral sites between the stacks of silicate rings in the beryl crystal structure. However, Maxixe beryl has a very low content of such ions (Roebeling and Tromnau, 1935) and the unusual blue colour centres of Maxixe and Maxixe-type beryl are instead located in the beryl channels.

Using EPR spectroscopy, Andersson (1979) determined that the colour centre in Maxixe beryl is the NO_3 molecule, while the colour centre in Maxixe-type beryl is CO_3^- . Since these centres have the same number of electrons in the same molecular orbitals (that is they are isoelectronic), their optical absorption spectra are very similar. However, their EPR spectra are different because the nuclei of the colour centres interact differently with the unpaired electron. The oxygen and carbon nuclei of CO_3^- have no influence on the EPR spectrum, but the nitrogen nucleus of NO_3 splits the EPR signal into three lines. It is therefore easy to separate Maxixe and Maxixe-type beryl by EPR spectroscopy.

Both the NO_3 and CO_3^- groups (radicals) are planar and fit in the widest part of the beryl channel where they are oriented with their trigonal symmetry axis parallel to the crystal *c*-axis. This well-defined orientation gives rise to the strong pleochroism of the blue colour.

Creation of NO_3 and CO_3^- colour centres in beryl

Nassau *et al.* (1976) concluded that the blue colour centre in Maxixe-type beryl is created by irradiation while the Maxixe colour centre is of natural origin. Different possibilities of how CO_3^- and NO_3 radicals could be created in beryl will now be considered.

One possibility is that CO_3^{2-} and NO_3^- ions existed in the original melt and were trapped in the channels of the beryl crystal during its formation. An electron can be removed from each of these ions by irradiation to create CO_3^- and NO_3 . The released electron can be caught by an impurity proton to form a hydrogen atom. Such atoms have been detected in both Maxixe and Maxixe-type beryl by EPR. If this scheme is correct, it can be concluded that both colour centres have been created by irradiation.

A second possibility is that CO_2 and NO_2 molecules were trapped from the original melt during the beryl crystal formation. Wood and Nassau (1967) observed the optical absorption of CO_2 in many beryl crystals and Andersson (1979 and 2010) observed the EPR signal of NO_2 in Maxixe beryl. It has been shown that H_2O molecules can diffuse in the beryl channel (Fukuda, 2009). If a water molecule enters a wide portion of the channel containing a NO_2 molecule, it can combine with this molecule to form NO_3 . The hydrogens are split off as single atoms, which have been detected in the EPR spectrum of Maxixe beryl. The probability that this combination of molecules will happen may be very small, so that it could have taken many thousands of years until a sufficient number of stable NO_3 molecules were created to give the Maxixe beryl its intense blue colour. This process was

proposed by Andersson (2008) to explain the existence of NO_3 in natural beryl crystals. The corresponding process forms CO_3^{2-} in beryl containing CO_2 and in this case the hydrogen is split off as protons. Irradiation creates the Maxixe-type colour centre CO_3^- and the released electron is captured by a proton to form a hydrogen atom.

A third possibility is that OH^- ions diffuse in the structural channel and combine with CO_2 or NO_2 to form CO_3^{2-} or NO_3^- . This possibility has been discussed in detail by Andersson (2006). As in the first possibility, irradiation is needed to create the Maxixe beryl.

Decay of the NO_3 and CO_3^- colour centres

Nassau *et al.* (1976) found that the colour of both Maxixe beryl and Maxixe-type beryl disappeared when the crystals were exposed to daylight for one week or were heated to 200°C for one hour. They observed that while the colour of Maxixe-type beryl was created in one single process, its decay exhibited one fast and one slow component. Edgar and Vance (1977) found that the decay of the CO_3^- EPR signal upon heating of Maxixe-type beryl at 175°C correlated very well with the decay of the optical absorption, while the decay of the hydrogen atom signal was less pronounced in the initial stage.

Both Maxixe and Maxixe-type beryl contain hydrogen atoms which are stable at room temperature, which is rather unusual. The hydrogen atom easily dissociates into a proton and an electron. The released electron can combine with CO_3^- to form a CO_3^{2-} ion or with NO_3 to form a NO_3^- ion, and the colour centres will disappear. I therefore suggest that the dissociation of the hydrogen atom is the cause of bleaching in Maxixe and Maxixe-type beryl. The hydrogen atom loses its electron and the bleaching occurs when the crystals are heated above 100°C or are exposed to light.

Andersson (2008) found that some of the electrons which were released by the irradiation of Maxixe-type beryl were trapped by CO_2 molecules to form

A Russian Maxixe beryl?

CO_2^- radicals. (This explains why the CO_2 absorption in the infrared spectrum of Krambrock *et al.* (2002) disappeared upon irradiation.) These radicals lose their electrons at a lower temperature than the hydrogen atoms and cause the initial decay of the CO_3^- colour centres. That is why the decay curve has two components in Maxixe-type beryl, with the slow component corresponding to the decay of the hydrogen atoms. The decay of colour in Maxixe beryl will have only one component.

NO_2 in Maxixe beryl and in a Russian beryl

The EPR signal of NO_2 has been detected in a colourless Russian beryl by Sukharzhevskii (1976). It is split into three lines by the nitrogen nucleus. These lines are of equal width and intensity when the magnetic field is oriented parallel to the crystal c -axis and in the spectrum they are separated by 66 Gauss, which in modern units is 6.6 milliTesla (mT). This beryl was found on the Kola peninsula in northwestern Russia (Sukharzhevskii, pers. comm., 2011). The Kola beryl has a high content of Cs ions, like the other beryls in which NO_2 has been observed.

Dr Gübelin of Lucerne kindly donated a piece from the Maxixe crystal in his collection for the EPR measurements, which were performed in 1977. I was not able to orient this irregular mm-size piece parallel to the c -axis, but a later extrapolation of the NO_2 signal positions observed at other angles converges to three narrow lines for the orientation parallel to the c -axis. This extrapolation (Andersson, 2010) was made before I was aware of the 1976 publication by Sukharzhevskii, but fits very well with his spectrum.

EPR spectra obtained with different orientations of the magnetic field give information about the orientation of the NO_2 molecule. Sukharzhevskii (1976) found that the molecular plane is perpendicular to the crystal c -axis and suggested that the NO_2 molecules are located between the stacks of silicate rings. Solntsev (1981) interpreted the data

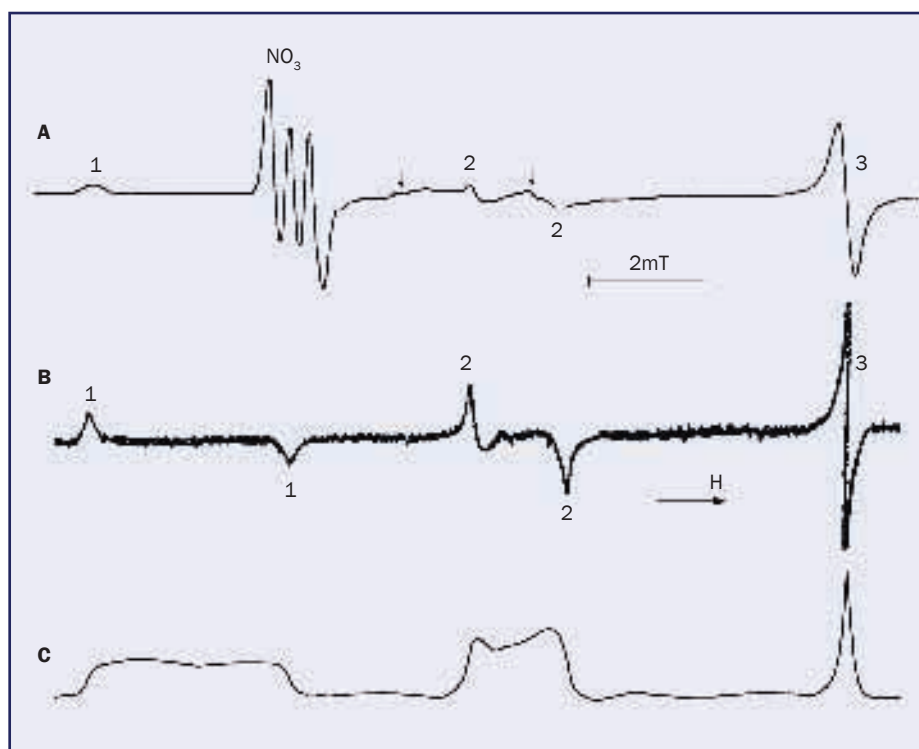


Figure 1: EPR spectra obtained at 9.2 GHz with the magnetic field H oriented perpendicular to the crystal c -axis. The strength of the field H is changed around the resonance field of the free electron near 330 mT. Trace A was obtained from Maxixe beryl at -180 °C and trace B from the Russian beryl at -196 °C. Trace C is the integral of the spectrum in trace B. Further explanations are given in the text.

differently and located the NO_2 molecules in the beryl channel, at the same position as the NO_3 molecules. He suggested that they are oriented in six equivalent positions in the hexagonal symmetry. Andersson (2010) found that the NO_2 molecules in Maxixe beryl are evenly distributed over all possible orientations in the plane perpendicular to the crystal c -axis.

The EPR spectra with the magnetic field oriented perpendicular to the crystal c -axis are shown for Maxixe beryl in trace A and for the Russian beryl in trace B of *Figure 1*. For technical reasons the EPR signal is recorded as the derivative of the absorption. An integration of trace B shows the three absorption lines in trace C of *Figure 1*. The two low field lines have been broadened. (Because of the background noise in trace B, the integral is not completely accurate: the areas beneath each of the three absorption lines should be equal.)

It can be seen that the intensity is evenly distributed over the range of the absorption for each of the two low field lines in trace C. If the NO_2 molecules had only six different orientations as suggested by Solntsev (1981), the low field lines should have consisted of a few separate absorptions. The absorption in trace C shows that there is an even distribution of NO_2 orientations over all angles in the Kola beryl, as there is in the Maxixe beryl.

The end points of the distributed absorptions appear clearly in the derivative spectrum in trace B and are marked with 1 and 2 for the two low field lines. These signals are also present in trace A from the Maxixe beryl. In this spectrum line 1 is partly overlapped by the signal from NO_3 , which has a much smaller splitting of 0.5 mT. The EPR signal of the hydrogen atom is outside the range of *Figure 1* because the hydrogen nucleus splits the signal into two lines 50 mT apart. The EPR signal from NO_2 can

A Russian Maxixe beryl?

only be observed at temperatures below $-140\text{ }^{\circ}\text{C}$ and is still somewhat broadened at $-180\text{ }^{\circ}\text{C}$. The derivative peaks are therefore not so sharp in trace A as in trace B which was obtained at $-196\text{ }^{\circ}\text{C}$.

Andersson (2010) has shown that it is a coincidence that line 3 has the same narrow shape as in the spectrum with the magnetic field parallel to the *c*-axis and that the spread of line 1 is twice as large as that of line 2. In the spectrum from an EPR spectrometer operating at another microwave frequency line 3 would also be broadened.

Discussion

Reports about NO_2 and NO_3 impurities in other beryls are rare and their concentrations have been so small that no colour has been observed. The EPR spectrum from the 1973 Maxixe-type beryl contains very small signals from NO_2 (Andersson, 2010) and NO_3 (Andersson, 1979). Solntsev (1981) reported EPR parameters for NO_2 and NO_3 in natural beryl and in synthetic hydrothermal beryl, but does not mention a blue colour or the origin of his samples. Krambrock *et al.* (2002) detected EPR signals from CO_3^- and NO_3 in natural pink beryl from Minas Gerais in Brazil. It is strange that CO_3^- is present in the unirradiated crystal and that a signal identified as NO_2 was observed only after irradiation. In a later publication, Pinheiro *et al.* (2007) reported that only the NO_3 signal was present in the natural crystal while the CO_3^- signal appeared after irradiation. The intensity of the NO_3 signal remained about the same before and after the irradiation.

An interpretation of the observations by Pinheiro *et al.* (2007) is that the natural crystal contained CO_3^{2-} and an amount of NO_3 which was not enough to give the crystal a colour. The irradiation created enough CO_3^- to colour the crystal blue but no additional NO_3 . If the natural crystal had contained NO_3^- , the irradiation should have created additional NO_3 .

Two of the possible processes for creation of the colour centre in Maxixe beryl involve NO_3^- ions and irradiation. The irradiation need not have been

artificial, but could have come from natural sources. Irradiation also creates CH_3 from CH_4 molecules in the beryl channel and the EPR signal from CH_3 can easily be detected in the spectrum from the artificially irradiated Maxixe-type beryl (Andersson, 2008). A much smaller CH_3 signal is detected in the Maxixe beryl and is indicated by arrows in trace A of *Figure 1*. Although natural radiation at the Maxixe locality may have created such a small signal, it was probably not sufficiently intense to have caused the much stronger NO_3 signal. (An alternative, but unlikely, interpretation is that the natural radiation was very strong and that the CH_4 content in Maxixe beryl was very small.) This supports the assumption that NO_3 was created by a different process and not by irradiation of NO_3^- .

The most likely process involves a combination of H_2O and NO_2 without the influence of radiation. The NO_2 molecules could have been trapped in the beryl crystals during their formation and some of these impurities have been transformed into NO_3 over geological time. This could have happened in both the Maxixe beryl and the Russian beryl. The NO_3 colour centres in the Kola beryl may then have been converted into NO_3^- by catching the electrons from the decay of the hydrogen atoms when the crystal was exposed to daylight or was heated above $100\text{ }^{\circ}\text{C}$ in recent geological time. Sukharzhevskii (1976) mentions that a zone of the crystal is weakly blue, which may indicate that some NO_3 remains.

The rest of the original NO_2 molecules are not influenced by heat or light and their EPR signal remains the same in both Maxixe and Kola beryl. The signals from the hydrogen atoms and NO_3 molecules in Maxixe beryl disappear when the crystal is bleached. The colour centres are then not converted back to NO_2 but are transformed to NO_3^- ions.

Nassau *et al.* (1976) found that the colour of bleached Maxixe beryl could be restored by irradiation with neutrons or γ -rays. This would be the case if the irradiation removes the electron from NO_3^- , which recreates the NO_3 colour centre.

Irradiation is therefore needed to restore the colour centre in Maxixe beryl, but not for its initial creation. Andersson (2008) showed that the colour of Maxixe-type beryl can be restored by UV irradiation. If this is the case also for Maxixe beryl, it may be possible that the Kola beryl could display the same deep blue colour as Maxixe beryl without the discolouring caused by more intense irradiation (Nassau *et al.*, 1976). This possibility should be borne in mind if such stones should appear in the gemstone market. Collectors and dealers should be aware that such a blue beryl would lose its colour upon extended exposure to daylight.

Conclusion

Considerable amounts of NO_2 impurities have been found in only two beryl crystals, the Kola beryl and the Maxixe beryl. The EPR spectrum of the colourless Kola beryl contains only the NO_2 signal, while that of the Maxixe beryl also contains NO_3 and hydrogen signals. The latter two signals disappear when the Maxixe beryl is bleached. The Kola beryl may therefore be a bleached Maxixe beryl and should turn blue when it is irradiated.

A definite classification of the Kola beryl as a Maxixe beryl could only be made if the NO_3 colour centre is detected after irradiation of a crystal from the same location as the beryl which was investigated in 1976.

References

- Andersson, L.O., 1979. The difference between Maxixe beryl and Maxixe-type beryl: an electron paramagnetic resonance investigation. *J. Gemm.*, **16**, 313–17
- Andersson, L.O., 2006. The positions of H^+ , Li^+ and Na^+ impurities in beryl. *Phys. Chem. Minerals*, **33**, 403–16
- Andersson, L.O., 2008. EPR investigation of the methyl radical, the hydrogen atom and carbon oxide radicals in Maxixe-type beryl. *Phys. Chem. Minerals*, **35**, 505–20

A Russian Maxixe beryl?

- Andersson, L.O., 2010. EPR investigation of NO₂ and CO₂⁻ and other radicals in beryl. *Phys. Chem. Minerals*, **37**, 435–51
- Edgar, A., and Vance, E.R. 1977. Electron paramagnetic resonance, optical absorption, and magnetic circular dichroism studies of the CO₃⁻ molecular-ion in irradiated natural beryl. *Phys. Chem. Minerals*, **1**, 165–78
- Fukuda, J., Shinoda, K., Nakashima, S., Miyoshi, N., and Aikawa, N., 2009. Polarized infrared spectroscopic study of diffusion of water molecules along structure channels in beryl. *Am. Mineral.*, **94**, 981–5
- Krambrock, K., Pinheiro, M.V.B., Guedes, K.J., Medeiros, S.M., Schweizer, S., Castaneda, C., Botelho, N.F., and Pedrosa-Soares, A.C., 2002. Radiation-induced centers in Cs-rich beryl studied by magnetic resonance, infrared and optical spectroscopy. *Nucl. Instrum. Methods B*, **191**, 285–90
- Nassau, K., Prescott, B.E., and Wood, D.L., 1976. The deep blue Maxixe-type color center in beryl. *Am. Mineral.*, **61**, 100–7
- Pinheiro, M.V.B., Krambrock, K., Guedes, K.J., and Spaeth, J.M., 2007. Optically-detected magnetic resonance of molecular color centers CO₃⁻ and NO₃ in gamma-irradiated beryl. *Phys. Stat. Sol. (c)*, **4**, 1293–6
- Roebling, W., and Tromnau, H.W., 1935. Maxixeberyll. II. *Zentralbl. Mineral. Geol. Paläont.*, **1935A**, 134–9
- Schiffman, C.A., 1977. Gemmologische Studie an einem Original-Maxixe-Beryll. *Z. Dt. Gemmol. Ges.*, **26**, 135–41
- Schlossmacher, K., and Klang, H., 1935. Der Maxixeberyll. I. *Zentralbl. Mineral. Geol. Paläont.*, **1935A**, 37–44
- Solntsev, V.P., 1981. The nature of colour centres and EPR in beryl and chrysoberyl. *Trudy Instituta Geologii i Geofiziki, Akademiya Nauk SSSR (Novosibirsk)*, **499**, 92–140 (in Russian)
- Sukharzhevskii, S.M., 1976. Investigation of the NO₂ molecular structure in beryl. In: *Problems in geochemistry and typomorphism of minerals*. Leningrad State University, Leningrad, 22–9 (in Russian)
- Wild, G.O., 1933. Mitteilung über ein anscheinend neues Berylliumsilikat. *Zentralbl. Mineral. Geol. Paläont.*, **1933A**, 38–9
- Wood, D.L., and Nassau, K., 1967. Infrared spectra of foreign molecules in beryl. *J. Chem. Phys.*, **47**, 2220–8

The Author

Dr Lars Olov Andersson
Brunnenweid 49, CH-5643 Sins, Switzerland

e-mail: loandersson@bluewin.ch

Raise your profile . . .

Raise customer confidence with

Gem-A Corporate Membership

Gain advantages including:

- Use of Gem-A logo or Coat of Arms (illustrated right)
- GIA Diamond Grading Reports via Gem-A
- Discounts on courses and workshops
- Discounts on books and instruments
- Regular meetings for information exchange and networking
- Gem-A's popular magazine *Gems & Jewellery*.

Any UK-based company may apply to become a Corporate Member of Gem-A if their business is the sale, auction, manufacture or appraisal of gems or gem-set jewellery

If you employ a Fellow (FGA) or Diamond member (DGA) of Gem-A you may apply for Gold Corporate Membership, entitling you to display the Gold Corporate Coat of Arms stating that you employ a qualified gemmologist – the ultimate sign of gem excellence.

The annual membership fee for Corporate Members and Gold Corporate Members for 2012 is £160.00.

However, it may cost you nothing extra for 2012 if you already employ and pay the subscriptions for two Fellow, Diamond or Associate Members of Gem-A. This is because the Corporate Membership subscription includes two individual subscriptions.

For further details and to apply, go to www.gem-a.com/membership/corporate-membership.aspx or contact the Membership Department on 020 7404 3334 email membership@gem-a.com

A Gem-A initiative to support your business

**Gem-A Corporate
Membership Logo**



**Gem-A
Gold Corporate
Coat of Arms**



The Gemmological Association of Great Britain

27 Greville Street (Saffron Hill entrance), London EC1N 8TN

tel: 020 7404 3334 fax: 020 7404 8843 email: information@gem-a.com

UK Registered Charity No. 1109555

Chemical and growth zoning in trapiche tourmaline from Zambia — a re-evaluation

Dr Karl Schmetzer, Dr Heinz-Jürgen Bernhardt and Thomas Hainschwang

Abstract: Trapiche tourmalines from Zambia show the hexagonal prism a $\{11\bar{2}0\}$, the positive pyramids r $\{10\bar{1}1\}$ and o $\{02\bar{2}1\}$ and the negative pyramid $-r$ $\{01\bar{1}\bar{1}\}$ as dominant external crystal forms. The trapiche pattern is formed by the positioning of liquid and solid inclusions which are trapped at growth boundaries between pyramidal and prismatic growth sectors. Growth-induced elongate voids are also formed perpendicular to the dominant growth faces, which are inclined at 27° , at 46° or at 90° to the pedion $\{0001\}$ of the tourmaline hosts.

All the trapiche tourmalines are chemically zoned with isomorphic substitutions of Ca by Na and Mg by Al, which is characteristic for tourmalines of the uvite-dravite solid solution series. Content of Na increases and of Ca decreases from core to rim of all tourmalines. However, at the boundaries between different growth sectors (forming the geometric trapiche pattern of the samples), tourmaline compositions with higher Na and lower Ca contents than measured in adjacent pyramidal and prismatic growth sectors were found.

The formation of this complex structural and chemical pattern is consistent with the formation of the tourmaline crystals in a two step process, with the skeletal growth of a sodium-rich dravite in a first step and the subsequent, layer-by-layer growth of a second tourmaline generation. The growth of the second generation started with calcium-rich fluor-uvite and was followed step-by-step by a more sodium-rich dravite. The green coloration of the samples is caused by minor contents of vanadium and chromium.



1. Introduction

Gem materials designated as trapiche are rare in the gemstone and mineral trade, and this is because there is only a limited number of mineral species which show a clear trapiche pattern, i.e. a pattern with a clear separation into distinct growth sectors, best seen in cabochons or polished slices. The boundaries of these

growth sectors are normally sharp and decorated with mineral or fluid inclusions, in this way separating a core from a rim or separating different parts within the rim. From these sector boundaries which are also described as arms of a fixed six-rayed or three-rayed star, growth tubes filled with mineral and/or fluid phases commonly run into the different

Above: Slices of trapiche tourmaline from Zambia cut perpendicular to the c-axis. In the centre of the slice, upper left, the dark arms of the fixed three-rayed star separate three pyramidal growth sectors. The slice, lower right, cut from the same tourmaline, has a rim with six prismatic growth sectors which are separated from each other and from the pyramidal growth sectors of the centre by less transparent boundaries. View parallel to the c-axis, size of the samples about 13×12 mm. Photos by T. Hainschwang.

Chemical and growth zoning in trapiche tourmaline from Zambia — a re-evaluation



Figure 1a: Three slices of trapiche tourmaline from Zambia with hexagonal outline cut from the same crystal perpendicular to the *c*-axis; in the centre, the arms of a fixed three-rayed star separate three pyramidal growth sectors of the tourmaline crystal; the rim consists of six prismatic growth sectors which are separated from each other and from the pyramidal growth sectors of the centre by less transparent boundaries; the sizes of cores and rims vary according to the position of the slices along the *c*-axis of the tourmaline crystal. Views parallel to the *c*-axis, the samples measure about 32 mm in diameter.

Figure 1b: Three slices of trapiche tourmaline from Zambia with trigonal outline cut from the same crystal perpendicular to the *c*-axis; in the centre, the arms of a fixed three-rayed star separate three pyramidal growth sectors of the tourmaline crystal; the rim consists of nine (three plus six) prismatic growth sectors which are separated from each other and from the pyramidal growth sectors of the centre by less transparent boundaries; the sizes of cores and rims vary according to the position of the slices along the *c*-axis of the tourmaline crystal. Views parallel to the *c*-axis, size of the samples about 7 × 8 mm.

Figure 1c: Two slices of trapiche tourmaline from Zambia with hexagonal outline cut perpendicular to the *c*-axis; in the centre, the boundaries distinguish six (three plus three) different pyramidal growth sectors; at the rim there are six prismatic growth sectors which are distinguished from each other and from the pyramidal growth sectors of the centre by more included borders or boundaries. Views parallel to the *c*-axis, size of the samples about 9 × 10 mm. All photos by T. Hainschwang: a and b in reflected light; c in transmitted light.

transparent growth sectors between these arms. The gem minerals showing a distinct trapiche pattern most commonly seen are emeralds from Colombia and rubies from Mong Hsu, Myanmar (Nassau and Jackson, 1970a,b; Schmetzer *et al.*, 1996). Different models have been described to explain the growth mechanism of the trapiche pattern (see, e.g., Nassau and Jackson, 1970 a,b; Sunagawa *et al.*, 1999). Recently, another trapiche mineral was added to this list, trapiche tourmaline from Zambia (Hainschwang *et al.*, 2007).

According to Hainschwang *et al.* (2007), the Zambian trapiche tourmalines originate from the Kavungu mine near

the small village of Jivunda, southwest of Mwinilunga in the northwestern part of the country near the border with Angola. Tourmaline crystals show the hexagonal prism a {11 $\bar{2}$ 0} as well as the positive rhombohedron r {10 $\bar{1}$ 1} and the negative rhombohedron $-r$ {10 $\bar{1}\bar{1}$ } as external crystal forms.

Slices of trapiche tourmalines cut perpendicular to the *c*-axis can show two different patterns (see photograph on page 151):

(a) a three-rayed star with three transparent tourmaline sectors between the three arms of the fixed star and, in most crystals,

(b) the pattern described above in the centre of the slice, surrounded by six transparent sectors of tourmaline, with six boundaries between the centre and the rim and six boundaries between the six sectors of the rim.

The crystals may also contain two types of channels, running “nearly parallel to the *c*-axis” and “close to perpendicular to the *c*-axis”.

After the description of trapiche tourmaline from Zambia was published, one author (KS) examined some crystals reportedly from the same occurrence which showed additional crystal faces not mentioned in the Hainschwang *et*

Chemical and growth zoning in trapiche tourmaline from Zambia — a re-evaluation

al. (2007) paper and which indicated that additional or different patterns not yet described could also be present. Furthermore, one author (TH) obtained additional samples from his suppliers, mostly in the form of polished slices cut perpendicular to the *c*-axis, which also revealed a somewhat different trapiche pattern. These specimens warranted a more detailed description.

The first 15 tourmaline crystals available to the authors were mostly broken along the columnar outline formed by various prism faces and were not complete doubly terminated crystals. Most slices had been cut perpendicular to the *c*-axis, but a series of slices cut from one crystal along the *c*-axis was also available. To obtain additional information, the authors purchased seven unbroken tourmalines from the stock of a mineral and gemstone dealer who had also a large number of cut and polished slices of trapiche tourmaline from Zambia. These crystals were used for the determination of the polarity of the tourmalines. This is described in terms of the antilogous (+) and the analogous poles (-) of the crystals, and some were sliced parallel to the *c*-axis to relate polarity to internal structures. Finally, the authors received a large parcel of tourmaline crystals and fragments from the same supplier as a donation for research purposes.

2. Determination of the external morphology

The numerous tourmaline slices cut perpendicular to the *c*-axis were subdivided into three basic types, designated A, B and C in the following description (Table I, Figure 1):

The main differences between the types are colour, outline, and number of growth sectors in core and rim. Also the numerous channel inclusions in the transparent tourmaline sectors show different orientations. In the rims of all samples, the channels run more or less perpendicular to the *c*-axis, but in all growth sectors of the core they are at various inclinations to it. Various slices parallel or perpendicular to the *c*-axis,

Table I: Main types of trapiche tourmalines from Zambia

	Type A (Figure 1a)	Type B (Figure 1b)	Type C (Figure 1c)
Colour	green, occasionally zoned	green	colourless
Outline of prism zone	hexagonal	trigonal	hexagonal
Clear transparent sectors in the core	3, with more or less broad, less transparent boundaries	3, with more or less broad, less transparent boundaries	6 (3 + 3), with more or less broad, less transparent boundaries
Clear transparent sectors in the rim	6, with more or less broad, less transparent boundaries	9 (3 + 6), with more or less broad, less transparent boundaries	6, with more or less broad, less transparent boundaries

which still show external prismatic or pyramidal crystal faces, indicate that all channels in the transparent growth sectors are perpendicular to these external prismatic or pyramidal crystal faces.

Although no direct internal growth planes were visible in our samples, using this information in combination with goniometric measurements of external crystal faces of several rough tourmalines, we were able to determine the morphology and orientation of type A samples, which represented more than 90% of the tourmalines available. The tourmaline samples of types B and C contained no complete crystals with both poles; most pieces were broken or sliced perpendicular to the *c*-axis and showed only the external prism faces with no pyramids. In those samples containing at

least one pole (end) of a rough crystal, the faces were not of suitable quality for goniometric measurement. Therefore, only an indirect reconstruction of crystal morphology on the basis of channel orientation was possible for types B and C.

2.1 External morphology of samples of type A

Most type A crystals show the hexagonal prism **a** as the dominant crystal form, sometimes in combination with a small trigonal prism **m** (see Table II). The few crystals which show trigonal prism faces **m** which are larger than the hexagonal prism faces **a** are classified as samples of type B. From goniometric measurements, the faces at the ends of the crystals were identified as the trigonal pyramids **r** or **o**, with some crystals having

Table II: Morphology and growth patterns of trapiche tourmalines from Zambia

	Crystal form	Designation (number of faces)	Miller indices	Inclination to the pedion <i>c</i> (°)
Antilogous pole (+)	trigonal pyramid	r (3)	{10 $\bar{1}$ 1}	27.35
		y (3)	{40 $\bar{4}$ 1}	64.21
		o (3)	{02 $\bar{2}$ 1}	45.97
Prism zone	hexagonal prism	a (6)	{11 $\bar{2}$ 0}	90
	trigonal prism	m (3)	{01 $\bar{1}$ 0}	90
Analogous pole (-)	trigonal pyramid	-r (3)	{01 $\bar{1}$ 1}	27.35
	pedion	-c (1)	{000 $\bar{1}$ }	0
Both poles	edge between two trigonal pyramids r and r' or -r and -r''	-	-	14.50

Chemical and growth zoning in trapiche tourmaline from Zambia — a re-evaluation

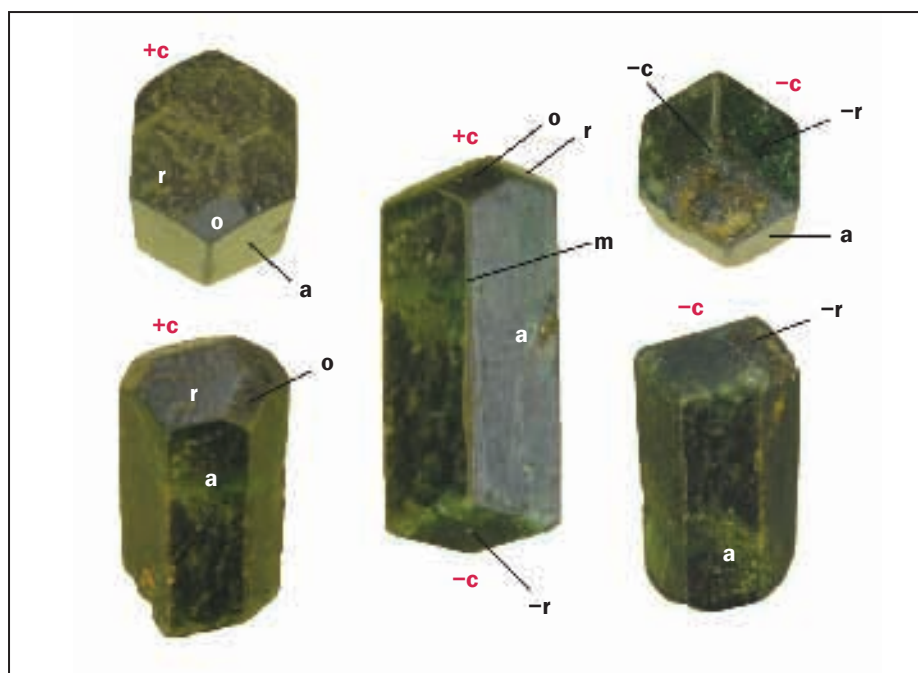


Figure 2: Trapiche tourmaline from Zambia: one crystal in different orientations. Centre: view perpendicular to the c-axis; left: view of the antilogous pole (+); right: view of the analogous pole (-); the pedion sign in red +c, -c indicates the polarity of the crystal. The prism zone is formed by the dominant hexagonal prism a and by subordinate trigonal prisms m, the antilogous pole consists of the trigonal pyramids r and o, the analogous pole consists of the trigonal pyramid -r and the pedion -c. Size of the crystal approx. 7.5 × 15.5 mm. Photos by K. Schmetzer.

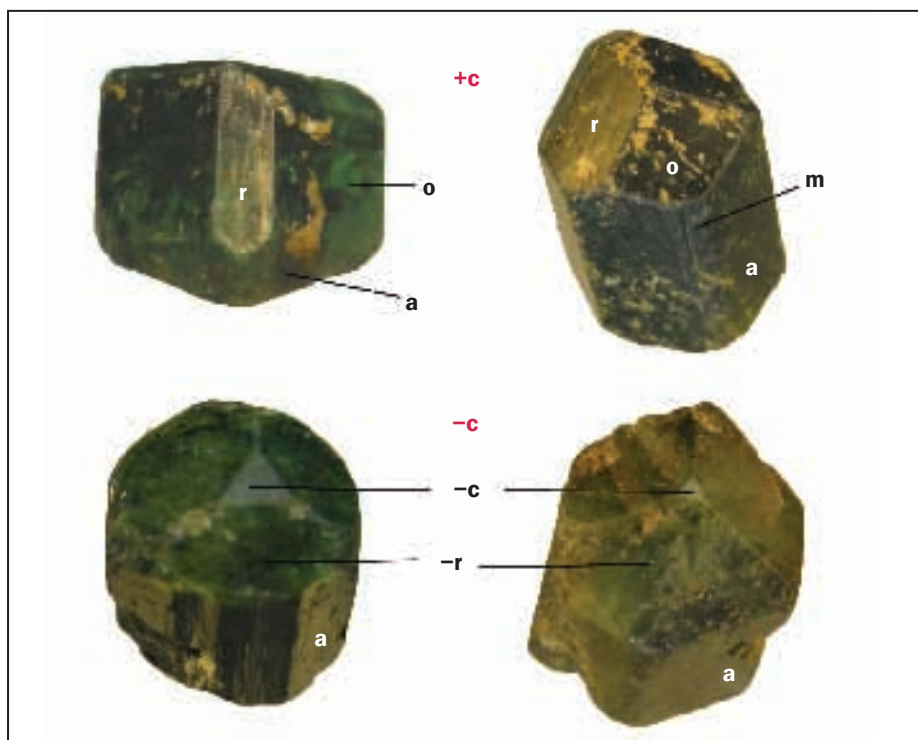


Figure 3: Trapiche tourmalines from Zambia in different orientations; top line: view of the antilogous pole of two crystals; bottom line: view of the analogous pole of two crystals. The pedion sign in red +c, -c indicates the polarity of the crystal. The prism zone is formed by the dominant hexagonal prism a and by subordinate trigonal prisms m, the antilogous pole consists of the trigonal pyramids r and o, the analogous pole consists of the trigonal pyramid -r and the pedion -c. Diameter of the crystals: top left 8 mm, top right 10.5 mm, bottom left 9.5 mm, bottom right 12 mm. Photos by K. Schmetzer.

combinations of r and o, or combinations of the trigonal pyramid r and the pedion c (Figures 2 and 3).

For the experimental determination of the antilogous and the analogous poles (ends) of the polar tourmaline crystals, the method of Kundt (1883) which is based on pyroelectricity (see also Takahashi and Sunagawa, 1998) was applied. Upon heating the antilogous end (+c) of the tourmaline crystal is negatively charged and the analogous end (-c) is positively charged (Dietrich, 1985). Kundt describes that, when a mixture of fine powdered sulphur and red lead oxide (Pb₃O₄, minium) is blown through a fine sieve on a crystal charged at an elevated temperature, the lead oxide is attracted by the negatively charged end of a crystal and the sulphur is attracted by the positively charged end of a crystal.

When the Zambian tourmalines were heated at a temperature below 120° C, i.e. below the melting point of sulphur, the effect seen was very small. After heating the tourmalines above 300 or 400°C, a mixture of sulphur and lead oxide blown onto the heated crystals showed a clear attraction of the lead oxide by the antilogous end and a repulsion of red lead oxide particles by the analogous end of the tourmalines. Consequently, after determination of the polarity of the Zambian tourmaline crystals we can summarize the morphology of type A tourmalines as follows (Figure 4 A,B,C):

In many tourmaline crystals, the antilogous end consists of three or six faces, i.e. of three r pyramids or of three o pyramids, but a combination of both faces, i.e. a combination of three r and three o pyramids, is also quite common. The analogous pole shows only three -r pyramids, often in combination with the pedion -c.

2.2 External morphology of tourmalines of types B and C

None of the tourmalines classified as B and C were complete crystals. Since only a clear outline of the external morphology of the prism zone can be obtained from slices perpendicular to the c-axis, this was combined with the

Chemical and growth zoning in trapiche tourmaline from Zambia — a re-evaluation

information available from the orientation of elongate voids in transparent internal growth sectors (see *Table II*).

Samples of type B (*Figure 4 D*) show trigonal habits with larger trigonal prism faces *m* and smaller hexagonal prisms *a*. The orientation of growth tubes indicates that the trigonal pyramid *r* is the dominant crystal form.

Samples of type C (*Figure 4 E*) show a hexagonal outline of the prism zone with larger hexagonal prism faces *a* and only subordinate trigonal prism faces *m*. Within the clear central growth sectors, two main orientations of needle-like growth tubes are visible and these indicate that two different trigonal pyramids, namely *o* and *y*, are present.

2.3 Single slices and series of slices of trapiche tourmalines from Zambia

For the European market, transparent tourmaline crystals or transparent parts within tourmaline crystals are normally sliced perpendicular to the *c*-axis and sold as individual slices or as complete series of tourmaline plates. Some crystals are cut as cabochons also in that particular orientation. Slices parallel to the *c*-axis were not available commercially.

Type A: In this study numerous single slices perpendicular to the *c*-axis and three complete series of slices consisting of seven, eight or nine individual tourmaline plates cut from almost completely transparent crystals or crystal fragments along the *c*-axis were examined.

From another six crystals, purchased from the trade, with at least partly transparent or translucent areas, individual slices perpendicular to the *c*-axis were prepared. Some non-transparent parts of crystals were not sliced.

Types B and C: From these categories, only slices perpendicular to the *c*-axis or fragments of prismatic crystals were available. It was possible to study small series of two or three slices cut along *c* from a few single crystals, but no slice parallel to *c* with a complete internal morphology could be obtained.

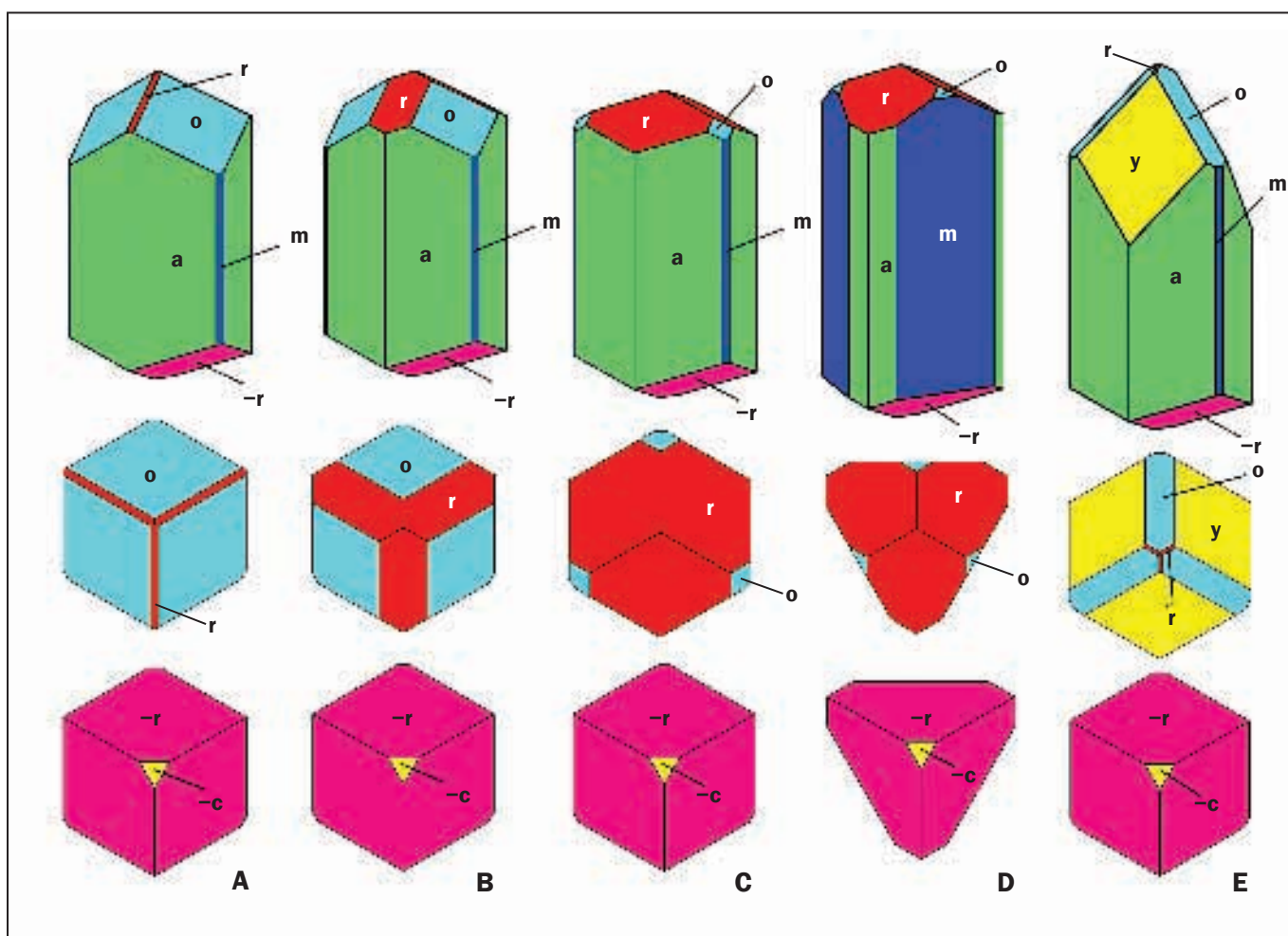


Figure 4: Morphology of trapiche tourmalines from Zambia; the prism zone is formed by the dominant hexagonal prism a and by subordinate trigonal prisms m (examples A,B,C,E); in example D, the prism zone is formed by three dominant trigonal prism faces m and subordinate hexagonal prisms a; the antilogous pole consists of the trigonal pyramids r, o and y, the analogous pole consists of the trigonal pyramid -r and the pedion -c. Top line: view perpendicular to the c-axis (clinographic projections), middle line: view parallel to the +c axis (parallel projections), bottom line: view parallel to the -c axis (parallel projections). Crystal drawings and artwork by K. Schmetzer.

Chemical and growth zoning in trapiche tourmaline from Zambia — a re-evaluation

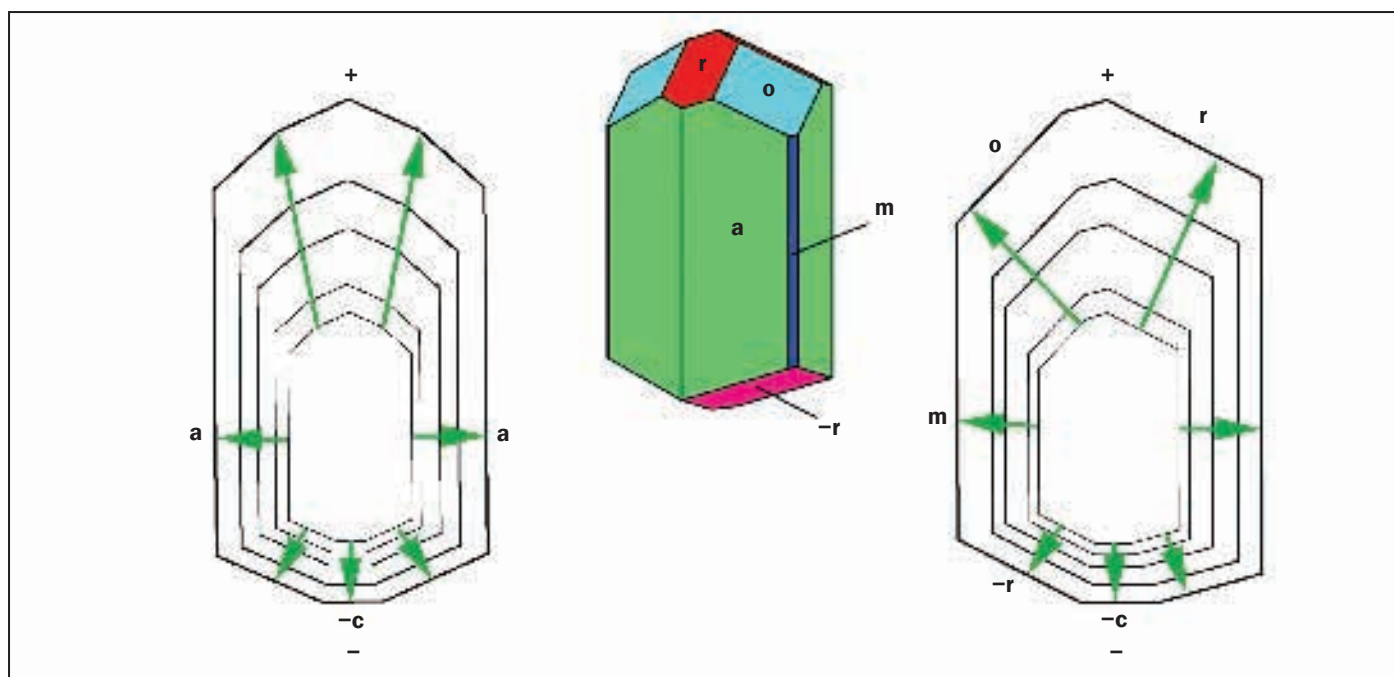


Figure 5: Schematic sections through a tourmaline crystal (top middle, clinographic projection) with orientation of the sections perpendicular to the prism **a** (left) and perpendicular to the prism **m** (right), only crystal faces are labelled but not crystal edges; the directions of crystal growth are indicated by green arrows; a preferential crystal growth at the antilogous pole compared to the analogous pole is indicated. Crystal drawings and artwork by K. Schmetzer.

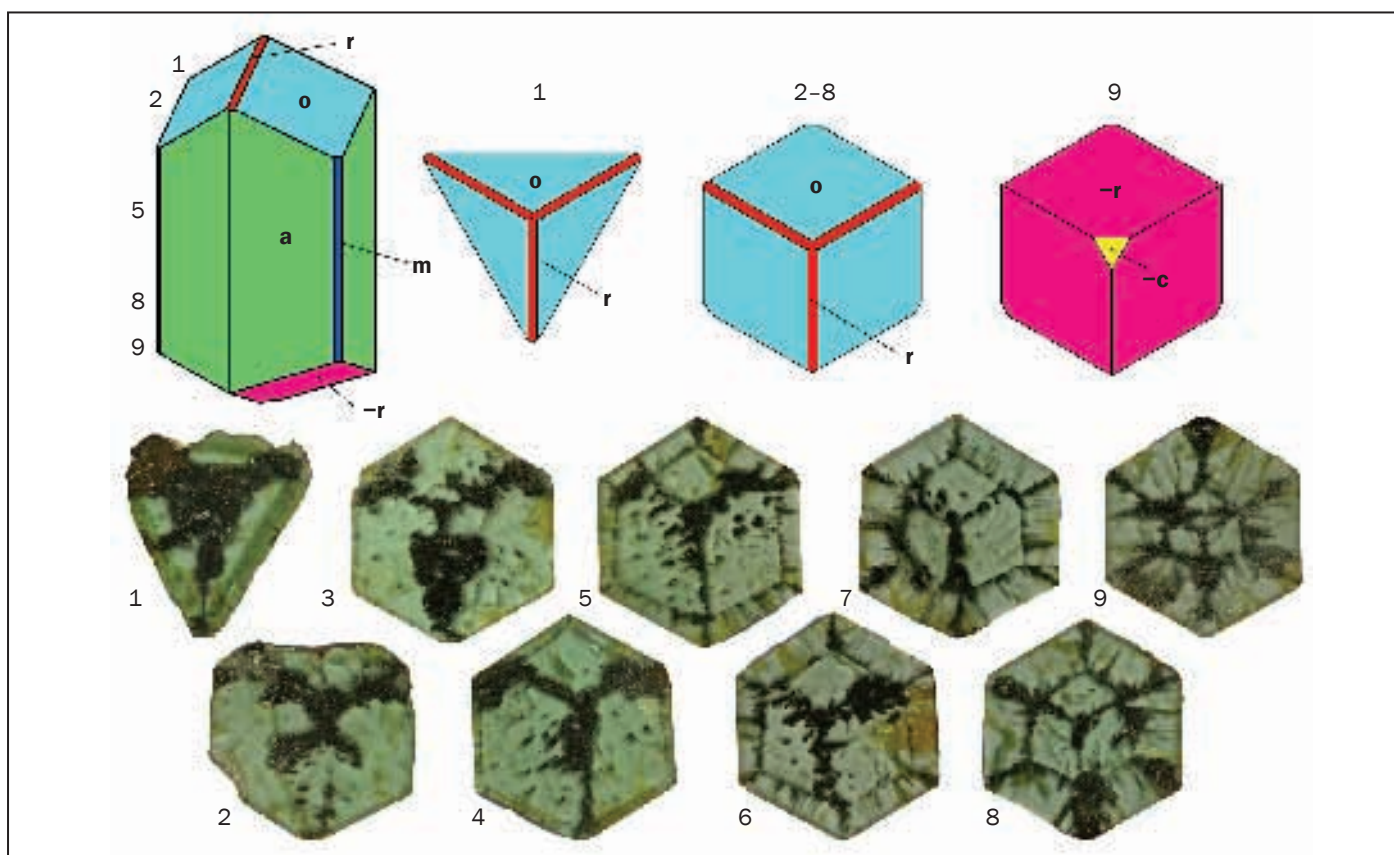


Figure 6: Series of slices of a trapiche tourmaline crystal from Zambia cut perpendicular to the *c*-axis (middle and lower line); the sequence of slices (Nos. 1 to 9) runs from the antilogous pole towards the analogous pole. Slice 1 represents a section through three trigonal pyramids **o**, slices 2 to 8 represent sections through three trigonal pyramids **o** and six prism faces **a**; slice 9 represents a section through three pyramids **-r** and six prism faces **a**; the approximate position of the slices within the complete crystal is given in the upper left diagram; the trigonal and hexagonal outline of the sections is also given in the upper line (middle and right). Diameter of slices 2 to 9 approx. 8 mm. Photos by T. Hainschwang, crystal drawings and artwork by K. Schmetzer.

Chemical and growth zoning in trapiche tourmaline from Zambia — a re-evaluation

3. The trapiche pattern: geometrical description

Tourmaline crystals from certain occurrences, especially samples from Madagascar, show a distinct growth and colour zoning with sharp boundaries (see, e.g., Benesch, 1990; Wöhrmann, 2002; Zang *et al.*, 2002; Rustemeyer, 2003; Lussier and Hawthorne, 2011). In cross sections parallel and perpendicular to the *c*-axis, growth and colour zoning parallel to the pedion as well as parallel to different prism and pyramidal faces is directly visible.

In contrast, the trapiche pattern in crystals from Zambia consists of different growth sectors, which are separated by more or less sharp boundaries. These boundaries, in general, are narrow areas within the tourmaline crystals with high concentrations of mineral and fluid inclusions, and where the elongated voids or channels were initiated to extend into the surrounding tourmaline sectors. These channels are always perpendicular to the growing crystal face of the relevant growth sector, i.e. perpendicular to the dominant hexagonal prism *a* or to one of the different trigonal pyramids *r*, *o*, *y* and $-r$.

Although individual growth layers with sharp boundaries are not visible, measurement of the inclination of the elongated voids allows the determination and identification of the growth plane and surrounding sector, i.e. the 'host' sector of the channel. The different positions of trapiche sector boundaries in successive slices of a crystal along the *c*-axis or the changes within trapiche sector boundaries allow an insight into the growth history of a crystal.

3.1 Samples of type A

From observations of slices parallel to the *c*-axis it is apparent that there was more crystal growth from the centre to the antilogous pole than from the centre to the analogous pole. In approximate terms, the length from the origin (centre) of crystal growth to the analogous end of the crystal is in the range of 5 to 15% of the total length of the crystal (Figure 5). Furthermore, where the parts of the crystal

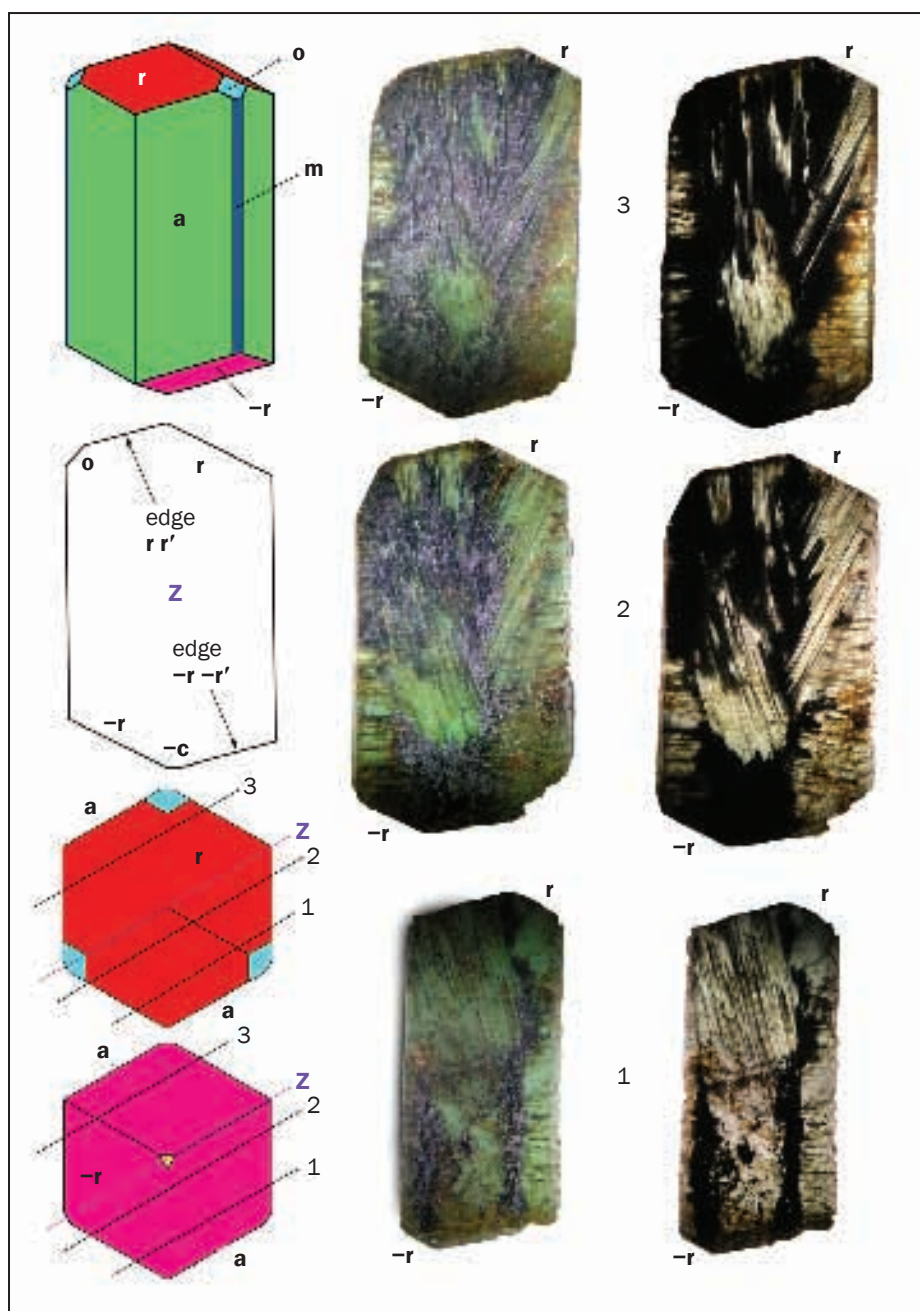


Figure 7: Series of slices of a trapiche tourmaline crystal from Zambia cut parallel to the *c*-axis (middle line in reflected light, right line in transmitted light); a schematic drawing of the original crystal (clinographic projection) is on the upper left; a schematic section through the centre (*Z*) of the tourmaline crystal is on the centre left; in views parallel to the $+c$ axis and the $-c$ axis (lower left), the approximate positions of the three sections are indicated. Size of the tourmaline slices: top 14 × 25 mm, middle 14 × 25 mm, bottom 11 × 25 mm. Photos by T. Hainschwang and K. Schmetzer, crystal drawings and artwork by K. Schmetzer.

between the centre and the analogous end are not transparent, those in the gem and mineral trade start a series of slices along the *c*-axis at or slightly above the crystal centre and run in a sequence towards its antilogous end. Several non-transparent ends of crystals, which were left over (i.e. which were not sliced) show the pedion $-c$ and the trigonal pyramid $-r$.

One series of nine slices examined (Figure 6) consists of one slice with three central growth sectors with channels inclined at about 27° to the *c*-axis (slice 9, representing a core with the trigonal pyramid $-r$), and eight successive slices with three central growth sectors with elongated voids inclined at about 45° to the *c*-axis (slices 1 to 8, representing a

Chemical and growth zoning in trapiche tourmaline from Zambia — a re-evaluation

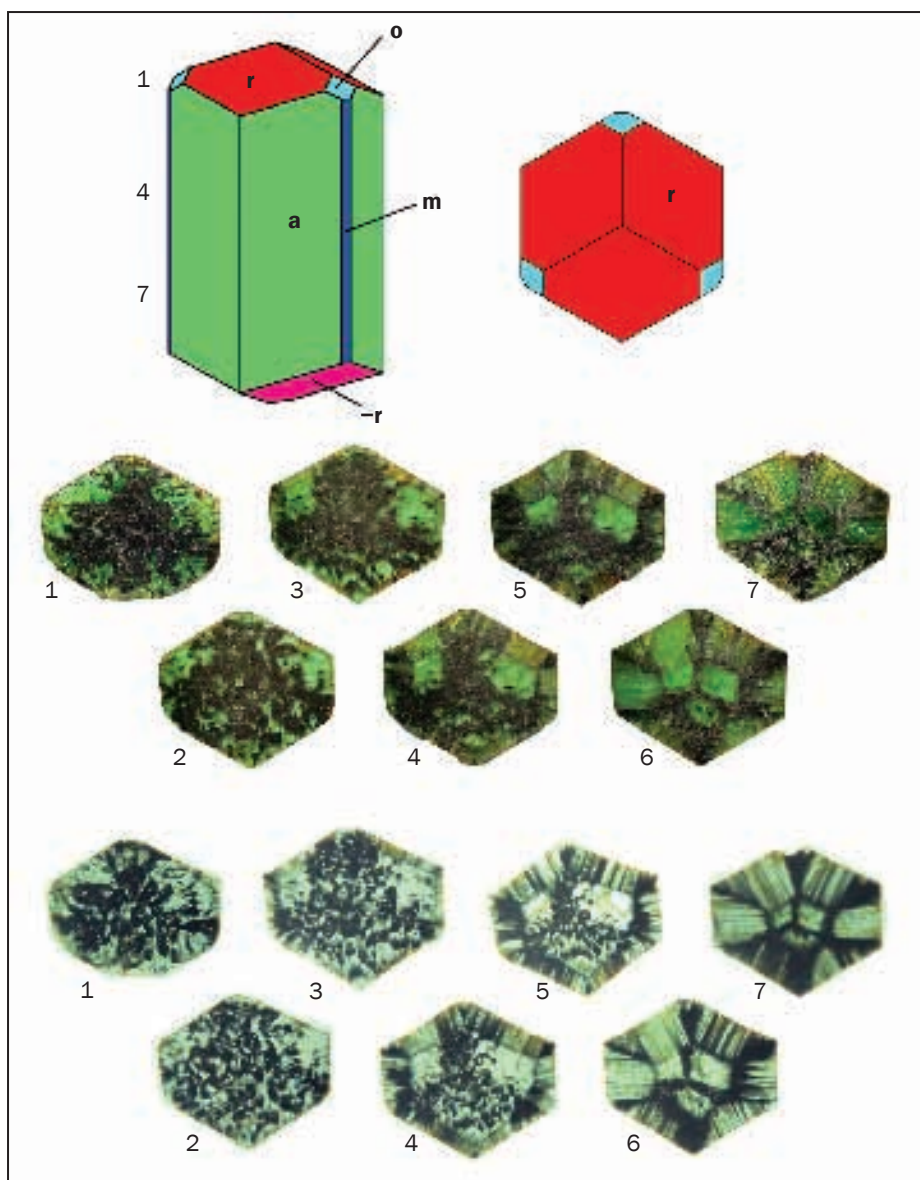


Figure 8: Series of slices of a trapiche tourmaline crystal from Zambia cut perpendicular to the c -axis (middle lines in reflected light, lower lines in transmitted light); as indicated in the diagram upper left, the sequence of slices (Nos 1 to 7) runs from the antilogous pole towards the analogous pole. Slices 1 to 7 represent sections through three trigonal pyramids r and six prism faces a . Size of the slices 16 × 18 mm. Photos by T. Hainschwang and K. Schmetzer, crystal drawings and artwork by K. Schmetzer.

core with the trigonal pyramid o). Slices 3 to 9, in addition, showed rims consisting of six growth sectors each, representing the hexagonal prism a . The two remaining slices in the series (slices 1 and 2) showed no rim related to prism zones.

Several slices of type A crystals parallel to the c -axis show external faces parallel to the prism a as well as parallel to the trigonal pyramids r (at the antilogous pole) and $-r$ (at the analogous pole). From one larger crystal (Figure 7) three slices show the edges between adjacent r or between adjacent

$-r$ pyramids, with an inclination of about 14.5° to the pedion c (Table II, Figure 7).

In Figure 7, it is apparent that these slices contain larger non-transparent areas of tourmaline with abundant trapped solid or liquid inclusions. Most of these channels are confined to margins between different growth sectors, and end irregularly within an adjacent transparent growth sector.

Two series of seven or eight tourmaline slices cut perpendicular to the c -axis are variably transparent (Figure 8). Both series started on the antilogous side

of the centre of crystal growth, so the analogous pole is not represented. In the slices closest to the crystal centres, the core of the crystals consists of three growth sectors with channels inclined at 27° to the c -axis, representing growth sectors related to the trigonal pyramid r . These are surrounded by six growth sectors with channels inclined at 90° to the c -axis, representing growth sectors related to the hexagonal prism a (slice 7 in Figure 8).

In both series of slices, the non-transparent margins between the three central r growth sectors become successively broader with distance from the centre of the crystal (slices 1 to 6 in Figure 8). Within these margins, numerous mineral and fluid inclusions were trapped, mostly in elongate voids. These channels are inclined at about 27° to the c -axis, which indicates that these areas represent growth sectors confined to the trigonal pyramid r . Within the two series of slices, the hexagonal prism growth zones gradually become smaller and are not present in the last tourmaline plates (slices 1 and 2) which show only larger, mostly non-transparent r growth sectors.

Slices 2 and 7 of the crystal depicted in Figure 8 were used for microprobe analyses (see also Figures 18 and 19).

3.2 Samples of type B and C

Each individual part of a type B crystal or single slice shows three central growth sectors with channels inclined at about 27° to the c -axis (representing the trigonal pyramids r or $-r$), and three larger growth sectors at the rim (representing the trigonal prism m). In some samples, smaller growth sectors related to the prism a are also present in the rim. Slices cut from a single crystal are shown in Figure 1b (see also Figure 4 D).

Type C tourmalines are mostly colourless and contain a core consisting of six transparent tourmaline growth sectors within a rim of six growth sectors related to the hexagonal prism a . The elongated voids within the six sectors of the central core show two different inclinations to c , which indicate that the faces within these zones are the trigonal pyramids

Chemical and growth zoning in trapiche tourmaline from Zambia — a re-evaluation

o and **y** (Figure 1c and see Figure 4 E). These observations indicate crystals with hexagonal habit but with somewhat steeper pyramidal faces **y** (Table II).

4. Thin sections of type A crystals parallel to the *c*-axis

In contrast to the slices parallel to *c* with thicknesses in the mm range several sections 60 μ m thick were prepared and two examples are shown in Figures 9 and 10. Each section was cut parallel to

one of the larger hexagonal prism faces **a**. One section shows a habit consisting predominantly of the hexagonal prism **a** in combination with **r** and $-\mathbf{r}$ pyramids (Figure 9) and the other shows additional **o** growth sectors increasing in size during crystal growth (Figure 10). With crossed polarizers, the orientation of numerous elongate voids is clearly visible and most channels are orientated perpendicular to the external crystal faces. Some channels however are inclined or even perpendicular to the plane of the section.

The sections parallel to the *c*-axis show external faces parallel to the prism **a**, the trigonal pyramids **r** and **o** (at the antilogous pole) and $-\mathbf{r}$ (at the analogous pole). The outlines of idealized sections through the three crystals are also given in Figures 9 and 10 and contain the edges between adjacent **r** or between adjacent $-\mathbf{r}$ pyramids, with an inclination of about 14.5° to the pedion **c** (see Table II). The individual growth zones within these sections were assigned to growth sectors related to the hexagonal prism **a** and

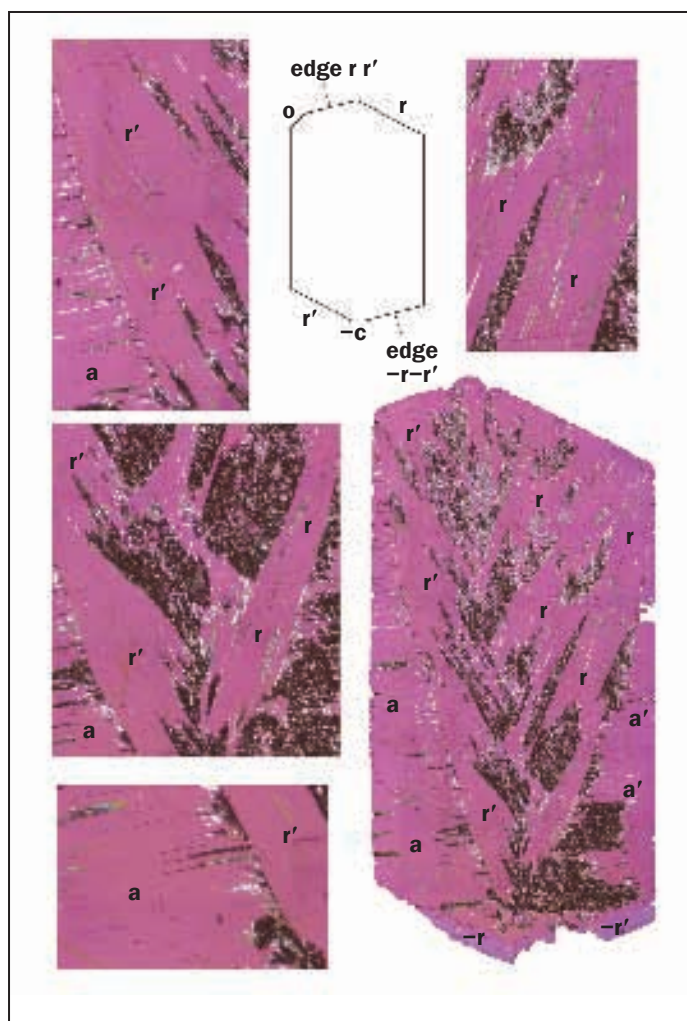


Figure 9: Section through a trapiche tourmaline crystal cut parallel to the *c*-axis; the complete crystal is in the lower right, a schematic section is in the upper line (middle), and enlarged views of different parts of the crystal are given in other photographs. Growth sectors belonging to the trigonal pyramids **r** and $-\mathbf{r}$ and the hexagonal prism **a** are indicated; the growth sectors are distinguished by margins with abundant solid and liquid inclusions; and within the transparent areas of various growth sectors, channels filled with liquid or solid matter and irregularly shaped areas with a high concentration of inclusions are visible. The prime symbol denotes another face in the same zone, so that **r**, **r'** and **r''** are the three pyramid faces of the **r** zone. Size of the crystal approx. 10 × 20 mm; thickness of the section approx. 60 μ m; crossed polarizers. Photos by H.-J. Bernhardt.

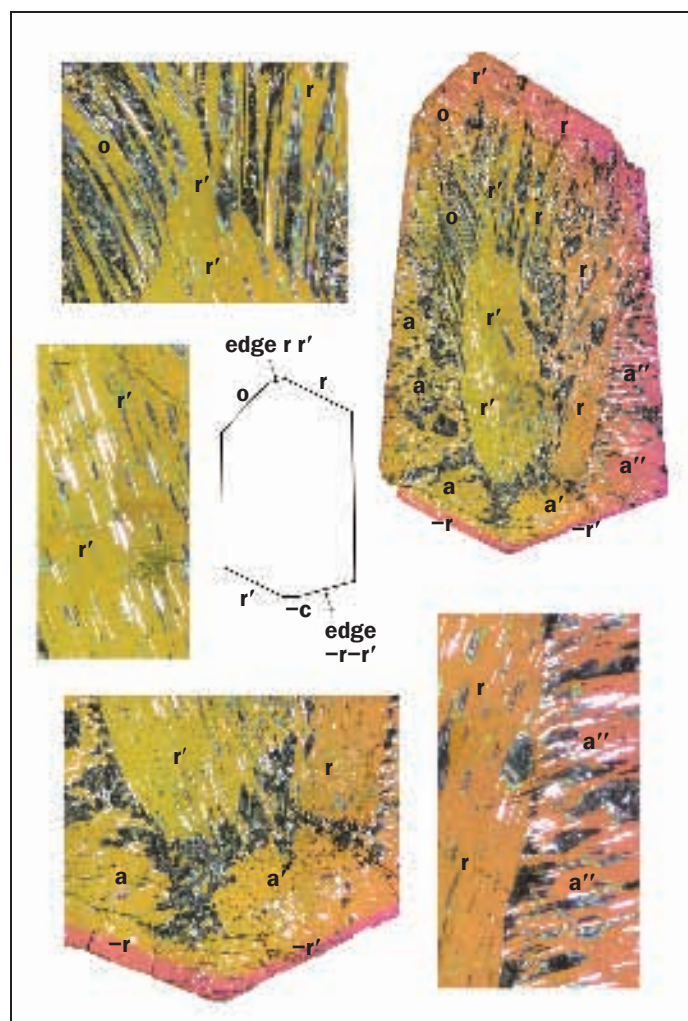


Figure 10: Section through a trapiche tourmaline crystal cut parallel to the *c*-axis; the complete crystal is in the upper right, a schematic section is in the centre and enlarged views of different parts of the crystal are given in other photographs. Growth sectors belonging to the trigonal pyramids **r**, **o** and $-\mathbf{r}$ and the hexagonal prism **a** are indicated; the growth sectors are distinguished by margins with high concentrations of solid and liquid inclusions; within the transparent areas of various growth sectors, channels filled with liquid or solid matter, and irregularly shaped areas with a high concentration of inclusions are visible. Size of the crystal approx. 10 × 16 mm; thickness of the section approx. 60 μ m; crossed polarizers. Photos by H.-J. Bernhardt.

Chemical and growth zoning in trapiche tourmaline from Zambia — a re-evaluation

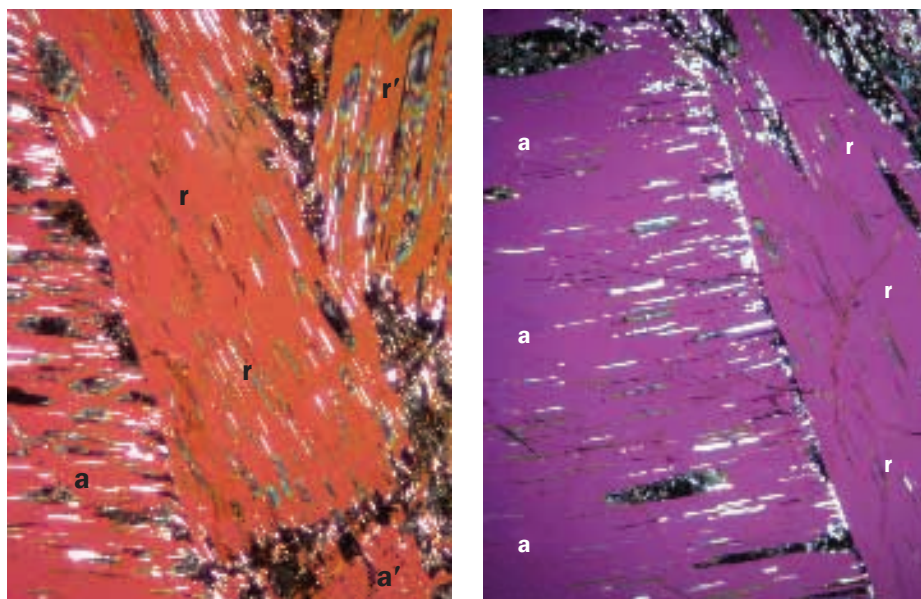


Figure 11: (a) In a section about 60 μm thick cut parallel to the c -axis, the pyramidal and prismatic growth sectors are separated by margins with abundant solid and liquid inclusions; (b) within the transparent areas of various growth sectors, channels filled with liquid or solid matter and irregularly shaped areas with a high concentration of inclusions are visible. Crossed polarizers, field of view (a) 2.04 \times 2.72 mm and (b) 3.04 \times 4.05 mm. Photos by H.-J. Bernhardt.

to different trigonal pyramids r and $-r$. Towards the antilogous end of the crystal pictured in Figure 10, there is also a small growth sector with an orientation of channels inclined at about 45° to the c -axis, corresponding with the trigonal pyramid o .

In detail, the thin section shown in Figure 9 represents a cut more or less through the centre of the crystal and shows two growth sectors related to the hexagonal prism (a and a') and two growth sectors related to the a trigonal pyramid (r and r'). The growth sectors of the trigonal pyramid ($-r$ and $-r'$) at the analogous pole are distinctly smaller than those towards the antilogous pole. This may indicate more preferential growth towards the antilogous end of the crystal (see Figure 5).

The other example (Figure 10) shows three prismatic growth sectors (a , a' and a'') which indicates that the cut represents a section not exactly through the centre of the crystal. The cut is not exactly parallel to the c -axis but inclined to it at about 10° , so the two edges running north-south are not exactly parallel. The section shows larger trigonal r and smaller $-r$ growth sectors. During growth of the crystal there

was a change of habit with development of growth sectors related to the trigonal pyramid o .

5. Fine structure and determination of inclusions

The trapiche pattern is formed by inclusions which are concentrated at the margins of adjacent growth sectors related to different crystal faces. Irregularly shaped areas with inclusions and individual elongate voids commonly originate at these sector boundaries and extend into more transparent tourmaline areas (Figure 11). The growth sectors of different crystal faces, such as r and o pyramids may contain different concentrations of inclusions, and there are also some bent channels (Figure 12) that follow closely the growth planes.

The inclusions were examined using optical microscopy and electron microprobe, and the main ones (i.e. non-tourmaline, see below) are graphite, calcite and dolomite, and irregularly shaped cavities or needle-like cavities filled with fluids of one or two phases (Figure 12a,b). A coating on the surface of some channels (Figure 12c), is most probably secondary iron oxide or iron

hydroxide on the basis of electron microprobe analyses. In some irregular fractures there is also some secondary fracture filling and staining by iron oxides and hydroxides.

6. Chemical composition

To evaluate chemical composition, zoning and colour variation, 10 sections of Zambian tourmaline were analysed using the electron microprobe. Four type A sections were parallel to the c -axis, five type A sections and one type B section were cut perpendicular to the c -axis. Two of the five sections of type A cut perpendicular to c represented different parts of one tourmaline crystal (sections of slices 2 and 7 of Figure 8). Thus, the chemical analyses presented have been obtained from 10 sections of nine tourmaline crystals.

Since the pattern of chemical zoning was found to be quite fine, the number of analysis points in different automatic scans was set at a range of 50 – 150 per scan. In total, 2922 point analyses were obtained, of which 326 analyses were deleted, because the chemical composition obtained did not represent tourmaline analyses of acceptable quality, being affected by inclusions or cavities. Consequently, the discussion of chemical composition in this paper is based on 2596 point analyses.

6.1 Range of chemical composition

The traverses across all 10 sections show a distinct variation of chemical composition within the dravite-uvite solid solution series. In general, the sections prepared parallel to the c -axis show a somewhat larger compositional range than the sections cut perpendicular to c . This is because the latter represent only part of the growth history, while the sections parallel to c and along the cores of euhedral crystals represent much more complete growth histories.

Tourmalines are borosilicates with a complex chemical composition and general formula:

$$\text{XY}_3\text{Z}_6(\text{T}_6\text{O}_{18})(\text{BO}_3)_3\text{V}_3\text{W}$$

(Schmetzer *et al.*, 2007; Novák *et al.*, 2009; Henry *et al.*, 2011)

Chemical and growth zoning in trapiche tourmaline from Zambia — a re-evaluation

For the two main magnesium-rich members of the tourmaline group, dravite and fluor-uvite, the following formulae are given:

Dravite: $\text{NaMg}_3\text{Al}_6(\text{Si}_6\text{O}_{18})(\text{BO}_3)_3(\text{OH})_3\text{OH}$

Fluor-uvite:

$\text{CaMg}_3(\text{Al}_5\text{Mg})(\text{Si}_6\text{O}_{18})(\text{BO}_3)_3(\text{OH})_3\text{F}$

Coupled isomorphous substitutions between dravite and fluor-uvite are established according to the formulae $\text{Na} + \text{Al} \leftrightarrow \text{Ca} + \text{Mg}$ and $\text{OH} \leftrightarrow \text{F}$

Average compositions of the tourmalines are given in *Table III*. In *Figure 13 a,b*, the atomic proportions of Na, Ca, Al and Mg obtained from the analyses of our four sections cut parallel to the *c*-axis and sample G (a total of 2101 analyses) are plotted. Isomorphous substitutions of Na and Ca, and of Al and Mg are evident. For calcium-rich (sodium-poor) tourmaline, the X sites are almost completely occupied by Ca and Na, with site vacancies mostly below 0.04 atoms per formula unit (apfu). For sodium-rich tourmalines, the number of vacancies in the X site increases to 0.15 apfu (*Figure 13c*) due to complex isomorphous substitution.

Sample A is the richest in fluorine (*Figure 13d*), and the substitution of fluorine and OH on the W position in the tourmaline structure is shown in *Figure 13e*. In general, Na-poor (Ca-rich) areas of the tourmalines show higher fluorine contents than areas with higher sodium contents.

The following formulae were calculated representing the compositional range of the nine tourmalines analysed:

A. for eight tourmalines with lower fluorine contents

dravite-rich $(\text{Na}_{0.81}\text{Ca}_{0.08})(\text{Mg}_{2.79}\text{Al}_{0.21})\text{Al}_6(\text{Si}_6\text{O}_{18})(\text{BO}_3)_3(\text{OH})_3(\text{F}_{0.2}\text{OH}_{0.62}\text{O}_{0.18})$
 uvite-rich $(\text{Na}_{0.20}\text{Ca}_{0.80})\text{Mg}_3(\text{Al}_{5.40}\text{Mg}_{0.60})(\text{Si}_6\text{O}_{18})(\text{BO}_3)_3(\text{OH}_{2.95}\text{O}_{0.05})(\text{F}_{0.85}\text{O}_{0.15})$

B. for one tourmaline with higher fluorine content

dravite-rich $(\text{Na}_{0.80}\text{Ca}_{0.06})(\text{Mg}_{2.75}\text{Al}_{0.25})\text{Al}_6(\text{Si}_6\text{O}_{18})(\text{BO}_3)_3(\text{OH})_3(\text{F}_{0.61}\text{OH}_{0.22}\text{O}_{0.17})$
 uvite-rich $(\text{Na}_{0.14}\text{Ca}_{0.86})\text{Mg}_3(\text{Al}_{5.30}\text{Mg}_{0.70})(\text{Si}_6\text{O}_{18})(\text{BO}_3)_3(\text{OH}_{2.77}\text{O}_{0.16}\text{F}_{0.07})(\text{F}_{1.00})$

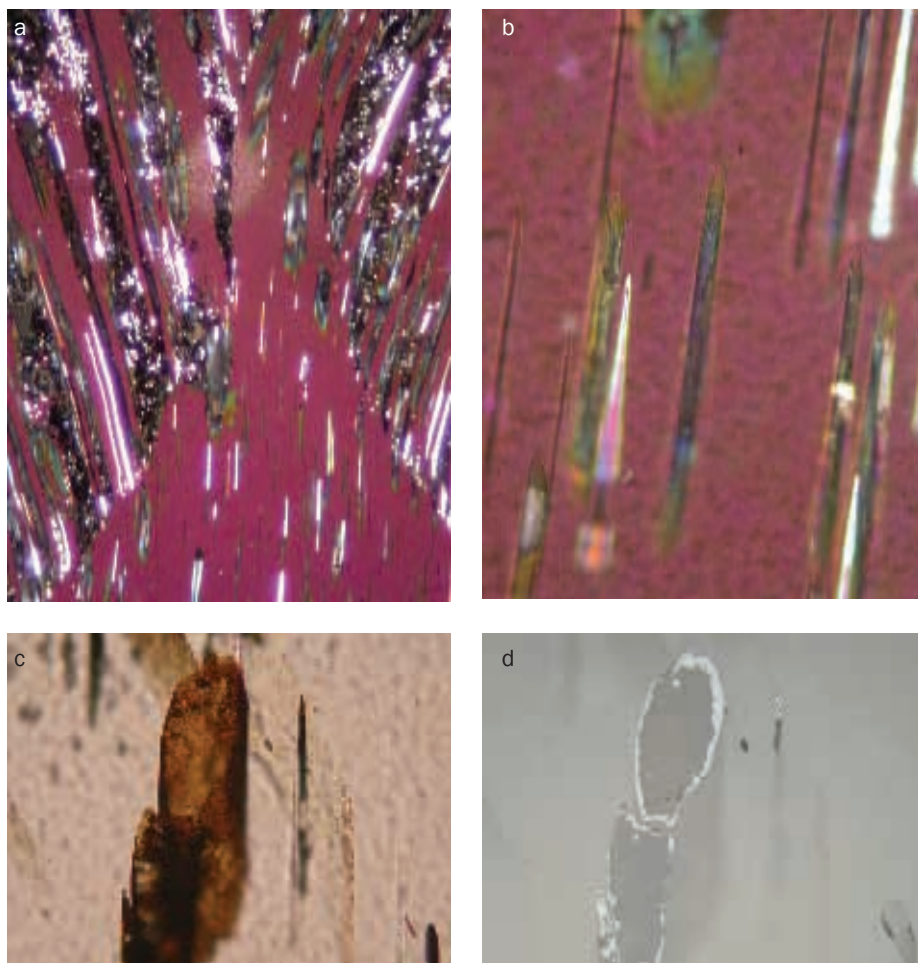


Figure 12 a,b: Different views of a section about 60 μm thick, cut parallel to the *c*-axis, showing channels filled with liquid or solid matter. Crossed polarizers, field of view (a) approx. 2.04 \times 2.72 mm, and (b) approx. 0.51 \times 0.68 mm; (c) and (d) view of an open channel which is stained with an iron-bearing mineral on its internal surface, in transmitted and reflected light respectively, field of view approx. 0.34 \times 0.26 mm. Photos by H.-J. Bernhardt.

Compared to an ideal intermediate composition between dravite and uvite, these analyses show some excess calcium and some sodium deficiency. For example, analyses with an intermediate composition between the ideal end-members dravite and uvite, with a composition of 3.5 apfu Mg and 5.5 apfu Al, show approximately 0.3 Na and 0.7 Ca rather than 0.5 Na and 0.5 Ca which would have been expected if isomorphous substitution had been ideal. A 'dravite' with an ideal composition of 3.0 apfu Mg and 6.0 apfu Al (which should be free of Ca) shows approximately 0.22 apfu Ca, and approximately 0.72 apfu Na (instead of 1.0 apfu Na which may have been expected from the theoretical composition). Consequently, if these compositions are compared with many quoted in textbooks, the Zambian

tourmalines would be considered as members of the dravite-uvite solid solution series but with excess calcium and deficient sodium.

6.2 Trace elements causing colour

Iron and manganese contents in all samples are each in the range of 0.01 to 0.02 wt.%, so neither trace element is likely to influence colour. The majority of the tourmalines (with smaller fluorine contents) contain vanadium in the range of 0.10 to 0.40 wt.% V_2O_3 and chromium between 0.0 and 0.27 wt.% Cr_2O_3 and the tourmalines with the higher contents of these elements are an attractive green (*Figure 13f*). In contrast, tourmaline A with the higher fluorine content (*Table III*) shows colour zoning with a colourless or almost colourless core and an intense green rim. The core contains 0.0 to 0.1

Chemical and growth zoning in trapiche tourmaline from Zambia — a re-evaluation

Table III: Mean chemical compositions of nine trapiche tourmalines from Zambia

Specimen	A	B	C*	D	E	F	G**	H	I
Orientation of section	∥ c	⊥ c	⊥ c	∥ c	⊥ c	∥ c	⊥ c	⊥ c	∥ c
Number of analyses	346	148	59	516	166	409	545	122	285
Wt. %									
SiO ₂	36.91	36.84	37.07	37.05	37.17	37.15	37.03	36.94	36.66
TiO ₂	0.10	0.21	0.18	0.22	0.21	0.19	0.21	0.20	0.18
B ₂ O ₃ ¹	10.73	10.73	10.78	10.73	10.78	10.77	10.71	10.67	10.64
Al ₂ O ₃	28.49	28.58	29.17	28.82	28.97	29.25	29.02	29.06	29.11
V ₂ O ₃	0.09	0.25	0.12	0.16	0.29	0.26	0.23	0.22	0.31
Cr ₂ O ₃	0.05	0.07	0.12	0.04	0.08	0.09	0.05	0.07	0.14
FeO ²	0.02	0.01	0.01	0.01	0.02	0.01	0.01	0.01	0.01
MnO	0.01	0.01	0.01	0.02	0.01	0.01	0.02	0.02	0.01
MgO	14.70	14.51	14.27	14.27	14.26	14.03	13.97	13.76	13.65
CaO	4.08	4.04	3.74	3.78	3.68	3.45	3.41	3.22	3.13
K ₂ O	0.01	0.01	0.01	0.01	0.01	0.01	0.01	0.02	0.01
Na ₂ O	0.91	0.94	1.07	1.09	1.15	1.25	1.28	1.35	1.38
F	1.98	1.65	1.73	1.55	1.55	1.55	1.54	1.51	1.50
H ₂ O ³	2.64	2.75	2.71	2.76	2.78	2.77	2.74	2.73	2.76
-O=F	0.83	0.70	0.73	0.65	0.65	0.65	0.65	0.64	0.63
Total	99.89	99.90	100.26	99.86	100.31	100.14	99.58	99.14	98.86

Number of ions based on 31 (O,OH,F)

Specimen	A	B	C	D	E	F	G	H	I
Si	5.978	5.969	5.979	5.999	5.993	5.994	6.007	6.017	5.997
Ti	0.012	0.025	0.022	0.026	0.026	0.023	0.026	0.024	0.022
B	3.000	3.000	3.000	3.000	3.000	3.000	3.000	3.000	3.000
Al	5.438	5.457	5.544	5.501	5.504	5.560	5.547	5.578	5.597
V	0.012	0.033	0.016	0.021	0.037	0.033	0.030	0.028	0.041
Cr	0.007	0.008	0.015	0.005	0.010	0.012	0.007	0.009	0.018
Fe	0.002	0.002	0.002	0.001	0.002	0.001	0.001	0.001	0.002
Mn	0.001	0.001	0.001	0.002	0.001	0.001	0.002	0.002	0.001
Mg	3.550	3.504	3.421	3.445	3.428	3.375	3.379	3.341	3.323
Ca	0.709	0.701	0.647	0.655	0.636	0.596	0.594	0.562	0.548
K	0.002	0.001	0.002	0.002	0.002	0.002	0.002	0.003	0.002
Na	0.285	0.294	0.335	0.341	0.360	0.392	0.402	0.427	0.436
F	1.012	0.848	0.881	0.793	0.791	0.793	0.788	0.780	0.775
OH	2.847	2.967	2.911	2.978	2.988	2.982	2.969	2.969	2.997

* Type B, all other samples type A

** two slices perpendicular to the c-axis

1 calculated as B = 3.00 atoms per formula unit (apfu)

2 total iron as FeO

3 calculated as OH + F + O = 31.00 apfu

wt.% V₂O₃ and between 0.0 and 0.06 wt.% Cr₂O₃, while the green rim has chromium up to 0.30 wt.% Cr₂O₃ and vanadium up to 0.8 wt.% V₂O₃. These elevated trace element contents are responsible for the intense green coloration of the rim of that particular sample.

6.3 Compositional zoning – scans across sections parallel and perpendicular to the c-axis

Chemical zoning in trapiche tourmalines from Zambia is extremely complex, especially because different patterns of zoning can be present in the same crystal. To demonstrate this, variation of sodium and calcium on the X positions in the tourmaline structure is shown, but the variation could be shown equally well by means of other element pairs such as magnesium and aluminium.

Numerous scans across the boundaries of prismatic/prismatic and pyramidal/pyramidal growth sectors in all analysed tourmalines show no changes in composition, but scans across adjacent prismatic and pyramidal growth sectors do show differences with higher sodium and lower calcium contents in the prismatic sectors (*Figure 14*). These differences for Na and Ca are in the range of 0.1 atoms per formula unit (apfu).

In transparent prismatic growth sectors the values obtained indicate that as growth proceeds there is a continuous increase of sodium content combined with a decrease of calcium content in the direction of growth, i.e. with increasing distance from the centre of the tourmaline crystals. This chemical variation is present both in sections perpendicular to the c-axis (*Figure 15*) and in sections parallel to the c-axis (*Figure 16*). In transparent pyramidal growth sectors of tourmalines cut parallel to the c-axis, a similar continuous increase of sodium contents coupled with a decrease of calcium contents also occurs in the direction of growth, i.e. in scans parallel to the c-axis (*Figures 16 and 17*). In scans of prismatic growth sectors with that particular direction however, the chemical composition is constant, because these analyses represent areas of the tourmaline

Chemical and growth zoning in trapiche tourmaline from Zambia — a re-evaluation

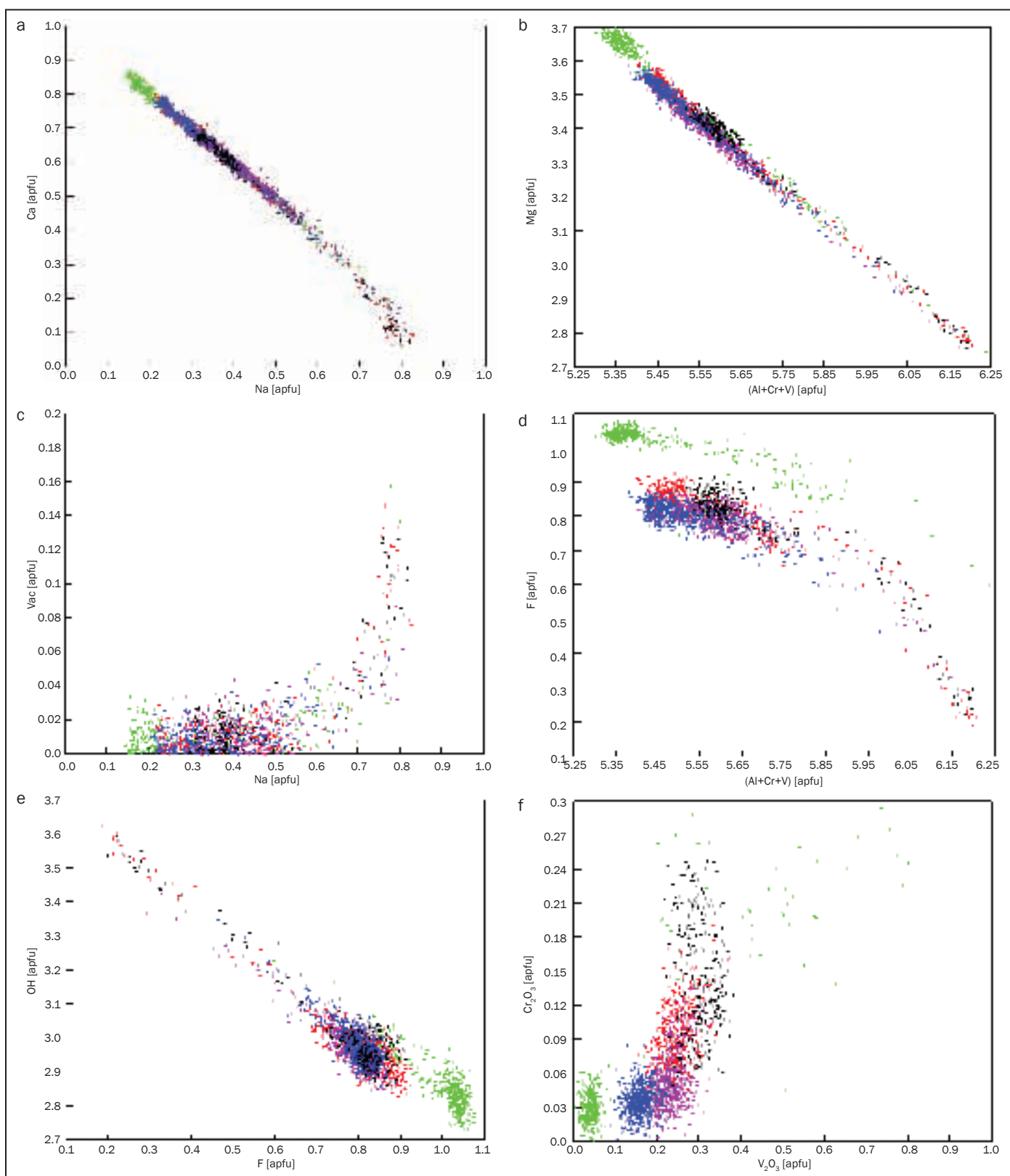


Figure 13: Variation of chemical composition in trapiche tourmalines from Zambia; five different colours indicate point analyses taken in various scans across the sections of five tourmalines, the diagrams represent a total of 2101 point analyses. (a) isomorphous substitution of calcium by sodium on X sites during tourmaline growth; (b) isomorphous substitution of magnesium on (Y+Z) sites by the sum of (aluminium plus chromium plus vanadium); (c) variation of vacancies with Na on X sites in the tourmaline; (d) variation of fluorine contents versus sum of (aluminium plus chromium plus vanadium); (e) variation of hydroxyl content versus fluorine content on W sites; (f) range of chromium and vanadium contents: A sample represented by green dots has a colourless core and an intensely green rim. All samples are members of the solid solution series between dravite and fluor-uvite and show a wide compositional range; one tourmaline (sample A in Table III represented by green dots) shows a higher fluorine content than the other four samples; apfu stands for 'atoms per formula unit'.

Chemical and growth zoning in trapiche tourmaline from Zambia — a re-evaluation

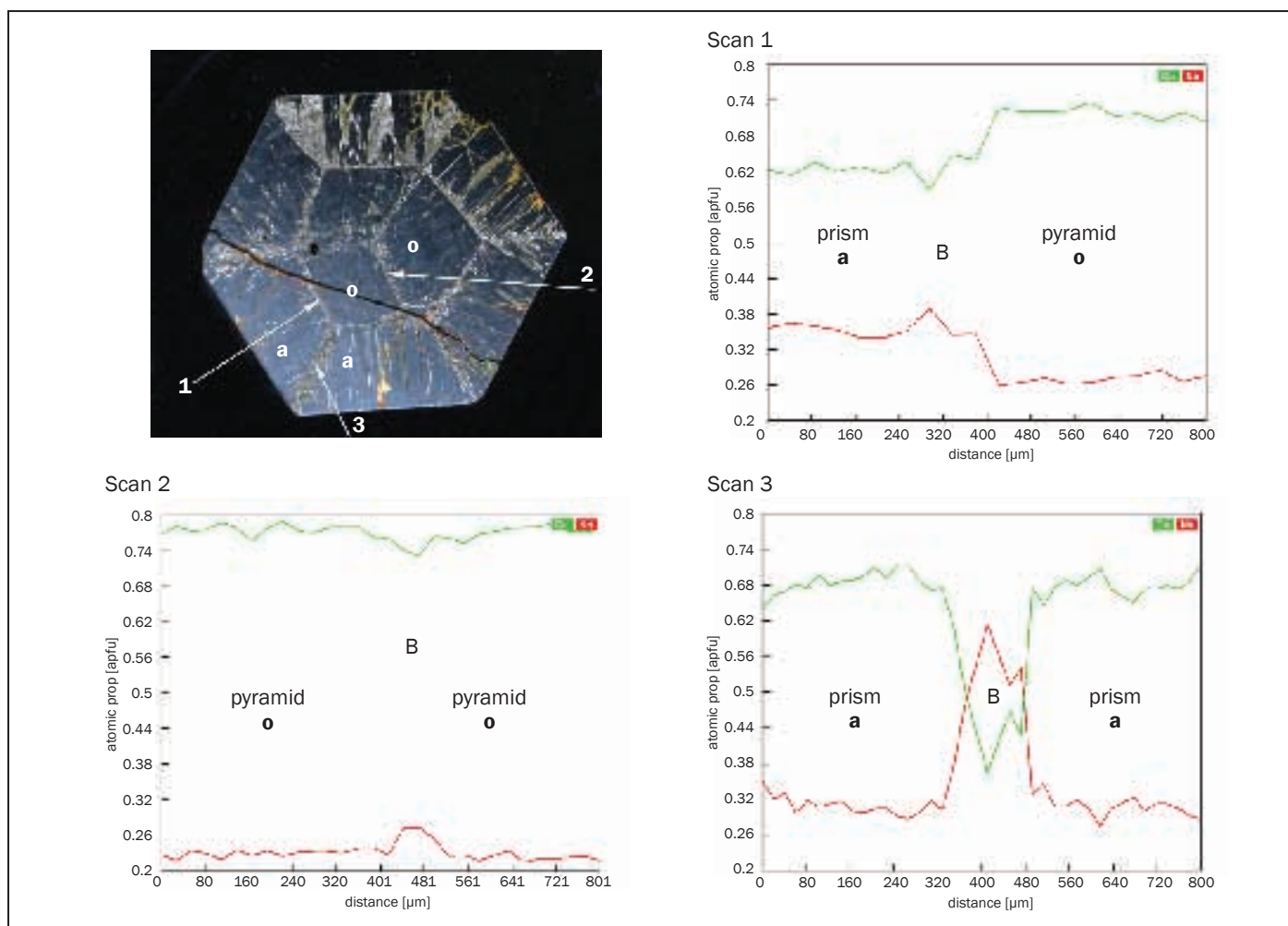


Figure 14: Ca (green) and Na (red) variation across prismatic **a** and pyramidal **o** growth sectors in trapiche tourmaline from Zambia; section perpendicular to the c-axis. Scans 1, 2 and 3 were performed across the sector boundaries indicated by B. Pyramidal **o** growth sectors show higher calcium and lower sodium contents than adjacent prismatic **a** growth sectors (scan 1); no significant difference in composition is present between the two adjacent pyramidal **o** growth sectors measured in scan 2 or between the adjacent prismatic **a** growth sectors in scan 3, but in scan 3 in the marginal area between the two **a** growth sectors, the tourmaline has higher sodium and lower calcium contents than in either growth sector. Diameter of the sample approx. 13 mm. Photo by H.-J. Bernhardt.

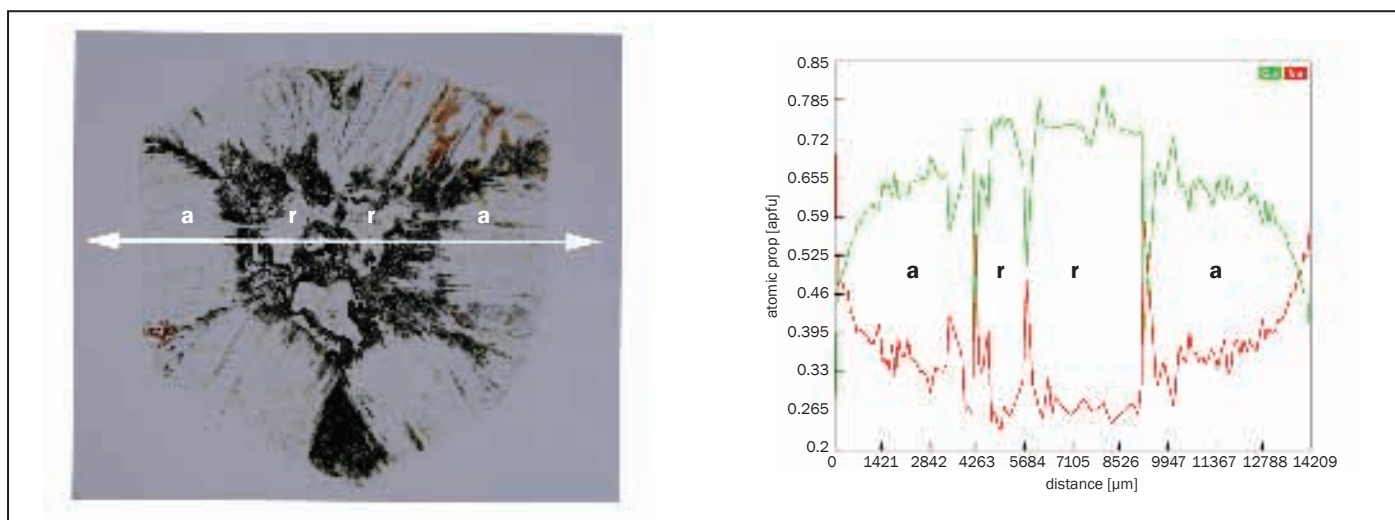


Figure 15: Ca (green) and Na (red) contents in a scan across two prismatic **a** and two pyramidal **r** growth sectors in a trapiche tourmaline from Zambia; section perpendicular to the c-axis. Pyramidal **r** growth sectors have higher calcium and lower sodium contents than adjacent prismatic **a** growth sectors. Within the prismatic **a** growth sector, sodium increases and calcium decreases from centre to rim; in the margins of the various growth sectors and in irregularly shaped areas with abundant trapped inclusions, the tourmaline has higher sodium and lower calcium contents. Size of the sample approx. 15 × 16 mm. Photo by H.-J. Bernhardt.

Chemical and growth zoning in trapiche tourmaline from Zambia — a re-evaluation

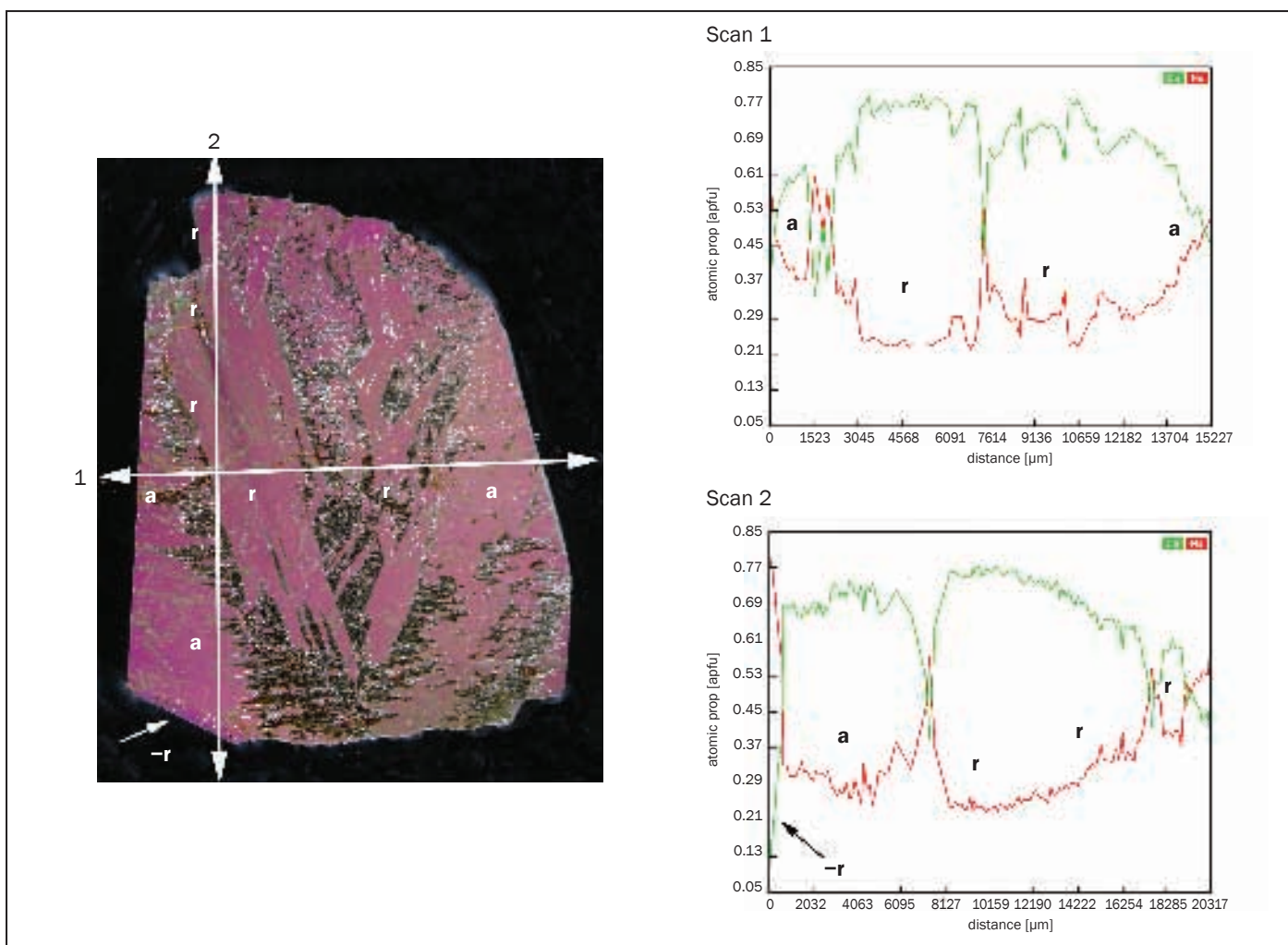


Figure 16: Ca (green) and Na (red) contents in scans across prismatic **a** and pyramidal **r** and **-r** growth sectors in trapiche tourmaline from Zambia; section parallel to the *c*-axis. In the prismatic **a** growth sectors, sodium increases and calcium decreases from centre to rim (scan 1); within pyramidal **r** and **-r** growth sectors, sodium increases and calcium decreases along the *c*-axis from the centre to both analogous and antilogous ends of the crystal (scan 2); as above, where there are abundant inclusions the tourmaline has higher sodium and lower calcium contents than that in the various growth sectors (scans 1 and 2). Size of the sample approx. 15 × 21 mm; crossed polarizers. Photo by H.-J. Bernhardt.

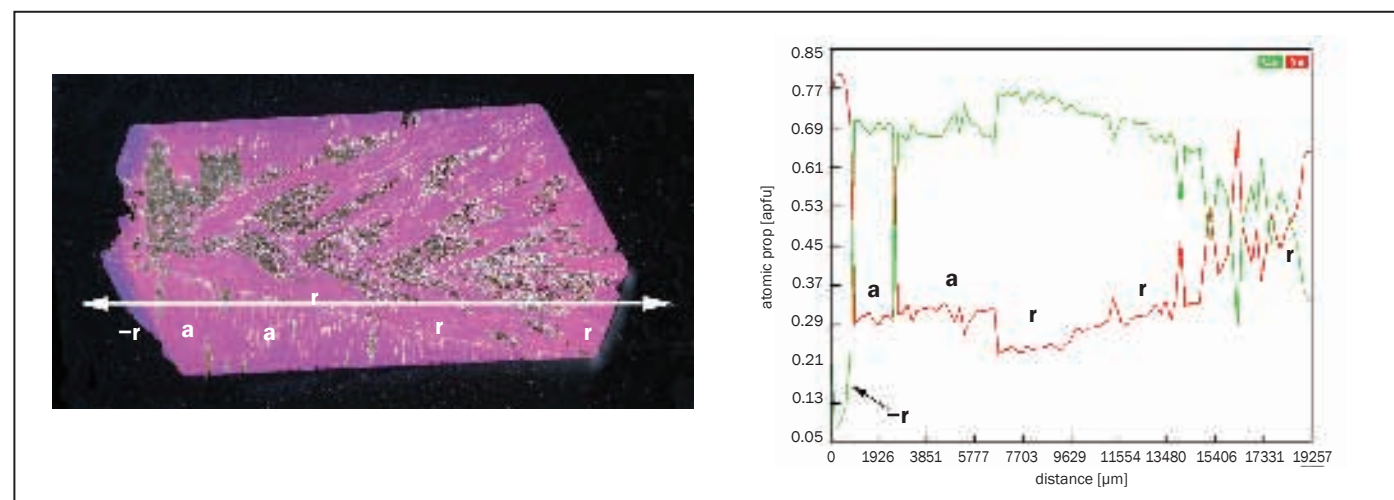


Figure 17: Ca (green) and Na (red) contents across prismatic **a** and pyramidal **r** and **-r** growth sectors along the *c*-axis in trapiche tourmaline from Zambia. Pyramidal **r** growth sectors have higher calcium and lower sodium contents than adjacent prismatic **a** growth sectors; within pyramidal **r** and **-r** growth sectors, sodium increases and calcium decreases along the *c*-axis from the centre to both analogous and antilogous ends of the crystal. At the margin of various growth sectors and in irregularly shaped areas with abundant trapped inclusions, the tourmaline host has higher sodium and lower calcium contents compared to that in the surrounding growth sectors. Size of the sample approx. 10 × 20 mm; crossed polarizers. Photo by H.-J. Bernhardt.

Chemical and growth zoning in trapiche tourmaline from Zambia — a re-evaluation

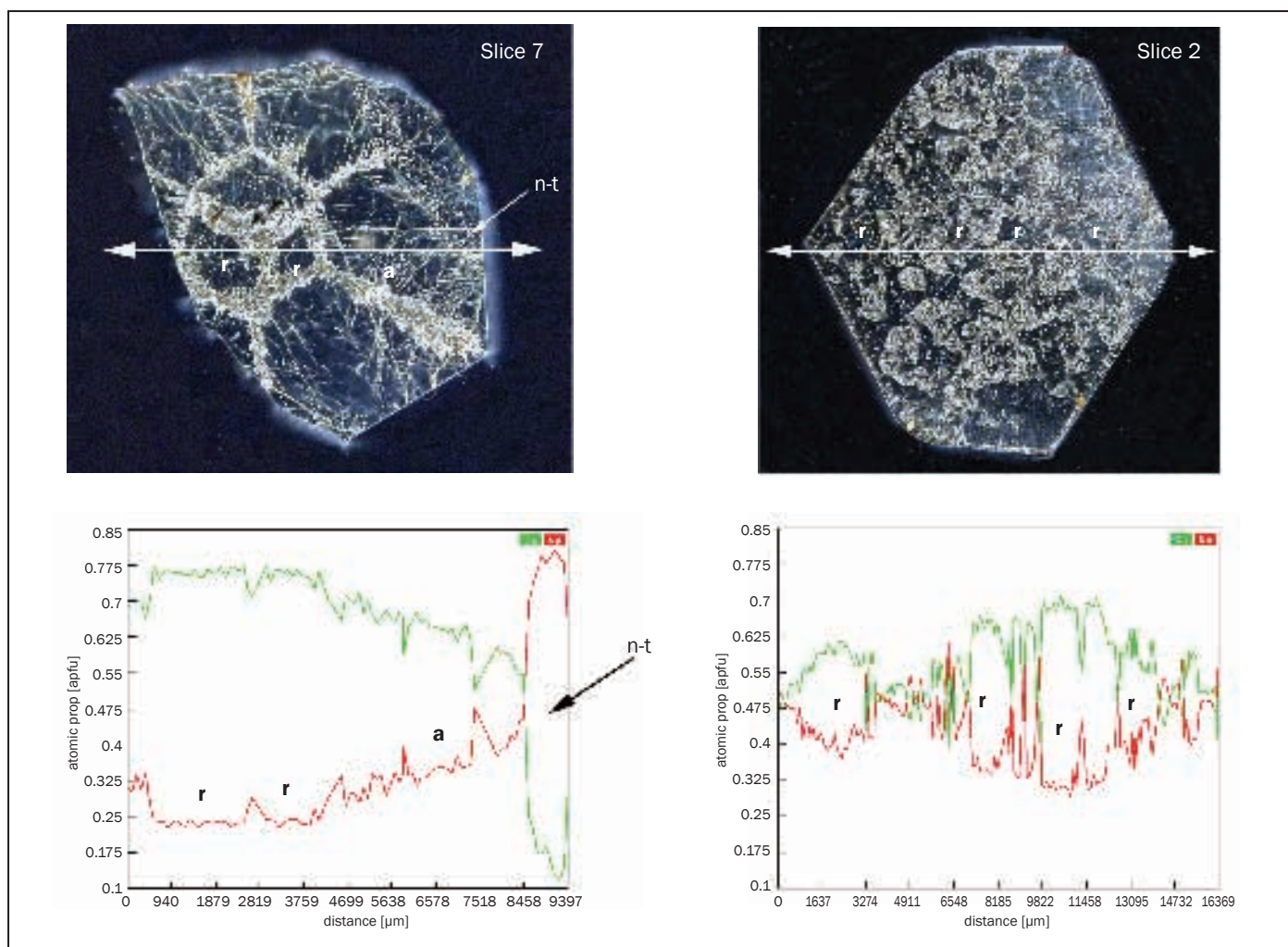


Figure 18: Ca (green) and Na (red) contents in trapiche tourmaline from Zambia. The slices are those shown in Figure 8 and are perpendicular to the c -axis; slice 7 was broken when repolished.

Thin section of slice 7: a scan across pyramidal r growth sectors shows higher calcium and lower sodium contents than the adjacent prismatic a growth sector; no differences in composition were observed between two adjacent pyramidal r growth sectors. Within the prismatic a growth sector, sodium increases and calcium decreases from the centre to the rim; these trends become extreme at the outermost part of the rim, which shows no trapiche pattern (indicated with $n-t$).

Thin section of slice 2: the scan across two r growth sectors shows that sodium (red) increases and calcium (green) decreases from centre to rim. The common occurrence of irregularly shaped areas with abundant inclusions, is reflected in the fluctuating sodium and calcium contents in the scan. Size of slice 7 approx. 11 × 14 mm and of slice 2 16 × 18 mm. Photos by H.-J. Bernhardt.

crystal at the same stage of growth.

In the growth areas related to the negative pyramid $-r$ (Figures 16 and 17), sodium contents are higher than in all other parts of the tourmaline crystals. Similar tourmaline compositions are present in the rim of a crystal with a normal trapiche pattern in the centre but which has an outer sector with no trapiche pattern (labelled $n-t$, Figure 18). Heavily included margins between adjacent growth sectors also have a more sodic tourmaline host than the non-transparent areas (Figures 15 to 17).

6.4 Compositional maps – the distribution of Na and Ca in tourmaline sections parallel and perpendicular to the c -axis

Na and Ca compositional maps were obtained on two sections of slices perpendicular to the c -axis, originating from the same rough crystal and for two sections of different crystals cut parallel to the c -axis. These show that in prismatic a growth sectors, the calcium contents are always somewhat lower than in adjacent pyramidal r growth sectors, while the sodium contents are higher (Figures 19a

and 20). In growth sectors confined to the negative pyramid $-r$, extreme chemical zoning is present on a small scale (Figure 20), and this represents the complete range of chemical variation along the c -axis.

At the boundaries between different prismatic or pyramidal growth sectors with abundant inclusions two types of areas with a composition different from the surrounding transparent tourmaline may be present (Figures 19 and 20). One shows pixels representing material with high calcium or a high calcium and magnesium content and represents the

Chemical and growth zoning in trapiche tourmaline from Zambia — a re-evaluation

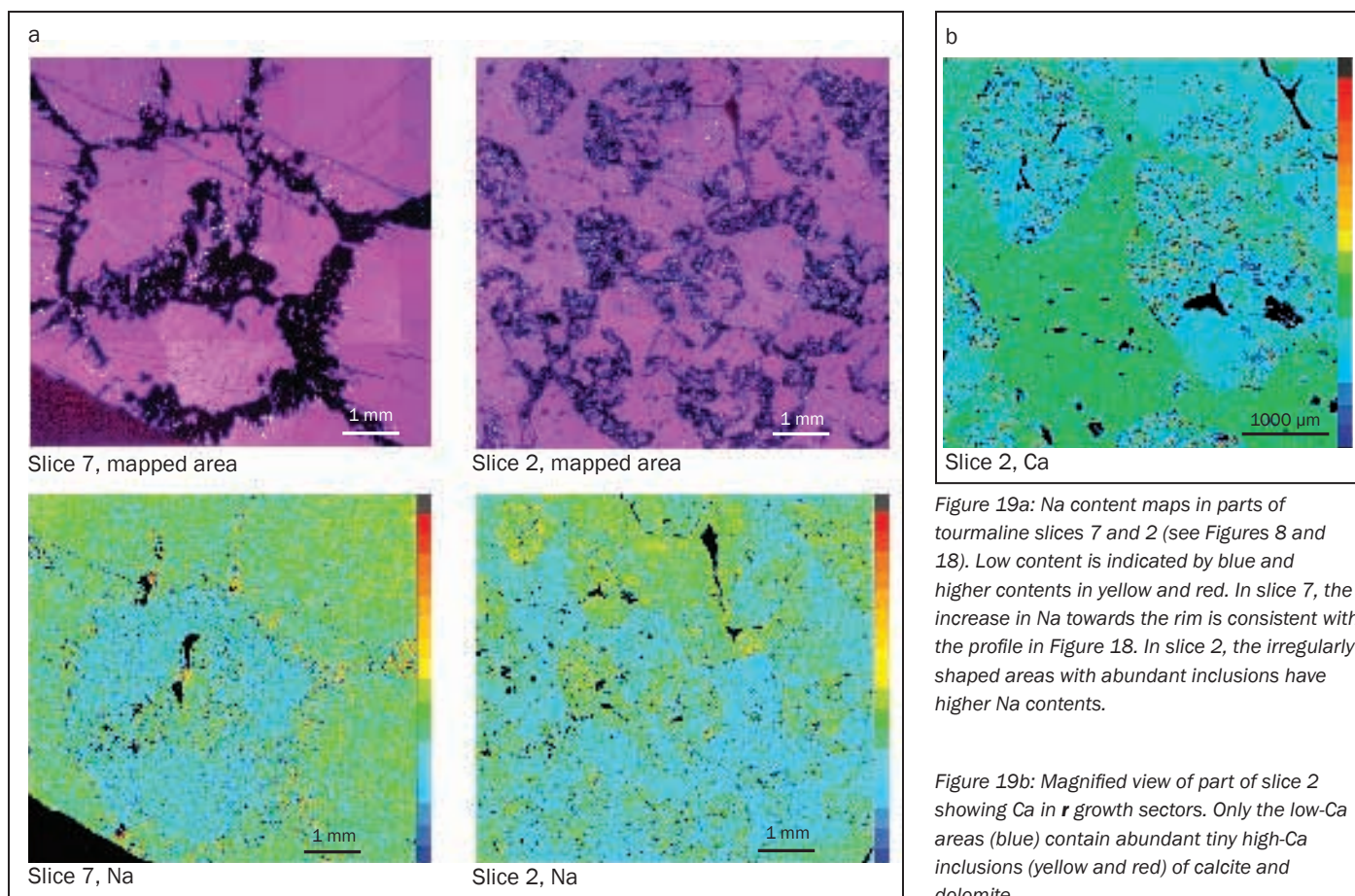


Figure 19a: Na content maps in parts of tourmaline slices 7 and 2 (see Figures 8 and 18). Low content is indicated by blue and higher contents in yellow and red. In slice 7, the increase in Na towards the rim is consistent with the profile in Figure 18. In slice 2, the irregularly shaped areas with abundant inclusions have higher Na contents.

Figure 19b: Magnified view of part of slice 2 showing Ca in r growth sectors. Only the low-Ca areas (blue) contain abundant tiny high-Ca inclusions (yellow and red) of calcite and dolomite.

many inclusions of magnesite or dolomite. The other type of pixel represents material with a somewhat higher sodium and lower calcium content than the surrounding tourmaline (Figure 20b).

7. Discussion — chemical zoning and formation of structural patterns

7.1 Compositional zoning

The complexity of structural and chemical zoning in tourmaline crystals from different localities is due to one or a combination of several mechanisms (see Benesch, 1990; Henry and Dutrow, 1992, 1996, 2001; Kazachenko *et al.*, 1993; Sperlich *et al.*, 1996; Takahashi and Sunagawa, 1998; Vergilov and Kostova, 2000; Agrosi *et al.*, 2006; van Hinsberg *et al.*, 2006; Lussier *et al.*, 2008; Lussier and Hawthorne, 2011).

(a) Chemical growth zoning. This type of compositional variation from core to rim is common in tourmalines from different localities.

(b) Compositional polarity. Tourmalines from some localities have antilogous and analogous ends of different composition.

(c) Sector zoning. Adjacent growth sectors can have different compositions.

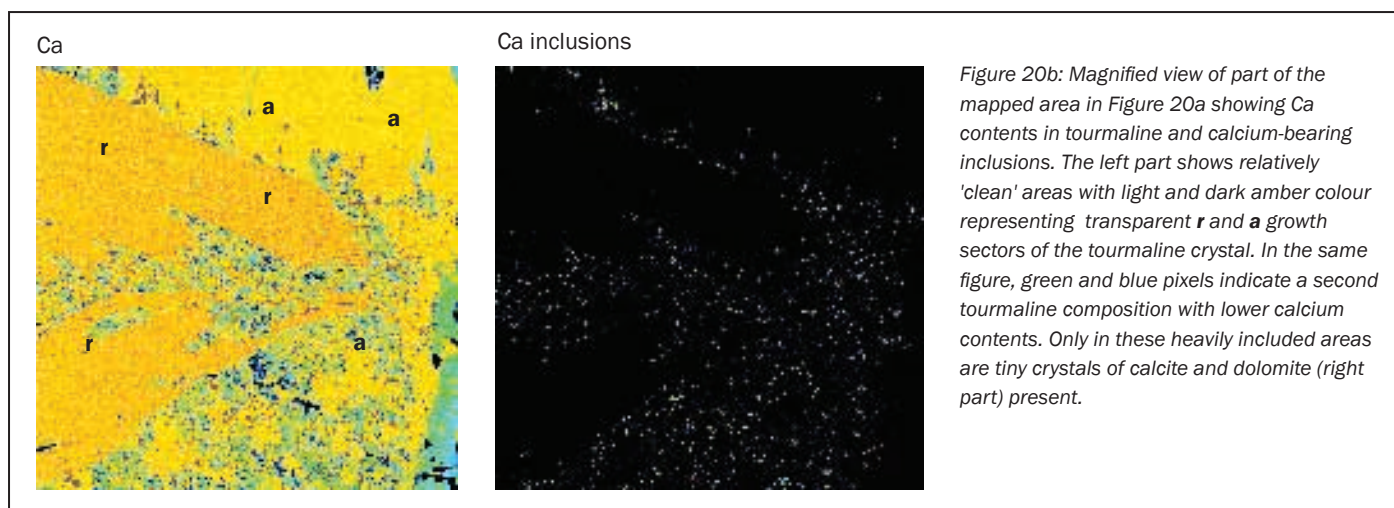
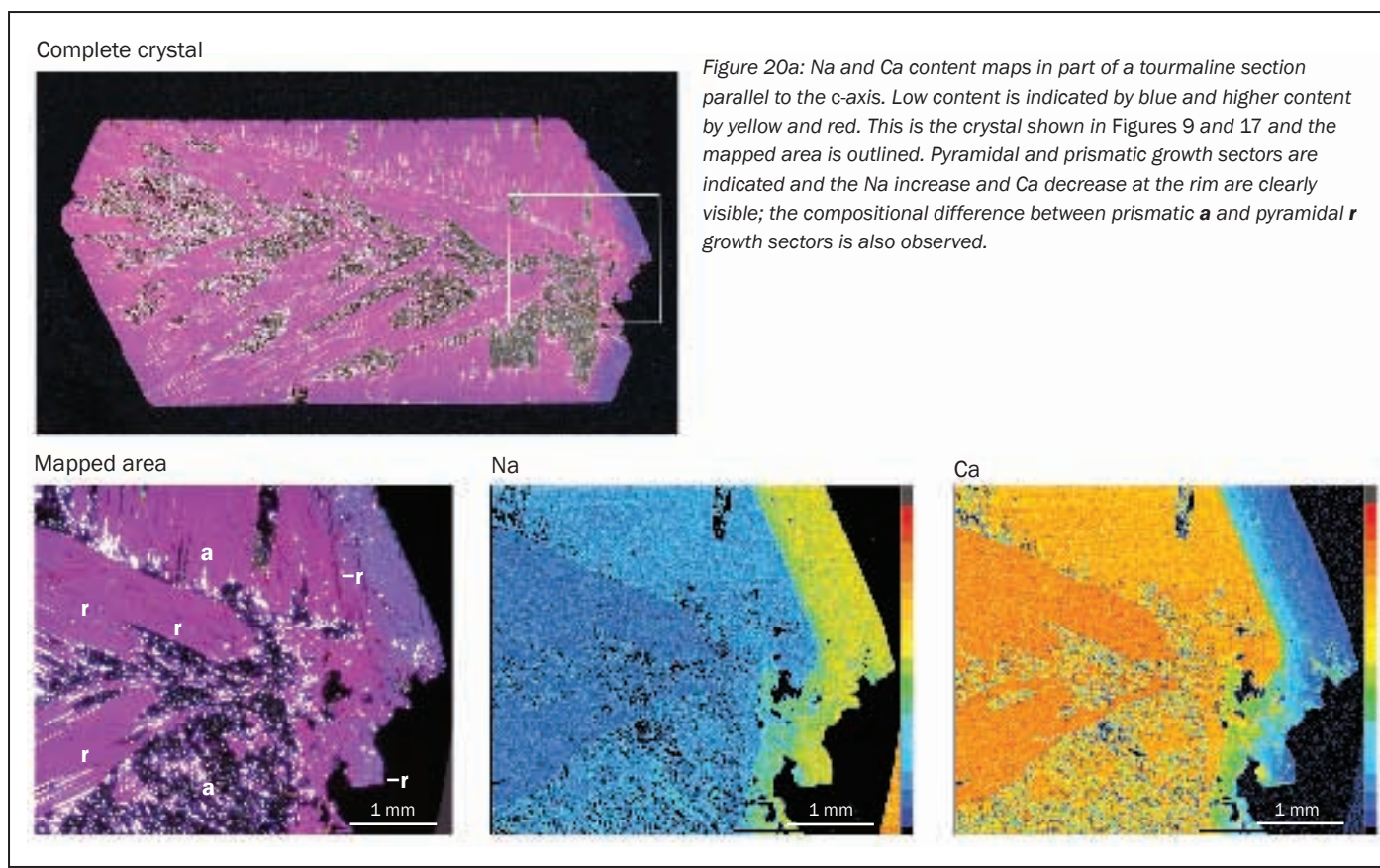
The chemical compositions of the transparent areas of all the trapiche tourmalines measured in this study varied from core to rim. At the beginning of crystal growth, a calcium-rich fluoruvite crystallized. Subsequently there was a continuous decrease of calcium, magnesium and fluorine contents with corresponding isomorphous substitutions of Ca by Na, Mg by Al and F by OH. Consequently, by the end of crystal growth, sodium-rich dravite was forming. Sector zoning is present in all samples, and some compositional polarity is present; details are given above. At the end of growth, the sodium content of the crystal's analogous end is higher than at its antilogous end. The variation described for sodium and calcium applies also for magnesium and aluminium and for

fluorine and hydroxyl groups.

The trapiche pattern is formed by numerous fluid and solid inclusions, mainly calcite and dolomite, at the margins of all combinations of pyramidal and prismatic growth sectors, i.e. at pyramidal/pyramidal, prismatic/prismatic and at pyramidal/prismatic growth sectors. Obviously, crystal growth was hindered by these inclusions for some period and then subsequent growth of tourmaline contained elongate voids. This mechanism of formation of the growth-induced elongate voids or channels has been described in detail by such authors as Slivko (1966) (see Figure 21 a,b), Liu and Lu (1986) and Rustemeyer (2003). The voids may form in two ways:

- Trapping of inclusions and formation of channels in the growth direction 'behind' these inclusions (Figure 21a).
- Trapping of inclusions and formation of channels in the growth direction with the inclusion moving 'in front' of the growth channel (Figure 21b). The formation of an elongate void

Chemical and growth zoning in trapiche tourmaline from Zambia — a re-evaluation



ends when the diameter of the channel diminishes and closes (case a, see *Figure 21a*) or when the inclusion at the forefront of the channel halts or is finally 'frozen' and normal tourmaline resumes growth (case b, see *Figure 21b*). One or both ways described could be responsible for the formation of channels in tourmaline cat's-eyes.

In some trapiche tourmalines, abundant channels of limited length are present only at the margins between

different growth sectors. If growth-induced channels are not limited to an area close to the sector boundaries, they continuously extend into the growing tourmaline sectors. In such samples, the last slices along the c-axis of the tourmalines show only small 'clean' transparent areas with few growth tubes.

The various growth processes suggested so far do not explain the tourmaline analyses in the arms of the star with sodium contents that are higher than

in the surrounding transparent tourmaline. Careful examination of thin sections showed that despite the difference, this tourmaline is not distinguishable from the main tourmaline on the basis of optical properties.

7.2 The trapiche pattern: nomenclature

Numerous gemstones have been designated as 'trapiche' in the trade and in various gemmological journals. In general

Chemical and growth zoning in trapiche tourmaline from Zambia — a re-evaluation

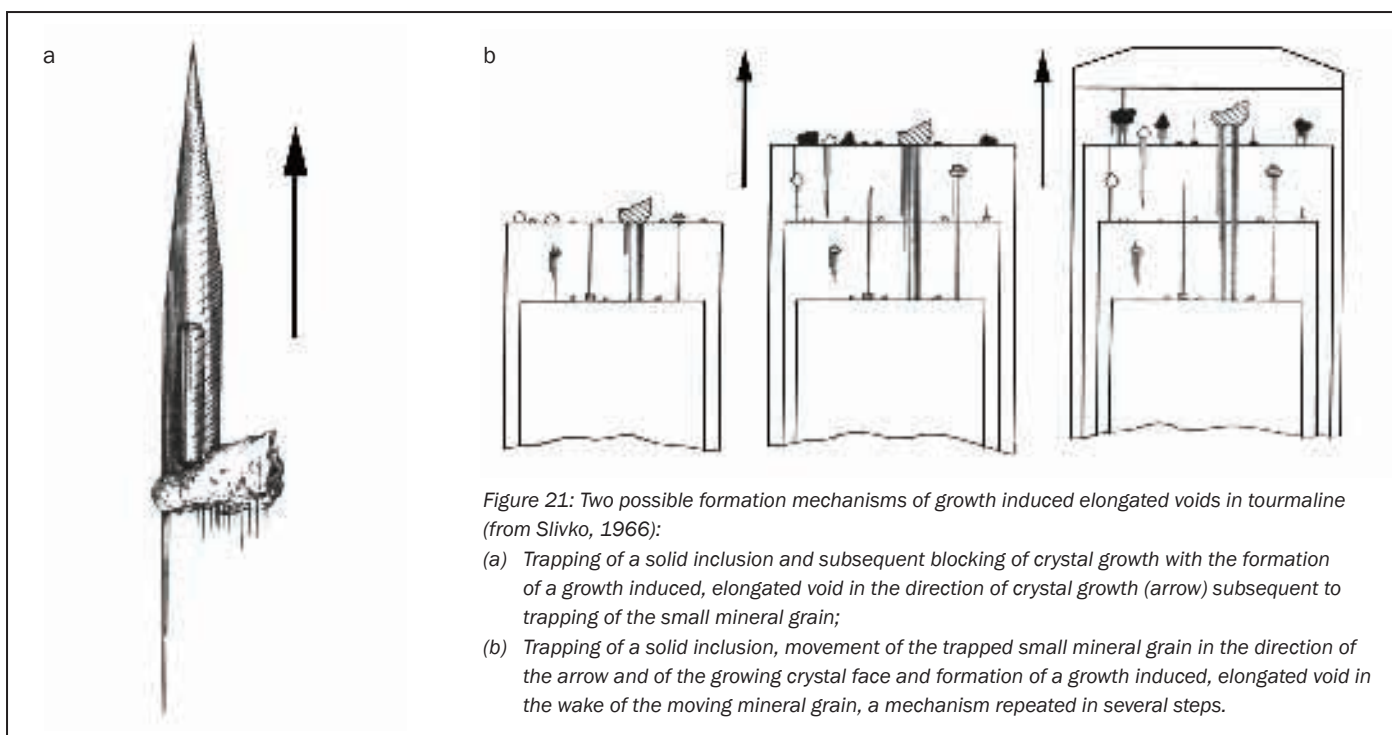


Figure 21: Two possible formation mechanisms of growth induced elongated voids in tourmaline (from Slivko, 1966):

- (a) Trapping of a solid inclusion and subsequent blocking of crystal growth with the formation of a growth induced, elongated void in the direction of crystal growth (arrow) subsequent to trapping of the small mineral grain;
- (b) Trapping of a solid inclusion, movement of the trapped small mineral grain in the direction of the arrow and of the growing crystal face and formation of a growth induced, elongated void in the wake of the moving mineral grain, a mechanism repeated in several steps.

the term is used to describe a pattern consisting of a fixed star in a transparent host matrix, with the arms of the star radiating from a central point or central core to the rim of the crystal, cabochon or slice. Several 'trapiche' materials with different visual appearance were recently described by Win (2005) and these can be considered in two groups.

The first group is characterized by more or less sharp boundaries, extending from a central intersection point or from the edges of a central core, which separate transparent to translucent growth sectors of the host (see ruby in Figure 22). The arms of the fixed star, which are formed by these boundaries, are mostly not transparent and run from the centre to the edges of the external crystal faces. They consist of the main mineral (e.g. beryl, corundum, tourmaline) and numerous tiny other mineral or fluid inclusions. Consequently, the areas separated by the arms of the star are crystallographically equivalent prismatic (beryl), dipyrnidal (corundum) or pyramidal (tourmaline) growth sectors of the crystal. The most prominent gem materials of this group (see Table IV) are Colombian emerald, ruby from Mong Hsu, Myanmar and the uvite-dravite tourmaline

from Zambia.

The second group is characterized by several alternating transparent and translucent areas which surround a central point or central core according to the symmetry of the host. The transparent and translucent areas are characterized by different concentrations of inclusions, which are trapped within specific central parts of symmetry-equivalent growth sectors of the host (see the sapphire in Figure 22). The sharp boundaries separating the different crystallographically equivalent growth sectors of the first group are not visible. The arms of the group 2 star are perpendicular to the external crystal faces, e.g. perpendicular to the hexagonal dipyrnids of corundum or perpendicular to the prism faces of beryl. The most prominent gem examples of this second group are the blue basaltic sapphires described recently by Khotchanin *et al.* (2009). Slices of these sapphires perpendicular to the *c*-axis consist of milky white, translucent areas with a high concentration of inclusions.

The following examples highlight the differences in star pattern. The milky white translucent areas with abundant inclusions in the sapphires of Khotchanin *et al.* (2009) are equivalent



Figure 22: Trapiche ruby from Mong Hsu, Myanmar (top) and trapiche-type sapphire from Hunan province, China (bottom); slices perpendicular to the *c*-axis, the hexagonal outlines of the rough crystals are represented by dipyrnidal faces. With identical crystallographic orientation of both corundum slices, the different orientation of the fixed star within these samples is observed. Diameter of the trapiche ruby 4.20 mm, size of the trapiche-type sapphire 10 × 12 mm. Photos by K. Schmetzer.

Chemical and growth zoning in trapiche tourmaline from Zambia — a re-evaluation

Table IV. Properties of gem materials with typical trapiche pattern

		Emerald, Colombia	Ruby, Myanmar	Tourmaline, Zambia ¹²
Type of crystals		Hexagonal prisms, rarely with basal faces ^{1,2,4,5}	Fragments confined by hexagonal dipyramids ω ⁷	Complete prismatic crystals
Sections or slices \perp to the <i>c</i> -axis	Geometrical pattern	Hexagonal core, rim formed by six trapezohedral sectors ^{1,2,3,4,5,6}	Hexagonal red, yellow or black core, rim formed by six red trapezohedral sectors ^{7,8,9,10,11} Growth zoning $\parallel \omega$ ¹⁰	Hexagonal core consisting of several pyramidal growth sectors, rim formed by six trapezohedral sectors
	Chemical zoning	Zoning of trace elements ⁶	Zoning of trace elements ^{8,9,11}	Uvite-dravite zoning
Fine structure in thin sections \perp to the <i>c</i> -axis, orientation of channels or needle-like inclusions		Fibrous texture \perp to the <i>c</i> -axis in the rim ^{1,5,6} growth planes parallel to the prism ^{1,5}	Channels \parallel to the <i>c</i> -axis and slightly inclined \perp to the <i>c</i> -axis ⁷	Channels \perp to the pyramids in the core and \perp to the prism in the rim
Sections or slices \parallel to the <i>c</i> -axis	Geometrical pattern	Tapered core ^{1,2,4,5}	Tapered core, end of cores red, yellow or black channels \perp to the dipyramids ω ⁷	Tapered core, sometimes skeleton growth
	Chemical zoning			Uvite-dravite zoning
Fine structure in thin sections \parallel to the <i>c</i> -axis, orientation of channels or needle-like inclusions		Fibrous texture \perp to the <i>c</i> -axis in the rim and \parallel to the <i>c</i> -axis in the core ¹		Channels \perp to the pyramids in the core and \perp to the prism in the rim
Main material trapped at the boundaries of growth sectors or in channels		Quartz, albite ^{3,5} or carbonaceous matter ⁵	Fluid, calcite, dolomite, silicates ^{7,8,11}	Graphite, calcite, dolomite, fluid

Emerald: 1 Bernauer, 1926; 2 McKague, 1964; 3 Schiffmann 1968, 1969; 4 Tripp and Hernandez, 1970; 5 Nassau and Jackson, 1970 a,b; 6 Ohnenstetter *et al.*, 1998

Ruby: 7 Schmetzer *et al.*, 1996; 8 Schmetzer *et al.*, 1998; 9 Sunagawa *et al.*, 1999; 10 Schmetzer and Schwarz, 2000; 11 Garnier *et al.*, 2002 a,b

Tourmaline: 12 this paper

to the transparent growth sectors of trapiche rubies (Figure 22, see Table IV), and the blue transparent areas of basaltic sapphires are equivalent to the sharp non-transparent boundaries of trapiche rubies. If the pattern of Colombian emeralds (Table IV) is compared with that in aquamarine from Namibia (Koivula, 2008), the non-transparent arms of Colombian emeralds are equivalent to the transparent areas within the aquamarine material from Pakistan, and the transparent growth sectors of the emeralds are equivalent to the heavily included milky white areas of these aquamarines. Another example is given by DelRe (1994) in which he

compares Colombian trapiche emerald with emeralds from Brazil which have a fixed six-rayed star with arms orientated perpendicular to the external prism faces of the beryl host. The author also mentioned that the two types of trapiche emeralds “almost seem to be a photographic negative” of each other.

These two star patterns indicate different mechanisms of formation. Consequently, to distinguish them, we suggest naming the first group (e.g. Colombian emeralds, ruby from Myanmar, tourmaline from Zambia) trapiche and the second group (e.g. basaltic sapphires from various origins) trapiche-type.

7.3 The trapiche pattern: formation

Several mechanisms of formation for the trapiche pattern have been suggested for the gemstones emerald and ruby, as well as for other non-gem materials such as cordierite or andalusite (chiastolite) (Petreus, 1974; Henderson, 1995).

A mineral which shows a clear trapiche pattern – cordierite from Japan – is not discussed in this paper because of the even more complex mechanism of formation, which includes a high temperature to low temperature transition between indialite and cordierite (see Rakovan *et al.*, 2006, and the papers cited therein). If we concentrate on the known

Chemical and growth zoning in trapiche tourmaline from Zambia — a re-evaluation

	emerald	ruby	tourmaline
core	basal pinacoid	basal pinacoid	different trigonal pyramids
rim	hexagonal prism	hexagonal dipyramid	hexagonal prism and/or trigonal prism

gem materials with trapiche patterns, i.e. emerald, ruby and tourmaline, we always have materials subdivided in growth zones related to a core and a rim. The equivalent faces of these growth zones are given above.

The most significant visual difference is the subdivision of the core of trapiche tourmalines into three different sectors, whereas the cores of emerald and rubies normally consist of a single hexagonally outlined area.

The formation of Colombian trapiche emeralds (Table IV) has been described as a process in which first the transparent core and then the rim (consisting of the six transparent sectors separated by non-transparent arms) were grown (McKague, 1964; Nassau and Jackson, 1970 a,b).

This mechanism does not explain the tapered form of the transparent core and the different orientations of the fibrous texture of the core and the rim (see Figure 23 by Bernauer, 1926). In addition, it is not clear how a rare type of trapiche emerald with opaque tapered core (as proposed by Nassau and Jackson from their observation and literature data) was formed. If the tapered form of the core and the growth planes within the outer trapezohedral areas as well as the orientation of fibrous textures indicate basal and prismatic growth sectors, a growth in several growth steps with the subsequent formation of the core and the six sectors of the rim is rather unlikely.

Trapiche rubies from Myanmar were extensively studied in basal slices and thin sections (see Table IV), but only limited information is available from slices or sections parallel to the *c*-axis. Within the arms of the six-rayed star, ruby zones with distinctly lower chromium contents compared to the higher chromium contents of the trapezohedral ruby sectors were analysed. Thus, a dendritic (skeletal) growth of the arms and a subsequent growth of the transparent trapezohedral ruby sectors were suggested by Sunagawa

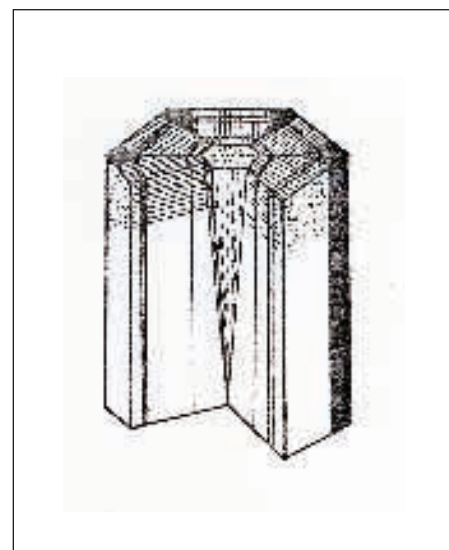
et al. (1999).

However, the growth sectors representing the different red, black or yellow cores of trapiche rubies and the transitions between these parts within the same sample were not resolved clearly (see Schmetzer *et al.*, 1996, 1998; Sunagawa *et al.*, 1999). In particular, it is not understood if the complex formation of non-trapiche rubies from Mong Hsu with subsequent red and black cores parallel to the *c*-axis as described by Peretti *et al.* (1995) is part of the formation of the differently coloured cores of the trapiche rubies from this occurrence.

The compositional zoning of the uvite-dravite tourmalines described in this paper and the geometrical pattern of a core consisting of pyramidal and prismatic growth sectors both separated by trapiche boundaries makes the possibility that a partial core (consisting only of pyramidal growth sectors) grew first, followed by a rim consisting of prismatic growth sectors very unlikely. The complex chemical zoning within all growth sectors of these tourmalines shows a successive, layer-by-layer growth from a calcium- and magnesium-rich uvite towards a sodium- and aluminium-rich dravite.

The presence of mineral grains and fluid inclusions at the margins of different growth sectors and in the less transparent areas of the crystals is apparent. The formation of fluid filled channels originating from these inclusions with an orientation perpendicular to the growing crystal face is consistent with the description of a similar mechanism of channel formation in tourmaline as described by Slivko (1966).

A sodium- and aluminium-rich dravite with a composition different from the tourmaline forming the larger transparent growth sectors was found in all non-transparent boundaries between different growth sectors and in the less transparent irregular growth zones of the tourmalines. Using the model of Sunagawa *et al.* (1999)



Figures 23: Schematic drawing of structural features in trapiche emerald from Colombia (from Bernauer, 1926). Fibrous textures within the tapered core are oriented parallel to the *c*-axis, and similar appearing fibrous textures within the rim are perpendicular to the external prism faces, layered growth zoning is observed within the prismatic growth sectors of the rim; the core and the six growth sectors of the rim are separated by dark non-transparent boundaries.

developed for trapiche rubies from Myanmar, this dravite is equivalent to the dendritic ruby forming the arms of trapiche rubies, and the transparent uvite-to-dravite growth sectors are equivalent to the trapezohedral growth sectors of these trapiche rubies. Consequently, the application of the model developed for trapiche rubies can explain the formation of the trapiche pattern in tourmaline from Zambia. First there was rapid skeletal growth of dravite with trapping of numerous inclusions followed by successive layer-by-layer growth of more transparent tourmaline. Starting this second generation of tourmaline growth with calcium-rich uvite, the composition slowly and continuously altered to a more sodium-rich dravite.

Acknowledgements

The authors are grateful to Prof. I. Sunagawa, Tokyo, Japan, for helpful comments and to D. Gravier, Poncin, France, who provided numerous samples of trapiche tourmaline for this research project.

Chemical and growth zoning in trapiche tourmaline from Zambia — a re-evaluation

References

- Agrosi, G., Bosi, F., Lucchesi, S., Melchiorre, G., and Scandale, E., 2006. Mn-tourmaline crystals from the island of Elba (Italy): Growth history and growth marks. *American Mineralogist*, **91**(5-6), 944–52
- Benesch, F., 1990. *Der Turmalin*. Urachhaus, Stuttgart. 380 pp
- Bernauer, F., 1926. Die sog. Smaragdsrillinge von Muzo und ihre optischen Anomalien. *Neues Jahrbuch für Mineralogie, Geologie und Paläontologie*, **54**, Beilage-Band, Abt. A, 205–42
- DelRe, N., 1994. Emerald, trapiche from a new locality. Gem Trade Lab notes. *Gems & Gemology*, **30**(2), 116–7
- Dietrich, R.V., 1985. *The tourmaline group*. Van Nostrand Reinhold Co. Inc., New York, pp. 12–15, 167–72
- Garnier, V., Ohnenstetter, D., Giuliani, G., Blanc, P., and Schwarz, D., 2002a. Trace-element contents and cathodoluminescence of “trapiche” rubies from Mong Hsu, Myanmar (Burma). *Mineralogy and Petrology*, **76**, 179–93
- Garnier, V., Ohnenstetter, D., Giuliani, G., and Schwarz, D., 2002b. Rubis trapiches de Mong Hsu, Myanmar. *Revue de Gemmologie A.F.G.*, **144**, 5–12
- Hainschwang, T., Notari, F., and Anckar, B., 2007. Trapiche tourmaline from Zambia. *Gems & Gemology*, **43**(1), 36–46
- Henderson, B., 1995. Inhibited growth of crystals. *Mineralogical Record*, **26**(3), 201–3
- Henry, D.J., and Dutrow, B.L., 1992. Tourmaline in a low grade clastic metasedimentary rock: an example of the petrogenetic potential of tourmaline. *Contributions to Mineralogy and Petrology*, **112**, 203–18
- Henry, D.J., and Dutrow, B.L., 1996. Metamorphic tourmaline and its petrologic applications. In: Grew, E.S., and Anovitz, L.M. (Eds), Boron. Mineralogy, petrology and geochemistry. Mineralogical Society of America. *Reviews in Mineralogy*, **33**, 503–57
- Henry, D.J., and Dutrow, B.L., 2001. Compositional zoning and element partitioning in nickeloan tourmaline from a metamorphosed karstbauxite from Samos, Greece. *American Mineralogist*, **86**(10), 1130–42
- Henry, D.J., Novak, M., Hawthorne, F.C., Ertl, A., Dutrow, B.L., Uher, P., and Pezzotta, F., 2011. Nomenclature of the tourmaline supergroup minerals. *American Mineralogist*, **96**(5–6), 895–613
- Kazachenko, V.T., Butsik, L.A., Sapin, V.I., Kitaev, I.V., Barinov, N.N., and Narnov, G.A., 1993. Vanadian-chromian tourmaline and vanadian muscovite in contact-metamorphosed carbonaceous rocks, Primorye, Russia. *Canadian Mineralogist*, **31**(2), 347–56
- Khotchanin, K., Thanasuthipitak, K., and Thanasuthipitak, T., 2009. The structure and chemical composition of trapiche blue sapphire from Southern Vietnam and Cambodia. *Journal of the Gemmological Association of Hong Kong*, **30**, 25–35
- Koivula, J.I., 2008. Two unusual aquamarines. *Gems & Gemology*, **44**(3), 275–6
- Kundt, A., 1883. Ueber eine einfache Methode zur Untersuchung der Thermo-, Actino- und Piëzoelectricität der Krystalle. *Wiedemanns Annalen der Physik und Chemie, Neue Folge*, **20**, 592–601
- Liu, G., and Lu, H., 1986. Fluid inclusion study of gem tourmaline from Xinjiang, China. *Geochemistry*, **5**(3), 234–40
- Lussier, A.J., and Hawthorne, F.C., 2011. Oscillatory zoned liddicoatite from Anjanabonoina, Central Madagascar. II. Compositional variation and mechanisms of substitution. *Canadian Mineralogist*, **49**(1), 89–104
- Lussier, A.J., Hawthorne, F.C., Herwig, S., Abdu, Y., Aguiar, P.M., Michaelis, V.K., and Kroeker, S., 2008. Mushroom elbaite from the Kat Chay mine, Momeik, near Mogok, Myanmar: II. Zoning and crystal growth. *Mineralogical Magazine*, **72**(5), 999–1010
- McKague, H.L., 1964. Trapiche emeralds from Colombia. *Gems & Gemology*, **11**(7), 210–13, 223
- Nassau, K., and Jackson, K.A., 1970a. Trapiche emeralds from Chivor and Muzo, Colombia. *American Mineralogist*, **55**(3-4), 416–27
- Nassau, K., and Jackson, K.A., 1970b. Trapiche emeralds from Chivor and Muzo, Colombia: Nature and origin. *Lapidary Journal*, **24**(1), 82–6
- Novák, M., Henry, D.J., Hawthorne, F.C., Ertl, A., Uher, P., Dutrow, B.L., and Pezzotta, F., 2009. Nomenclature of the tourmaline-group minerals. Report of the subcommittee on tourmaline nomenclature to the International Mineralogical Association's Commission on New Minerals, Nomenclature and Classification, 45 pp (unpublished draft)
- Ohnenstetter, D., Giuliani, G., and Bustos, O., 1998. Émeraudes trapiches colombiennes. In: Giard, D. et al. (Eds), *L'Émeraude. Connaissances actuelles et perspectives futures*. Livre Edition, Association Française de Gemmologie, Paris, 119–24
- Peretti, A., Schmetzer, K., Bernhardt, H.-J., and Mouawad, F., 1995. Rubies from Mong Hsu. *Gems & Gemology*, **31**(1), 2–26
- Petres, I., 1974. The divided structure of crystals. *Neues Jahrbuch für Mineralogie Abhandlungen*, **122**(3), 314–38
- Rakovan, J., Kitamura, M., and Tamada, O., 2006. Sakura Ishi (Cherry Blossom Stones): Mica pseudomorphs of complex cordierite-indialite intergrowths from Kameoka, Kyoto Prefecture, Japan. *Rocks & Minerals*, **81**, 284–92
- Rustemeyer, P., 2003. *Faszination Turmalin*. Formen, Farben, Strukturen. Spektrum Akademischer Verlag, Berlin. 310 pp
- Schiffman, C.A., 1968. Unusual emeralds. *Journal of Gemmology*, **11**(4), 105–14
- Schiffman, C.A., 1969. Unusual emeralds. *Lapidary Journal*, **23**(6), 828–31
- Schmetzer, K., Bernhardt, H.-J., Dunaigre, C., and Krzemnicki, M.S., 2007.

Chemical and growth zoning in trapiche tourmaline from Zambia — a re-evaluation

- Vanadium-bearing gem-quality tourmalines from Madagascar. *Journal of Gemmology*, **30**(7/8), 413–33
- Schmetzer, K., Hänni, H.A., Bernhardt, H.-J., and Schwarz, D., 1996. Trapiche rubies. *Gems & Gemology*, **32**(4), 242–50
- Schmetzer, K., and Schwarz, D., 2000. Trapiche ruby: an update. *Gems & Gemology*, **36**(2), 168–169
- Schmetzer, K., Zhang, B., Gao, Y., Bernhardt, H.-J., and Hänni, H.A., 1998. Element mapping of trapiche rubies. *Journal of Gemmology*, **26**(5), 289–301
- Slivko, M.M., 1966. Repulsion and capture of solid particles by growing tourmaline crystals. In: Grigoriev, D.P. (Ed.) *Genezis Mineralnych Individov i Agregatov*. Akademija Nauk SSSR, pp 116–21 (in Russian)
- Sperlich, R., Gierè, R., and Frey, M., 1996. Evolution of compositional polarity and zoning in tourmaline during prograde metamorphism of sedimentary rocks in the Swiss Central Alps. *American Mineralogist*, **81**(9-10), 1222–36
- Sunagawa, I., Bernhardt, H.-J., and Schmetzer, K., 1999. Texture formation and element partitioning in trapiche ruby. *Journal of Crystal Growth*, **206**, 322–30
- Takahashi, Y., and Sunagawa, I., 1998. Tourmaline: morphological and compositional variations during the history of uvite single crystals. *Journal of Gemmology*, **26**(4), 226–37
- Tripp, E.J., and Hernandez, L.H., 1970. The complete trapiche emerald picture. *Lapidary Journal*, **24**(1), 97–104
- Van Hinsberg, V.J., Schumacher, J.C., Kearns, S., Mason, P.R.D., and Franz, G., 2006. Hourglass sector zoning in metamorphic tourmaline and resultant major and trace-element fractionation. *American Mineralogist*, **91**(5-6), 717–28
- Vergilov, Z., and Kostova, B., 2000. Composition, anatomy and growth mechanism of tourmalines from Vitosha pegmatites. *Annuaire de l'Universite de Sofia "St. Kliment Obriidski", Faculte de Geologie et Geographie, Livre 1 – Geologie*, **92**, 105–19
- Win, K.K., 2005. Trapiche of Myanmar. *Australian Gemmologist*, **22**(6), 269–70
- Wöhrmann, B., 2002. Cut longitudinally with drafting pen and paint brush. In: Falster, A.U., *et al.* (Eds), Tourmaline, a gemstone spectrum. *ExtraLapis English*, **3**, 34–8
- Zang, J., Falster, A.U., and Simmons, W.B., 2002. News about the star. In: Falster, A.U., *et al.* (Eds), Tourmaline, a gemstone spectrum. *ExtraLapis English*, **3**, 39–41

The Authors

Dr Karl Schmetzer

Taubenweg 16, 85238 Petershausen, Germany
 Email: SchmetzerKarl@hotmail.com

Dr Heinz-Jürgen Bernhardt

ZEM, Institut für Geologie, Mineralogie und Geophysik, Ruhr-University,
 D-44780 Bochum, Germany
 Email: Heinz-Juergen.Bernhardt@rub.de

Thomas Hainschwang

GGTL Laboratories, Gemlab (Liechtenstein)/GemTechLab, FL 9496 Balzers,
 Liechtenstein/CH 1227 Geneva, Switzerland
 Email: thomas.hainschwang@ggtl-lab.org

Untreated yellowish orange sapphire exhibiting its natural colour

J.M. Duroc-Danner, Dip. IUED, DUG, FGA, GG

Abstract: Orange sapphires of natural colour are rather rare. A 3.85 ct sapphire recently submitted for identification was confirmed as natural using conventional gemmological equipment and infrared spectrometry. Colour zoning, inclusions and twinning are described and compared with the features shown by synthetic sapphires.

Keywords: colour zoning, heat treatment, inclusions, infrared spectra, orange sapphire, synthetic



Introduction

Recently, the author received a 3.85 ct pear-shaped yellowish orange gemstone, measuring 11.38 × 9.55 × 4.88 mm, for identification (*Figure 1*).

The refractive index (RI) determinations were carried out using a Rayner Dialdex critical angle refractometer with the use of a polarizing filter and monochromatic sodium light. Using the table facet, the stone was rotated every 45° and the indices recorded until a rotation of 180° was reached. The indices obtained showed two constant and parallel shadow edges, 1.762 and 1.770 (birefringence 0.008), proving the stone uniaxial, with its table facet cut perpendicular to the optic axis. A polarizing filter is needed to obtain the optic sign (Sturman and Parker, 2010), and this was checked by testing one of the pavilion facets, under the same working conditions, this gave $\epsilon = 1.762$, $\omega = 1.770$, optic sign U/-.

To confirm the uniaxial nature of the stone, it was examined table down in a Gem Illuminator Polariscope, set to its dark position (where the vibration

directions of the polarizer and analyser are perpendicular to one another) and with a conoscope placed on the stone's pavilion; a uniaxial interference figure could be seen.

The specific gravity (SG) was obtained by hydrostatic weighing of the stone, employing a Mettler PL 300c electronic balance (accuracy ± 0.001 ct) with SG attachments. The SG is 3.99.

The pleochroism observed through the pavilion with a Rayner calcite dichroscope was very weak with a small range from yellow orange to slightly darker yellow orange.

The absorption spectrum seen through a Gem Beck Spectroscope Unit, showed no lines in the blue portion of the visible spectrum, but lines in the red at 660 and 680 nm.

A faint uneven dark apricot fluorescence could be seen with a Multispec combined LW/SW unit.

These physical properties correspond to those of corundum, yellowish orange sapphire, so to determine whether it was natural or synthetic, treated or untreated, further testing was necessary.

Distinguishing natural from synthetic corundum

Synthetic corundum was first obtained by M.A. Gaudin in 1837 by the Verneuil flame-fusion process (Bourgeois, 1884); this was followed by J. Czochralski in 1918 using the pulling method (Elwell, 1979), later by C.C. Chatham and F.T. Brown by flux fusion in the mid 1960s (Nassau, 1980) and more recently by Taurus using hydrothermal synthesis in the 1990s (Koivula *et al.*, 2000).

To test whether this orange yellow sapphire was synthetic, the stone was examined under a Bausch & Lomb Mark V Gemolite binocular microscope using dark field illumination or overhead lighting as appropriate. It revealed immediately under the table facet, broad parallel straight growth zonal striae lying in different planes, crossing each other at angles (*Figure 2*). Numerous clouds of exsolved substances are aligned with these zonal striae and are responsible for

Figure 1 (above): Pear-shaped yellowish orange sapphire of 3.85 ct. Magnification 10×.

Untreated yellowish orange sapphire exhibiting its natural colour



Figure 2: Broad parallel straight growth zonal striae lying in different planes and crossing each other at angles. Dark field illumination, magnification 15x.

the 'sleepy' appearance of the stone. Lying in the bottom of the pavilion, parallel to a basal pinacoid is a tiny 'feather' consisting of very fine acicular droplets (Figure 3). Polysynthetic twin lamellae (Figure 4) are visible with the stone immersed in ethyl alcohol between crossed polaroids.

These inclusions exclude Verneuil and Czochralski synthesis which display curved colour and growth banding (Gübelin and Koivula, 1986, 2008), often in the company of rounded gas bubbles with notably bold edges (although there is polysynthetic twinning in some Verneuil synthetics; Duroc-Danner, 1985).

In contrast, the most common inclusions in flux-grown sapphires are twisted veils of flux resembling net curtains or veils blowing in the wind (O'Donoghue, 2005; Gübelin and Koivula, 1986). While hexagonal, herring-bone or sets of straight growth bands forming an angle can occur in flux-grown synthetics, their synthetic origin can be ascertained by crystallographic investigation of structural features such as morphology and growth components. Straight parallel

growth planes of the second-order hexagonal prism as well as growth planes parallel to different second-order hexagonal dipyrramids (with the exception of n ($2\bar{2}43$)), do not appear in this type of synthesis (Schmetzer, 1986; Kiefert and Schmetzer, 1988, 1991). Occasionally one encounters inclusions of angular platelets of metallic appearance, often triangular or hexagonal in shape, but also in other forms such as needles. These originate from the platinum crucible in which the corundum is grown and have not been encountered in natural corundum (Gübelin and Koivula, 1986).

Hydrothermally grown synthetic corundums usually show fluid inclusions composed at room temperature of H_2O (liquid), H_2O (vapour) and carbonate solid daughter minerals (such as $CaCO_3$ and $KHCO_3$), while the fluid inclusions found in the natural counterparts (including the heat-treated ones) are composed of CO_2 -rich compositions with completely different reactions to heating and freezing. By studying these reactions, it is therefore possible to identify this type of synthetic (Peretti *et al.*, 1997). Roiled-to-angular growth structures, sometimes described as chevron-spaced, and scattered flake-like 'breadcrumbs' can also occur (Renfro *et al.*, 2010). Solid inclusions are sometimes also observed, consisting of copper alloys, derived from the steel autoclave (copper inclusions have not yet been observed in natural corundum). Hydrothermally produced yellow, green, blue-green and blue synthetic sapphires owe their colour only to nickel, whereas blue-violet to violet orange and reddish-orange synthetic

hydrothermal sapphires are coloured by traces of both chromium and nickel, while the three main causes of colour in natural corundum are due to colour centres or Fe^{3+} for yellow sapphires; Fe^{2+}/Ti^{4+} ion pairs with or without additional Fe^{2+}/Fe^{3+} pairs, for blue to violet sapphires; and Cr^{3+} for rubies (Schmetzer and Peretti, 1999, 2000).

Magmatic or metamorphic corundum

Corundum can be of two different types:

- Magmatic yellowish orange sapphires owe their colour chiefly to Fe^{2+}/Fe^{3+} , Fe^{3+} and Fe^{3+}/Fe^{3+} , and to a lesser degree to IVCT $Fe^{2+} \rightarrow Ti^{4+}$, with high Ga^{3+} and minor Cr^{3+} .
- Metamorphic yellowish orange sapphires can owe their colour partially or wholly to trapped-hole centres, or mainly to Fe^{3+} , Fe^{3+}/Fe^{3+} , with sometimes minor IVCT $Fe^{2+} \rightarrow Ti^{4+}$, added to some Mg^{2+} and Cr^{3+} (F.L. Sutherland pers. comm., 2011; Schmetzer and Schwarz, 2005).

Some magmatic sapphires may be transported as xenocrystic passengers by basalt and brought to the surface from depths of up to 100 km (Keller, 1990, p.71) during volcanic eruptions. The infrared spectra of these magmatic sapphires show a peak at ± 3309 cm^{-1} , which is not present in natural metamorphic sapphires, nor in all (non-heat treated) synthetic sapphires except those issued from the Verneuil flame-fusion syntheses; this is due (as for peaks

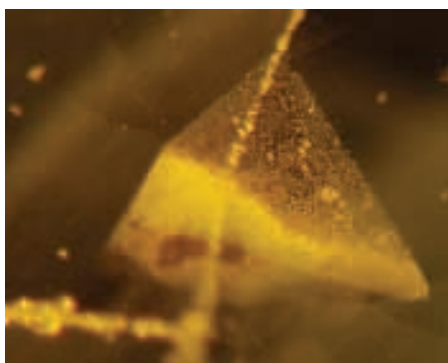


Figure 3: Tiny 'feather' consisting of very fine acicular droplets. Dark field illumination, magnification 30x.

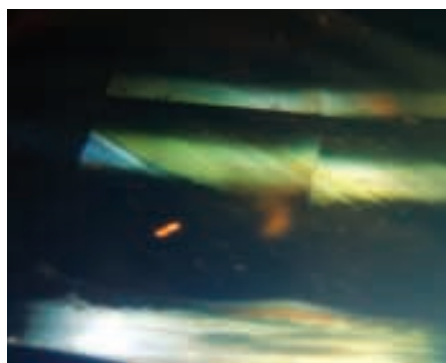
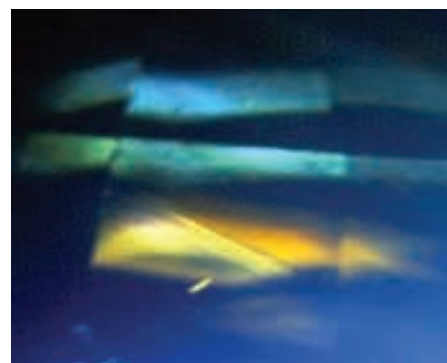


Figure 4: Polysynthetic twin lamellae, stone immersed in ethyl alcohol, between crossed polaroids, magnification 20x.



Untreated yellowish orange sapphire exhibiting its natural colour

$\pm 3295 \text{ cm}^{-1}$, $\pm 3232 \text{ cm}^{-1}$, and $\pm 3185 \text{ cm}^{-1}$) to a OH-dipole linked to atoms of iron and titanium in the corundum structure. The peak $\pm 3366 \text{ cm}^{-1}$ is due to OH clusters linked to a titanium atom (Duroc-Danner, 2002).

The FTIR spectrum in the mid-infrared region between 4000 and 2100 cm^{-1} of the yellowish orange sapphire is shown in *Figure 5*. There is a strong absorption in the range $2300\text{--}1700 \text{ cm}^{-1}$, a 3161 cm^{-1} peak, accompanied by peaks at 3240 cm^{-1} and 3354 cm^{-1} .

The 3161-series occurs most commonly in natural-colour yellow-to-orange and padparadscha sapphires from low-iron metamorphic environments, which owe their colour partially or wholly to trapped-hole centres. LA-ICP-MS chemical data and heating experiments suggest that the 3161-series is actually due to structurally bonded OH associated with Mg^{2+} (Smith and Van der Bogert, 2006).

The absence of a 3309 cm^{-1} peak (location indicated on *Figure 5*), also confirms that this yellowish orange sapphire is of non-magmatic origin (probably metamorphic) and has not suffered heat-treatment.

Natural colour versus beryllium treated corundum

Heat-treatment of corundum, with more or less colour improvement occurred in Sri Lanka around the second century AD, and is still performed today. Corundums were embedded in an open charcoal fire and air was blown through a bamboo pipe to raise the temperature



Figure 6: Straight angular yellow zoning alternating with colourless areas. Immersed in ethyl alcohol, magnification $10\times$.

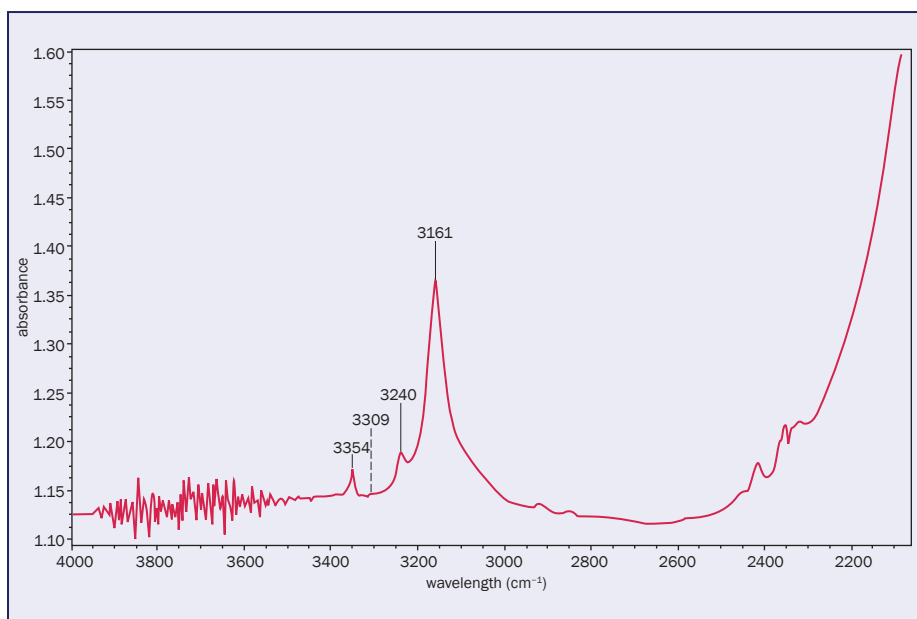


Figure 5: FTIR spectrum showing the 3161 cm^{-1} series of peaks due to structurally bonded OH associated with Mg^{2+} , and the absence of a 3309 cm^{-1} peak (indicated on the spectrum to show its location).

up to 1000°C (Gunaratne, 1981; Hughes, 1988; Themelis, 1992, pp 113–14; Notari and Grobon, 2002).

More modern heat-treatment techniques were discovered apparently in the 1960s (translucent milky white Geuda sapphires from Sri Lanka transformed by atmosphere-controlled high temperatures around 1500°C into transparent richly coloured sapphires). Diffusion-treated corundum which first appeared on the world market in the late 1970s (heating in the range 1800°C with addition of colour-causing elements such as titanium results in a thin outer layer of saturated blue in otherwise colourless or pale coloured sapphire) produced dramatic results when compared with the subtle changes of the past (Kane *et al.*, 1990; Emmett *et al.*, 2003).

More recently, in late 2001, beryllium-diffused treated rubies and sapphires were produced (heating the corundum to around 1800°C with the beryllium obtained, for example, by crushed chrysoberyl, BeAl_2O_4). The reaction penetrates the entire sapphire to impart relatively homogeneous yellow-to-orange hues, although early examples of this treatment could be recognized when the stone was immersed in methylene iodide or ethyl alcohol by the presence of a

colour zone that conforms to the external faceted shape of the stone (Emmett *et al.*, 2003). As can be seen in *Figure 6*, when immersed in ethyl alcohol the present yellowish orange sapphire has a colour distribution of angular yellow zoning alternating with colourless areas, which is characteristic of natural growth origin (Hurwit, 1987).

Discussion

Standard gemmological properties, such as RI, optic character and sign, and SG, confirm that the stone is corundum, variety yellowish orange sapphire, but do not help in determining whether it is natural or synthetic.

Nowadays at least four kinds of process are used worldwide on a commercial basis to produce synthetic corundum, and the products are becoming more sophisticated, thus posing a real challenge to the unwary jeweller:

- Verneuil inverted blow-pipe process (Hrand Djévahirdjian S.A., Switzerland; Union Carbide, U.S.A.; Nakazumi Earth Crystals, Japan; Wiedes Carbidwerke Freyung, Germany; etc).
- Czochralski (pulling) growth technique (Union Carbide, U.S.A.; Deltronics, New Jersey, U.S.A.; Crystal

Untreated yellowish orange sapphire exhibiting its natural colour

- Optics Research, California, U.S.A.; Kyocera International Inc., Japan; etc).
- Flux fusion growth technique (C.C. Chatham, California; Douros, Greece; J. Osmer Crystals Co., California, U.S.A.; Kashan Inc., Texas, U.S.A.; P.O. Knischka, Austria; J. Lechleitner, Austria; etc).
 - Hydrothermal growth process (Tairus Co., Thailand and Russia; etc).
- Also most natural corundums in the gem market are heat-treated between 1000° and 1500°C. Additionally, some are diffusion-treated with colour-causing elements such as titanium (Ti) or more recently beryllium (Be), which can be detected using Secondary Ion Mass Spectrometry (SIMS) or Laser Ablation-Inductively Coupled Plasma-Mass Spectrometry (LA-ICP-MS).

The present yellowish orange sapphire was identified with conventional gemmological equipment and infrared spectroscopy, so recourse to the expensive SIMS or LA-ICP-MS facilities was not necessary.

The inclusions and internal characteristics point towards a natural stone devoid of heat-treatment (Panjekar and Panjekar, 2011).

The FTIR spectrum not only confirmed that the stone was not heat-treated, but also established its non-magmatic origin (probably metamorphic).

The faint uneven dark apricot luminescence to ultraviolet radiation provided helpful indications for non-Be-diffusion treatment since Be-diffused areas usually fluoresce a distinctive homogeneous orange (Notari *et al.*, 2003). This indication is also consistent with the angular yellow zoning alternating with colourless areas, which is characteristic of natural origin.

References

- Bourgeois, M.L., 1884. *Reproduction artificielle des minéraux*. Dunod, éditeur, Paris, 62–5
- Duroc-Danner, J.M., 1985. Polysynthetic twin lamellae in synthetic Verneuil sapphire. *Journal of Gemmology*, **19**(6), 479–83
- Duroc-Danner, J.M., 2002. *A study of Colombian corundum*. Diplôme d'Université de Gemmologie de Nantes, 217 pp
- Elwell, D., 1979. *Man-made gemstones*. Ellis Horwood Ltd., Chichester. 52–7
- Emmett, J.L., Scarratt, K., McClure, S.F., Moses, T., Douthit, T.R., Hughes, R., Novak, S., Shigley, J.E., Wang, W., Bordelon, O., and Kane, R.E., 2003. Beryllium diffusion of ruby and sapphire. *Gems & Gemology*, **39**(2), 84–135
- Gübelin, E.J., and Koivula, J.I., 1986. *Photoatlas of Inclusions in Gemstones*. ABC Verlag, Zürich. 532 pp
- Gübelin, E.J., and Koivula, J.I., 2008. *Photoatlas of Inclusions in Gemstones*. 3. Opinio Publishers, Basel. 672 pp
- Gunaratne, H.S., 1981. "Geuda sapphires" — Their colouring elements and their reaction to heat. *Journal of Gemmology*, **17**(5), 292–300
- Hughes, R.W., 1988. Identifying yellow sapphires – two important techniques. *Journal of Gemmology*, **21**(1), 23–5
- Hughes, R.W., 1997. *Ruby and Sapphire*. RWH Publishing, Boulder, CO. 511 pp
- Hurwit, K.N., 1987. Heat-treated yellow sapphire. Gem Trade lab notes. *Gems & Gemology*, **23**(3), 167
- Kane, R.E., Kammerling, R.C., Koivula, J.I., Shigley, E., and Fritsch, E., 1990. The identification of blue diffusion-treated sapphires. *Gems & Gemology*, **26**(2), 115–33
- Keller, P.C., 1990. *Gemstones and their origins*. Van Nostrand Reinhold, New York, 144 pp
- Kiefert, L., and Schmetzer, K., 1988. Morphology and twinning in Chatham synthetic blue sapphire. *Journal of Gemmology*, **21**(1), 16–22
- Kiefert, L., and Schmetzer, K., 1991. The microscopic determination of structural properties for the characterization of optical uniaxial natural and synthetic gemstones. Part 3: Examples for the applicability of structural features for the distinction of natural and synthetic sapphire, ruby, amethyst and citrine. *Journal of Gemmology*, **22**(8), 471–82
- Koivula, J.I., Tannous, M., and Schmetzer, K., 2000. Synthetic gem materials and simulants in the 1990s. *Gems & Gemology*, **36**(4), 360–79
- Notari, F., and Grobon, C., 2002. *Gemmologie du corindon et du spinelle*. Minéraux et Fossiles, Paris, Hors-série No.15, 48–59
- Notari, F., Fritsch, E., and Grobon, C., 2003. Comment l'observation de la luminescence (fluorescence) peut aider à l'identification des corindons jaunes, rose orangé et orange, traités par diffusion de béryllium. *Revue de Gemmologie A.F.G.*, 148, 40–3
- Nassau, K., 1980. *Gems made by man*. Chilton Book Company, Radnor, Pennsylvania, 83
- O'Donoghue, M., 2005. *Artificial gemstones*. NAG Press, London, 109–42
- Panjekar, J., and Panjekar, A., 2011. *Importance of various "feather type" inclusions for the identification of natural, treated, synthetic and treated-synthetic yellow sapphire*. 32nd IGC Abstracts, 85–8
- Peretti, A., Mullis, J., Mouawad, F., and Guggenheim, R., 1997. Inclusions in synthetic rubies and synthetic sapphires produced by hydrothermal methods (Tairus, Novosibirsk, Russia). *Journal of Gemmology*, **25**(8), 541–61
- Renfro, N., Koivula, J.I., Wang, W., and Roskin, G., 2010. Synthetic gem materials in the 2000s: A decade in review. *Gems & Gemology*, **46**(4), 260–73
- Schmetzer, K., 1986. An improved sample holder and its use in the distinction of natural and synthetic ruby as well as natural and synthetic amethyst. *Journal of Gemmology*, **20**(1), 20–33
- Schmetzer, K., and Peretti, A., 1999. Some diagnostic features of Russian hydrothermal synthetic sapphires. *Gems & Gemology*, **35**(1), 17–28

Untreated yellowish orange sapphire exhibiting its natural colour

- Schmetzer, K., and Peretti, A., 2000.
Characterization of a group of experimental Russian hydrothermal synthetic sapphires. *Journal of Gemmology*, **27**(1), 1–7
- Schmetzer, K., and Schwarz, D., 2005. A microscopy-based screening system to identify natural and treated sapphires in the yellow to reddish-orange colour range. *Journal of Gemmology*, **29**(7), 407–49
- Smith, C.P., and Van der Bogert, C., 2006. Infrared spectra of gem corundum. *Gems & Gemology*, **42**(3), 92–3
- Sturman, D.B., and Parker, D., 2010. Use of the polarizing filter on the refractometer in determination of the optic sign or optic character of a gemstone. *Journal of Gemmology*, **31**(1–4), 90–100
- Themelis, T., 1992. *The heat treatment of ruby and sapphire*. Gemlab Inc., U.S.A., 236 pp

The Author

J.M. Duroc Danner

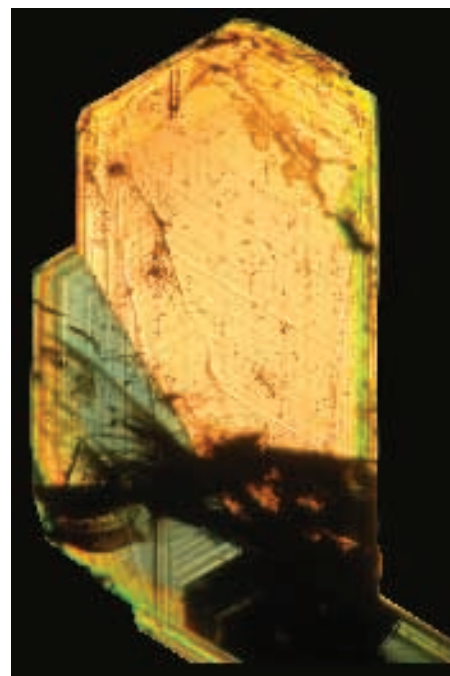
Geneva, Switzerland

e-mail: durocdanner22@bluewin.ch

Alexandrite and colour-change chrysoberyl from the Lake Manyara alexandrite-emerald deposit in northern Tanzania

Dr Karl Schmetzer and Anna-Kathrin Malsy

Abstract: Mineralogical and gemmological properties of alexandrite from the Mayoka deposit, Lake Manyara mining area, Tanzania, are described. The alexandrite crystals are located in a phlogopite-bearing schist which is part of a metamorphic-metasomatic association of mafic or ultramafic rocks in contact with pegmatitic intrusions. Emeralds are associated with the pegmatites. Single crystals, contact twins, penetration twins and cyclic twins (trillings) are all present in this area and are developed in two major habits, one tabular parallel to the *a* pinacoid and the other columnar along the *a*-axis. Microscopic features of faceted and rough alexandrites are characterized by internal growth structures reflecting the external morphology of the samples. Common mineral inclusions are phlogopite, apatite and zircon. Associated with series of channels parallel to the *a*-axis three groups of elongated or tabular negative crystals oriented in a plane parallel to the *a* pinacoid form milky white zones in some samples. The complexity of alexandrite colours is clarified to some extent by correlation of colorimetric parameters with trace element contents and with the orientation of the alexandrites. The designation of samples as alexandrites and a possible distinction from colour-change chrysoberyl is discussed. Alexandrite and green chrysoberyl from Lake Manyara is compared with samples from other occurrences in phlogopite-bearing schist such as the 'classical' alexandrite deposits in the Urals, Russia, and from Novello, Zimbabwe.



*Irregular alexandrite twin from Lake Manyara, Tanzania; view parallel to the *a*-axis, immersion, crossed polarizers, field of view 6.5 × 4.9 mm. Photo by K. Schmetzer.*

Historical background

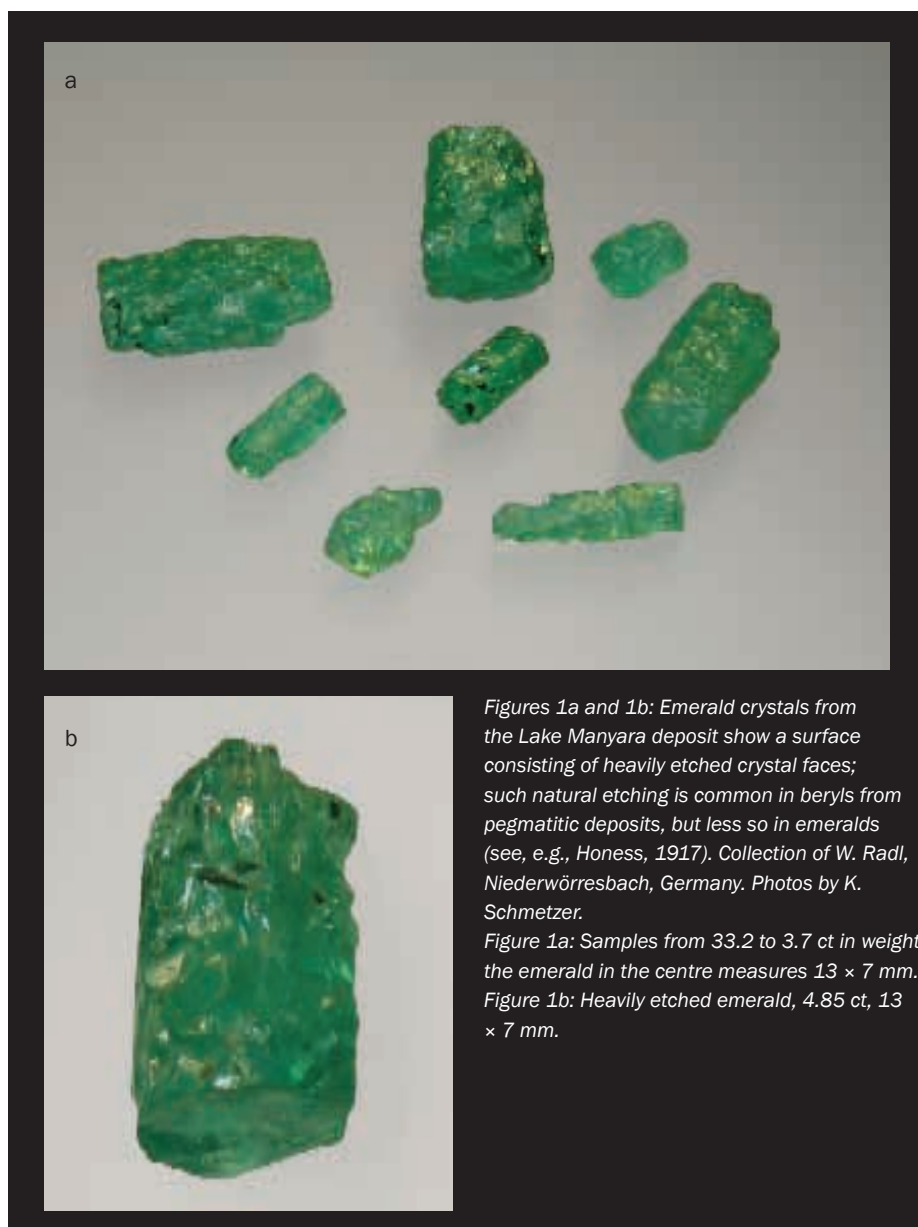
The first emeralds originating from the Lake Manyara alexandrite-emerald deposit were discovered in 1968 or 1969 by local residents and after some time appeared in Arusha, in northeastern Tanzania, where they were seen by the prospector Hans Kristen. He and some of his group were able to trace the emeralds back to a place called Maji Moto (hot springs) in the Lake Manyara area. In February 1970,

after months of prospecting activities, they finally discovered the primary deposit on the western bank of Lake Manyara. The mining rights were given to and the mine was exploited by Galai Mining Company Ltd., headed by George 'Papas' Papaeliopoulos (also spelled in the literature Papaleoupoulos, Papadopoulos) until 1973. Within this period, more than 100 workers were employed in the mine yielding more than 200 kilos of emerald

(July 1970 to April 1972). In contrast, an official report by Mwakisunga (1972 a,b), a geologist who examined the mining area from July to September 1972 for Tanzania Gemstone Industries Ltd, a subsidiary of the State Mining Corporation, mentioned only the possible occurrence of gem materials in the mine and no commercial production.

In February 1973, the activities of Galai Mining Company were stopped by

Alexandrite and colour-change chrysoberyl from the Lake Manyara alexandrite-emerald deposit in northern Tanzania



Figures 1a and 1b: Emerald crystals from the Lake Manyara deposit show a surface consisting of heavily etched crystal faces; such natural etching is common in beryls from pegmatitic deposits, but less so in emeralds (see, e.g., Honess, 1917). Collection of W. Radl, Niederwöresbach, Germany. Photos by K. Schmetzer.
 Figure 1a: Samples from 33.2 to 3.7 ct in weight, the emerald in the centre measures 13 × 7 mm.
 Figure 1b: Heavily etched emerald, 4.85 ct, 13 × 7 mm.



Figure 2: These two recently found alexandrite crystals were shown to the visitors at Mayoka mine in October 2009. Photo by Willow Wight.

the Tanzanian government and the mine was nationalized. The government had decided to take over the mine because no production figures had been reported for several months and no emeralds had ever been exported officially. G. Papas was arrested and imprisoned, being accused of smuggling emeralds out of the country. The mining activities continued under the guidance of Kristen for the state-owned Manyara Emerald Co. During their stay in Tanzania in November 1973 and July 1974, E. Gübelin from Lucerne and H. Bank from Idar-Oberstein were allowed to visit the mine. They reported on a mine in full production with several dozens of labourers. In 1976 the so-called Mayoka mine was taken over by the state-owned Stamico (State Mining Company). Activities declined and finally the mine was abandoned. Prospecting work was performed in the late 1970s and early 1980s by the companies Stamico and Gemco Ltd. (for the history from the discovery of the deposit to the 1980s see Mwakisunga, 1972 a,b; Thurm, 1972, a,b,c; Bank, 1974; Gübelin, 1974, 1976; Bank and Gübelin, 1976; Viswanatha and Shah, 1983).

For almost three decades, only limited mining activity in the area by local farmers or other residents has been reported; they sporadically worked, legally or illegally, the old veins in the Mayoka mine and other pits nearby (Simonet, 1997, 2010; Werner Radl and John Saul, pers. comm., 2010, 2011). Only small parcels of gem-quality emerald (Figures 1a and 1b) or alexandrite (Figure 2) from this source reached the market.

In October 2009, participants of the International Gemmological Conference were able to visit the area and allowed to see a mine, which was operated by Charles Perfect (Coldham and Payette, 2010; Wight and Wight, 2010). The visitors were told that active mining had started only some months ago. They reported on an area with deeply weathered country rocks with darker bands, some metres wide (Figure 3), which appeared to be deeply weathered amphibolite-, actinolite- and phlogopite-bearing schist, intruded by pegmatites. These darker

Alexandrite and colour-change chrysoberyl from the Lake Manyara alexandrite-emerald deposit in northern Tanzania

rocks were indicated by the miners as possibly alexandrite-bearing or as possibly emerald-bearing veins. To find emerald (Figures 1a and 1b) or alexandrite (Figure 2), the miners follow these dark, possibly emerald- or alexandrite-bearing amphibolite-actinolite-phlogopite bands in different parts of the mine (Figures 4 and 5) and remove these darker layers from the more or less weathered lighter country rock (Anne and George Bosshart, Terry Coldham, Francine Payette, Willow and Quintin Wight, Hanco Zwaan; pers. comm., 2010, 2011).

At present (2011) the mine visited by participants of the International Gemmological Conference in 2009 is still operated by Charles Perfect, and the gem material is marketed by Sailesh Pandit of Signature Gems, Arusha, Tanzania (Werner Radl, pers. comm., 2011). The claim adjacent to this location is exploited by Emanuel Pengo (Figure 6). The term 'Mayoka' is used for both mining areas, but it is not clear to the present authors, which parts of these claims were originally covered by the claims of G. Papas in the early 1970s (see above).

The Mayoka mine was originally located close to the boundary of the Lake Manyara Game Reserve, but at least partly outside the park. Due to an expansion of the Reserve, the mining area is nowadays located completely within the park. This created a conflict (see Kondo, 2005; Nkwame, 2009) which was settled in December 2010 by a Tanzanian court allowing the continuation of mining activities in the main Lake Manyara

Figure 3 : Detailed view of the deeply weathered country rock traversed by darker bands of what appear to be actinolite-phlogopite-bearing zones or layers, mostly some metres wide. These bands were indicated by the miners at Mayoka mine as either alexandrite- or emerald-bearing veins. Photo by Quintin Wight.

Figure 4 : 'Emerald adit' at Mayoka mine with miner removing the rocks of the darker emerald-bearing vein from the surrounding country rock. Photo by Francine Payette.

Figure 5 : Miner digging for alexandrite in a weathered zone of the actinolite-phlogopite schist at Mayoka mine. Photo by Willow Wight.



Alexandrite and colour-change chrysoberyl from the Lake Manyara alexandrite-emerald deposit in northern Tanzania



Figure 6: Another area next to the Mayoka mine visited by participants of the International Gemmological Conference in 2009 is exploited by E. Pengo who is using also the term 'Mayoka' for his claim. Mayoka is also the name of a small village nearby. Photo (taken in 2011) courtesy of Werner Radl.

alexandrite-emerald deposit and also for some local miners working in the area.

Formation of emerald and alexandrite

The formation of emerald and alexandrite in phlogopite-bearing host rocks was recently summarized by Schmetzer *et al.* (2011). Alexandrite and emerald are the rare green varieties of chrysoberyl (BeAl_2O_4) and beryl ($\text{Be}_3\text{Al}_2\text{Si}_6\text{O}_{18}$), respectively. Trace amounts of chromium are the principal cause of the green colours of both gem minerals and are responsible for the colour-change of alexandrite. The development of both gemstones in a rock requires the simultaneous availability of beryllium and chromium and it is not uncommon to find both minerals near to each other but not in contact. Chromium is present to some extent in ultramafic rocks, such as dunite and peridotite and their metamorphic equivalents, serpentinite and talc schist. Although beryllium is usually associated with specific types of granitic pegmatites in which it commonly occurs as beryl, it can also be derived from feldspars and other minerals independent of a

pegmatitic source.

It follows therefore that an interaction between a beryllium-rich pegmatite and an ultramafic or mafic host would provide a suitable environment for the formation of emerald and/or alexandrite, mostly in a complex metamorphic-metasomatic alteration process. The emerald occurs within and in close proximity to the pegmatite; the rarer alexandrite and chrysoberyl formed under silicon-poor conditions and occurs more distally. It need not be directly associated with the pegmatite. Deposits with a similar paragenesis, especially those containing alexandrite in phlogopite lenses or phlogopite bodies, include the Russian emerald-alexandrite-phenakite deposits in the Urals and the emerald-alexandrite occurrence from the Novello deposit, Masvingo District, Zimbabwe.

Geology of the Lake Manyara deposit, Tanzania

Several authors have mentioned that the Lake Manyara deposit belongs to the classical phlogopite-related metamorphic-metasomatic type described for the alexandrite occurrences in the Urals or in

Novello (see Box 1). The most detailed description of the country rocks found in the area and the reaction zone between ultramafic or suitable mafic rocks and pegmatite veins at the Lake Manyara deposit is in an unpublished report by Viswanatha and Shah (1983):

“The rock types within the area consist of permeated gabbroic amphibolite and meta-pyroxenite bordered on either side by banded granodioritic to granitic gneisses....The borders of the pyroxenite with the amphibolite are traversed by veins of pegmatite and quartzo-feldspathic permeations and are marked by the development of alteration zones rich in acicular bunches of actinolite and tremolite with interlocked flakes of vermiculite. Some of these pegmatites along this contact carry gem quality emerald, green aquamarine, chrysoberyl cat's-eye, alexandrite, alexandrite cat's-eye, ruby and garnet.”

A more recent summary is in another unpublished report by Simonet (1997):

“The Manyara deposit belongs to the

Box 1

In some older papers, the mica associated with emerald and alexandrite is described as biotite, but modern analyses show that most brownish micas in these alteration zones contain less iron than in biotite and, thus should be designated phlogopite. The actual analyses of some micas on rough alexandrite samples from Lake Manyara and from inclusions in faceted Lake Manyara alexandrites by the present authors gave between 7.86 and 8.57 wt% FeO. All micas analysed contained significant amounts of potassium and, thus, the samples were designated phlogopite and not vermiculite. This is consistent with the analysis of phlogopite inclusions in Lake Manyara emeralds reported by Moroz and Eliezri (1999).

Alexandrite and colour-change chrysoberyl from the Lake Manyara alexandrite-emerald deposit in northern Tanzania

category of emeralds in micaschists. Its main characteristics are the following: It is evidently associated with an alignment of altered ultrabasic bodies, which follows a big shear zone. Many pegmatite dikes have been observed and are thought to be the source of the beryllium. In one of the pits I visited, mineralizations are strikingly associated with black biotite veins, one to several meters thick, with strongly marked orientation, and surrounded by black amphibolites. Emerald is present as isolated crystals in biotitites, or in pockets associated with transparent quartz. Alexandrite appears in lumps of a whitish rock inside the emerald bearing biotitites, or associated with mica, in desilicified pegmatites."

Most other authors have described the emerald host rocks as massive biotite schists or biotite lenses and less commonly as pegmatites with emeralds occurring in these types of host rocks and especially at the contact between pegmatites and biotite schists (Thurm, 1972 a,b,c; Gübelin, 1974; Bank and Gübelin, 1976; Bridges, 1982). Mineral and fluid inclusions in Lake Manyara emeralds were examined with modern analytical methods by Moroz and Eliezri (1999) and Moroz *et al.* (2001). The P-T conditions of emerald growth are given as: T = 370-470 °C, P = 3.0-7.0 kbar.

Furthermore, alexandrite is mentioned to occur together with emerald in the biotite schist (Thurm, 1972 a,b,c), occasionally also together with emerald and ruby (Bank, 1974; Amstutz and Bank, 1977). However, the alexandrite has also been found in actinolite schist (Gübelin, 1976; Bank and Gübelin, 1976).

In summary, emeralds are found in the phlogopite and at the contact between phlogopite and pegmatite veins, while alexandrites are found in the phlogopite and within masses of deeply weathered white feldspar originating from desilicified pegmatite veins.

So far, the details described in the two unpublished reports by Viswanatha and Shah (1983) and Simonet (1997) and in



Figure 7: Alexandrite trilling in different orientations and mirrored to show habit, and faceted alexandrite from Lake Manyara, Tanzania, shown in both daylight and incandescent light; these extraordinary pieces are from the collection of W. Radl, Niederwörresbach, Germany. The trilling weighs 132 g, view almost parallel to the a-axis, size 62 x 43 mm, thickness along the a-axis 29 mm; the faceted alexandrite weighs 0.71 ct, size 4.8 x 4.7 mm. Photos and artwork by K. Schmetzer.

various other papers are not completely consistent (see also the summary of Keller, 1992, 49-59) but fit within the general concept of formation of alexandrite and emerald in a complex metamorphic-metasomatic phlogopite-bearing alteration zone formed between an intruding pegmatite and mafic or ultramafic rocks. Consequently, the Mayoka mining area close to Lake Manyara is a deposit of the same kind as those metamorphic-metasomatic deposits in the alexandrite-

emerald mining belt of the Urals, Russia, and the Novello deposit, Zimbabwe.

Scope of the present paper

Mineralogical and gemmological descriptions of alexandrite from Lake Manyara were made of a limited number of samples in the 1970s (Dunn, 1976; Gübelin, 1976; Liddicoat, 1976; Bank and Gübelin, 1976). Morphological properties of rough crystals are only briefly mentioned, and growth patterns in rough

Alexandrite and colour-change chrysoberyl from the Lake Manyara alexandrite-emerald deposit in northern Tanzania

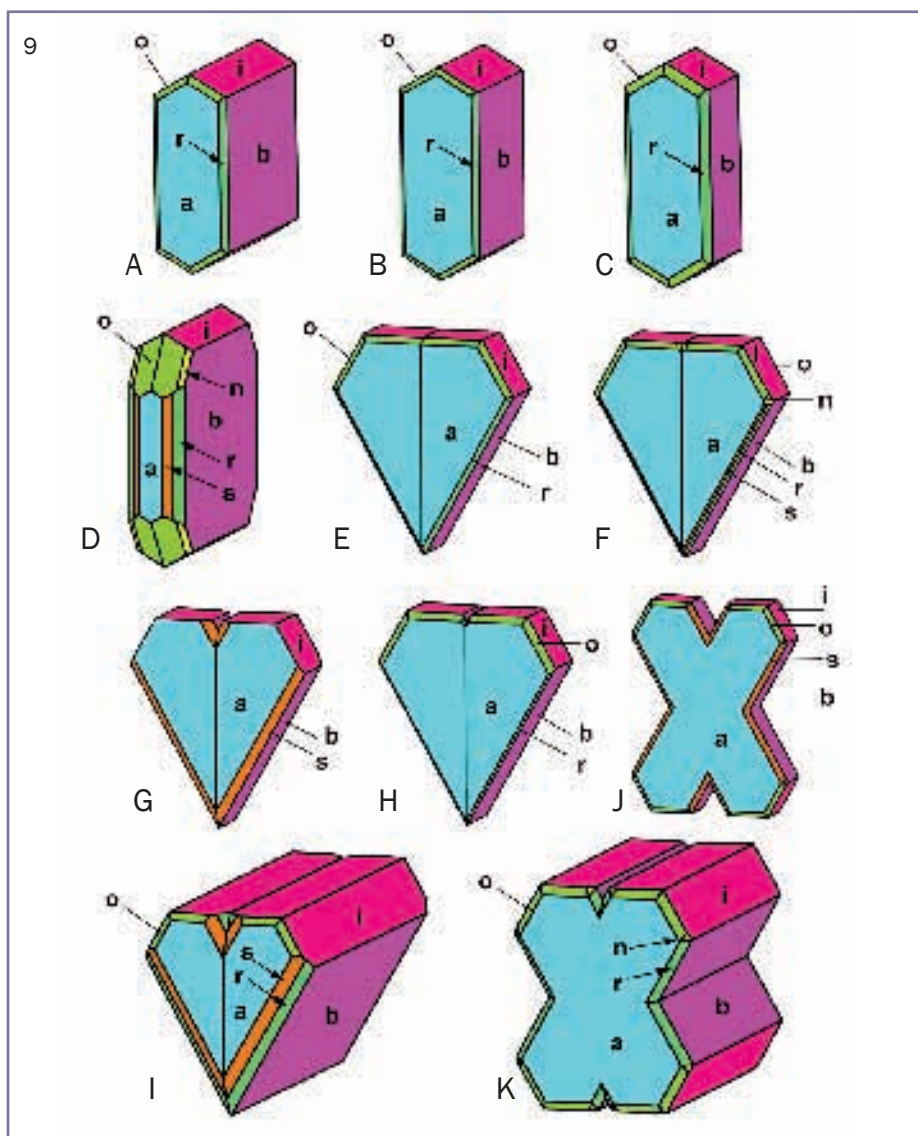
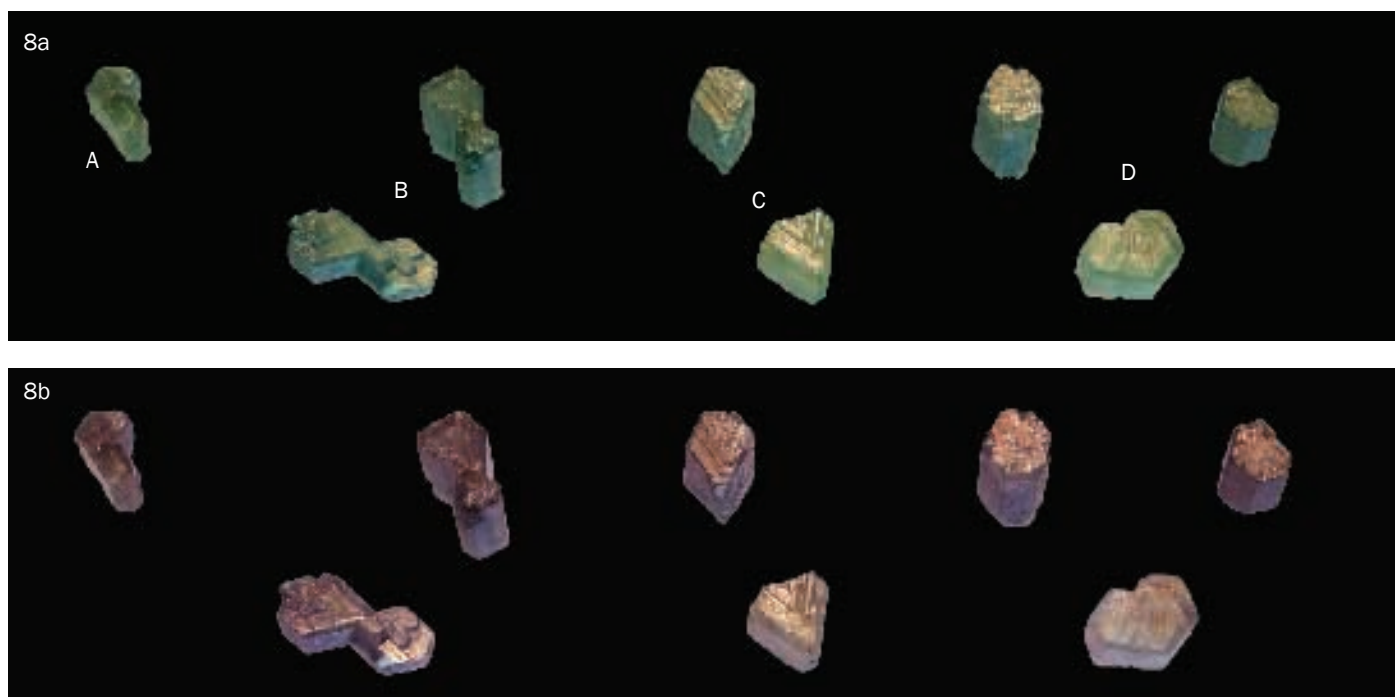


Figure 8: Alexandrite crystals from Lake Manyara, Tanzania, shown in both daylight (a) and incandescent light (b); The alexandrites are found as single crystals (A), interpenetrant twins (B), contact twins (C) or cyclic twins (trillings, D); in the upper row, the crystals show columnar habit along the crystallographic a-axis, in the lower row, the crystals show tabular habit parallel to the a pinacoid. The two interpenetrant twins (B) measure 10.0 × 6.5 mm, length along the a-axis 10.0 mm (sample in the upper row) and 14.1 × 7.5 mm, thickness along the a-axis 3.8 mm (sample in the lower row). Collections of SSEF, Basel, Switzerland (H.A. Hänni collection), and W. Radl, Niederwörresbach, Germany. Photo by K. Schmetzer.

Figure 9: Schematic drawings of alexandrites from the Lake Manyara deposit, Tanzania. Single crystals (A to D), contact twins (E to I) and interpenetrant twins (J, K) are shown. The single crystals and twins are drawn in a view parallel to the a-axis, single crystals show tabular habit parallel b (A, D) or tabular habit parallel a (B, C), twins show tabular habit parallel a (E to H, J) or columnar habit along the a-axis (I, K). Crystal drawings and artwork by K. Schmetzer.

Alexandrite and colour-change chrysoberyl from the Lake Manyara alexandrite-emerald deposit in northern Tanzania

Table I: Morphological properties of alexandrites from Lake Manyara, Tanzania.

Possible crystal forms and designation

Crystal form	Designation	Miller indices (hkl)*	Number of faces
Pinacoid	a	(100)	2
	b	(010)	2
Prism	i	(011)	4
	s	(120)	4
	r	(130)	4
Dipyramid	o	(111)	8
	n	(121)	8
	w	(122)	8

*Based on a morphological cell with a 4.42, b 9.39, c 5.47

Crystal class $2/m\ 2/m\ 2/m = D_{2h}$, single and repeated twinning on (031) and (0 $\bar{3}$ 1)

Habit of single crystals, twins and cyclic twins (trillings)

	Habit	Dominant forms	Subordinate forms	Accessory forms	Drawings in Figure
Single crystals	Tabular parallel a	a	b, i	o, r	9 C
	Tabular parallel b or columnar along a -axis	a, b, i		s, r, o, n	9 A, B, D
Contact twins	Tabular parallel a	a	b, i	s, r, o, n	9 E, F, G, H
	Columnar along a -axis	a, b, i		s, r, o, n	9 I
Penetration twins	Tabular parallel a	a	b, i	s, r, o, n	9 J
	Columnar along a -axis	a, b, i		s, r, o, n	9 K
Cyclic twins (trillings)	Tabular parallel a	a	b, i	o	14 A, B, C
	Columnar along a -axis	a, (b), i		o	14 D, E, F

or faceted samples were not reported. Analytical data for trace element contents or analytical determination of inclusions are limited. Thus, in the present account, the authors will try to fill this gap using numerous rough and faceted samples available from collectors closely associated with the Tanzanian gem trade for many years, from the reference collections of gemmological laboratories and from the gem trade.

Subsequent to the recent monograph containing detailed descriptions of the properties of alexandrite from the Uralian deposits (Schmetzer, 2010), and from the emerald-alexandrite occurrence at Novello, Zimbabwe (Schmetzer *et al.*, 2011), the current authors were also interested in comparing the mineralogical and gemmological characteristics of Lake

Manyara alexandrite with stones from the other sources mentioned. Although the general occurrence of alexandrite from these deposits in a phlogopite matrix has been discussed in the literature, a detailed comparison of their characteristic features is not available.

Research materials

In the current investigation, the authors examined more than 200 complete crystals and crystal groups as well as crystal fragments, together with some alexandrite in matrix. Furthermore, 45 faceted stones in the range of 0.15 to 3 ct were available for examination (Figure 7). The samples originated from private collections, from the reference collections of gemmological laboratories and from the

stock of several companies. The samples are drawn from stones collected over the full time scale of four decades from the discovery of the mining area in the early 1970s to the most recent production (2009). No significant differences were found between samples unearthed in different decades within the Lake Manyara deposit.

Morphology, twinning and colour

Alexandrites from Lake Manyara show some variability in morphology, and especially in different forms of twinning. The crystals were determined as single crystals, contact twins, penetration twins or cyclic twins (trillings). Two major habits are found within each group (Figures 8, 9 and 14), which can be described as

- I. tabular parallel to the **a** (100) pinacoid or
- II. tabular parallel to the **b** (010) pinacoid or columnar along the a [100] axis.

From the crystal material available, the authors were able to determine seven external crystal forms for the orthorhombic chrysoberyls, namely the pinacoids **a** and **b**, the prisms **i**, **s**, and **r**, and the dipyramids **o** and **n** (Table I). The habit of all crystals is determined by three crystal forms, the two pinacoids **a** and **b** and the prism **i**. The remaining prisms **s** and **r** and dipyramids **o** and **n**, are accessory forms only. The dipyramid **w** was only found as an internal growth feature.

All samples which are tabular parallel to the **a** pinacoid (group D), show dominant **a** pinacoids and somewhat smaller **b** and **i** faces. If the **b** pinacoids as well as the **i** prism faces are larger and dominant with **a** faces still being present (group II), the samples are mostly columnar along the a -axis or rarely tabular parallel **b** (Table I).

Single crystals of both groups (Figures 9 and 10) are rare. The largest single crystal examined weighing 30 g is pictured in Figure 11. In contrast, contact twins with tabular habit are common, while columnar contact twins are rare (Figure 12). Tabular penetration twins are rare,

Alexandrite and colour-change chrysoberyl from the Lake Manyara alexandrite-emerald deposit in northern Tanzania

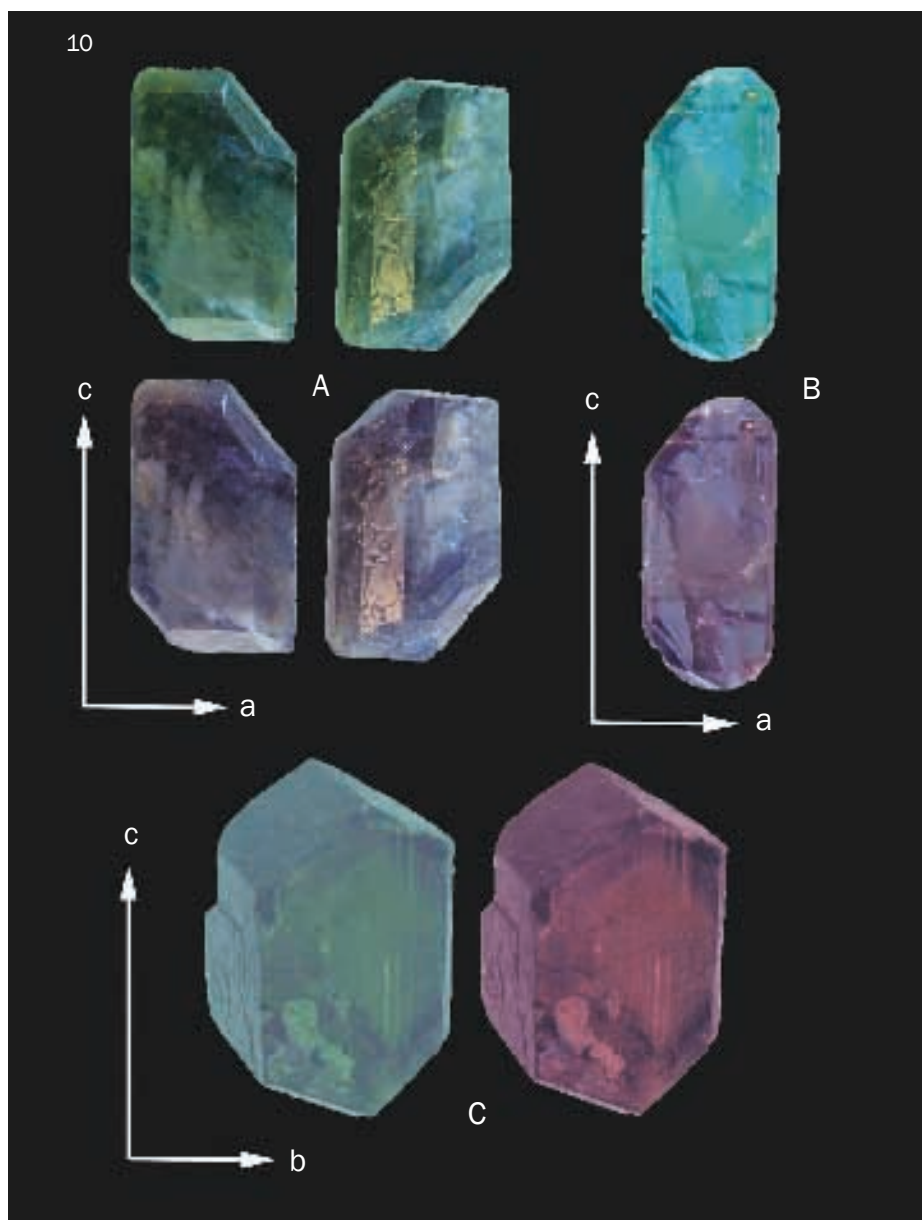
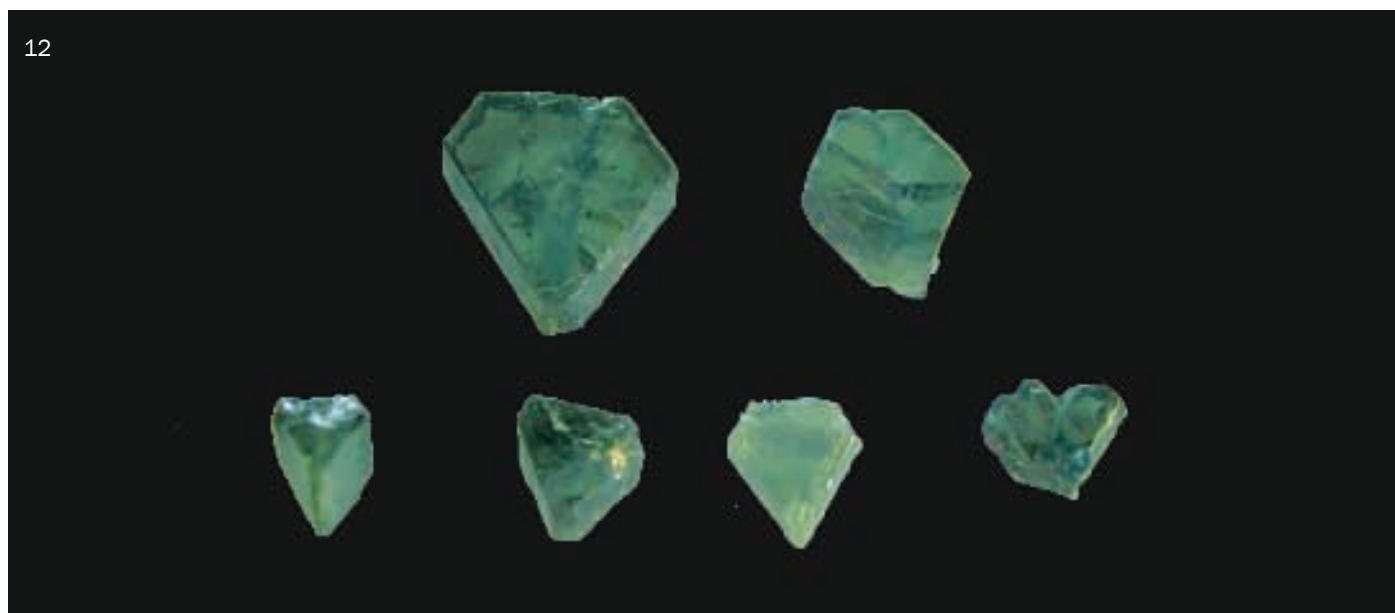


Figure 10: Alexandrite single crystals from the Manyara area, Tanzania, shown in both daylight and incandescent light. Upper row: crystals A and B with tabular habit parallel **b**, lower row: crystal C with tabular habit parallel **a**; samples not to scale, sample A 15 × 9 mm, sample B 8.7 × 4.1 mm, sample C 16.5 × 10.5 mm. Collection of W. Radl, Niederwörresbach, Germany. Photos and artwork by K. Schmetzer.

Figure 11: Alexandrite single crystal from Manyara, Tanzania; view almost parallel to the a-axis, weight 30 g, size 32 × 28 mm, thickness along the a-axis 15 mm. Collection of J.M. Saul, Paris, France. Photo by K. Schmetzer.

Figure 12: Contact twins of alexandrite from Lake Manyara, Tanzania; view almost parallel to the a-axis, the crystal on the upper left measures 10.2 × 9.1 mm, thickness along the a-axis 3.0 mm. Collection of W. Radl, Niederwörresbach, Germany. Photo by K. Schmetzer.



Alexandrite and colour-change chrysoberyl from the Lake Manyara alexandrite-emerald deposit in northern Tanzania

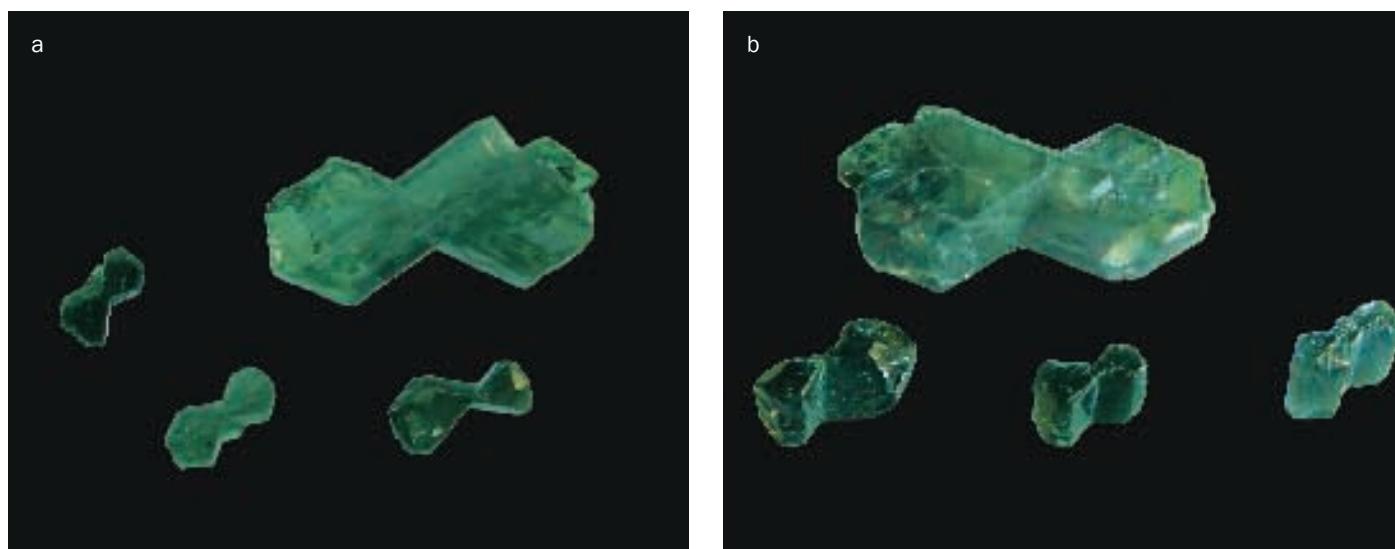


Figure 13: Penetration twins of alexandrite from Lake Manyara, Tanzania; view almost parallel to the a-axis (a) and oblique to the a-axis (b), the largest sample shows tabular habit parallel a, the three smaller twins show columnar habit along the a-axis; size of the largest crystal 14.1 x 7.5 mm, thickness along the a-axis 3.8 mm. Collection of W. Radl, Niederwörresbach, Germany. Photos by K. Schmetzer.

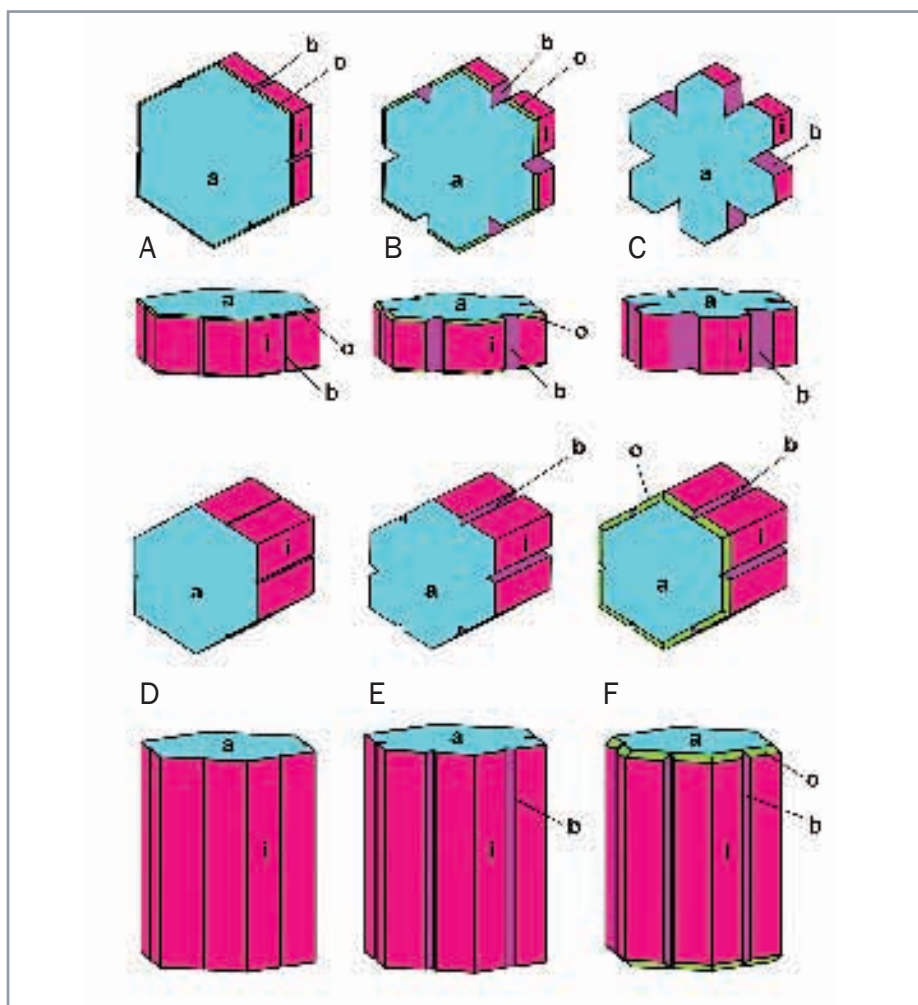


Figure 14: Schematic drawings of alexandrite cyclic twins (trillings) from the Lake Manyara deposit, Tanzania. The cyclic twins are shown in views parallel to the a-axis (upper rows) and perpendicular to the a-axis (lower rows); the trillings show tabular habit parallel a (A to C) or columnar habit along the a-axis (D to F). Crystal drawings and artwork by K. Schmetzer.

and columnar penetration twins were seen only occasionally (Figure 13). On the other hand, tabular trillings (cyclic twins) are common (Figures 14 and 15), but only a few columnar trillings were seen (Figure 16). Tabular trillings commonly show colour zoning with a transparent light green rim and an off-white, translucent core. In several samples, between rim and core, there are transparent green and translucent off-white layers. The two largest somewhat distorted trillings seen by the present authors weigh 132 and 16 g respectively (Figures 7 and 17).

Some more irregular twins can be described as contact twins with an additional crystal in twin position (Figure 18 and 19, sample A), as part of a penetration twin (Figure 19, sample B) or as part of a trilling (Figure 20).

In summary, the variability of morphology, i.e. the presence of single crystals and a wide range of twins and trillings, is enormous. It is comparable with or even exceeds the wide variability of alexandrites from the large Uralian mining area in Russia. Two types of samples are commonest: tabular contact twins (Figure 12) and tabular trillings (Figure 15), both with dominant a pinacoids and subordinate i prism faces and b pinacoids. Tabular contact twins commonly show small o dipyrramids and one or two

Alexandrite and colour-change chrysoberyl from the Lake Manyara alexandrite-emerald deposit in northern Tanzania

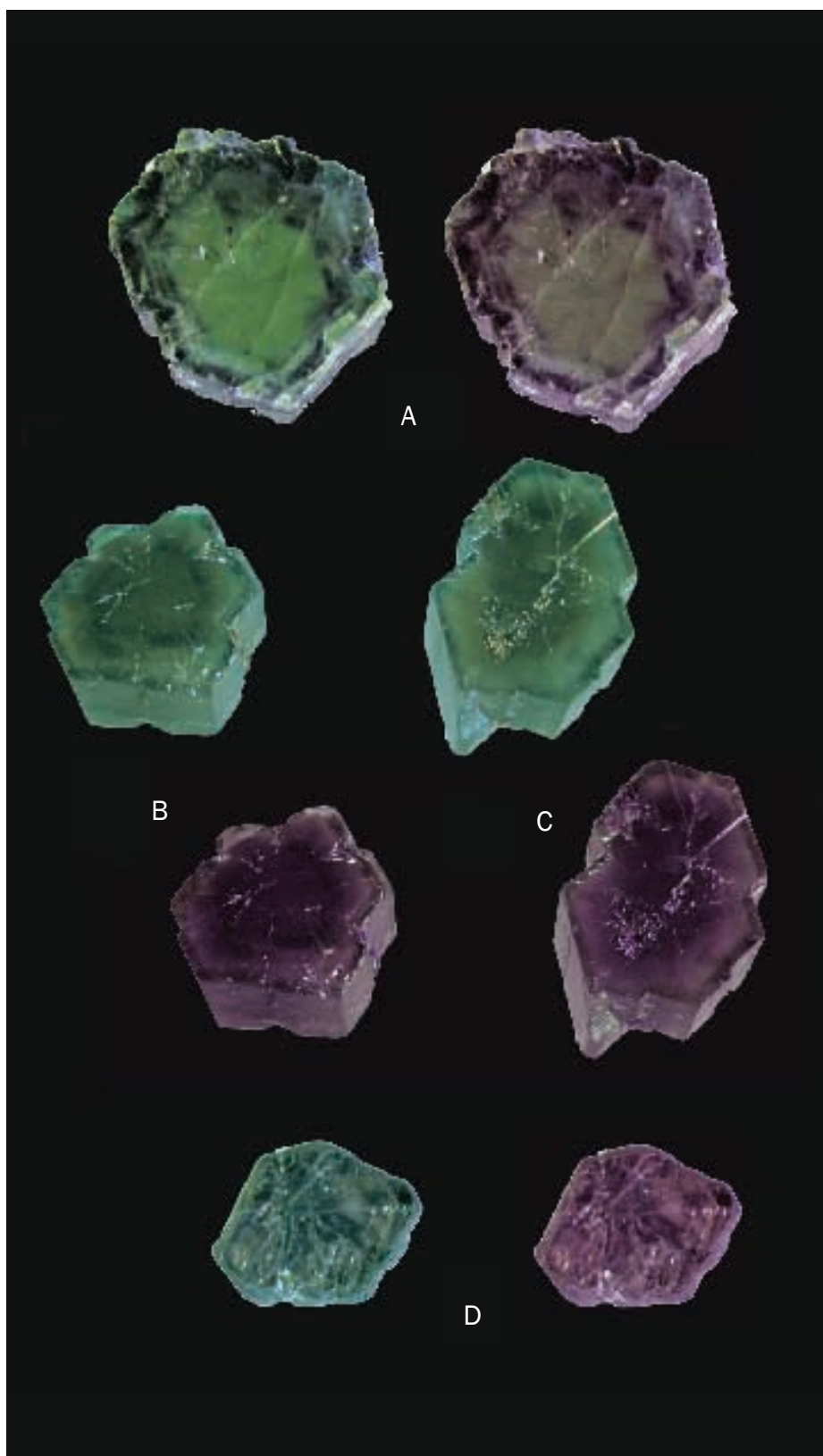


Figure 15: Cyclic twins (trillings) of alexandrite from Lake Manyara, Tanzania, with tabular habit parallel *a* shown in both daylight and incandescent light, view almost parallel to the *a*-axis; samples A to C show distinct zoning with alternating green and milky white layers. Samples not to scale; sample A 21 × 17.5 mm, thickness along the *a*-axis 8.0 mm; sample B 8.8 × 8.2 mm, thickness along the *a*-axis 5.2 mm; sample C 12.5 × 8.5 mm, thickness along the *a*-axis 5.3 mm; sample D 11.0 × 9.0 mm, thickness along the *a*-axis 4.7 mm. Collection of W. Radl, Niederwörresbach, Germany. Photos and artwork by K. Schmetzer.



Figure 16: Cyclic twin (trilling) of alexandrite from Lake Manyara, Tanzania, with columnar habit along the *a*-axis shown in both daylight and incandescent light; diameter of sample 9.5 × 9.0 mm, length along the *a*-axis 11.0 mm. Collection of F. Jurkutat, Einbeck, Germany. Photo by K. Schmetzer.



Figure 17: Alexandrite trilling from Lake Manyara, Tanzania. The trilling weighs 16 g, view almost parallel to the *a*-axis, size 27.5 × 14.5 mm, thickness along the *a*-axis 11.0 mm. Collection of Paul Wild Company, Kirschweiler, Germany. Photo by K. Schmetzer.

Alexandrite and colour-change chrysoberyl from the Lake Manyara alexandrite-emerald deposit in northern Tanzania

smaller prism faces (**s** or **r**). Tabular trillings, in general, show only small **o** dipyrramids, but no **s** or **r** prism faces.

The colours of rough alexandrites and chrysoberyls from Lake Manyara range (in daylight) from various shades and intensities of green to yellowish green or bluish green. The pleochroism of Lake Manyara alexandrites in polarized light is distinct, and is as seen in most alexandrites from different sources (for the description of colour in different directions of view, i.e. pleochroism in non-polarized light, see below).

Pleochroism of alexandrite from Lake Manyara, Tanzania, in polarized light

	Daylight	Incandescent light
X a	yellow green	purple to purplish red
Y b	yellow	orange
Z c	blue green	blue green

Microscopic features of crystals

To understand the structural pattern, colour zoning and zoning of inclusions of faceted gemstones, it is helpful to examine the microscopic characteristics of transparent rough single and twinned crystals. The microscopic characteristics of contact twins and penetration twins are shown in *Figure 21*, and examples for cyclic twins are shown in *Figure 22*. In views parallel to the *a*-axis (in most cases perpendicular to the large **a** pinacoids of the crystals), a growth pattern with dominant **i** prism faces as growth structures is present. In some crystals, we noted also growth structures parallel to the **b** pinacoid. If a twin plane or several twin planes are present, the twin planes are perpendicular to **i** prism faces of the different parts of the twin.

In the centres of crystals, i.e. in the first stages of crystal growth, the faces **a**, **b**, **i**, **o** and **w** can be present (see *Table D*), but in later stages of growth, the

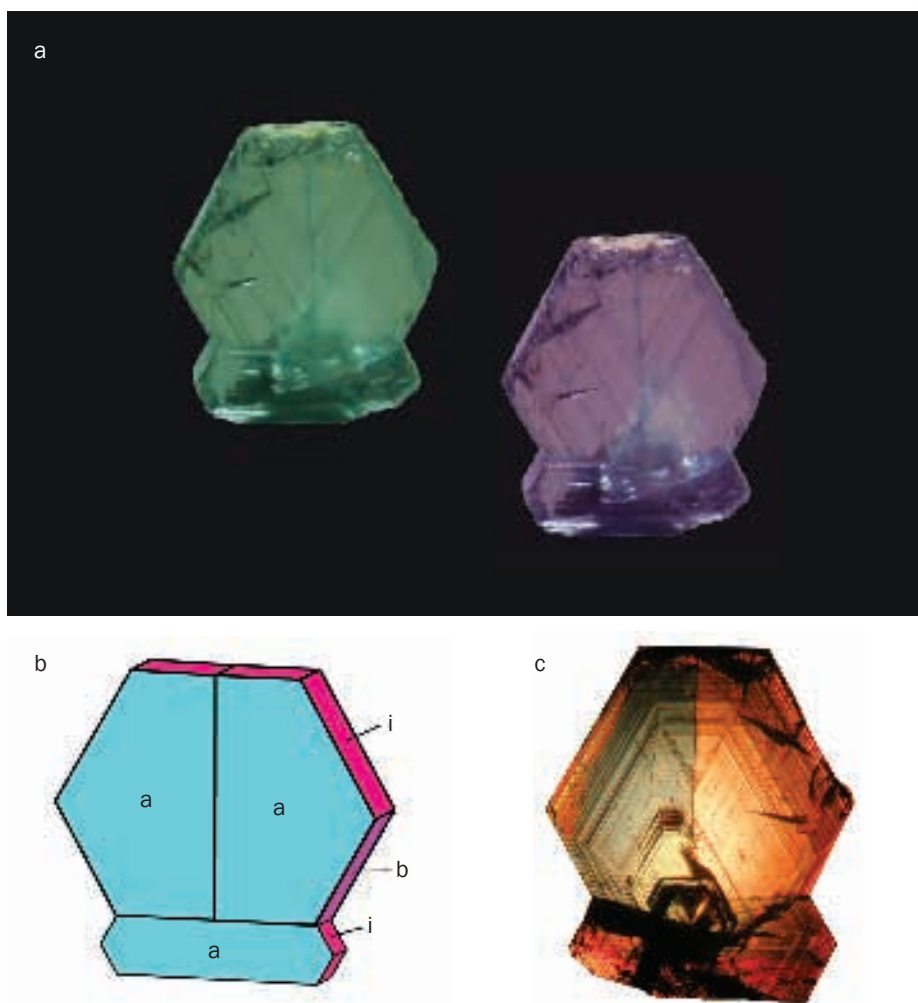


Figure 18 a to c: Irregular alexandrite contact twin with tabular habit parallel **a** from Lake Manyara, Tanzania: (a) in both daylight and incandescent light; (b) in a schematic crystal drawing; and (c) in immersion showing growth planes and inclusion distribution. The crystal consists of three twinned individuals; view almost parallel to the *a*-axis, size 8.5 × 7.2 mm, thickness along the *a*-axis 2.7 mm. Collection of J.M. Saul, Paris, France. Photos and crystal drawing by K. Schmetzer.

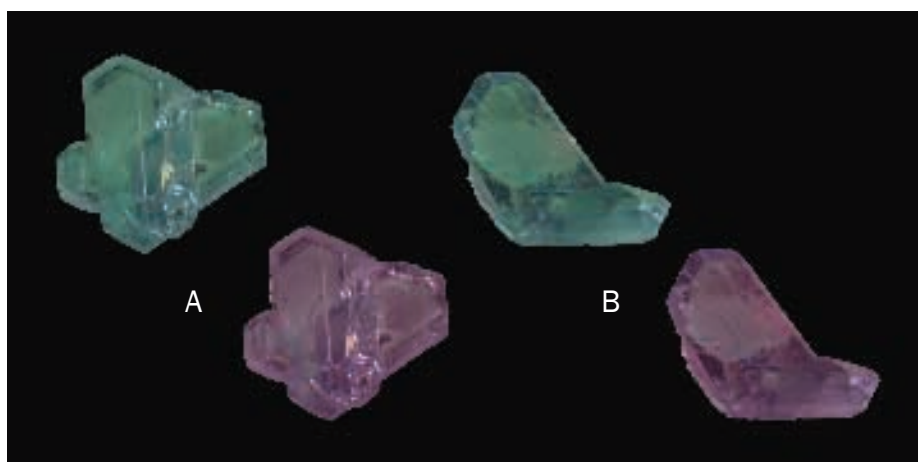


Figure 19: Irregular alexandrite contact twins with tabular habit parallel **a** from Lake Manyara, Tanzania shown in both daylight and incandescent light; crystal A consists of three twinned individuals and crystal B consists of two twinned individuals; view almost parallel to the *a*-axis; sample A size 6.2 × 6.1 mm, thickness along the *a*-axis 3.2 and 1.8 mm (in different parts), sample B size 5.5 × 4.5 mm, thickness along the *a*-axis 2.7 mm. Collection of W. Radl, Niederwörresbach, Germany. Photos by K. Schmetzer.

Alexandrite and colour-change chrysoberyl from the Lake Manyara alexandrite-emerald deposit in northern Tanzania

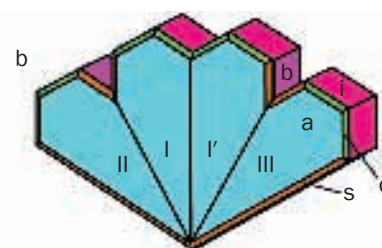
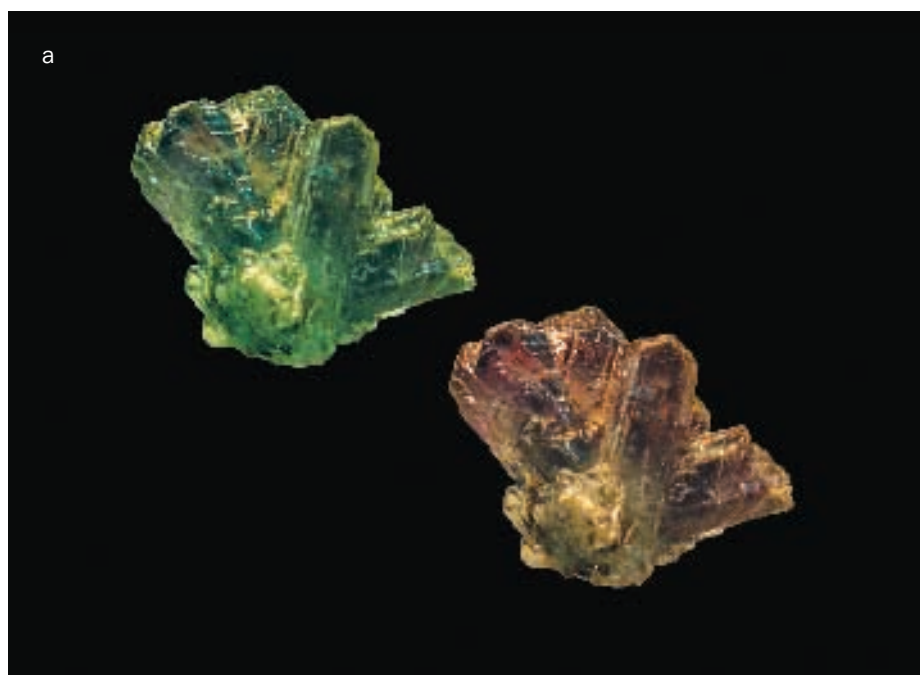


Figure 20 a,b: Irregular alexandrite contact twin with tabular habit parallel to **a** from Lake Manyara, Tanzania, (a) in daylight and incandescent light; (b) schematic drawing; the crystal consists of four twinned individuals, two of the four crystals (in the middle, labelled I and I') with parallel orientation are intergrown parallel to a virtual **b** plane, each of these two crystals is twinned with another crystal (labelled II and III); view almost parallel to the a-axis, size 23 × 17 mm, thickness along the a-axis 8.5 and 6.5 mm (in different parts). Collection of J.M. Saul, Paris, France. Photo and crystal drawing by K. Schmetzer.

dipyramid **w** (122) is absent. An example of a single crystal showing this internal growth zoning reflecting the growth history of the alexandrites is given in Figure 23. This pattern is typical of rough single crystals and twins, which do not show the **w** dipyramid as an external crystal face.

Growth layers with milky white zones are common. They are separated from transparent zones by normal growth planes, mostly parallel to **i** prism faces (Figure 24), and some parallel to **b** pinacoids. In views perpendicular to the *a*-axis, the milky zones can be seen to be formed by small needles, particles or channels with a dominant orientation parallel to the *a*-axis.

Microscopic features of faceted stones

Structural properties: growth structures and twinning

Faceted alexandrites from Lake Manyara commonly show growth structures and twinning. Under the microscope, twin boundaries can be separated from growth planes according to differences in the interference pattern visible under crossed polarizers (Figure 25 a,b). Twinned individuals can also be distinguished by the different (pleochroic)

colours of the parts of the twin using just plane polarized light. The growth patterns seen in faceted samples closely reflect the external morphologies of single crystals and twins. Dominant growth planes present are the pinacoids **a** and **b** and the prism **i**, in some stones in combination with smaller dipyramids (**o** and **n**) or smaller prism faces (**s** and **r**).

The most characteristic growth pattern in alexandrites from Lake Manyara is seen in a view parallel to the *a*-axis and consists of two **i** prism faces (Figure 25c), occasionally in combination with **b** pinacoids. In twinned stones, a more complex pattern with a twin plane as well as **i** prism faces and **b** pinacoids from both parts of the twinned individual is present (Figure 25d). In a direction of view perpendicular to a twin plane, i.e. in a direction inclined to the *b*- and *c*-axes, a pattern consisting of dominant **a** and **i** faces in combination with smaller **o** dipyramids is common (Figure 25, e,f). In the same direction of view, this pattern can also be seen in untwinned stones.

Oriented particles and needles

In numerous alexandrites there are tiny, in most cases somewhat elongated particles or even needles or channels, which are orientated in one particular direction (Figure 25 g to i). This preferred

direction was determined as the *a*-axis of the chrysoberyl crystals or twins (Figure 25j). In a view parallel to the needle axis, i.e. parallel to the *a*-axis, these needle-like particles are frequently zoned parallel to **i** prism faces (Figure 25k), occasionally also parallel to **b** pinacoids. In other samples, these 'needles' form special areas, zones or lines, which are inclined to the dominant **i** or **b** crystal faces (Figure 25l). However, the 'needles' are all parallel to the *a*-axis of the alexandrite host (Figure 26 a to d).

In some stones, there is a second type of tiny inclusion, in most cases in addition to the needle-like particles described above (Figure 26d). These tiny inclusions are concentrated on specific planes parallel to **a** pinacoids. Consequently, in a direction perpendicular to the *a*-axes, i.e. in a view perpendicular to the 'needle'-axes, a combination of both structural features is seen (Figure 26 e to g). In this direction of view, the 'needles' parallel to the *a*-axis and the areas on **a** pinacoids intersect at right angles. If both structural inclusion patterns are very dense, samples with complete off-white reflecting areas are present, consisting of numerous oriented reflecting particles (Figure 26 h,i; see also the section below 'Stones with larger milky white zones').

Alexandrite and colour-change chrysoberyl from the Lake Manyara alexandrite-emerald deposit in northern Tanzania

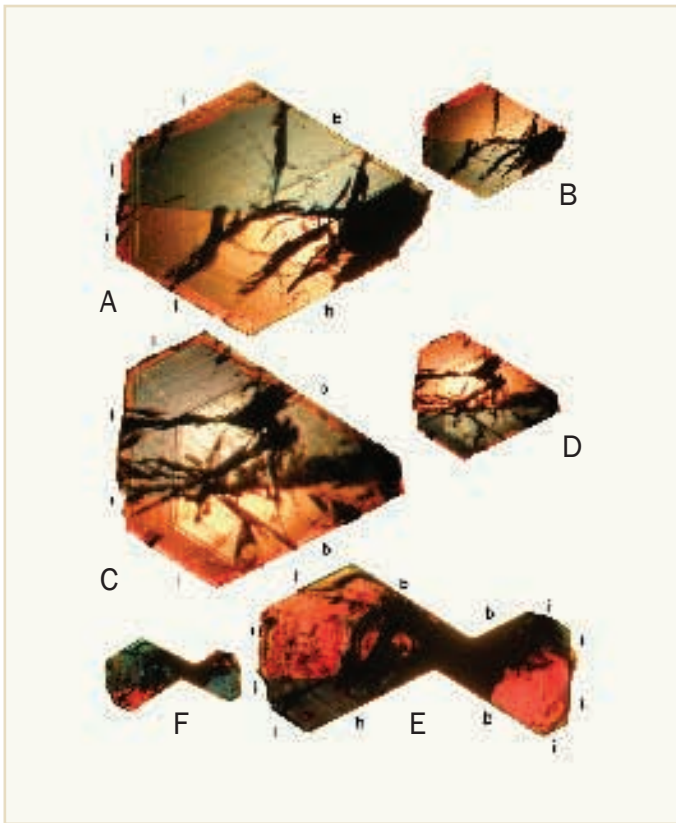


Figure 21: Growth structures and twinning in two alexandrite contact twins (A,B and C,D) and one interpenetrant twin (E,F) with tabular habit; the samples are shown in a view parallel to the a-axis in polarized light with different orientations of the polarizer, which highlights the pleochroic colours. The dominant growth structures seen in this orientation are planes parallel to the prism *i*, subordinate growth structures are planes parallel to the *b* pinacoid. Immersion, samples not to scale, size of the twin A,B 8.2 × 6.8 mm; size of the twin C,D 10.2 × 9.1 mm, size of the twin E, F 6.2 × 3.2 mm. Photos and artwork by K. Schmetzer.

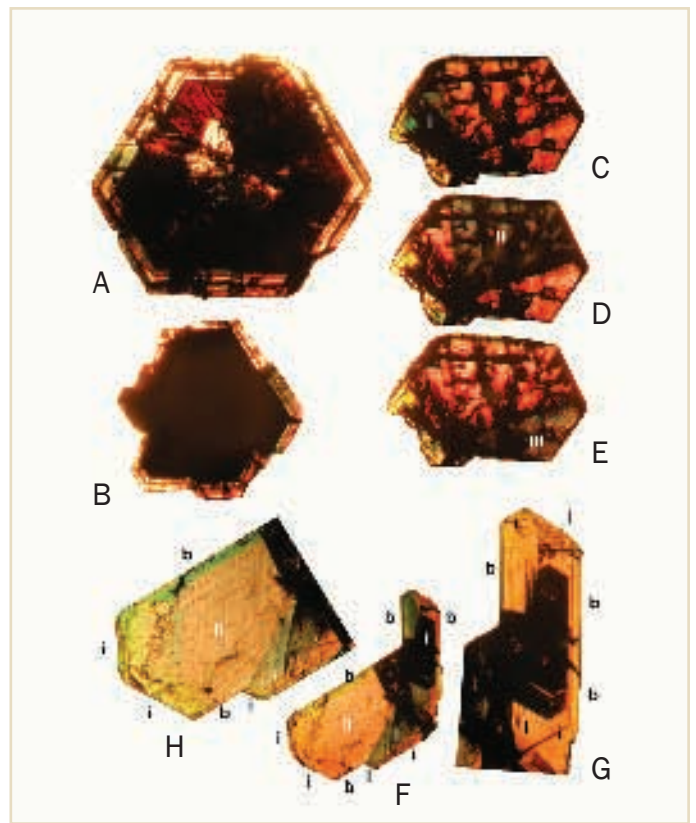


Figure 22: Growth structures and twinning in three alexandrite trillings (A, B and C to E) and one irregular alexandrite contact twin (F to H) with tabular habit; the samples are shown in views parallel to the a-axis. The two trillings pictured in A and B show an intense growth zoning with alternating transparent and milky white layers; the trilling pictured in C to E is shown in polarized light with different orientations of the polarizer. The irregular contact twin shown in F (parts magnified in G and H) consists of two individuals, I and II, growth structures are seen parallel to the prism *i* and the pinacoid *b*. Immersion, samples not to scale, size of trilling A 5.5 × 5.2 mm; size of trilling B 8.8 × 8.2 mm, size of trilling C to E 3.8 × 2.6 mm, size of twin F to H 5.5 × 4.5 mm. Photos and artwork by K. Schmetzer.

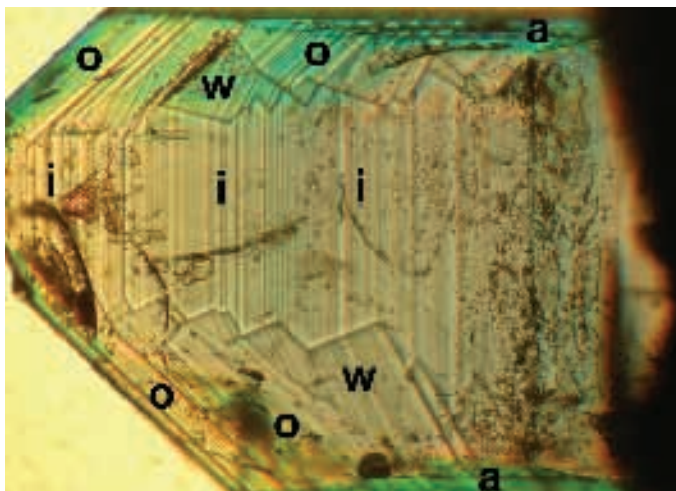


Fig 23: Growth structures in an alexandrite single crystal (untwinned) from Lake Manyara, Tanzania. The internal growth pattern shows growth planes parallel to the pinacoid *a*, the prism *i* and the dipramids *o* and *w*; in the final stages of crystal growth, the face *w* is not developed and is not seen as an external crystal face. Immersion, 40x. Photo by K. Schmetzer.

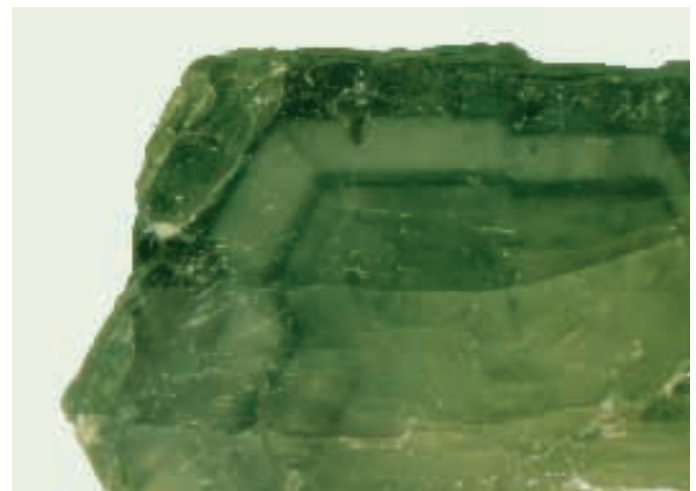


Figure 24: Many alexandrite samples, especially trillings, from Lake Manyara show zoning which consists of alternating transparent zones of variable intensities of green and milky white layers; this milky whiteness is due to channels which are oriented parallel to the a-axis and small negative crystals in the *a* pinacoid. View parallel to the a-axis, field of view 11.5 × 8.6 mm. Photo by K. Schmetzer.

Alexandrite and colour-change chrysoberyl from the Lake Manyara alexandrite-emerald deposit in northern Tanzania

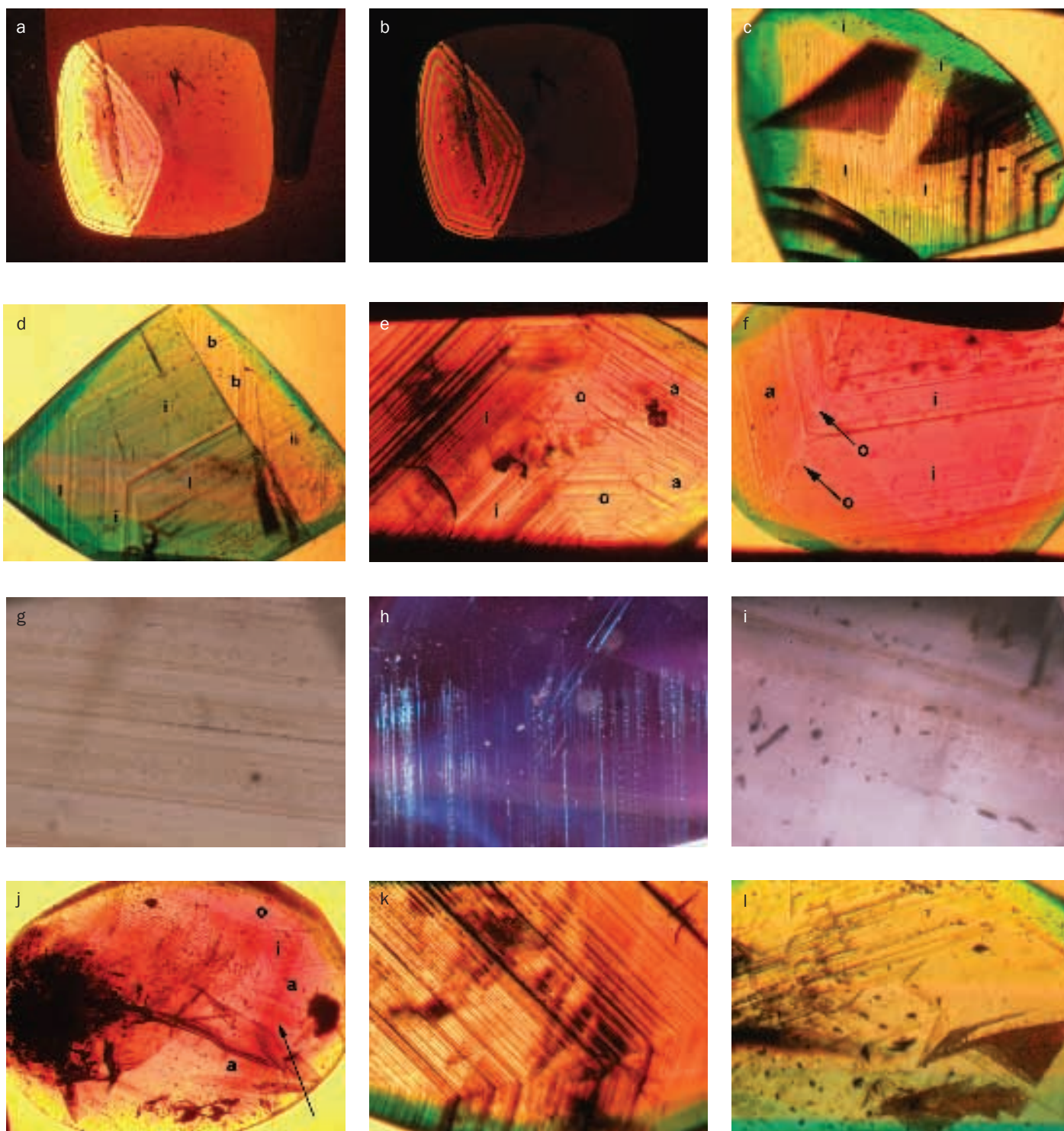


Figure 25 a to l: Microscopic properties of alexandrite and chrysoberyl from Lake Manyara, Tanzania.

(a and b) Twin boundary showing interference patterns: (a) immersion; (b) same sample with crossed polarizers, 25 \times .

(c to f) Characteristic growth structures consisting of **a** and **b** pinacoids, **i** prism faces and **o** dipyramids; in (d) a twin boundary is also present; immersion (c,d) 25 \times ; (e) 50 \times ; (f) 60 \times .

(g to i) Orientated needle-like particles or channels: (g) darkfield, 80 \times ; (h,i) brightfield, 80 \times .

(j) Growth structures parallel to the faces **a**, **i** and **o** with channels perpendicular to the **a** pinacoid (arrow), immersion, 35 \times .

(k) View parallel to the a-axis, showing a concentration of needles or channels or other inclusions on **i** prism planes, 50 \times .

(l) View parallel to the a-axis, showing a concentration of channels on **i** prism planes (upper part) or an irregular arrangement along specific planes or within specific zones (lower right), immersion, 60 \times .

Photos a to f, j to l by K. Schmetzer, g to i by A.-K. Malsy.

Alexandrite and colour-change chrysoberyl from the Lake Manyara alexandrite-emerald deposit in northern Tanzania

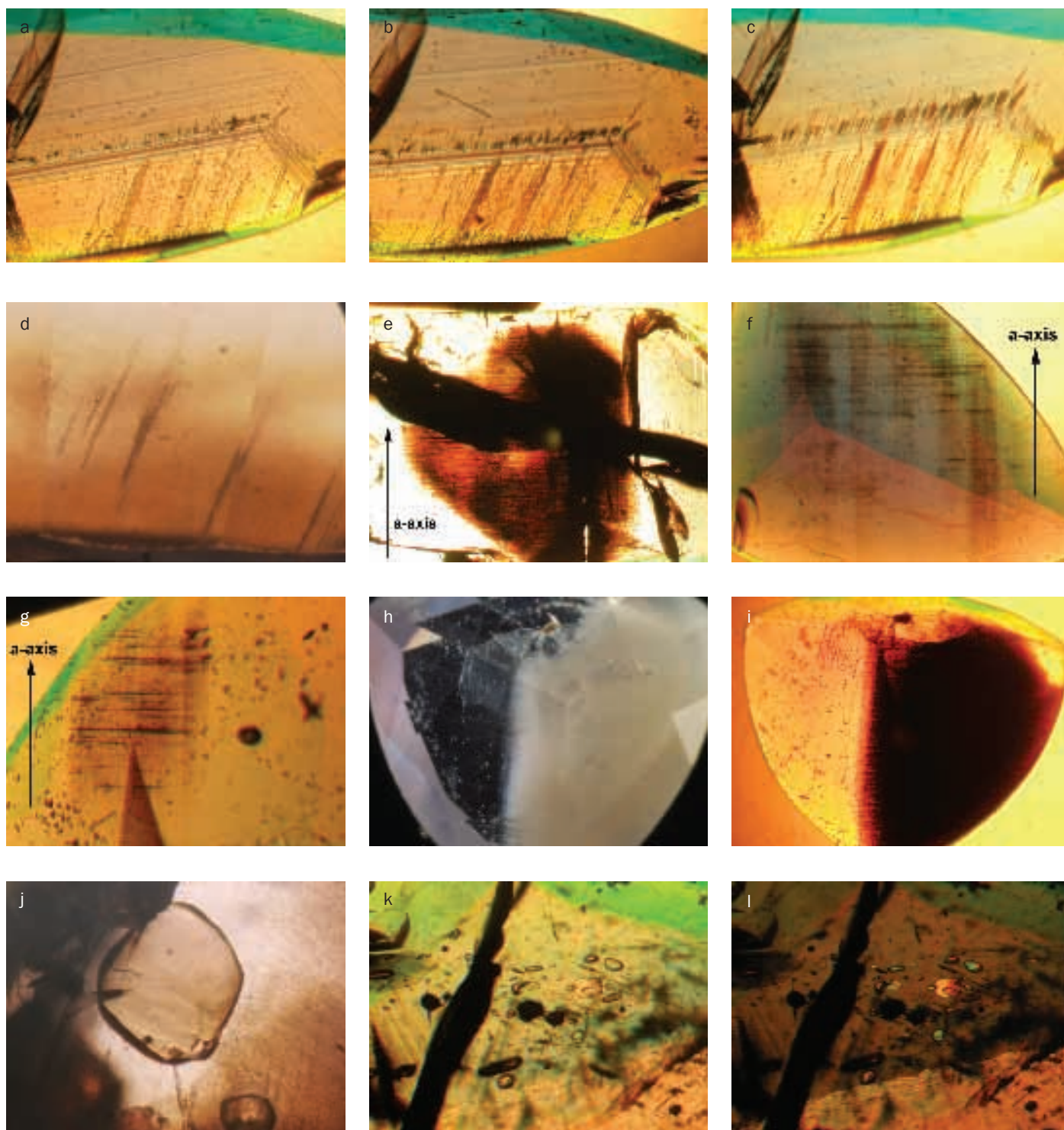


Figure 26 a to l: Microscopic properties of alexandrite and chrysoberyl from Lake Manyara, Tanzania:

(a to c) Channels with an orientation along the a-axis in different views: (a) parallel to the a-axis; (b) slightly inclined to the a-axis; and (c) inclined to the a-axis; the channels are concentrated on $\{111\}$ prism planes or show an irregular arrangement along specific other planes or within specific growth zones (lower part), immersion, 60 \times .

(d to i) Two types of inclusions are developed as needles or channels parallel to the a-axis and as smaller particles concentrated on planes perpendicular to the a-axis; in high concentration, these inclusions cause a milky white appearance (h); (d) brightfield, 80 \times ; (e) immersion, 40 \times ; (f,g) immersion, 60 \times ; (h) darkfield, 35 \times ; (i) (same sample as h) immersion, 30 \times .

(j to l) Phlogopite inclusions: (j) brightfield, 80 \times ; (k,l) immersion; (l) with crossed polarizers, 60 \times .

Photos a to c, e to g, i, k, l by K. Schmetzer, d, h, j by A.-K. Malsy.

Alexandrite and colour-change chrysoberyl from the Lake Manyara alexandrite-emerald deposit in northern Tanzania

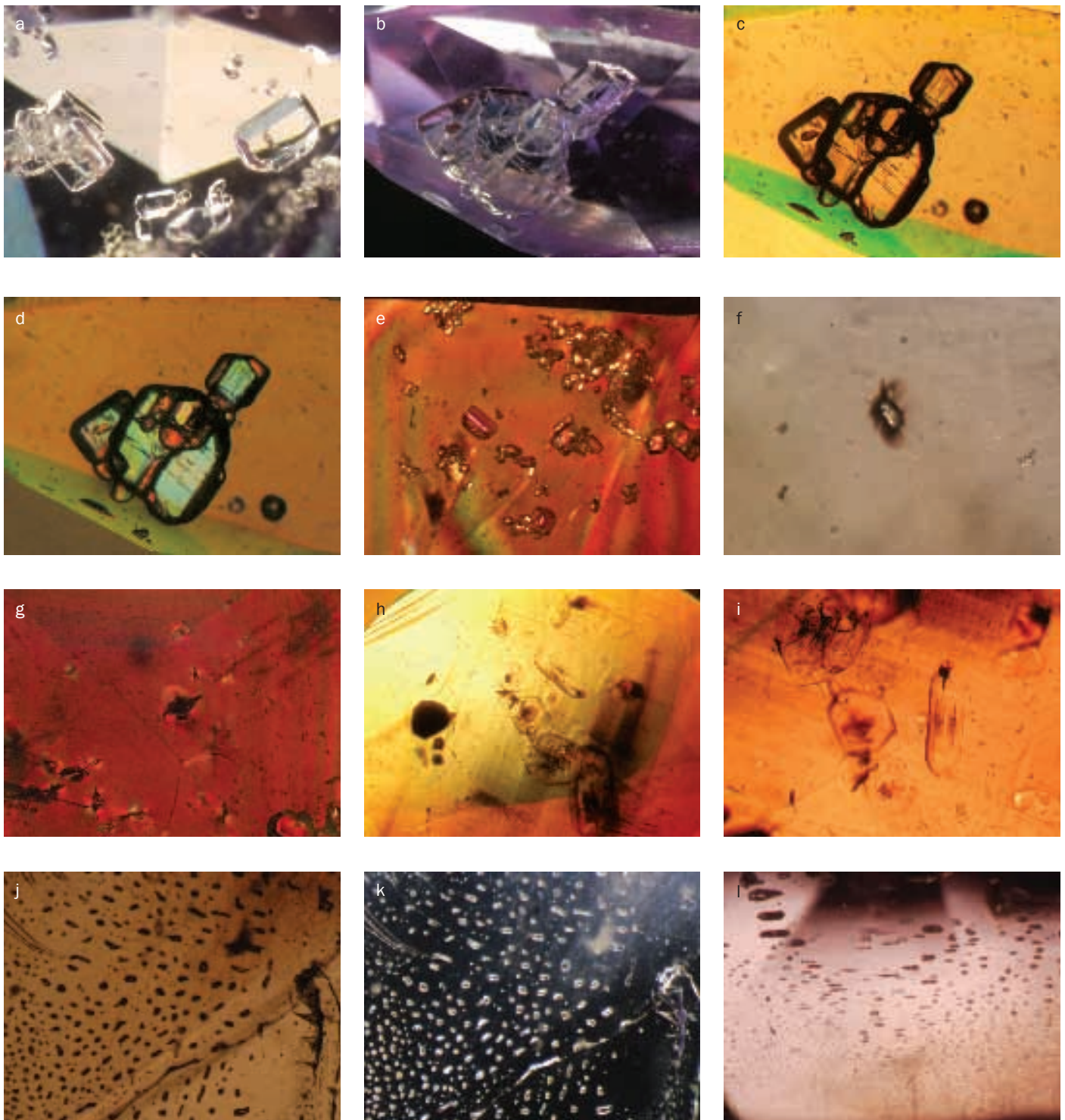


Figure 27 a to l: Microscopic properties of alexandrite and chrysoberyl from Lake Manyara, Tanzania.

(a to e) Inclusions of apatite crystals and apatite clusters (e): (a) brightfield, 50x; (b to d) same sample, (b) brightfield, (c) immersion, (d) immersion, crossed polarizers, all 60x; (e) immersion, crossed polarizers, 70x.

(f,g) Zircon crystals with tension cracks: (f) brightfield, 80x; (g) immersion, crossed polarizers, 60x.

(h,i) Chrysoberyl inclusions in alexandrite, immersion, crossed polarizers: (h) 40x; (i) 60x.

(j,k) Healing feathers consisting of small irregular liquid-filled cavities: (j) brightfield, 80x; (k) darkfield, 80x.

(l) Healing feather with two-phase inclusions in negative crystals, brightfield, 80x.

Photos c to e, g to i by K. Schmetzer, a, b, f, j to l by A.-K. Malsy.

Alexandrite and colour-change chrysoberyl from the Lake Manyara alexandrite-emerald deposit in northern Tanzania

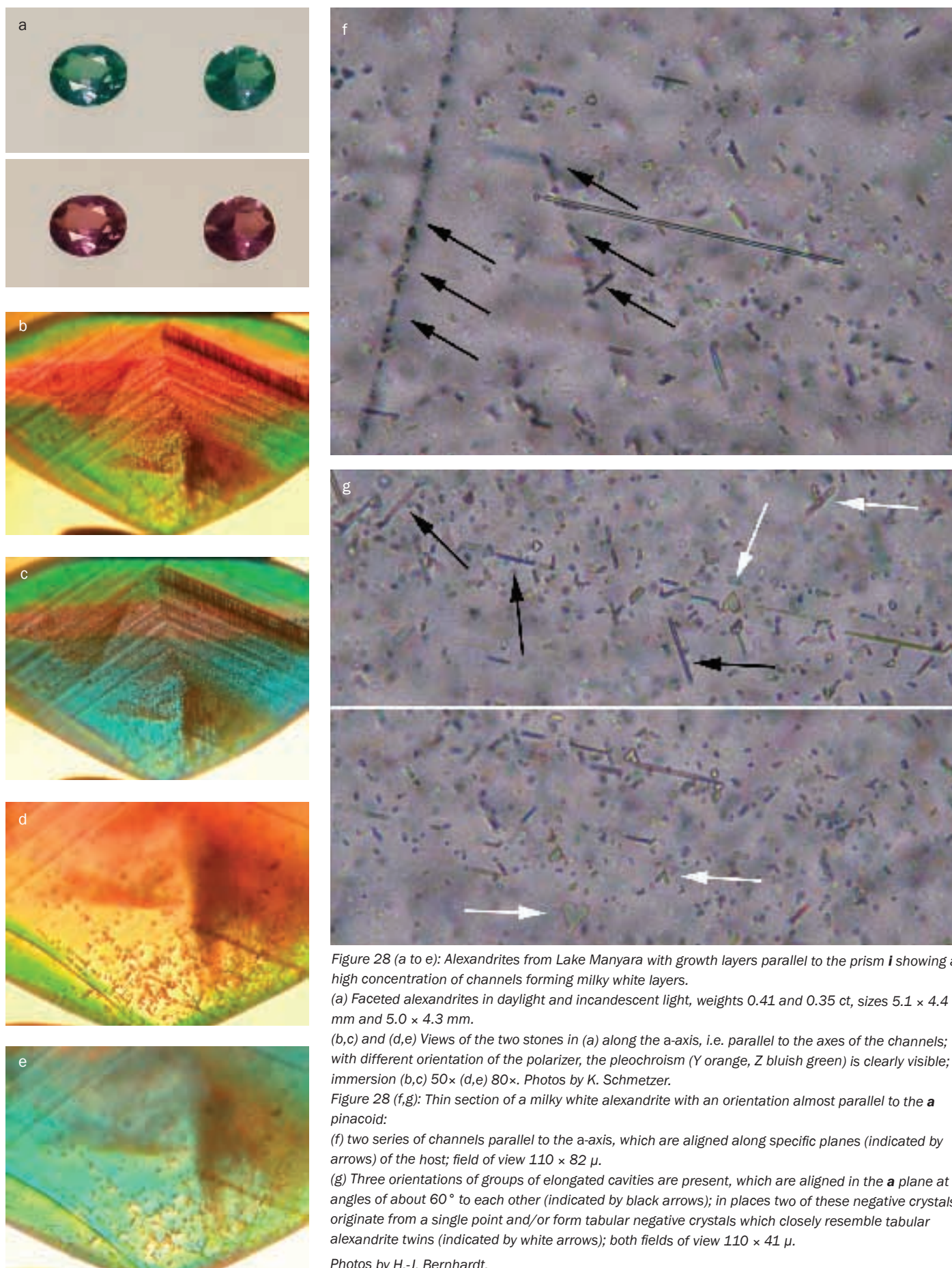


Figure 28 (a to e): Alexandrites from Lake Manyara with growth layers parallel to the prism \bar{i} showing a high concentration of channels forming milky white layers.

(a) Faceted alexandrites in daylight and incandescent light, weights 0.41 and 0.35 ct, sizes 5.1 × 4.4 mm and 5.0 × 4.3 mm.

(b,c) and (d,e) Views of the two stones in (a) along the a-axis, i.e. parallel to the axes of the channels; with different orientation of the polarizer, the pleochroism (Y orange, Z bluish green) is clearly visible; immersion (b,c) 50× (d,e) 80×. Photos by K. Schmetzer.

Figure 28 (f,g): Thin section of a milky white alexandrite with an orientation almost parallel to the **a** pinacoid:

(f) two series of channels parallel to the a-axis, which are aligned along specific planes (indicated by arrows) of the host; field of view 110 × 82 μ .

(g) Three orientations of groups of elongated cavities are present, which are aligned in the **a** plane at angles of about 60° to each other (indicated by black arrows); in places two of these negative crystals originate from a single point and/or form tabular negative crystals which closely resemble tabular alexandrite twins (indicated by white arrows); both fields of view 110 × 41 μ .

Photos by H.-J. Bernhardt.

Alexandrite and colour-change chrysoberyl from the Lake Manyara alexandrite-emerald deposit in northern Tanzania

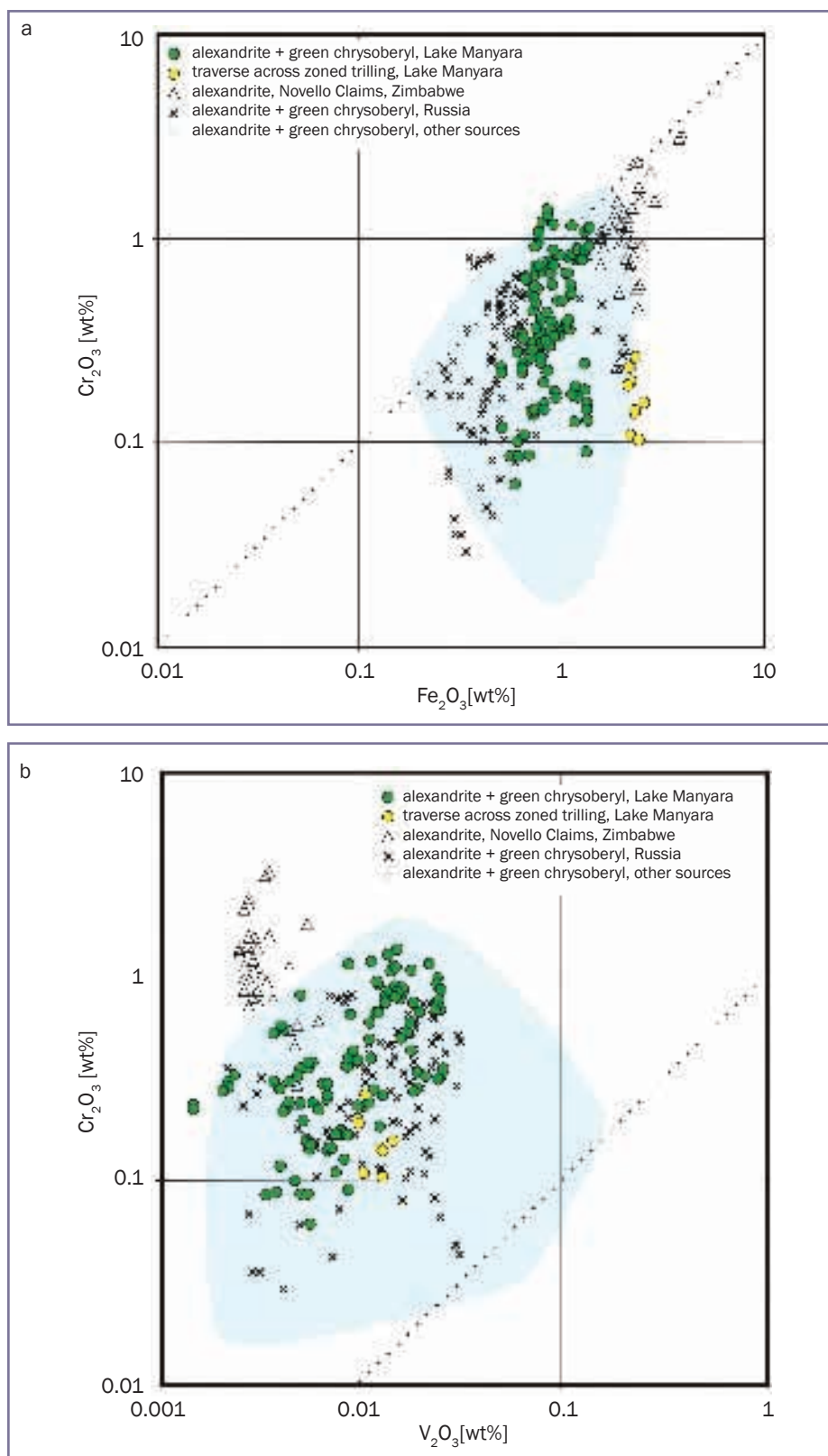


Figure 29 a,b: Iron/chromium and vanadium/chromium binary diagrams showing the variability of these trace element contents in alexandrites and green chrysoberyls from Lake Manyara compared to alexandrites and green chrysoberyls from Russia, from Zimbabwe and other localities (pale blue area representing more than 220 samples including all market relevant sources). The individual points represent measurements on various alexandrites; multiple analyses of different spots on the same crystal are plotted separately. Iron contents in alexandrites from Lake Manyara are intermediate between those in samples from Russia and Zimbabwe, vanadium and chromium contents for all three sources overlap. Artwork by A.-K. Malsy.

Mineral and fluid inclusions

Numerous mineral inclusions were identified using Raman microspectroscopy and laser ablation inductively coupled plasma mass spectrometry (LA-ICP-MS) by one author (A.-K.M.). The results are given below.

Although alexandrites from Lake Manyara are found in phlogopite schist, mica (phlogopite) inclusions are not common in gem-quality samples (Figure 26 j to l). The commonest inclusions were identified as prismatic apatite crystals or clusters of apatites (Figure 27 a to e). In several samples isolated zircons or groups of zircons, mostly surrounded by tension cracks (Figure 27 f,g) are also present. One alexandrite contains a group of well developed alexandrite crystals in no particular orientation (Figure 27 h,i).

Some alexandrites also contain healed fractures with residual fluid inclusions (Figure 27 j,k), and others may contain negative crystals filled with liquid or two-phase (liquid-gas) inclusions (Figure 27l).

Stones with larger milky white zones

It should be mentioned that alexandrite crystals with larger milky white zones (see again Figure 24) can yield attractive gems if the direction of cut is carefully chosen. The two samples depicted in Figure 28a were cut with the table facet formed of a transparent zone which was free of any milky white reflecting particles as inclusions. The growth zones below the table facets consist of successive layers with different concentrations of milky white reflecting needles or channels (Figure 28 b,c). The different growth layers are separated by two *i* (011) prism faces. This microscopic feature, however, does not disturb the overall appearance of the gems.

In a view perpendicular to the needle axis, the elongated particles within the milky white zones are clearly visible. In a view parallel to the crystallographic *a*-axis, i.e. parallel to the needle axis, the observer has the impression of looking into a fibre optic with light emanating from the needles. A view at somewhat higher magnification (Figure 28 d,e) indicates

Alexandrite and colour-change chrysoberyl from the Lake Manyara alexandrite-emerald deposit in northern Tanzania

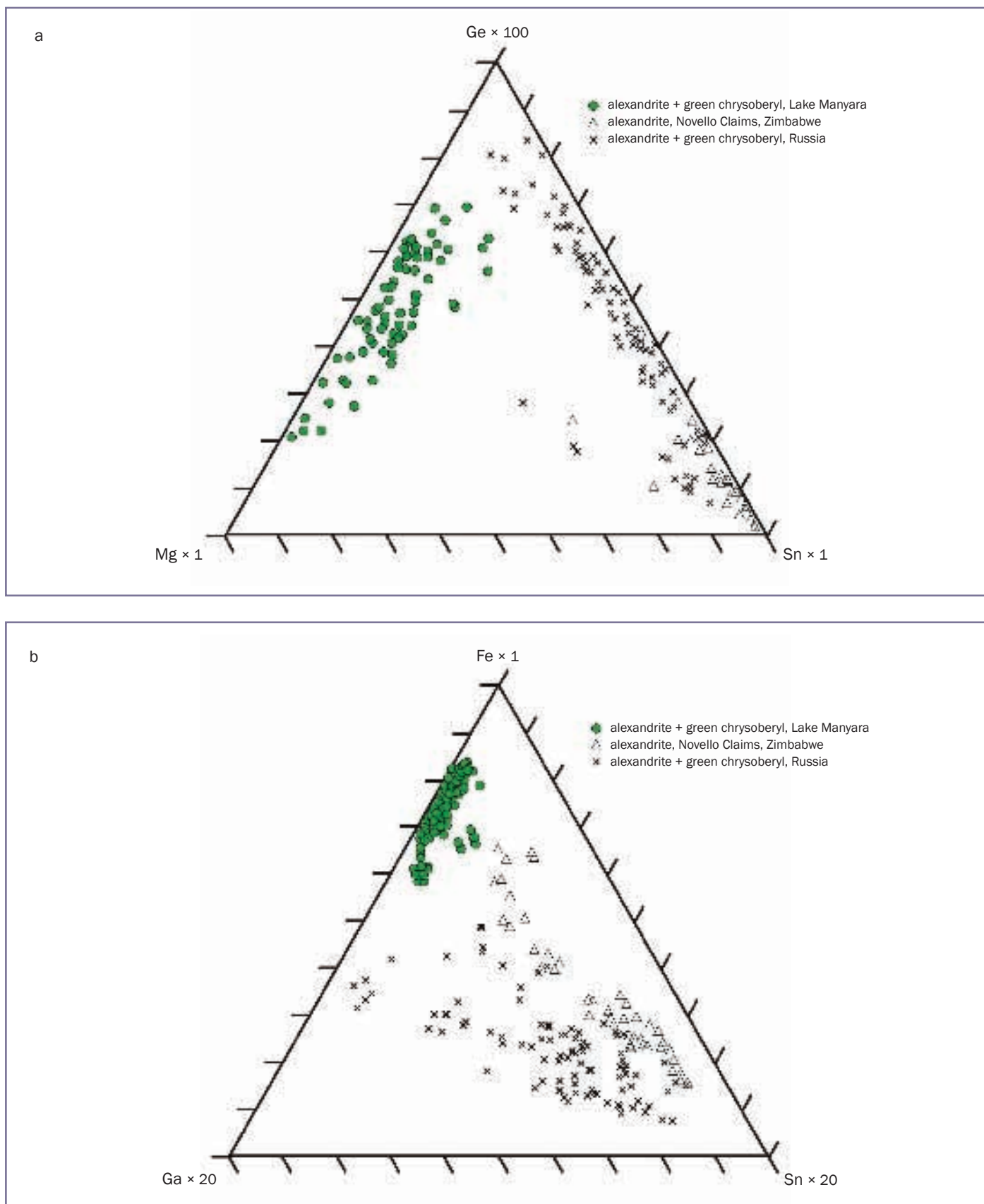


Figure 30 a,b: Ternary diagrams showing relative proportions of magnesium-germanium-tin and iron-gallium-tin in alexandrites and green chrysoberyls from Lake Manyara, Tanzania, Zimbabwe and Russia. The individual points represent measurements on various alexandrites; multiple analyses of different spots on the same crystal are plotted separately. The potential of trace element chemistry for distinguishing alexandrites from various localities is evident. Artwork by A.-K. Malsy.

Alexandrite and colour-change chrysoberyl from the Lake Manyara alexandrite-emerald deposit in northern Tanzania

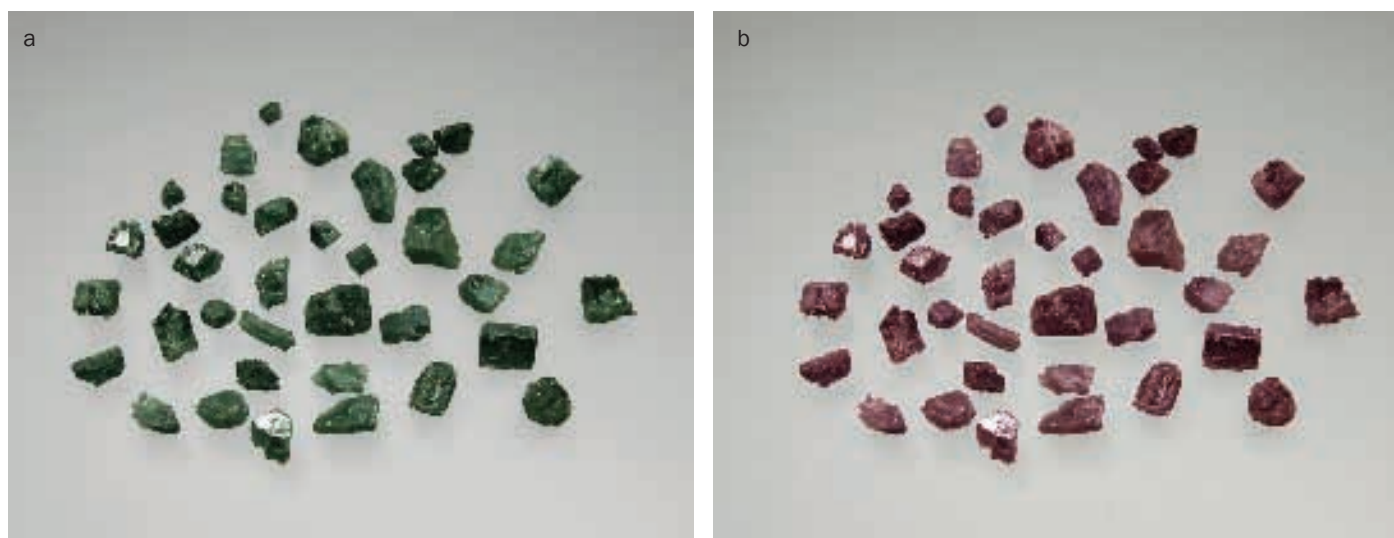


Figure 31: Rough alexandrite crystals and fragments from Lake Manyara with colour change from green or bluish green in daylight (a) to purple or reddish purple in incandescent light (b). The largest crystal measures about 7 × 6 mm. Photo by K. Schmetzer.

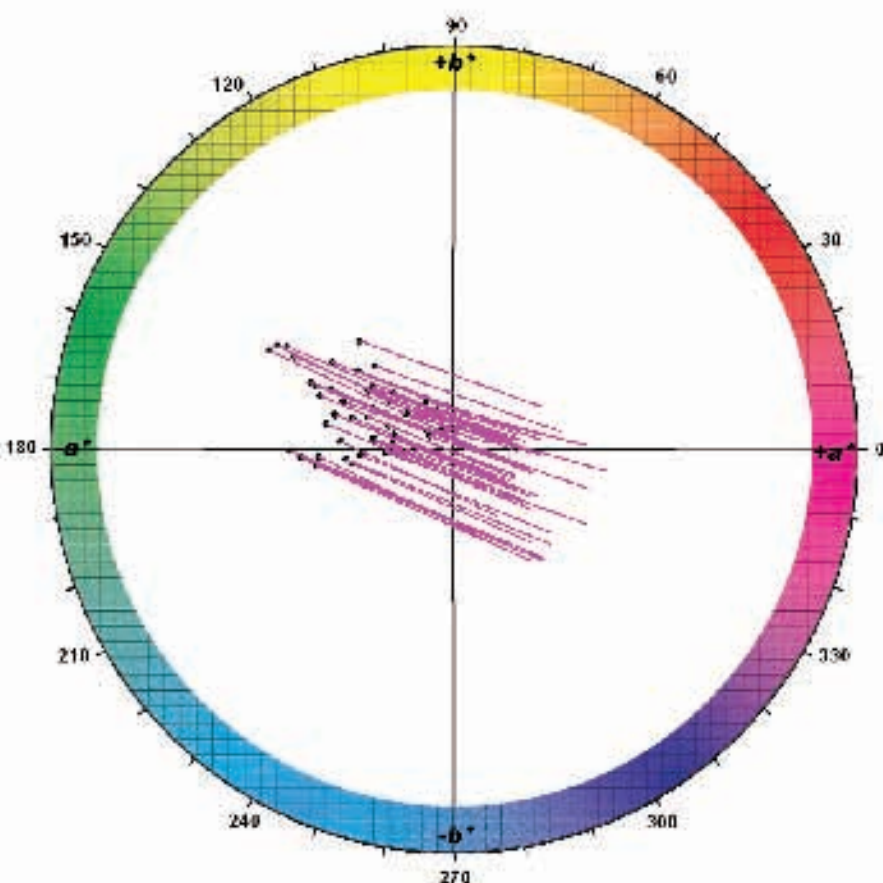


Figure 32: Colorimetric parameters of rough alexandrites shown in Figure 31 in the CIELAB colour circle; the neutral point (white point) is in the centre of the a^*b^* coordinate system; the small black circles represent the coordinates in the daylight source D_{65} and the ends of the differently coloured bars represent the coordinates in tungsten light A, the outer circle represents a chroma of 18. These parameters show the typical alexandrite-like colour change from daylight to incandescent light. Colorimetric measurements of various samples by A.-K. Malsy and G. Bosshart.

that at least part of these structures are hollow channels and not mineral inclusions such as rutile.

To identify all the needles and/or channels in Lake Manyara alexandrites and to further evaluate the inclusions causing the milky white appearance, a thin section almost parallel to the a pinacoid was prepared. The thin section showed several series of channels parallel to the a -axis, which were aligned along specific planes of the host (Figure 28f). In addition, three groups of elongated cavities were present, which are aligned in the a plane at angles of about 60° to each other (Figure 28g). Occasionally, two of these negative crystals originate from a single point and/or form tabular negative crystals which closely resemble tabular alexandrite twins in appearance (Figure 28g, compare Figure 9, especially crystal G). These results, indicating that the milky white zones are caused by channels parallel to the a -axis, occasionally in combination with negative crystals along the a plane, are confirmed by the chemical properties of a zoned green/milky white sample (see below).

We would like to mention that – although not found in our study – there might be also needle-like mineral inclusions in other samples of alexandrite from Lake Manyara and especially in chrysoberyl from other sources. It was found in numerous samples from different

Alexandrite and colour-change chrysoberyl from the Lake Manyara alexandrite-emerald deposit in northern Tanzania

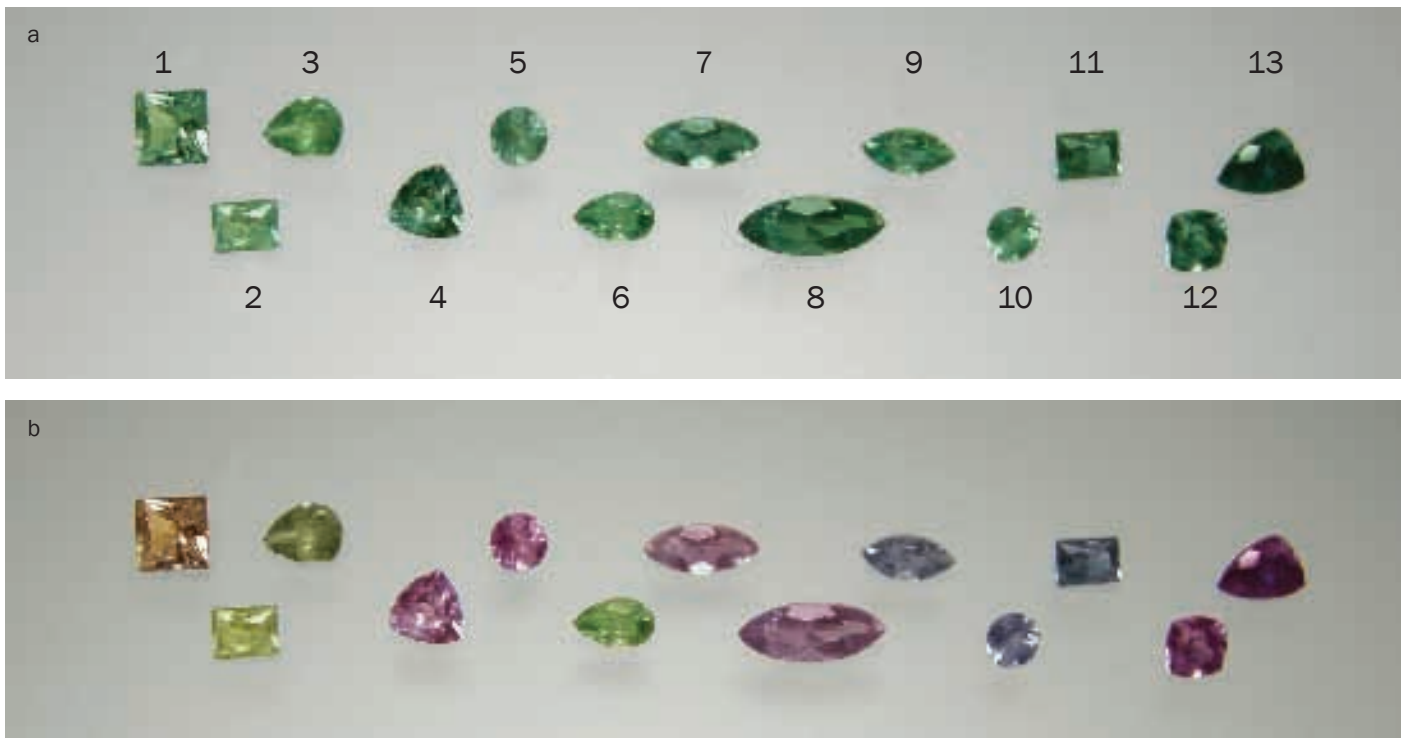
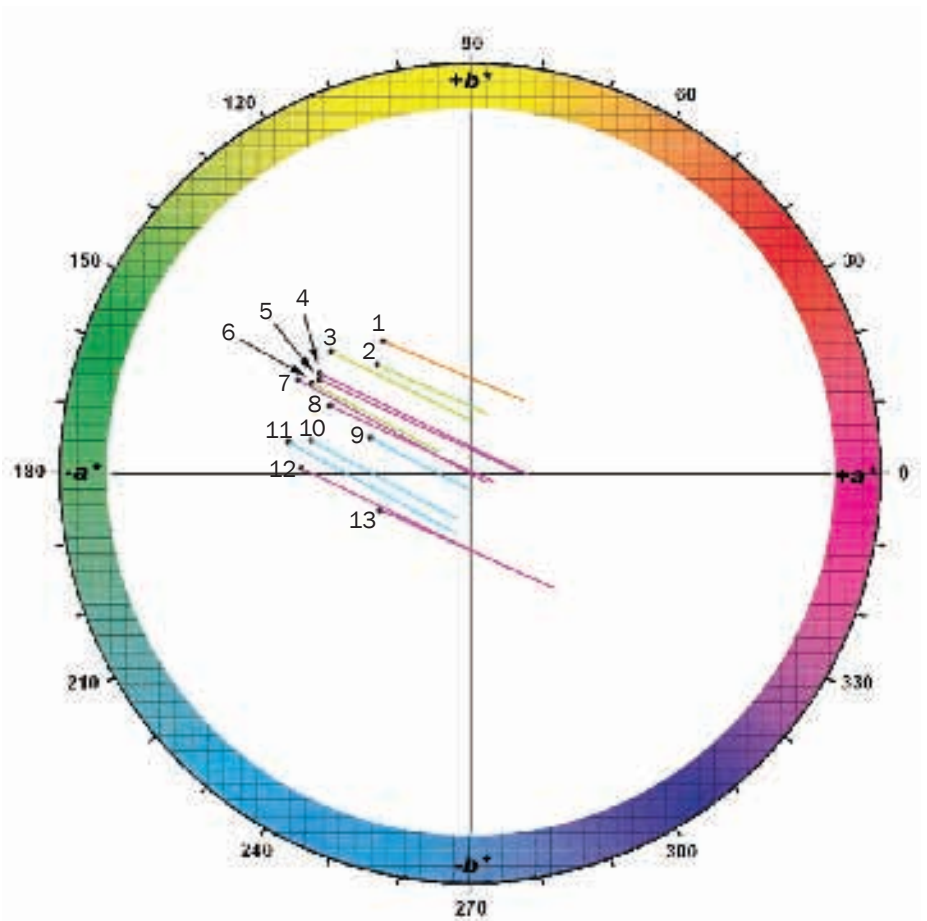


Figure 33: Faceted alexandrites and green chrysoberyls from Lake Manyara show a range of colours in daylight (a) and a much greater range in incandescent light (b); the numbers correspond to the numbers and their colorimetric parameters in the CIELAB diagram in Figure 34. Weights of samples from 0.16 to 0.68 ct, the square cut stone (1) weighs 0.56 ct, size 4.4 mm square. Photo by K. Schmetzer.

localities by microscopic examination by one of the present authors (K.S.) that chatoyancy in chrysoberyl or alexandrite is due to needle-like particles or channels with a preferred orientation parallel to the *a*-axis. However, to determine the exact nature of all different types of needles and/or channels in chrysoberyls and alexandrites from different sources, additional research is necessary, which is beyond the scope of the present paper.

Figure 34: Colorimetric parameters of faceted alexandrites and green chrysoberyls originating from the Lake Manyara deposit, Tanzania, in the CIELAB colour circle; the neutral point (white point) is in the centre of the *a***b** coordinate system; the small black circles represent the coordinates in daylight *D*₆₅ and the ends of the differently coloured bars represent the coordinates for tungsten light A, the outer circle represents a chroma of 18. Only a few stones show the typical alexandrite colour change of green to purplish red (e.g. 4, 5, 12, 13, represented by purple bars); other stones are green or yellow, orange or bluish grey in incandescent light. Colorimetric measurements of various samples by A.-K. Malsy. The numbers represent the stones in Figure 33 in daylight and incandescent light.



Alexandrite and colour-change chrysoberyl from the Lake Manyara alexandrite-emerald deposit in northern Tanzania

Composition

The compositions of ten rough crystals (with colour change from an intense green or bluish green to purple or reddish purple, see *Figure 31*) and 28 faceted alexandrites and green to yellowish green chrysoberyl (with variable colour change, see *Figure 33*) using LA-ICP-MS were determined (for details of the technique, see Malsy, 2010). In addition, there was a traverse of nine analysis points across the a pinacoid of a rough alexandrite trilling with zoning consisting of alternating transparent and off-white layers from the centre to the rim (see *Figure 24*).

Trace elements responsible for colour

The contents of trace elements that influence the colour of a stone are summarized in *Table II*. Vanadium, chromium and iron values for rough and faceted samples from the Lake Manyara deposit show a wide variability. The data, based on the analyses of 38 samples, are plotted in *Figure 29 a,b* and are compared with data from Russian samples (Malsy, 2010) and samples from the Novello mine in Zimbabwe (Schmetzer *et al.*, 2011). In all three localities, alexandrites or green chrysoberyls occur mainly in phlogopite schists and have a similar formation history.

In the Lake Manyara stones, chromium contents are always dominant over vanadium contents by a factor of at least 5. Chromium and iron values are found in comparable ranges. The iron contents of the zoned alexandrite trilling exceed the values found in other samples. This stone (see again *Figure 24*) also showed decreasing chromium values from the centre to the rim. Transparent areas showed titanium contents in the range of 278–317 ppm Ti, and in milky white areas titanium contents in the range of 298–362 ppm Ti were determined. Thus, the average titanium contents in milky white areas is only slightly higher than titanium contents of transparent green zones. This indicates that the particles responsible for the milky white appearance are not rutile needles, because — in that case — the difference in titanium contents

Table II. Ranges of trace element contents in differently coloured alexandrites and chrysoberyl from Lake Manyara, Tanzania (in wt%).

Samples	Colour in incandescent light	V ₂ O ₃	Cr ₂ O ₃	Fe ₂ O ₃
Rough (<i>Figure 31</i>)	purple to reddish purple	0.002 – 0.016	0.28 – 1.38	0.70 – 1.35
Faceted (<i>Figure 33</i>)	purple to reddish purple	0.004 – 0.019	0.22 – 0.68	0.58 – 0.78
	bluish grey	0.007 – 0.012	0.14 – 0.25	0.70 – 1.29
	orange	0.004 – 0.005	0.10 – 0.12	0.51 – 0.60
	yellow to green	0.003 – 0.009	0.09 – 0.18	0.55 – 1.34
Traverse across zoned trilling (<i>Figure 24</i>)	purple, transparent	0.013 – 0.013	0.11 – 0.14	2.29 – 2.41
	milky white	0.009 – 0.014	0.15 – 1.27	2.13 – 2.55

of transparent to non-transparent zones should be distinctly higher.

The average iron content for all Lake Manyara chrysoberyls and alexandrites lies between the average iron content measured for Russian samples and alexandrites from Zimbabwe. Chromium and vanadium contents of Lake Manyara stones lie in the range of the Russian samples, and the average chromium content is somewhat smaller than that measured for alexandrites from Zimbabwe. In the light of these results, it is evident that these trace element values should not be considered as distinctive criteria for source determination.

Trace elements of potential use for origin determination

For origin determination, various ternary diagrams containing diagnostic trace element contents can be applied. Useful elements include boron, magnesium, gallium, tin and germanium, amongst others. Two examples (*Figure 30 a,b*) of ternary diagrams show a possible means of distinguishing Lake Manyara alexandrites from those of Zimbabwe and Russia. However, according to the particular nature of any stone, different combinations of elements may have to be plotted to establish its origin.

Colorimetric data and nomenclature

Colorimetric systems are used for the quantitative description and prediction of

colour phenomena. For the description of colour, special coordinate systems, known as colour spaces, were developed. The CIELAB colour space is the most complete colour model conventionally used to describe colours and colour differences visible to the human eye. A detailed description of this uniform colour space, the application of this model to colour-change garnets as well as Russian alexandrites and experimental details of colour measurement are given by Schmetzer *et al.* (2009) and Schmetzer and Bosshart (2010). There is also an ongoing discussion in the gem trade and in gemmological laboratories about the border between colour-change chrysoberyl and alexandrite.

To describe colour for alexandrite and chrysoberyl from the Lake Manyara deposit in daylight and incandescent light and to evaluate the extent of colour change, the authors measured two groups of samples and calculated the CIELAB parameters for daylight (standard light source D₆₅) and incandescent light (standard light source A):

1. We visually selected 42 small crystals or crystal fragments with a distinct colour change from green or bluish green in daylight to violet purple, purple, reddish purple or purplish red in incandescent light (*Figure 31*) from several lots consisting of at least 300 rough samples. Absorption spectra were measured and colorimetric data were calculated for all 42 alexandrites.

Alexandrite and colour-change chrysoberyl from the Lake Manyara alexandrite-emerald deposit in northern Tanzania

For a group of 15 samples the spectra in different directions were also measured, if the morphology of the rough irregular fragments allowed this procedure. In summary, colorimetric data from 65 measured spectra were calculated and plotted in *Figure 32*. Ten of this group were also chemically analysed to determine the trace element contents (see above).

- For the 28 faceted chrysoberyls and alexandrites, which were chemically analysed (see above), absorption spectra were measured and colorimetric data were calculated. These alexandrites and chrysoberyls show great variability of colour change between daylight and incandescent light and were selected to cover the full range of colour change present in Lake Manyara stones. The colour in daylight ranged from green either to bluish green or to yellowish green, with a large colour variability in incandescent light, which allowed subdivision of the samples into four subgroups according to their colour in incandescent light: (a) orange, (b) yellow to green, (c) grey to bluish grey, and (d) purple to purplish red. From these 28 spectroscopically examined samples 13 faceted stones were selected (*Figure 33*), to represent the full range of colour and colour change in the population for the graphical presentation of colorimetric data (*Figure 34*).

All colorimetric data closely reflect the visually observed colour (*Figures 31 to 34*). Colorimetric parameters of all rough alexandrites of the first group (*Figures 31 and 32*) reveal a large hue angle difference between daylight and incandescent light as well as a distinct colour difference between both light sources. These colorimetric parameters are typical for an alexandrite-like colour change from green or bluish green in daylight to a colour ranging from violet purple to purplish red in incandescent light.

All 13 faceted gemstones of the second group also reveal a distinct colour change between daylight and incandescent light, and a wide range of colours under the

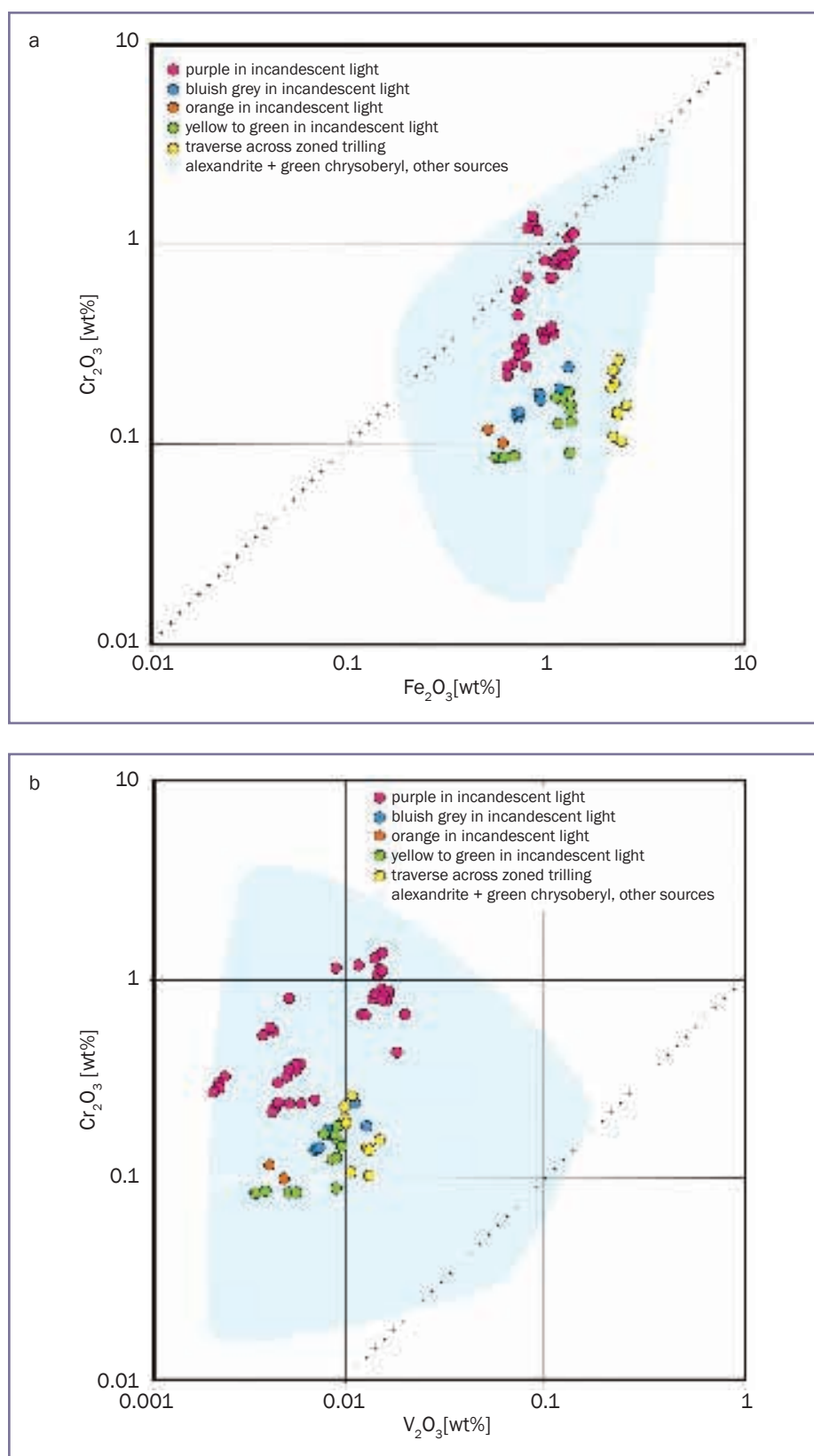


Figure 35 a,b: Iron, chromium and vanadium contents of alexandrites and green chrysoberyls from Lake Manyara and from other localities. The general light blue area represents more than 220 samples including all market relevant sources. The differently coloured symbols represent the approximate colours of the samples observed in incandescent light. Chromium contents in alexandrites from Lake Manyara with a colour change to purple or reddish purple are above the values measured in samples with other colours in incandescent light; the values for iron and vanadium, on the other hand, are comparable. Artwork by A.-K. Malsy.

Alexandrite and colour-change chrysoberyl from the Lake Manyara alexandrite-emerald deposit in northern Tanzania

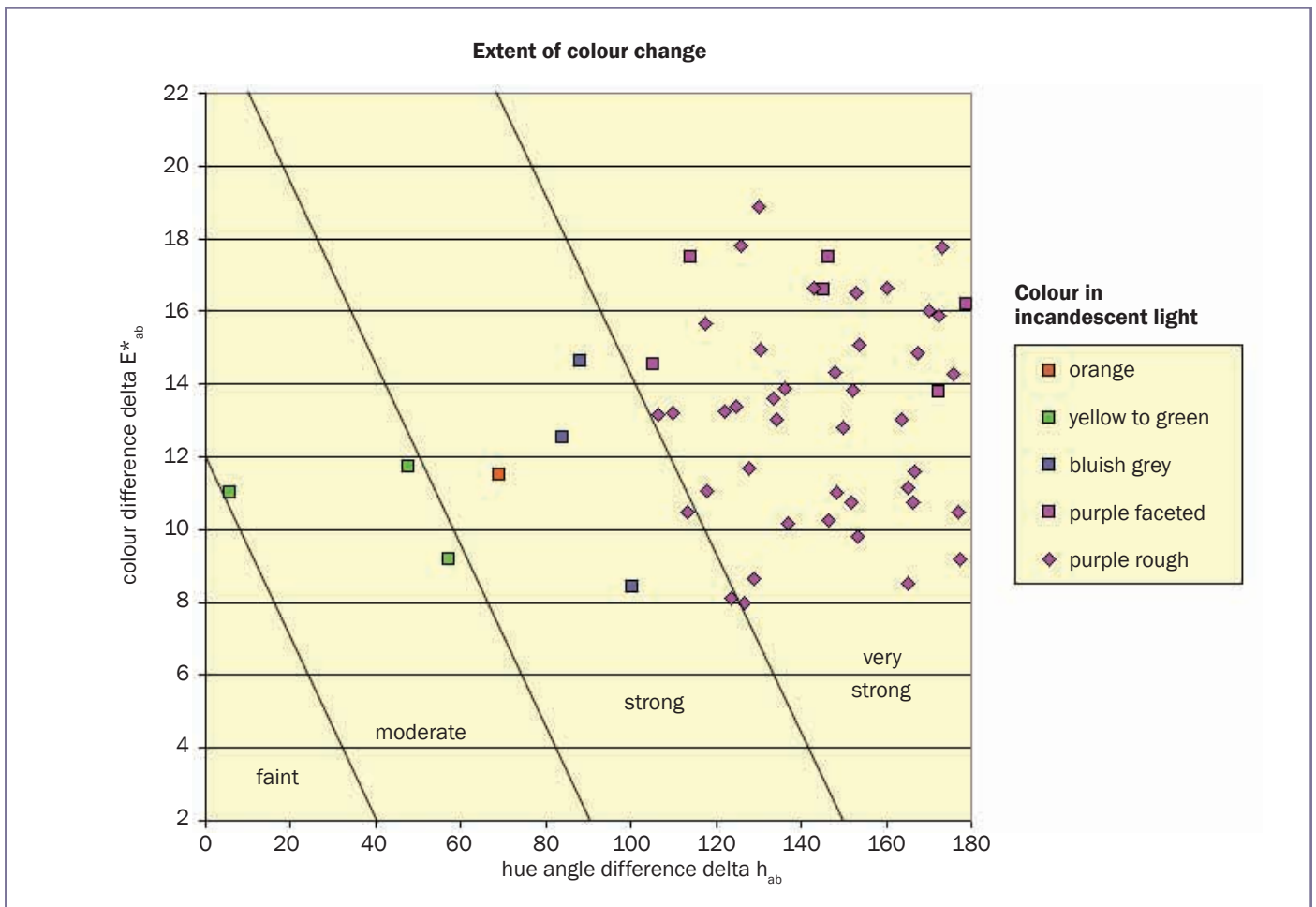


Figure 36: Graph showing the correlation of the main colorimetric parameters of hue angle difference and colour difference in alexandrites and colour-change chrysoberyls from Lake Manyara, with correlations representing the extent of colour change referred to as faint, moderate, strong and very strong. The extent of colour change for rough and faceted alexandrites with a purple or reddish purple coloration in incandescent light [samples of group I and of group II, subgroup (d)] is very strong, the extent of colour change for samples with different coloration in incandescent light [orange, yellow to green or bluish grey; samples of group II, subgroups (a), (b) and (c)] is moderate to strong. Artwork by K. Schmetzer.

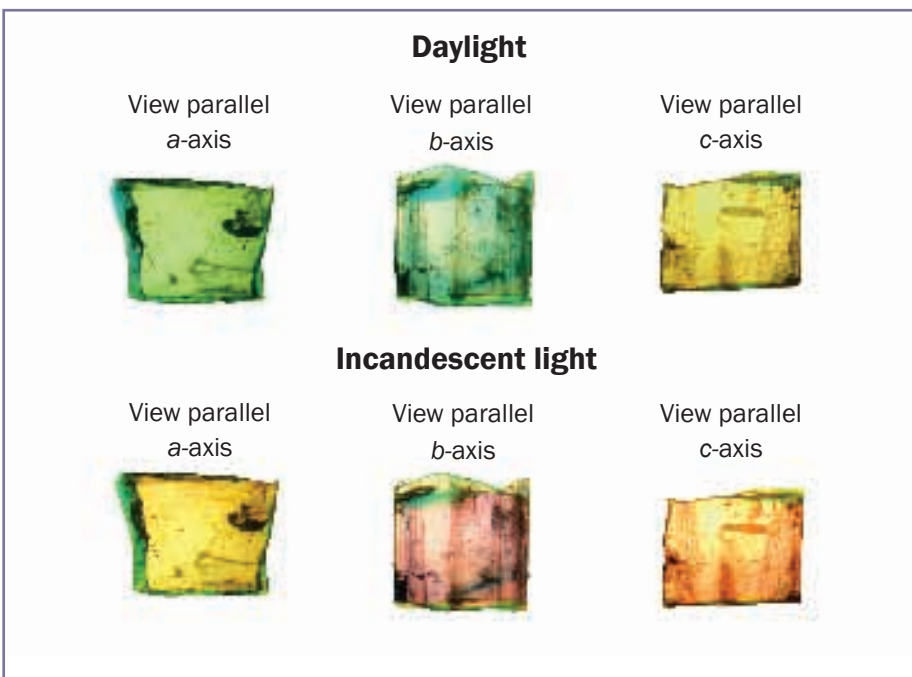
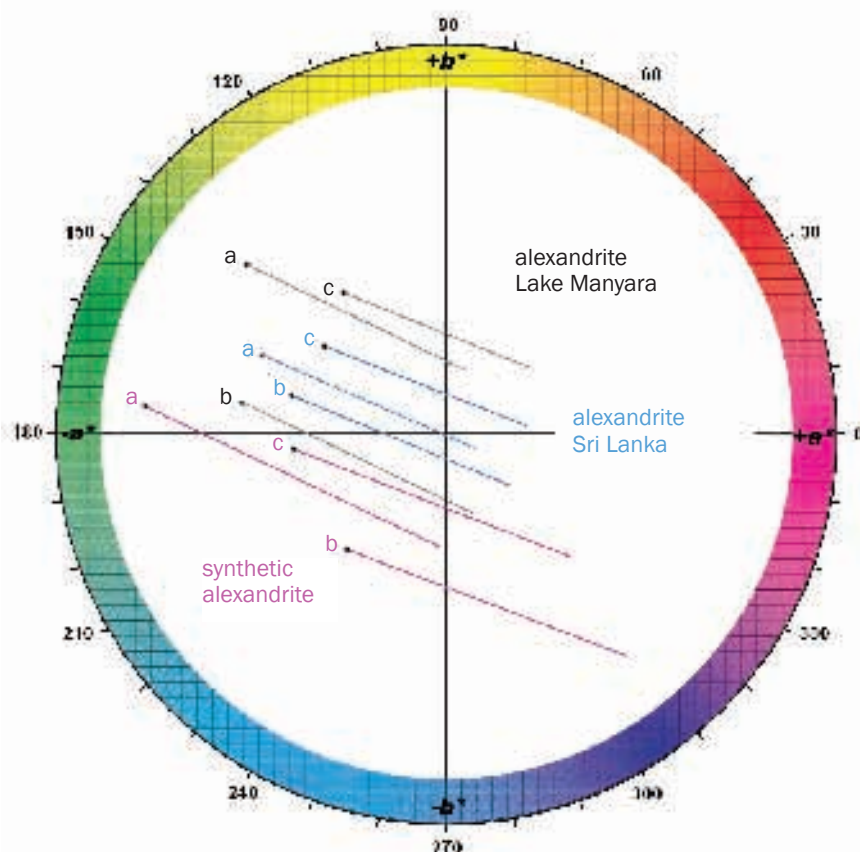


Figure 37: Colour and pleochroism in a natural alexandrite single crystal from Lake Manyara, Tanzania, in daylight and incandescent light in views parallel to the a-, b- and c-axes. The crystal fragment shows a and b pinacoids and is broken at both terminations, size of the crystal 3.8 × 3.5 × 3.2 mm. With the unaided eye (non-polarized light), the observed coloration in all three directions varies distinctly, with the 'best' colour change in the view parallel to the b-axis. Parallel to the a-axis, the red colour component in incandescent light is very small. Photographs and artwork by K. Schmetzer.

Alexandrite and colour-change chrysoberyl from the Lake Manyara alexandrite-emerald deposit in northern Tanzania

Figure 38: Colorimetric parameters of three alexandrite cubes, i.e. of natural alexandrite from Lake Manyara, Tanzania (see Figure 37), and natural alexandrite from Sri Lanka as well as Czochralski-grown synthetic alexandrite from Russia plotted in the CIELAB colour circle. Each stone was measured parallel to the crystallographic a-, b- and c-axis) and the coordinates labelled accordingly; the neutral point (white point) is in the centre of the a*b* coordinate system; the small black circles represent the coordinates in daylight D₆₅ and the ends of the differently coloured bars represent the coordinates in tungsten light A; the outer circle represents a chroma of 18. The typical alexandrite-like colour change from daylight to incandescent light is apparent in views parallel to the b-axis and partly also in views parallel to the c-axis. The red colour component in incandescent light is distinctly weaker in views parallel to the a-axis. Data for the synthetic Russian alexandrite from Schmetzer and Bosshart (2010), data for the natural samples from Tanzania and Sri Lanka measured by A.-K. Malsy.



latter (Figures 33 and 34). Only six samples (subgroup d) show a colour change to purple or purplish red in incandescent light, which represents a typical alexandrite-like colour change between daylight and incandescent light. The other groups of samples [subgroups (b) and (c)] show a colour change to yellow or green or to greyish blue in incandescent light, and one stone [subgroup (a)] became brownish orange in incandescent light.

Chromium, vanadium and iron contents of rough alexandrite crystals and of the four different groups of faceted stones are plotted in Figure 35 a,b. It is evident that chromium contents of most samples with a typical alexandrite-like colour change of green to purplish red in daylight to incandescent light (rough samples of group I [Figure 31] and faceted samples of group II, subgroup (d) of [Figure 33]) exceed the chromium contents of samples with colour change to bluish grey, orange or yellowish green to yellow in incandescent light (faceted samples of group II, subgroups (a), (b), and (c) [Figure 33]). Vanadium and iron contents, on the other hand, are in similar ranges.

Table III. Trace element contents, colour and pleochroism in selected alexandrites.

Samples	Czochralski-grown synthetic alexandrite, Russia	Natural alexandrite, Lake Manyara, Tanzania	Natural alexandrite, Sri Lanka
Size (mm)	9.2 × 9.0 × 9.0	3.8 × 3.5 × 3.2	6.6 × 6.1 × 6.0
Trace element contents (wt%)			
V ₂ O ₃	0.09	0.01	0.01
Cr ₂ O ₃	0.21	0.60	0.15
Fe ₂ O ₃	< 0.01	1.23	0.80
Colour to the unaided eye in daylight			
View a-axis	intense green	green	green
View b-axis	greenish blue	bluish green	bluish green
View c-axis	light green	yellowish green	yellowish green
Colour to the unaided eye in incandescent light			
View a-axis	bluish grey	yellow	purplish grey, almost colourless
View b-axis	intense purple	violet purple	intense purple
View c-axis	light greyish purple	orange	purplish red

To evaluate the extent of colour change, the two relevant colorimetric data, i.e. colour difference ΔE^*_{ab} versus hue angle difference Δh_{ab} were plotted in Figure 36. The rough and faceted samples with

a typical alexandrite-like colour change [rough samples, group I, and faceted samples, group II, subgroup (d)] showed a wide variation of hue angle difference (from about 100° to 180°) and colour

Alexandrite and colour-change chrysoberyl from the Lake Manyara alexandrite-emerald deposit in northern Tanzania

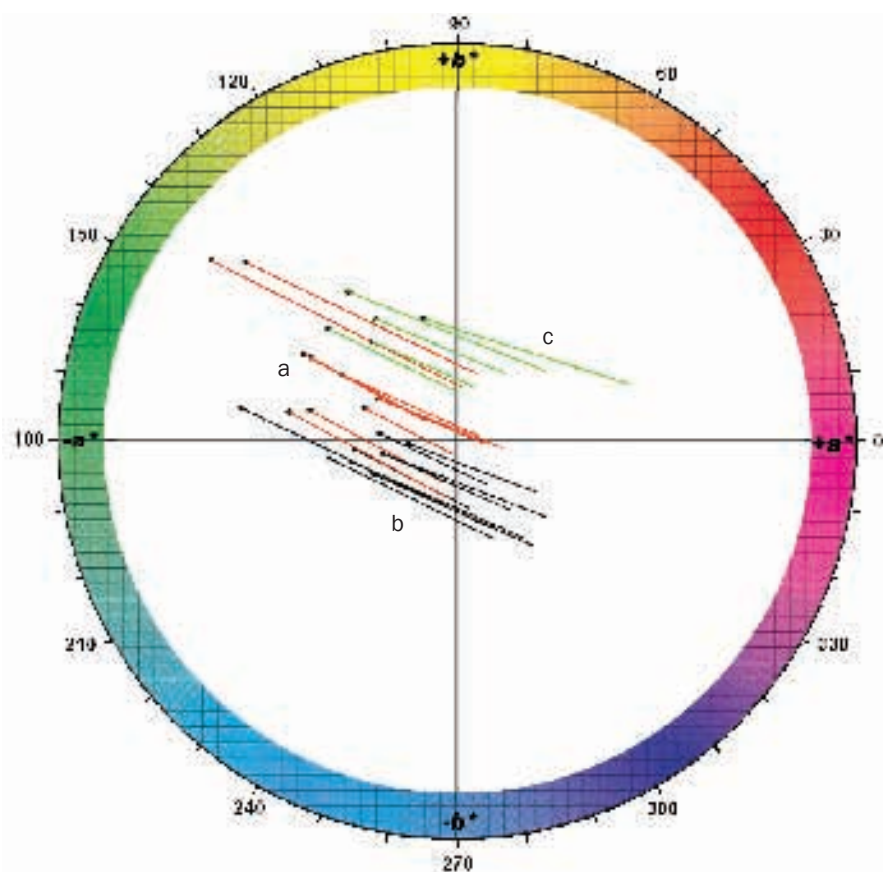


Figure 39: Colorimetric parameters of rough and faceted alexandrites and chrysoberyls from Lake Manyara in the CIELAB colour circle; the neutral point (white point) is in the centre of the a^*b^* coordinate system; the small black circles represent the coordinates in daylight D_{65} and the ends of the differently coloured bars represent the coordinates for tungsten light A; the outer circle represents a chroma of 18. The coloured bars represent measurements of different samples with a predominant path of light parallel to the a -axis (red), parallel to the b -axis (black) and parallel to the c -axis (green) of each sample. The dependency of colour and colour change on stone orientation is evident. Colorimetric measurements of various samples by A.-K. Malsy and G. Bosshart.

differences (between 8 and 19 CIELAB units). Using the definition for the extent of colour change given by Schmetzer *et al.* (2009) and Schmetzer and Bosshart (2010), the extent of colour change for all these alexandrites is very strong. The other samples show colour differences in the same range, but smaller hue angle differences. Although these samples show moderate [group II, subgroup (b), yellow to green,] or strong colour change [group II, subgroup (a), brownish orange sample, and subgroup (c), bluish grey samples], they do not show the traditional alexandrite colours in incandescent light.

The association or correlation of chemical properties, especially chromium contents, and colorimetric parameters, however, does not completely explain

the pattern of colour change observed. It is generally known in the gem trade and especially by cutters of alexandrite rough, that the colours observable in incandescent light are strongly dependent on the orientation of the samples (Fischer, 1954, 94–6). This was demonstrated with colorimetric parameters measured for alexandrites in different orientations versus the non-polarized primary spectrometer beam (Schmetzer and Bosshart, 2010). In particular, colorimetric parameters were described for an exactly oriented, Czochralski-grown cube of synthetic alexandrite.

Similar orientation dependencies were observed and measured in two natural alexandrites. One fragment of an untwinned crystal from Lake Manyara is

shown in Figure 37 in different orientations in daylight and incandescent light. For comparison, an alexandrite cube from Sri Lanka was also measured. The size, chemical properties and colours to the unaided eye in daylight and incandescent light of the two samples are summarized in Table III, the colorimetric parameters are plotted in Figure 38. The parameters of the synthetic alexandrite cube mentioned above are also given.

The sample loci within the CIELAB colour circle (Figure 38) represent the colours for daylight and incandescent light. Although the connecting bars between the loci measured for a specific orientation of the three cubes are almost parallel to each other, the positions of the endpoints differ significantly and demonstrate the distinct pleochroism of alexandrite. The lengths of the bars are a graphical representation of colour difference in the a^*b^* plane of the CIELAB colour circle.

Although the three samples show large differences according to various trace element contents and variable paths of light (sample thickness), a general scheme is apparent for all three alexandrites. In daylight, in a view parallel to the a -axis, the most intense and pure green is visible. In a view parallel to the b -axis, the alexandrites are more bluish green and in a view parallel to the c -axis, the alexandrites are less intense green or more yellowish green. The most intense colour change is always parallel to the b -axis; the change is somewhat weaker parallel to the c -axis. In incandescent light, the colour parallel to the a -axis in these three samples changed only to yellow, bluish grey or purplish grey, in general without a distinct red colour component.

In the gem trade, only a small percentage of faceted alexandrites will be cut so that the table facets are exactly perpendicular to one of the three crystallographic axes a , b or c . To evaluate the orientation dependency of colour change in faceted alexandrites and green chrysoberyls from Lake Manyara, we determined the orientation of the table facets for colorimetrically measured and chemically analysed samples by optical

Alexandrite and colour-change chrysoberyl from the Lake Manyara alexandrite-emerald deposit in northern Tanzania

means (pleochroism, growth structures, twinning, observation of optical axes; see Schmetzer, 2011). We also selected the rough samples which had been colorimetrically measured through a natural crystal face (in this case, through an **a** or **b** pinacoid) and chemically analysed and examined all samples for the presence or absence of twinning, i.e. if the samples were single crystals or twins. According to the twin law of chrysoberyl, the *a*-axes of twinned individuals are parallel to each other, but the *b*- and *c*-axes are not. Thus, twinned samples can be measured through the **a** pinacoid to determine colorimetric parameters, but not through the **b** pinacoid (the **c** pinacoid is not present in Lake Manyara samples).

The above constraints meant that we could only use some of the faceted and rough samples for this research, simply because some stones were cut with a table facet oblique to the crystallographic axes or some broken crystals did not show an **a** or **b** pinacoid suitable for oriented spectroscopic measurement. Also, twinned stones were rejected. It should also be mentioned that the different cut and/or thickness of the faceted stone plays a certain role. Therefore we also tried to use samples of comparable thickness for this research. The results are plotted in Figure 39.

In general, the trend described above for the three cubes (Figure 38) was confirmed. Most stones with a table facet predominantly perpendicular to the crystallographic *a*-axis (i.e. in a view parallel to the *a*-axis) showed an intense green coloration in daylight. Samples examined parallel to the *b*-axis are less intense green or more bluish green. Samples viewed parallel to the *c*-axis are more yellowish green in daylight. For stones with a table facet predominantly perpendicular to the *b*-axis, various shades and intensities of purple to purplish red are shown in incandescent light. For samples with a table facet predominantly perpendicular to the *c*-axis, the colour in incandescent light varied between orange, yellow and green. Some samples viewed parallel to the *a*-axis did not show a distinct red colour component

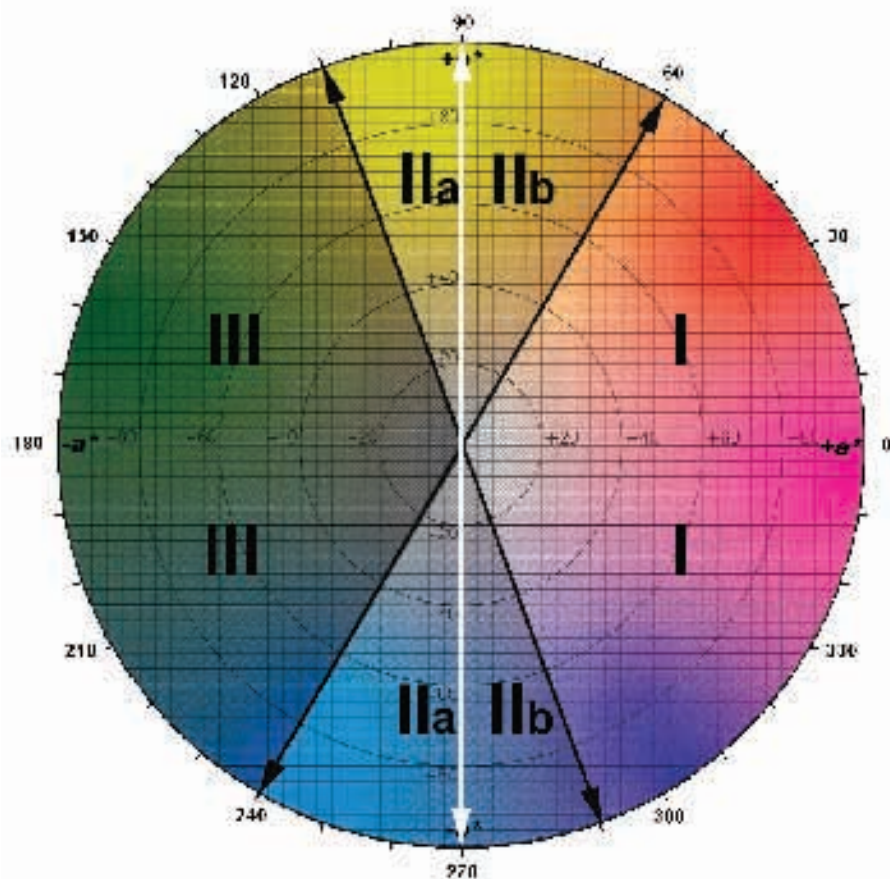


Figure 40: This schematic diagram is designed to aid thinking about the distinction and naming of alexandrite and green chrysoberyl in the gem trade. The colour wheel represents colours of these gems in incandescent light; the white line separates those with a red colour component (sectors I and IIb) from those without red (sectors III and IIa). Stones with colours in sector I are – in general – accepted as alexandrites in the trade, whereas those with colours in sector III are – in general – not designated as alexandrites. There are, however, some stones with colours in the yellow to orange or in the blue to blue violet ranges (sectors IIa and IIb), which are accepted by only some in the gem trade as alexandrites. The position of the boundaries between sectors I and IIb, representing possible boundaries between alexandrite and colour-change chrysoberyl, is also a matter of discussion. Artwork by K. Schmetzer.

in incandescent light. In a view parallel to the *a*-axis, only stones with chromium contents in the range of 0.9 wt% Cr₂O₃ or above were red to purple in incandescent light.

These results enable one to explain the extreme variability of colour change of faceted and rough alexandrites. It is evident that the orientation of the table facet or the direction of view in rough samples plays a dominant role in establishing the extent and nature of the colour change and the classification of the faceted or rough stone as alexandrite or chrysoberyl. Therefore, the distinction of alexandrite from chrysoberyl based on the presence or absence of chromium and even the quantitative determination

of chromium contents in specific samples is not sufficient to solve this nomenclature problem. The presence of a certain amount of chromium is necessary to produce a colour change in chrysoberyl, but in our opinion, there must be a distinct red colour component in incandescent light to call a stone alexandrite.

A chrysoberyl, rough or faceted, can show an alexandrite-like colour change in a specific direction of view, but not in others. Therefore, a faceted stone should only be assessed in a face-up orientation if the correct designation has to be given to a customer in the trade. However, it should be appreciated that in its current cut, a gemstone may not appear as an

Alexandrite and colour-change chrysoberyl from the Lake Manyara alexandrite-emerald deposit in northern Tanzania

alexandrite, but it might show a different colour change with different orientation of its table facet.

In the trade, there is a wide variation of opinion about the correct designation of alexandrites and chrysoberyls. If we apply our colorimetric measurements and place the sample loci for chrysoberyl and alexandrite samples in incandescent light into the colour wheel, we can subdivide the colour wheel into different areas (*Figure 40*). In general, it is agreed that chrysoberyls with a coloration in the colour range designated as sector I should be called alexandrites, while those in a sector designated III should not be called alexandrites. In between, the areas IIa and IIb contain the colours of chrysoberyls subject to most variation in designation. These areas are centred in the blue and yellow. Although we do not want to formally define a boundary between alexandrite and chrysoberyl (boundaries between sectors labelled I and IIb in *Figure 40*), at present we would not designate samples with a colour in incandescent light represented by areas labelled IIa in *Figure 40* (e.g. yellow samples) as alexandrites, simply because they do not show any red colour component in incandescent light.

A system used by some in the gem trade which describes the colour change of alexandrites in terms of a certain percentage, e.g. 30 % colour change, 50 % colour change, is, in our view, not very helpful because neither the colour in daylight nor that in incandescent light is given or can be deduced from such a simple percentage figure.

Using the Lake Manyara stones pictured in *Figure 33* in daylight and incandescent light with sample loci plotted into the CIELAB colour circle in *Figure 34*, we contacted numerous people in the gem trade and found a wide range of opinions. The great majority told us that they would not designate our samples 1, 2, 3 and 6 as alexandrites, but a minority would do so for samples 1, 2 and 3, or only for sample 1. The opinions about samples 9, 10 and 11 with bluish grey colour in incandescent light were also different, with some dealers

accepting these stones as alexandrites, and others not.

Discussion and comparison of the Lake Manyara material with alexandrites from other phlogopite-bearing schist-type deposits

Alexandrites from Lake Manyara, Tanzania, from various localities in the Urals, Russia, and from Novello, Zimbabwe, occur in a common type of emerald-alexandrite deposit comprising seams, layers or irregularly shaped ore bodies of phlogopite. This common lithological host had already been recognized in the 1960s, shortly after the discovery of the occurrence at Novello (Martin, 1962; Bank, 1964; Bank and Okrusch, 1967; Okrusch, 1971) and was again underlined in the 1970s after the discovery of the Lake Manyara deposit (Thurm, 1972 a,b,c; Bank, 1974; Gübelin, 1974, 1976).

Although emerald and alexandrite are occasionally found together in such deposits, they mostly form at some distance from each other. In the Novello area, the main emerald- and alexandrite-bearing bodies were found about 1 km apart (Taylor, 1976; Metson and Taylor, 1977). In Lake Manyara, the distance is very variable, between a few tens of centimetres to a few metres or tens of metres. Although details of the emerald-alexandrite formation within these schist-type deposits are still under discussion, a multistage metamorphic genesis in so-called 'blackwall' contact zones is generally accepted for this type of deposit (see detailed review by Franz and Morteani, 2002).

A comparison of alexandrites originating from massive phlogopite host rocks indicates that the samples from Novello are most similar to some of the Russian material and that an equivalent to the Lake Manyara material is also found in Russia. However, it must be emphasised that the Russian samples originate

from numerous deposits exploited by surface and underground mining over a considerably larger area than the Lake Manyara and Novello sources. Consequently, the Russian samples show a larger variability of characteristic mineralogical and gemmological features.

The most impressive rough crystals from all three mining areas are cyclic twins (trillings), which show two main types of habit: dipyrnidal-equidimensional-columnar or tabular. Below we compare samples with dipyrnidal to columnar habit, but similar results would be obtained for trillings with tabular habit, twins or single crystals. The growth sequence of alexandrite trillings is given as a schematic overview in *Figure 41*. The first stage of crystal growth (A) is characterized by a simple dipyrnidal habit with the dipyrnidal **o** and the pinacoid **a** as dominant crystal forms. In the last step of crystal growth (H), the columnar trillings are characterized by the prism **i** and the pinacoid **a**. Intermediate steps (B to G) are described as a step-by-step increase in size of **i** and a corresponding decrease in size of **o**. During this sequence, the dipyrnidal **w** also grows but only temporarily (E).

Specimens from Russia can show any or all the habits shown in *Figure 41*, but generally only two or three steps within this sequence are found within one alexandrite trilling. For example, a sample might show an external morphology as described in crystal (E), and with the microscope, a morphology varying from C (in the centre of the crystal) over D (in the middle) to E (at the outermost rim) might be seen. Another example with an external morphology of crystal G might show internal growth structures represented schematically by drawings E and F.

Specimens from Novello (Schmetzer *et al.*, 2011) show two types of trillings, both with **o**, **b**, **i** and occasionally with **w** faces (examples D and E). In the first type, these faces are combined with the **a** pinacoid, a feature also commonly observed in Russian samples from the Malysheva Mine (Schmetzer, 2010). On the

Alexandrite and colour-change chrysoberyl from the Lake Manyara alexandrite-emerald deposit in northern Tanzania

other hand, the second type from Novello with smaller or no *a* pinacoids and larger *m* prism faces, is extremely rare in Russian samples. Instead of the *m* prism, which is a larger face in Novello samples, alexandrite from the Urals commonly shows the *s* prism. Some of the Russian samples do not show the *i* prism and the *w* dipyramid, a common feature in crystals from Novello.

Trillings from Lake Manyara, on the other hand, show two dominant faces, the *a* pinacoid and the *i* prism, mostly in combination with small *o* dipyramids and *b* pinacoidal faces (see again Figure 41, examples F to H). Under the microscope growth patterns at the beginning of crystal growth showing the *w* dipyramid (E) are visible; this is not seen macroscopically on the mature crystals (see again Figure 23). This morphology has recently been found in Russian alexandrites which have been unearthed within the last two decades from the Malysheva Mine, but only in smaller crystals with columnar habit. In contrast to Russian samples and crystals from Novello, single crystals and twins from Lake Manyara commonly show the prism *r*.

The general crystal morphology of twinned and untwinned chrysoberyls from the Lake Manyara deposit is reflected in their growth patterns and consists of dominant *a* pinacoids and *i* prism faces with subordinate (smaller) *o* dipyramids. In contrast to some alexandrites from Russia and most from Zimbabwe, intense colour zoning is not present in the Tanzanian stones.

Inclusions or platelets of phlogopite mica are present in the chrysoberyls from all three areas. Other mineral inclusions which are common in material from Lake Manyara are apatite and zircon; channels parallel to the *a*-axis are also common.

Compositionally, Zimbabwean stones have higher chromium contents than most Russian alexandrites, while in samples from Lake Manyara, chromium contents are variable and overlap with those in Russian samples. It was also found that Lake Manyara alexandrites have iron contents intermediate between those in

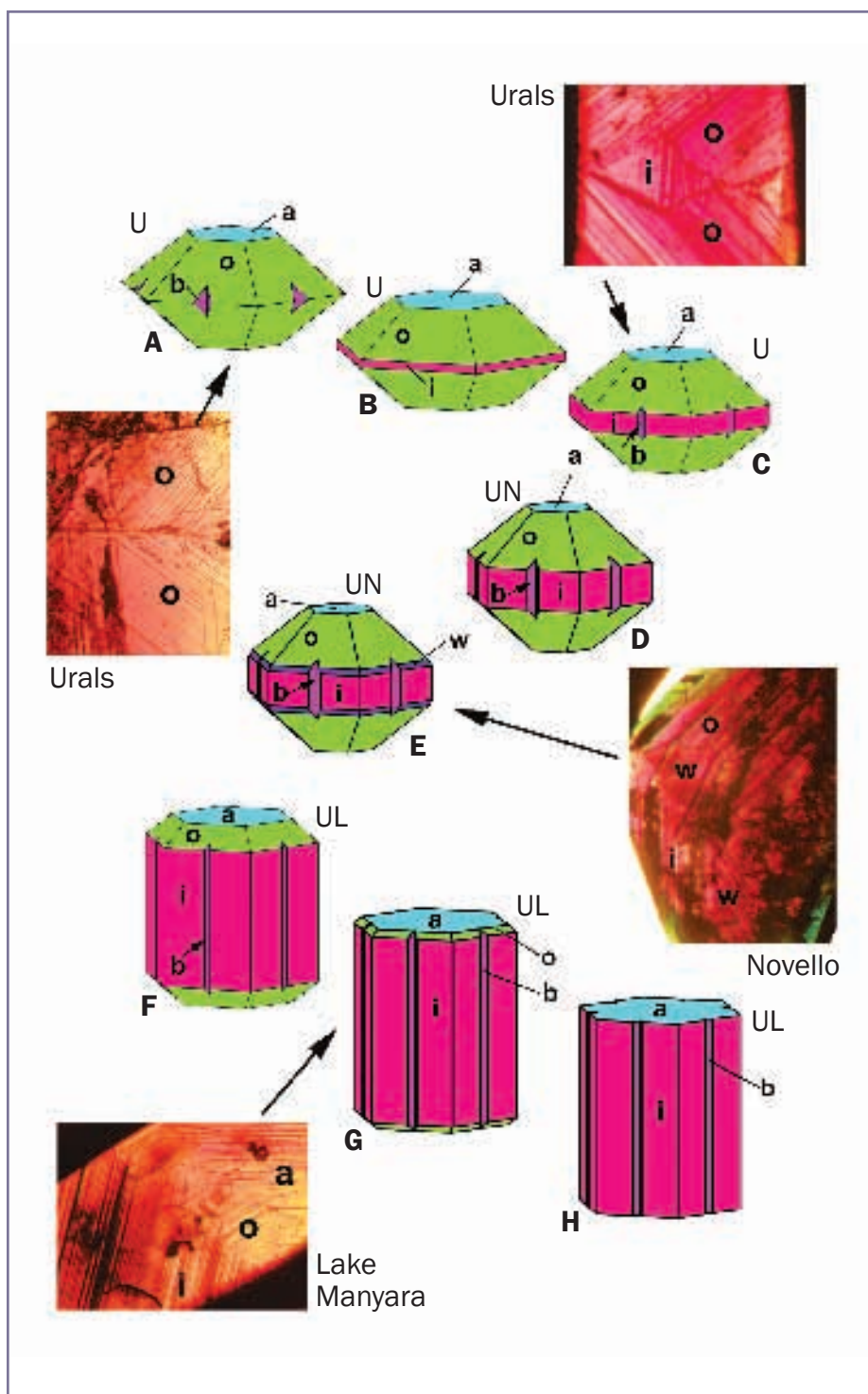


Figure 41: Growth sequence of alexandrite and chrysoberyl trillings with dipyramidal to columnar habit originating from phlogopite schist-related deposits. Examples of the complete growth sequence from A to H can be obtained from stones mined from the Uralian emerald-alexandrite belt (U), Russia, crystals A to C represent typical habits which were unearthed in the nineteenth century, samples D and E represent crystals mined in the twentieth century in the famous Malysheva Mine, and habits F to H represent mostly smaller crystals from the more recent production from Malysheva. Crystals D and E are typical examples of alexandrite trillings from the Novello deposit, Zimbabwe (N). Also E represents a morphology developed at the beginning of crystal growth in the Lake Manyara deposit, Tanzania, but not seen in well developed crystals from this deposit. F to H represent later stages of Lake Manyara (L) material and these habits are common in trillings from this locality. Examples of characteristic internal growth patterns corresponding to the external morphologies are also shown. Photos, crystal drawings and artwork by K. Schmetzer.

Alexandrite and colour-change chrysoberyl from the Lake Manyara alexandrite-emerald deposit in northern Tanzania

Russian and Zimbabwean alexandrites. A more fruitful distinction of stones from these three sources on the basis of composition can be made using various trace elements, such as boron, magnesium, gallium, germanium and tin.

The colour changes observed in alexandrites and chrysoberyls from Tanzania are extremely variable, and relate directly to their chromium contents and the orientation of the table facet with respect to the crystallographic axes.

Acknowledgements

Information about the history of the mine and unpublished geological reports were obtained by Werner Radl, Niederwörresbach, Germany, John M. Saul, Paris, France, and Mark Saul, Swala Gem Traders, Arusha, Tanzania. Cedric Simonet, Nairobi, Kenya, submitted two of his unpublished geological reports for information. Some of the samples examined were from the private collections of the authors, and additional alexandrites from the Lake Manyara area were kindly submitted from the following private collections or from the stock of their companies, which is greatly appreciated:

George Bosshart, Horgen, Switzerland;
Terry Coldham, Sydney, Australia;
Rolf Goerlitz, Rolf Goerlitz Company, Idar-Oberstein;
Frank Jurkutat, Einbeck, Germany;
Michael Krzemnicki, SSEF, Swiss Gemmological Institute, Basel, Switzerland;
Francine Payette, Perth, Australia;
Werner Radl, Mawingu Gems Company, Niederwörresbach, Germany;
John M. Saul, Paris, France;
Markus Wild, Paul Wild Company, Kirschweiler, Germany;
Karl Egon Wild, Wild & Petsch Company, Kirschweiler, Germany.
Frank-Jürgen Schupp, Pforzheim, Germany, kindly submitted the alexandrite cube from Sri Lanka;
George Bosshart, Horgen, Switzerland, measured numerous rough alexandrite crystals and crystal fragments with his

Zeiss MCS 311 colorimeter. Christopher Cavey, London, UK, is thanked for various discussions concerning the alexandrite/chrysoberyl nomenclature.

References

- Amstutz, G.C., and Bank, H., 1977. Geologische, petrographische und mineralogische Beobachtungen in einigen Minen von Smaragd, Tansanit, Tsavorit und Rubin in Tansania und Kenya. *Zeitschrift der Deutschen Gemmologischen Gesellschaft*, **26**(3), 118–27
- Bank, H., 1964. Alexandritvorkommen in Südrhodesien. *Zeitschrift der Deutschen Gesellschaft für Edelsteinkunde*, **47**, 11–15
- Bank, H., 1974. Smaragd, Alexandrit und Rubin als Komponenten einer Paragenese vom Lake Manyara in Tansania. *Zeitschrift der Deutschen Gemmologischen Gesellschaft*, **23**(1), 62–3
- Bank, H., and Okrusch, M., 1967. Mineralogische Untersuchungen am Alexandrit der Novello Claims, Rhodesien. *Zeitschrift der Deutschen Gesellschaft für Edelsteinkunde*, **61**, 33–49
- Bank, H., and Gübelin, E., 1976. Das Smaragd-Alexandritvorkommen von Lake Manyara/Tansania. *Zeitschrift der Deutschen Gemmologischen Gesellschaft*, **25**(3), 130–47
- Bridges, C.R., 1982. Gemstones of East Africa. In: Eash, D.M. (Ed.), *International Gemological Symposium Proceedings 1982*, Gemological Institute of America, 263–75
- Coldham, T., and Payette, F., 2010. The 31st International Gemmological Conference. *Australian Gemmologist*, **24**(1), 17–22
- Dunn, P.J., 1976. Gemmological Notes. *Journal of Gemmology*, **15**(3), 113–18
- Fischer, W., 1954. *Praktische Edelsteinkunde*. 2nd Edn. Kettwig/Ruhr, Verlag Gustav Feller-Nottuln, 187 pp
- Franz, G., and Morteani, G., 2002. Be-minerals: synthesis, stability, and occurrence in metamorphic rocks. In: Grew, E.S. (Ed.), *Beryllium: mineralogy, petrology, and geochemistry*. *Reviews in Mineralogy*, **50**, 551–89
- Gübelin, E.J., 1974. The emerald deposit at Lake Manyara, Tanzania. *Lapidary Journal*, **28**(2), 338–60
- Gübelin, E., 1976. Alexandrite from Lake Manyara, Tanzania. *Gems & Gemology*, **15**(7), 203–9
- Honess, A.P., 1917. On the etching figures of beryl. *American Journal of Science, Series 4*, **43**, 223–36
- Keller, P.C., 1992. Emerald and alexandrite from Tanzania. In: *Gemstones of East Africa*. Geoscience Press, Phoenix, Arizona, 144 pp
- Liddicoat, R.T. Jr., 1976. African alexandrites? *Gems & Gemology*, **15**(7), 211–13
- Malsy, A.-K., 2010. Trace element chemistry and locality determination. In: Schmetzer, K. *Russian alexandrites*. Schweizerbart Science Publishers, Stuttgart, pp 121–6
- Martin, H.J., 1962. Some observations on Southern Rhodesian emeralds and chrysoberyl. *Chamber of Mines Journal*, **4**, 34–8
- Metson, N.A., and Taylor, A.M., 1977. Observations on some Rhodesian emerald occurrences. *Journal of Gemmology*, **15**(8), 422–34
- Moroz, I.I., and Eliezri, I.Z., 1999. Mineral inclusions in emeralds from different sources. *Journal of Gemmology*, **26**(6), 357–63
- Moroz, I., Vapnik, Y., Eliezri, I., and Roth, M., 2001. Mineral and fluid inclusions of emeralds from the Lake Manyara and Sumbawanga deposits, Tanzania. *Journal of African Earth Sciences*, **33**(2), 377–90
- Mwakisunga, M.A., 1972a. Geological report of Mayoka beryl occurrence, Lake Manyara. Unpublished report, 3 pp
- Mwakisunga, M.A., 1972b. Preliminary summary report on Mayoka beryl occurrence — Lake Manyara. Unpublished report, 6 pp
- Okrusch, M., 1971. Zur Genese der Chrysoberyll- und Alexandritlagerstätten. Eine Literaturübersicht. *Zeitschrift der Deutschen Gemmologischen Gesellschaft*, **20**(3), 114–24

Alexandrite and colour-change chrysoberyl from the Lake Manyara alexandrite-emerald deposit in northern Tanzania

- Schmetzer, K., 2010. *Russian alexandrites*. Schweizerbart Science Publishers, Stuttgart, 141 pp
- Schmetzer, K., 2011. Measurement and interpretation of growth patterns in chrysoberyl, including alexandrite. *Journal of Gemmology*, **32**(5-8), 129–44
- Schmetzer, K., Bernhardt, H.-J., Bosshart, G., and Hainschwang, T., 2009. Colour-change garnets from Madagascar: variation of chemical, spectroscopic and colorimetric properties. *Journal of Gemmology*, **31**(5–8), 235–82
- Schmetzer, K., and Bosshart, G., 2010. Colorimetric data of Russian alexandrite and yellowish green to green chrysoberyl. In: Schmetzer, K. *Russian alexandrites*. Schweizerbart Science Publishers, Stuttgart, pp 107–20
- Schmetzer, K., Stocklmayer, S., Stocklmayer, V., and Malsy, A.-K., 2011. Alexandrites from the Novello alexandrite-emerald deposit, Masvingo District, Zimbabwe. *Australian Gemmologist*, **24**(6), 133–47
- Simonet, C., 1997. The Manyara emerald mine – proposals for the re-opening. Unpublished report, October 1997, 7 pp
- Simonet, C., 2010. Manyara alexandrite and emerald. Unpublished report, August 2010, 9 pp
- Taylor, A., 1976. African clues to the great emerald mystery. *Lapidary Journal*, **30**(3), 692–722
- Thurm, R., 1972a. Smaragde vom Lake Manyara in Tansania. *Zeitschrift der Deutschen Gemmologischen Gesellschaft*, **21**(1), 9–12
- Thurm, R.E., 1972b. Die Manyara-Smaragde von Tansania. *Goldschmiede Zeitung*, **70**(5), 62–63
- Thurm, R.E., 1972c. The Lake-Manyara emeralds of Tanzania. *Journal of Gemmology*, **13**(3), 98–9
- Viswanatha, M.N., and Shah, A.P., 1983. Geology and gem potentiality of the emerald deposit at Lake Manyara (Arusha region) Tanzania. Unpublished report, 10 pp
- Wight, Q., and Wight, W., 2010. The 31st International Gemmological Conference Arusha, Tanzania, October, 2009. *Canadian Gemmologist*, **31**(1-3), 16–26

Web list

- Kondo, H., 2005. Manyara: Living on memories. Available at: <http://www.ganoksin.com/borisat/nenam/tanzania-mines.htm>
- Nkwame, M., 2009. Lake Manyara National Park to be expanded. Available at: <http://www.dailynews.co.tz/home/?n=5713&cat=home>

The Authors

Dr Karl Schmetzer

Taubenweg 16, 85238 Petershausen, Germany
email: SchmetzerKarl@hotmail.com

Anna-Kathrin Malsy

Gübelin Gem Lab, Gübelin Gemmological Laboratory, Maihofstr. 102, 6006 Lucerne, Switzerland and Institute of Geological Sciences, Mineralogical Crystallography, University of Berne, Freiestrasse 3, 3012 Bern, Switzerland.
email: A.Malsy@gubelingemlab.ch

The Gem-A TravelGem Microscope

A compact microscope designed for gemmologists — ideal for students, valuers and gem dealers.



Price: £325.00

plus VAT, postage and packing

A 10% discount is given on all instruments ordered by Gem-A members and Gem-A registered students.

- Fitted aluminium travel case
- 10x, 20x, 30x and 60x magnification
- Stone holder and dark field assembly can be removed to examine jewellery
- Runs on 110 and 220 volts (built in transformer)
- Bright field, dark field and top lighting

To order your TravelGem Microscope from the Gem-A shop go to www.gem-a.com/shop.aspx or contact Alan Clark on +44 (0)20 7404 3334, email shop@gem-a.com.



Gem-A

THE GEMMOLOGICAL ASSOCIATION
OF GREAT BRITAIN

Review of ultraviolet sources for gem fluorescence and testing

Grant Pearson, FGAA

Abstract: The ultraviolet-visible spectra of emissions from mercury discharge lamps and light emitting diodes (LEDs) have been recorded. The emissions from five Hg discharge lamps nominally labelled to produce short wave ultraviolet (SWUV) radiation were found to also contain significant long wave (LWUV) components. The emissions of LWUV lamps also were found to contain wavelengths in addition to 365 nm LWUV mercury (Hg) line. This compromises the effectiveness of such lamps for diagnostic gem testing. The emission spectra of LWUV and violet LEDs were collected and found to show spreads of up to 20 nm either side of the nominal emission wavelength. Excitation-fluorescence diagrams obtained by Hoover¹ indicate that some gems such as ruby may not fluoresce when stimulated by SWUV at 254 nm, contrary to present gemmological belief. Experiments carried out with Wood's glass and with nickel sulphate and cobalt sulphate solutions indicate that they do not absorb all LWUV from nominal SWUV sources, so such filters for UV sources are not a reliable tool in gem testing.

Keywords: fluorescence, gem testing, Hg-discharge tubes, light-emitting diodes, ultraviolet, UV-visible emission spectra, Wood's glass filter



1. Introduction

Fluorescence responses evoked by ultraviolet light are frequently used as identity indicators for many gem species, particularly for those containing chromium. However, there has been little investigation and reporting of the consistency and purity of emission of ultraviolet radiation from the low-pressure mercury discharge tubes which have been generally assumed to emit just 365 nm (long wave ultraviolet, LWUV) and 254 nm (short wave ultraviolet, SWUV) radiation. These mercury discharge emissions are filtered by Wood's glass, a visibly

opaque but UV-transparent glass with a high nickel content, or by other similar screening compositions to supposedly exclude all wavelengths other than the two mentioned above.

As a first step in establishing the nature of UV and visible emissions from UV sources used in gem testing, the writer's USB 'Ocean Optics' USB2000 CCD miniature spectrometer was used.

2. Equipment and procedures

The UV source equipment tested includes a dual handpiece instrument

manufactured by the Gemmological Association of All Japan (GAJJ), a dual wavelength single handpiece instrument from UltraViolet Products (UVP), the UVSL-15 with selectable LW or SW outputs, and a smaller unbranded dual-band unit also with LW or SW outputs, all shown in *Figures 1, 2 and 3* respectively.

The USB2000 CCD spectrometer directly registers light emissions between 200 and 850 nm on 2048 discrete CCD channels. This contrasts with many analytical spectrophotometers which determine the relative transparency of a specimen to a monochromatic beam as its wavelength scans across the spectrum.

Review of ultraviolet sources for gem fluorescence and testing



Figure 1: Separate LWUV and SWUV lamps manufactured by the Gemmological Association of All Japan (GAAJ).



Figure 2: A combined LW and SWUV lamp UVSL-15 from UltraViolet Products (UVP).



Figure 3: A combined LW and SWUV lamp, unbranded.

Such instruments cannot register direct emissions from external radiant sources.

Emissions from the three UV sources mentioned above were scanned several times each at appropriate distances from the Ocean Optics USB2000 spectrometer's input optic fibre aperture to develop suitable spectra. This enabled the overall general shapes of their emission envelopes and the specific peak apex or peak centre locations to be recorded together with any wavelengths additional to the nominal ones. The scans are shown in *Figures 4, 5 and 6*, where the relative intensity of radiation is plotted against wavelength.

3. Results and discussion

The scan of the GAAJ shortwave source shown in *Figure 4* contains not just the emission at 254 nm but also SWUV emissions at 267 and 295 nm, LWUV emissions at 310, 334 and 365 nm, and visible emissions at 405 and 437 nm. The LWUV and visible emissions are of total energy exceeding that of the SWUV emissions, based on the relative areas beneath the curve representing the energy received.

Inspection of the GAAJ LWUV-output spectrum, *Figure 4*, shows that the 365 nm line which is supposed to be exclusively generated is actually accompanied by continuous and far more abundant LWUV emission ranging between about 320 and 390 nm. Any LWUV fluorescent reaction observed in a gem or mineral specimen examined with this illumination could then have been excited by any or all of the wavelengths represented in this

emission. That is, a fluorescent reaction may not necessarily be specifically generated by only the 365 nm mercury line, but may be caused by any or all of the available LWUV wavelengths being emitted. Consequently, minerals or gems that may fluoresce to very specific and selective narrow LWUV excitations, not necessarily even the presumed 365 nm line, may give a positive but clearly erroneous reaction to this emission which is supposed to be exclusively the 365 nm line. A false-positive indication of identity could then result.

In addition, any gem that fluoresces to LWUV, especially at or near the 365 nm wavelength, will inevitably react positively to the source in *Figure 4* which is labelled short wave, because of its additional emissions. Despite the apparently visible SWUV fluorescence of a specimen, it could really be quite inert to any or all of the SWUV being generated, responding only to the accompanying LWUV. Any observed SWUV fluorescence that is visibly similar to its LWUV response should therefore be treated suspiciously until a genuine fluorescence excitation by

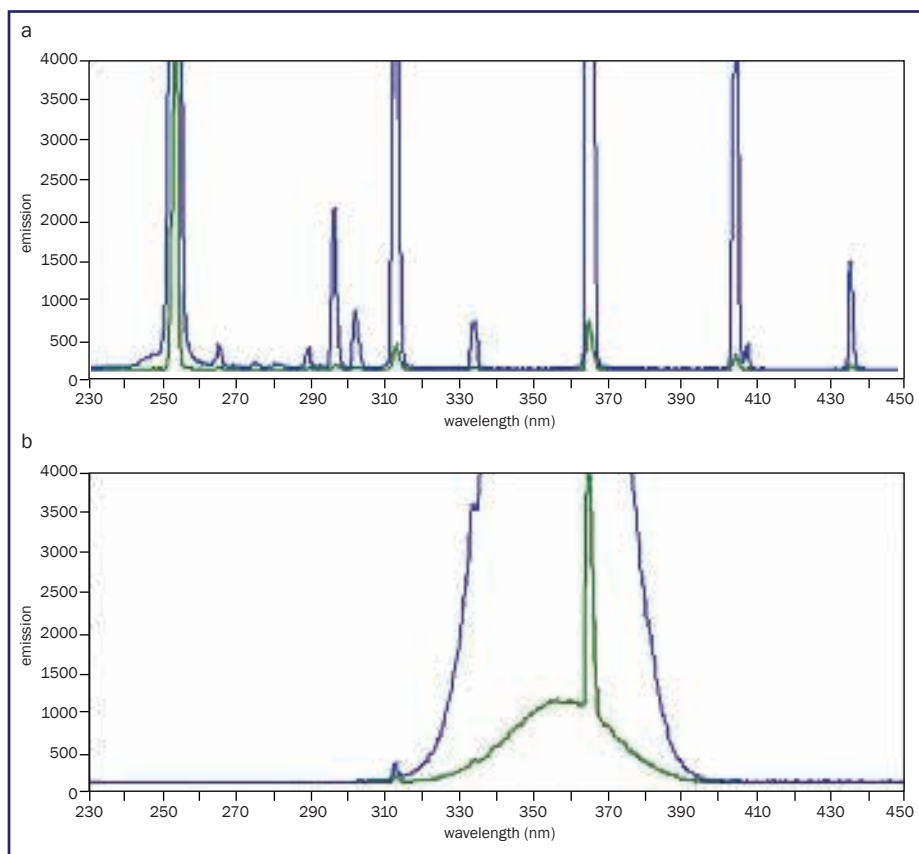


Figure 4: Emission spectra of GAAJ lamps: (a) SWUV range, (b) LWUV range.

Review of ultraviolet sources for gem fluorescence and testing

exclusively SWUV can be demonstrated, rather than by any unsuspected accompanying LWUV.

The spectrum of the SWUV emission from the UVSL-15 lamps shown in *Figure 5* indicates a definite emission near 254 nm accompanied by a substantially larger output in the long wave region which is perhaps comparable with that from the nominal LWUV-only output (see lower graph). So, any visible fluorescence evoked in a gem by such LWUV will also appear when it is placed under the SWUV lamp. Any genuine fluorescence stimulated by the SWUV may not be perceptible since it could be overwhelmed by fluorescence excited by the more intense accompanying LW radiation, especially if the fluorescent emission wavelengths are visibly similar.

Examination of the SWUV emission spectrum of the unbranded dual-band UV unit shown in *Figure 6* also indicates the presence of substantial amounts of LWUV. This common feature of all three commercial lamps suggests that many if not most Hg-discharge UV lamps may suffer from this shortcoming. This implies that any fluorescence displayed by a gem under one of these lights may or may not be due to short-wave stimulation, which in turn casts doubt on attributions of cause and interpretations published in the past.

Just like the other two LWUV maps, the unbranded lamp emits light with a distinct peak near 405 nm. This is significant, since many chromiferous minerals and gems may strongly fluoresce red to the visible shorter wavelengths, often more intensely than to the shorter 365 nm LWUV band to which they may even be negligibly sensitive. This effect is at the core of the 'crossed filters technique' where fluorescence of a specimen is preferentially excited by visible blue light. Appropriate blue light can be screened from initially white continuous light by a solution of a blue copper salt such as the nitrate or sulphate to remove all wavelengths other than the blue to visible-violet (see the transmission spectrum of saturated copper nitrate solution produced by the writer on a

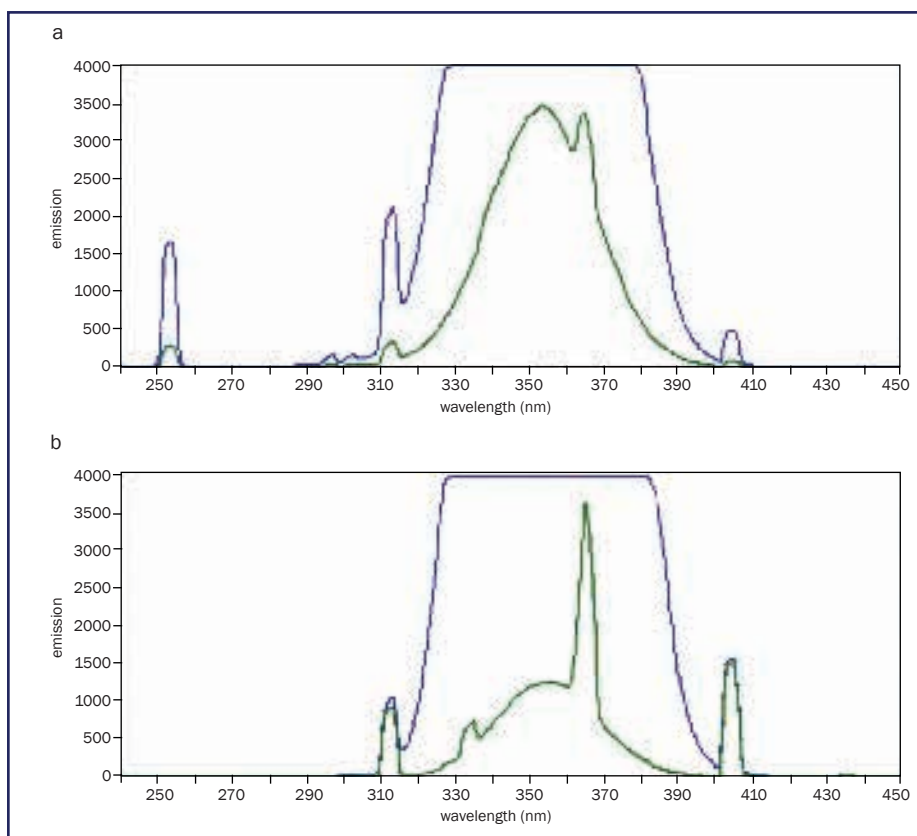


Figure 5: Emission spectra of UVSL-15 lamp: (a) in SWUV mode, (b) in LWUV mode.

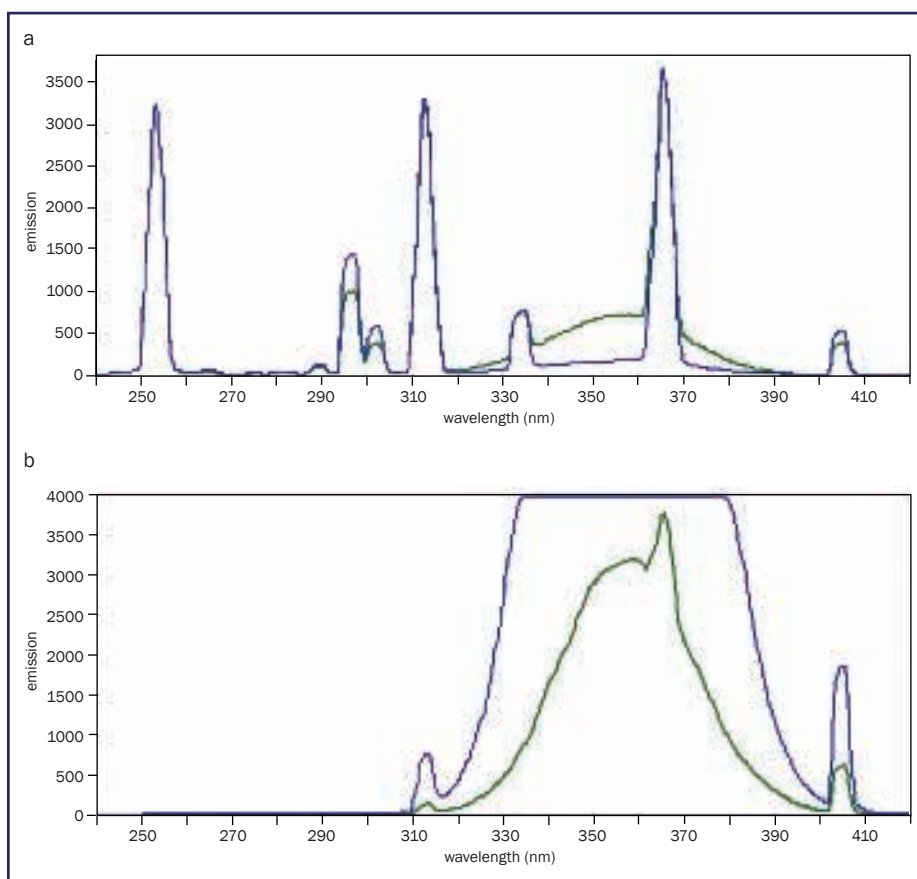


Figure 6: Emission spectra of unbranded lamp: (a) SWUV source, (b) LWUV source.

Review of ultraviolet sources for gem fluorescence and testing

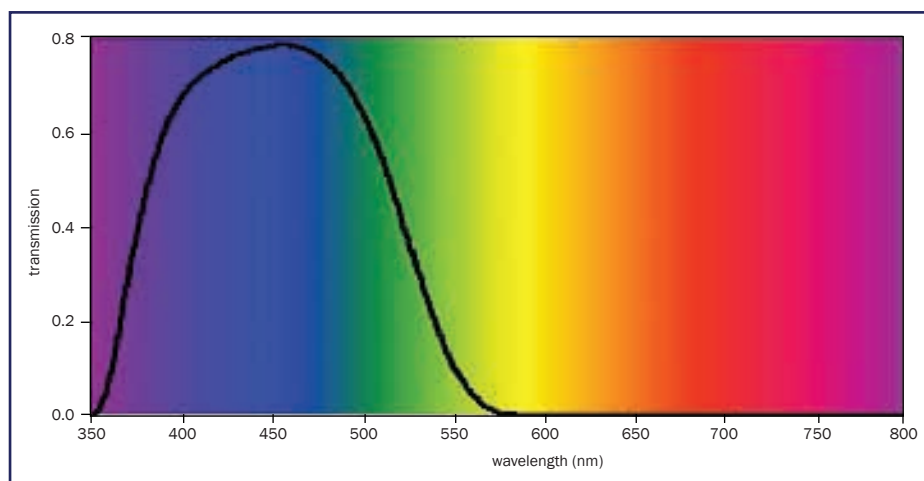


Figure 7: Spectrum showing transmission of visible light through a concentrated aqueous solution of $\text{Cu}(\text{NO}_3)_2$, used as the blue filter in the 'crossed filters' technique.

Varian Cary 3 spectrophotometer, Figure 7) and then viewing any red fluorescence of a specimen through an isolating red 'barrier' filter.² Consequently, any red fluorescence supposedly excited by the 365 nm LWUV could actually be due, partially or totally, to the accompanying blue-violet 405 nm Hg-emission band.

In order to decide how to clarify and improve the use of UV radiation in gem testing, a number of aspects need to be discussed in more detail. These include (a) materials which fluoresce under SWUV but not LWUV, (b) excitation-emission properties of minerals and (c) investigation of light emitting diodes (LEDs), filters and discharge tubes. The

discussion is illustrated by the spectral excitation-emission spectra produced by Hoover and Theisen.¹

(a) *Minerals which fluoresce under SWUV*

A few gem minerals fluoresce when stimulated by wavelengths in the 200 to 300 nm range. In Figure 8 scheelite, benitoite, Verneuil synthetic spinel and hyalite are shown in ordinary light, then under the GAAJ lamp in SW mode. These substances yield genuine and unequivocal SWUV responses since they are inert to excitation by wavelengths in the LWUV 300 to 400 nm range.

(b) *Excitation-emission properties of minerals*

Using a unique, purpose-built

fluorescence spectrophotometer, red fluorescence of various chromium-bearing minerals stimulated by UV and visible wavelengths was demonstrated by Hoover in a series of diagrams reproduced here in Figure 9, a to n. The application of fluorescence stimulated by visible wavelengths to gem testing was then expanded by Hoover and Williams² in their update of the 'crossed filters' technique. In this, they discussed the use of LEDs rather than an incandescent white light and filters of blue solutions of copper salts.

The graphs of excitation wavelength against the fluorescence wavelength stimulated in Figure 9 reveal that significant fluorescence is not generated in many gem species by wavelengths in the SWUV. Unfortunately Hoover's experimental limit of 270 nm is not quite as low as the Hg discharge emission at 254 nm which has hitherto been considered the standard SWUV gem testing wavelength, so at present, the discussion is limited and based on the trends exhibited by the varying strengths of fluorescence to longer wavelengths.

For example, consideration of the three graphs for the different varieties of natural chromiferous corundum, i.e. purple sapphire, Burmese ruby and Thai ruby (see Figure 9 j, k, l) indicates that visible fluorescence, i.e. developed at

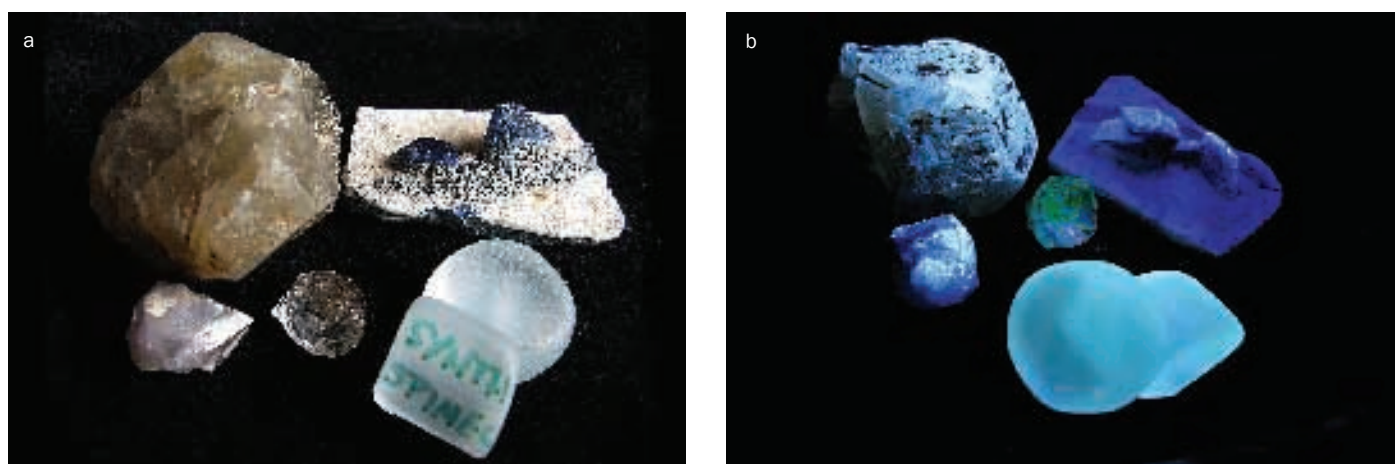


Figure 8: Minerals pictured in daylight and SWUV.

(a) (Clockwise from lower left) Daylight appearance of scheelite (Chinese, Australian crystals), benitoite crystals on natrolite matrix (California), synthetic Verneuil spinel and hyalite opal.

(b) SWUV (GAAJ lamp) fluorescent appearance of scheelite crystals (chalky bluish white to greenish white), benitoite crystals (chalky blue white) on natrolite matrix (also weakly fluorescing, probably due to the contaminating LWUV), synthetic Verneuil spinel (bright greenish white) and hyalite opal (vivid bright green).

Review of ultraviolet sources for gem fluorescence and testing

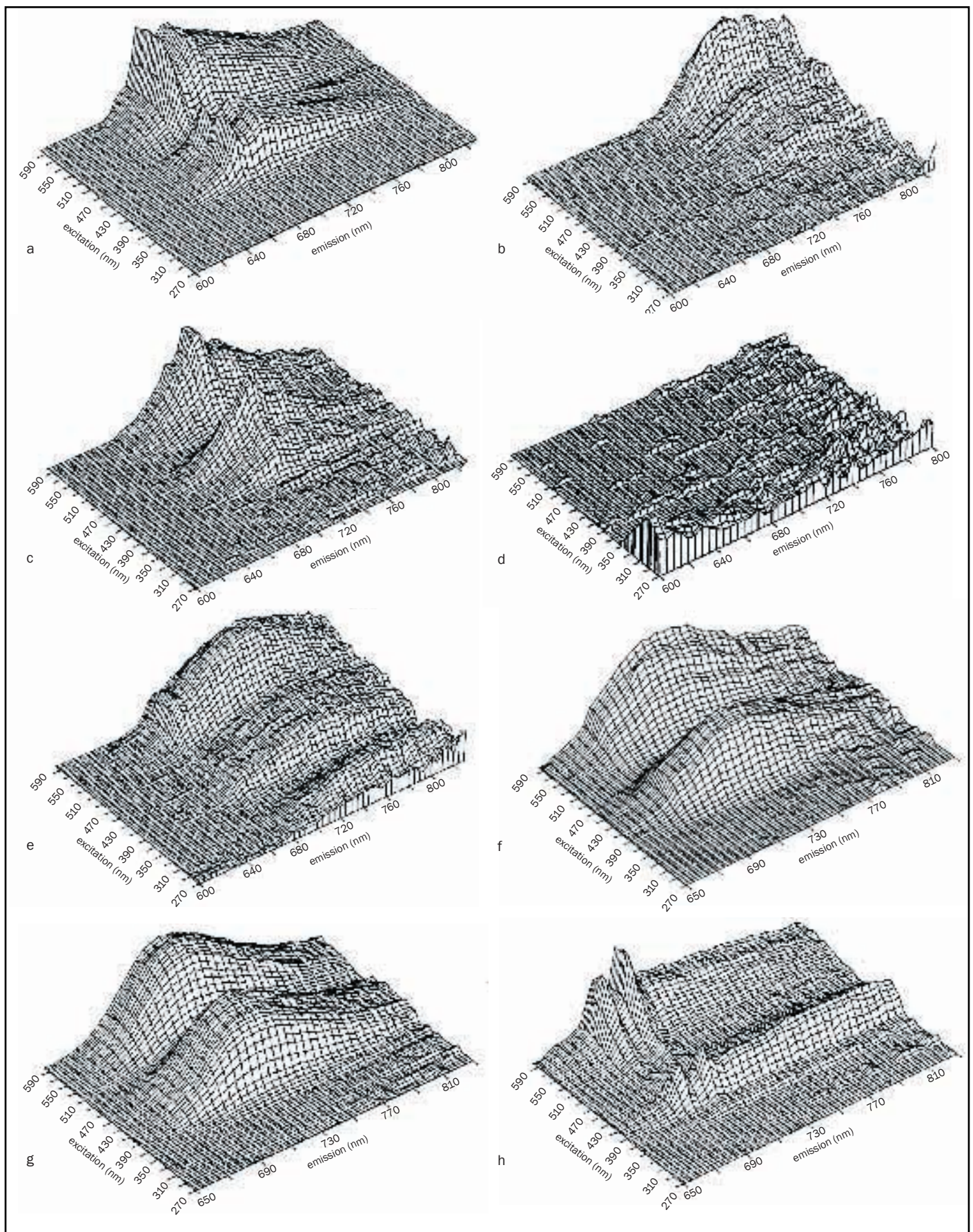


Figure 9 a–h: Fluorescence-excitation contour diagrams for (a) alexandrite, (b) chrome diopside, (c) chrome grossular, (d) chrome korerupine, (e) chrome tourmaline, (f) Australian emerald, (g) Brazilian emerald, and (h) chrome kyanite.

Review of ultraviolet sources for gem fluorescence and testing

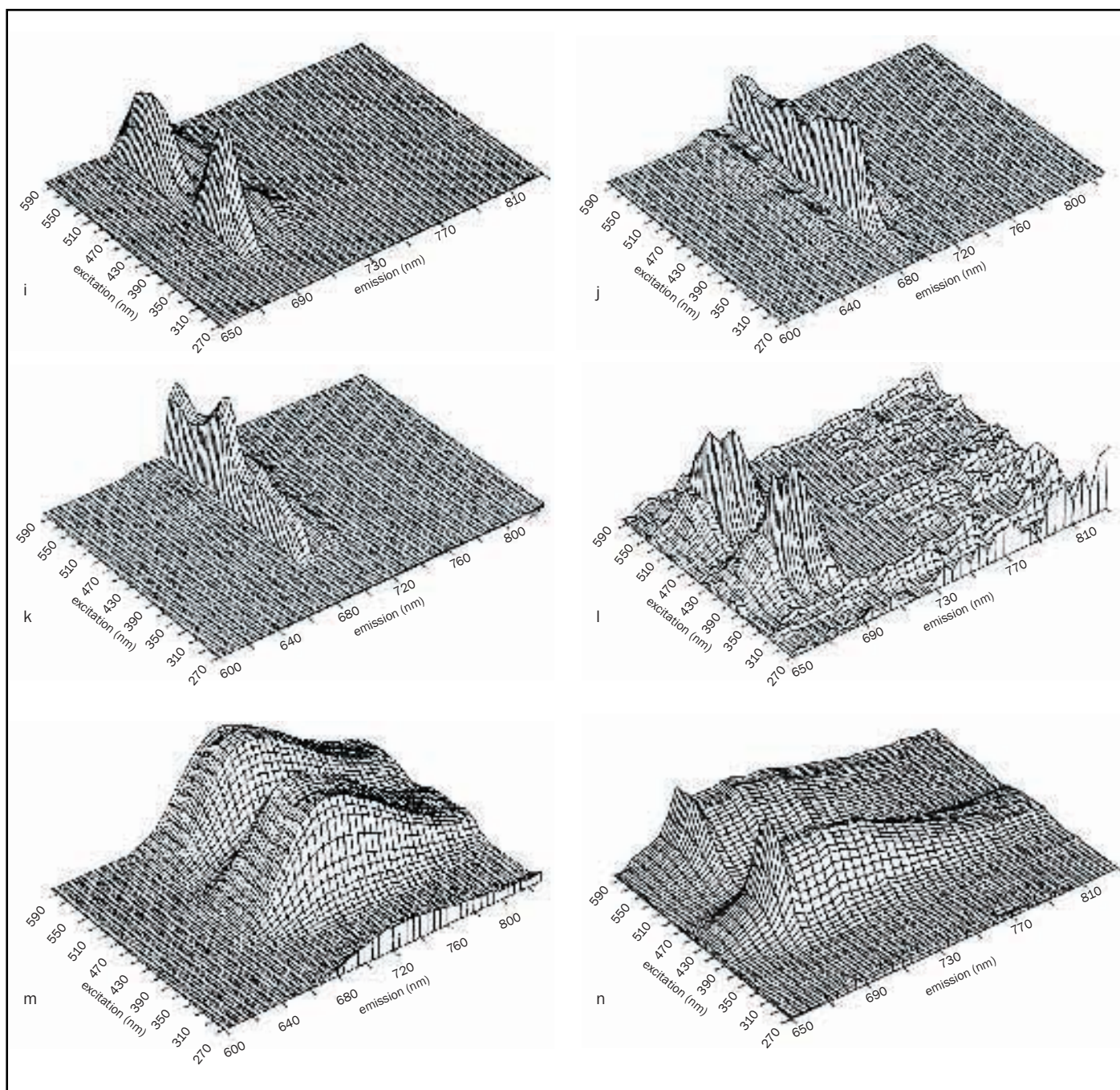


Figure 9 i-n: Fluorescence-excitation contour diagrams for (i) purple sapphire, (j) Burmese ruby, (k) Thai ruby, (l) purple spinel (Sri Lanka), (m) synthetic emerald, (n) pink topaz (Brazil).

wavelengths less than 700 nm, occurs only for excitation wavelengths in the LWUV, and even then only at values greater than about 350 nm for each of them, and with no indication of any fluorescence by excitation at any shorter wavelengths.

The onset of visible fluorescence of the natural Brazilian alexandrite (Figure 9a) only commences at excitation by wavelengths greater than 370 nm, again with no indication of any fluorescence from any shorter excitation wavelengths.

Exactly as for the alexandrite, the chrome grossular (Figure 9c) including green garnets such as Merelani 'mint' garnet or chrome-rich tsavorite), the Australian natural emerald (Figure 9f), the Brazilian natural emerald (Figure 9g), the Kenyan chrome tourmaline (Figure 9e) and the Brazilian pink topaz (Figure 9n), also fluoresce but only to excitation wavelengths greater than 370 nm, suggesting that fluorescence to the usual 365 nm LWUV should not

even be observed and that any detected fluorescence is due to the longer LWUV continuum up to about 390 nm. Some very minor longer wavelength fluorescence was noted for the chrome tourmaline at shorter excitations.

Chrome kyanite (Figure 9b) does not begin to significantly fluoresce until the excitation reaches as much as 390 nm and should be inert to 365 nm LWUV. Purple (chrome-rich) Sri Lankan spinel (Figure 9l), did fluoresce red to 365 nm,

Review of ultraviolet sources for gem fluorescence and testing

beginning at slightly shorter excitation wavelengths around 350 nm with some comparatively minor activity at even shorter excitation wavelengths.

The synthetic emerald (*Figure 9m*) shows the same fluorescence pattern as the two natural emeralds except that additional visible fluorescence does begin to develop as low as about 300 nm, and the fluorescence intensity is still increasing as the excitation wavelength falls to 270 nm. This suggests that this undisclosed variety of synthetic emerald may well fluoresce to some excitation band in the SWUV including 254 nm, in contrast to the natural emeralds.

African chrome kornerupine (*Figure 9d*) develops fluorescence to shorter excitation wavelengths from 350 nm down to at least 270 nm with trending indications that fluorescence may well also occur at the SWUV 254 nm and perhaps even at shorter wavelengths. Chrome diopside fluoresced strongly to excitation, but only emitted at greater than about 390 nm although its fluorescence was confined to the near-infrared with negligible visible fluorescence.

Of all of these instances discussed, only the synthetic emerald displayed significant fluorescence to wavelengths in the part of the SWUV band portrayed, i.e. 270 to 300 nm, and none except the chrome kornerupine showed any trends suggesting that fluorescence to 254 nm might be encountered. None of the various minerals, spinel, corundum, etc, usually considered to develop red diagnostic chrome fluorescence to SWUV, i.e. 254 nm, as well as to the usual LWUV band, actually displayed significant observable fluorescence to the available lower limit of 270 nm. This is consistent with the conclusion indicated above that previously noted fluorescence reactions to SWUV are false and really due to other wavelengths from the lamp emission that extend into the LWUV region.

(c) LEDs, discharge tubes and filters

LEDs have become useful illumination sources in gemmology, especially including some of the shorter-wavelength emitters which can stimulate possibly diagnostic fluorescence in various

Figure 10: Multiple-LED battery-powered torch with a Wood's glass filter and nominal 385 nm emission.

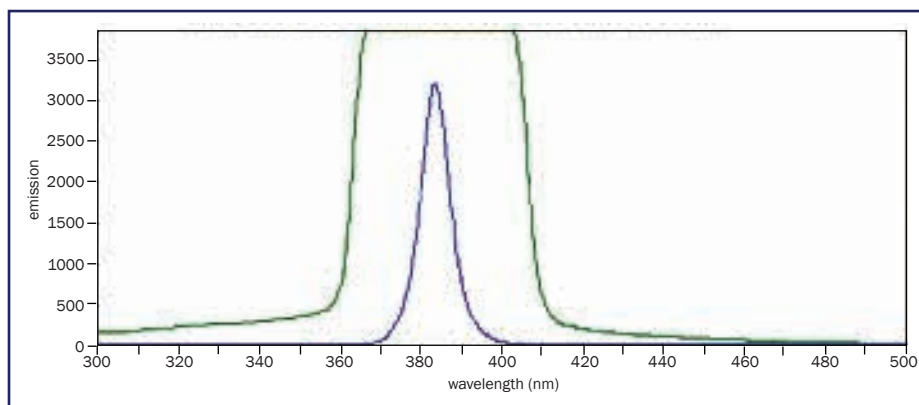


Figure 11: Emission spectrum from LED torch shown in Figure 10. At close range (green trace) the emission band is 50 nm wide but this surprisingly narrows with distance from the source (blue trace).

materials. LEDs producing visible deep blue from about 450 to 400 nm as well as some that generate LWUV at wavelengths near 395 and 385 nm have shown potential for gemmological identification, especially for stimulating fluorescence in susceptible diamonds and in chromiferous materials. The chromiferous gems particularly include ruby, red spinel, alexandrite and even some varieties of emerald. LEDs have significant advantages such as compactness, simplicity and portability, operating from low voltages while drawing only milliwatts of power and developing locally high light intensities appropriate for gemmology. One inexpensive recent development is the manufacture of a torch (*Figure 10*) containing several 385 nm LEDs with their output being filtered by a disc of Wood's glass (*Figure 11*) to remove most of the accompanying visible deep blue to violet emission. The deep blue to violet could mask visible fluorescence results (see the illustrations in *Figure 12* of visible

emissions from a blue LED torch and the 385 nm filtered LED torch). Wood's glass is coloured with nickel, but unlike most bright-green nickel salts, Wood's glass is deep purple and essentially opaque to the visible spectrum although it is transparent to much of the LWUV range. The emissions from several different LED sources, including the 405 nm violet-LED torch (see *Figure 12* (left) and *Figure 13*), a single 405 nm violet LED 'key-ring' torch and a single isolated violet LED were scanned to determine the extents of their outputs (*Figures 14* and *15*).

Another source of LWUV is the fluorescent 'black light' which basically consists of an ordinary fluorescent tube with its glass tube consisting of Wood's glass filter to exclude the visible spectrum. The usual phosphors to convert the UV emissions of Hg into visible light have probably been replaced by ones which emit LWUV (see Gleason⁴). Also, information posted on the internet suggests that compositions such as

Review of ultraviolet sources for gem fluorescence and testing



Figure 12: Multiple-LED torch of Figure 10 on the right next to a multiple-LED torch on the left which is unfiltered and emits light at and around 405 nm.



Figure 13: Another view of the torch on the left in Figure 12.

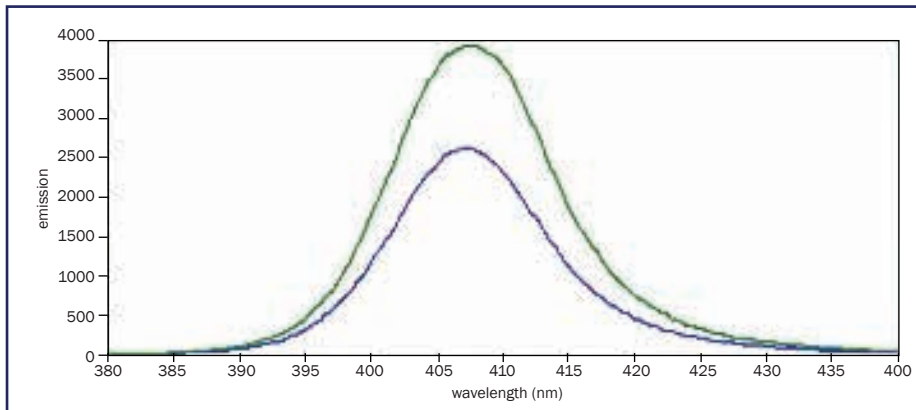


Figure 14: Emission spectrum of the multiple-LED torch of Figure 13, unfiltered and showing a spread from about 390 to 430 nm and centred about 407 nm. The green trace was measured closer to the source.

europium-doped strontium fluoroborate, europium-doped strontium borate or lead-doped barium silicate are often used as phosphors in these 'black-light-blue' or 'BLB' black-light tubes. This would explain the abundant wideband continuous

emission accompanying the line spectra in the LWUV from Hg discharge tubes. Wide band emission is often a typical feature of some fluorescence. Black-lights have been used in various commercial applications such as advertising, counterfeit detection,

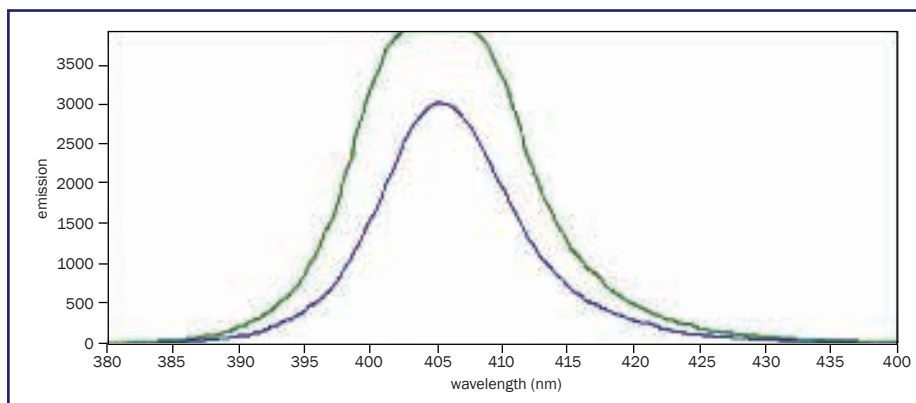


Figure 15: Emission spectrum of a single LED 'key ring' torch showing a range from 390 to 430 nm and centring about 405 nm. The green trace is closer to the source.

skin-tanning and decoration, but their LWUV spectra and their applicability for gemmological purposes have not been widely discussed. The LWUV spectrum of the small (4 watt) BLB black-light fluorescent tube (Figure 16) was scanned (Figure 18) to compare it with those of the proprietary ultraviolet mercury-discharge lamps shown in Figures 4 to 6 with which it is nearly identical.

Another lamp that has applications to gemmological testing is the 'germicidal' fluorescent tube with a SWUV-transparent envelope (Figures 16 and 17). The output is unfiltered and consists of mercury SWUV emission together with LWUV radiation and some visible emission. An earlier commercially unsuccessful attempt to employ this germicidal lamp for development of mineralogical and gemmological fluorescence employed a unique but rather fragile liquid filter. It consisted of a UV-transparent fused-silica ('vycor') tube filled with an iron-free and saturated aqueous solution of cobaltous sulphate. The spectrum of the LWUV BLB fluorescent tube is illustrated in Figure 18 and the emission of the SWUV liquid-filtered prototype lamp is presented in Figure 19. The filtered germicidal tube develops a quite satisfactorily intense SWUV emission but is also accompanied by significant interfering LWUV and visible emissions.

To be an effective liquid filter for excluding visible light from ultraviolet

Review of ultraviolet sources for gem fluorescence and testing



Figure 16: Small BLB 'black light' fluorescent LWUV tube (4 watt) above a 'germicidal' SWUV mercury based (4 watt) fluorescent tube fitted with a CoSO_4 solution filter and green sleeve.

Figure 17: Another view of the 'germicidal' SWUV tube shown in Figure 16.

emission, Strong (1938)⁵ had suggested that the solution should be 3 cm thick and contain not only 100 grammes per litre (g/L) cobalt sulphate but also 140 g/L nickel sulphate which is then perhaps a composition perhaps rather analogous to Wood's glass. Backstrom (1933)⁶ had also suggested that this solution transmits only 3.5% of the 334 nm Hg-emission, but 96% of the 313 emission, and that its transparency in the SWUV extends to 230 nm, thus apparently isolating SWUV from most UV of longer wavelengths, excepting 313 nm.

An experimental solution of this composition was prepared in distilled water using the usual commercial form of hydrated nickel sulphate, the hexahydrate, $\text{NiSO}_4 \cdot 6\text{H}_2\text{O}$ of AR purity ('Analytical Reagent' grade) together with the usual commercial form of cobalt sulphate, the heptahydrate, $\text{CoSO}_4 \cdot 7\text{H}_2\text{O}$, also of AR grade. A suitable source of full spectrum ultraviolet with a multiple line discharge spectrum (Figure 20a) was improvised using an unshielded high-pressure 100 watt mercury discharge tube (Figure 21). It is notable that there was also an appreciable odour of ozone generation which usually occurs with emissions in the range of about 180 to 190 nm, very close to the transmission limit of silica.

In order to determine the UV transparency of each constituent in the experiment, the lamp emission itself

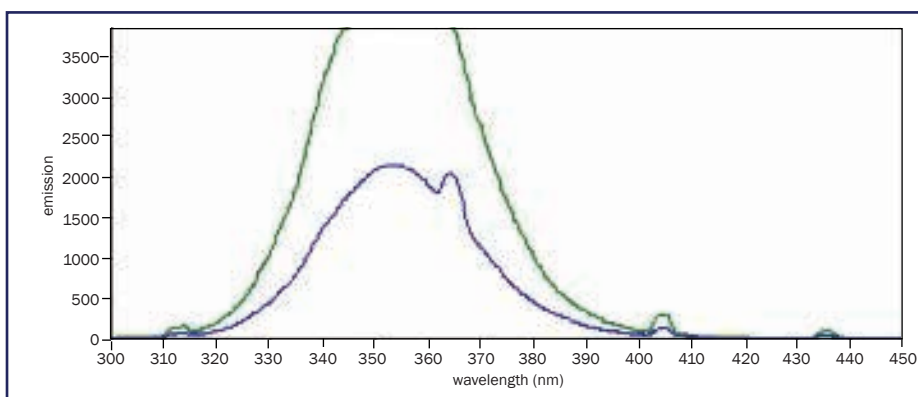


Figure 18: Emission spectrum of the BLB 'black light' fluorescent tube, showing a spread of emission wavelengths probably due to special phosphors.

was scanned in duplicate to ensure reproducibility, then the quartz cuvette filled only with water; and finally the $\text{NiSO}_4/\text{CoSO}_4$ solution in the quartz cuvette to record its UV filtering effect. (The first 'silica' cuvette used turned out to be glass which was opaque to UV

below 300 nm!)

The spectra in Figure 20 indicate that the solution removes much of the visible light between 440 and 550 nm from the emission but certainly does not remove any substantial proportion of the wavelengths between 300 and 370 nm.

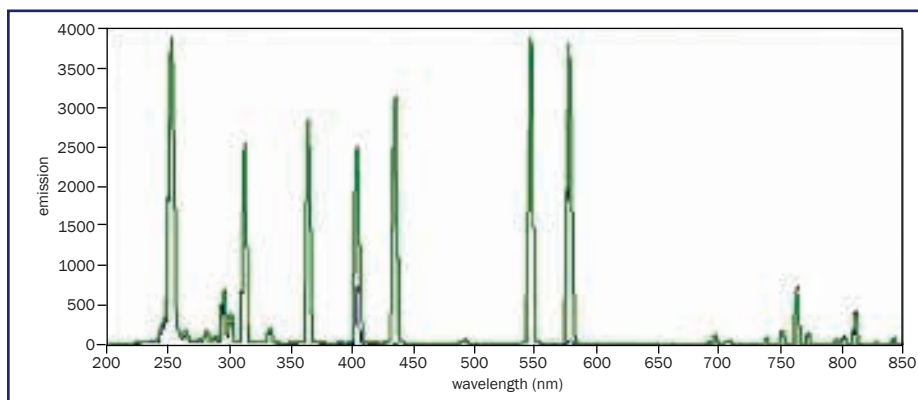


Figure 19: Emission spectrum of the 'germicidal' SWUV fluorescent tube showing multiple sharp Hg lines. The spectrum is very similar to that of the GAAJ SWUV tube shown in Figure 4.

Review of ultraviolet sources for gem fluorescence and testing

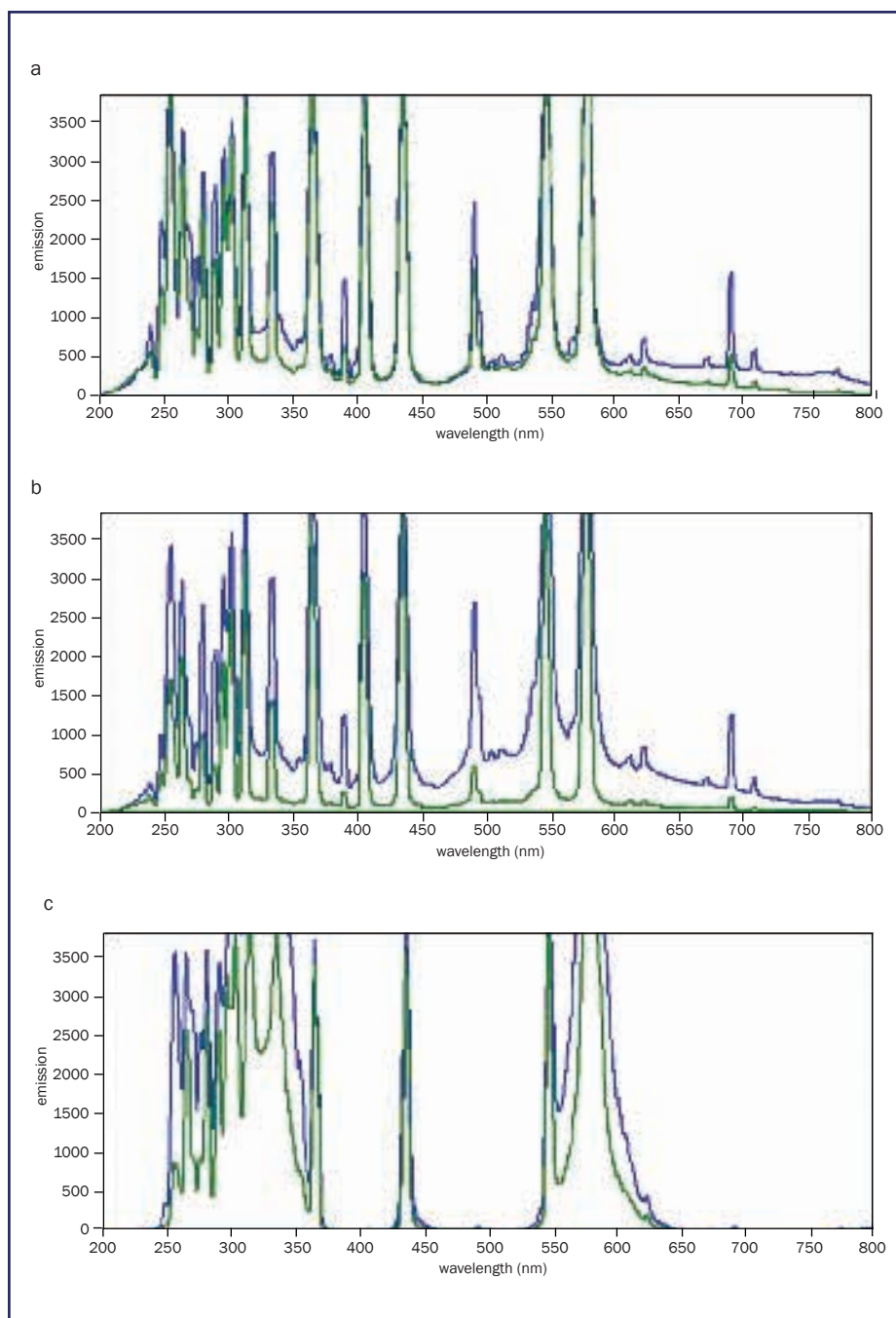


Figure 20: Emission spectra from the high-pressure mercury discharge lamp shown in Figure 21. (a) Unfiltered; (b) filtered by silica cuvette containing water; (c) filtered by silica cuvette containing CoSO_4 and NiSO_4 solution. Note that LWUV radiation between 300 and 370 nm is transmitted by this assembly.

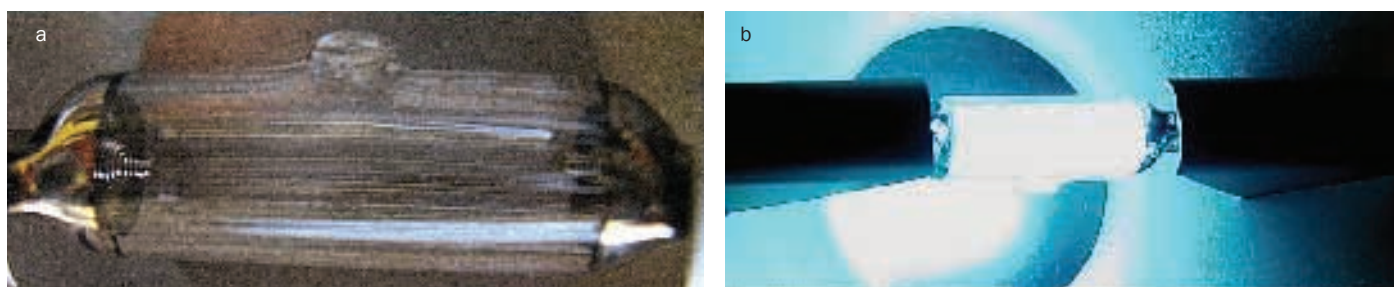


Figure 21: High pressure mercury-discharge unshielded bulb used as a broadband source of discontinuous line discharge of SWUV and LWUV (a) and the bulb upon ignition (b).

The solution is not effective to isolate SWUV from unwanted LWUV.

It is also well known that filters of the Wood's glass type suffer from 'solarisation' which is a progressive loss of SWUV transparency and performance with continued exposure to SWUV which is chemically more active than longer wavelengths (see also Gleason⁴). Consequently, the SWUV performance of frequently used SWUV lamps may progressively deteriorate and any fluorescence effect from the accompanying LWUV can become even more accentuated. Gleason⁴ (p.14) and Strong⁵ (p.252) both suggest that solarisation is remediable by carefully heating the degraded glass filter in air just below 550°F (290°C) for several hours before slowly cooling to restore its original SWUV transparency.

A SWUV tube of Philips manufacture (TUV 4W 57416E/40) is shown in Figure 22. This is unshielded and unfiltered, and gives a bright blue central discharge and red glow around cold electrode terminals, emitting the spectra in Figure 23(a) and (b). These reveal the usual Hg lines at 254 and 365 nm and various other Hg emission lines despite no liquid mercury droplets being visible before ignition.

The electrode red glow spectrum, shown in Figure 23(b), suggests that the starter or carrier gas is probably neon with its characteristic red discharge consisting of numerous closely spaced sharp lines in the red. These emissions should clearly be excluded from any desired ultraviolet content to avoid confusion with any red fluorescence of the specimen. This SWUV source is obviously very similar to the filtered germicidal tube, and also

Review of ultraviolet sources for gem fluorescence and testing

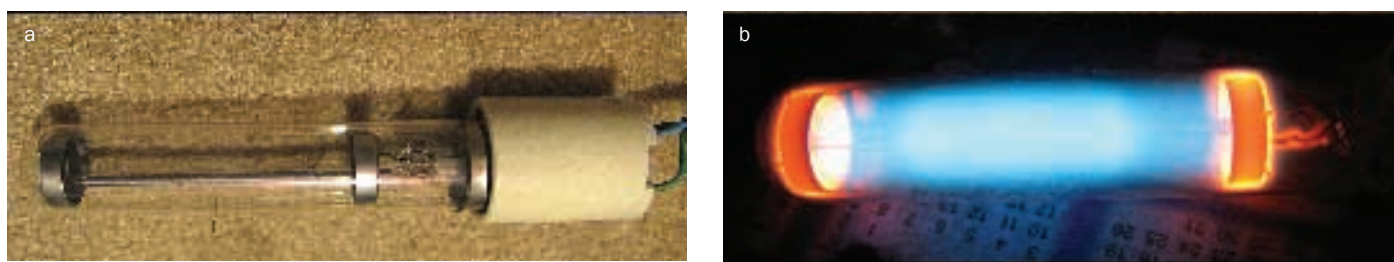


Figure 22: Unshielded SWUV discharge tube (a) and (b) in operation. The red glow at each end of the blue discharge indicates that the medium is a gas consisting of Ne and Hg.

to the GAAJ SWUV tube even with its Wood's glass filter. It appears to offer no advantage over the other proprietary SWUV sources regarding purity of any SWUV emission line(s).

Sunlight may contain variable amounts of UV depending upon latitude, atmospheric conditions, the season and even the time of day. Such UV, although not deliberately applicable to the induction of diagnostic fluorescence effects, can lead to uncontrolled fluorescence, such as bluish tints in some diamonds, red enhancement of some rubies or the well known green fluorescence in the bright yellow Verneuil synthetic spinel doped with manganese. An indication of the variability of the relative amount of UV that may occur in Melbourne early-afternoon summer daylight is illustrated in Figure 24. Solar spectra are recorded, from a clear blue sky a mildly overcast white sky, and through a glass window pane. Various Fraunhofer lines are visible, but the significant differences between the scans occur at wavelengths only below about 470 nm, and especially below 400 nm. Blue-sky LWUV was detected down to almost 300 nm although essentially all LWUV was removed by the glass window pane.

4. Conclusions

Each of the three investigated proprietary UV lamps was based upon low pressure Hg-discharge and all showed appreciable contents of accompanying LWUV when operated in the SWUV mode. Any fluorescence stimulated in a gem in SWUV mode may thus be due to either SWUV or LWUV or both. This casts doubt on whether some fluorescence previously attributed to stimulation by

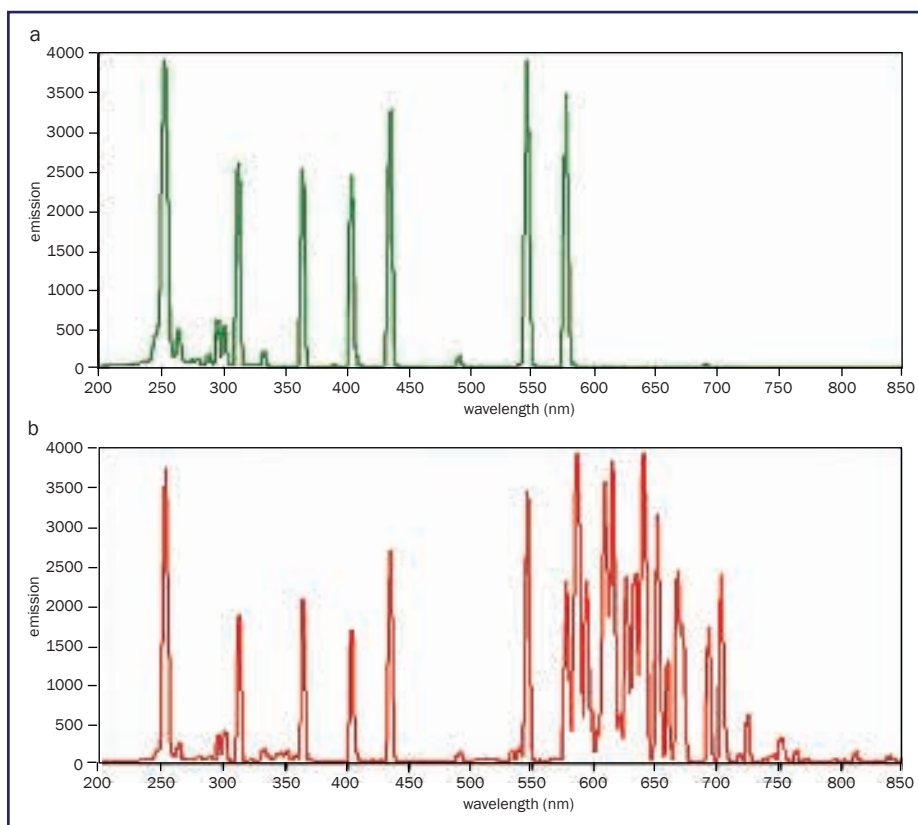


Figure 23: (a) Emission spectrum of discharge from the centre of the tube shown in Figure 22. (b) Emission spectrum of the blue and red components showing numerous neon lines.

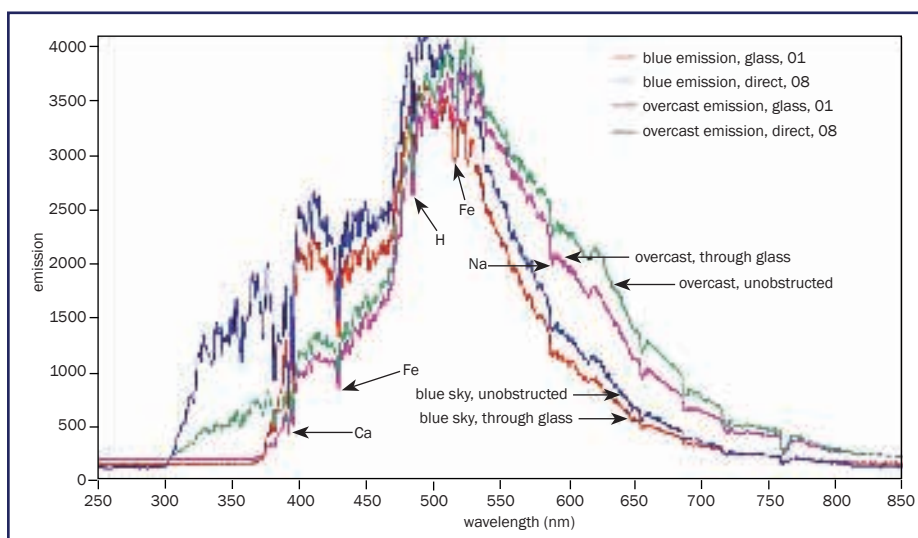


Figure 24: Spectral wavelength distribution of daylight showing differences due to cloud cover and filtering by window glass. Some Fraunhofer absorption lines are labelled.

Review of ultraviolet sources for gem fluorescence and testing

SWUV actually occurs, especially in many chromiferous gems. Unless the SWUV fluorescence response is observably different and distinguishable from any LWUV induced fluorescence generated by the accompanying contaminating LWUV emissions, fluorescence supposedly generated by 254 nm SWUV may actually be due to the LWUV contaminating 'bleed'. The contaminating LWUV 'bleed' in the SWUV mode may even be almost as intense as in the nominal LWUV-emission mode.

The excitation/fluorescence diagrams obtained by Hoover suggest that many LWUV-fluorescent gems, including ruby for instance, may show negligible fluorescence to shorter wavelengths — at least down to 270 nm which was the limit of that experiment. So, until exclusively monochromatic or specific narrow-band SWUV sources are available to the gemmological fraternity, it is suggested that any fluorescent responses in gems to discharge tubes in the SWUV mode and being used for identification purposes, are treated with suspicion.

In both LW and SW modes the emission spectra of the discharge tubes indicate the presence of many emissions at wavelengths in addition to those at 254 and 365 nm. In the SW region, these include emissions at 265, 288 and 296 nm, and in the (nominal) LW region, at 303 and 313 nm. All or any could evoke fluorescence that might otherwise be attributed to the 254 nm emission which in turn could result in an erroneous interpretation. Also in the LW mode, the nature of the '365 nm emission' is in reality broadband and only centred on 365 nm, and fluorescence could be stimulated by any or all wavelengths in this range. Again, erroneous interpretation could result if stimulation by exclusively 365 nm emission was assumed. The selective fluorescence response to particular LW emissions is indicated in Hoover and Theisen's diagrams.

It is suggested that the output

from an ultraviolet lamp intended for gemmological identification purposes, both SWUV and LWUV ranges, should be scanned spectrometrically. Any fluorescence responses observed with its use can then be interpreted with the appreciation and knowledge of its actual radiation, rather than simply assuming that its emissions consist solely of the 254 nm SWUV Hg-line discharge and the 365 nm LWUV Hg-line discharges. Lamps apparently intended primarily to develop aesthetically attractive fluorescent-display responses from minerals may not be directly suitable for diagnosing fluorescence in gems unless their spectral emission content is known and the response is appropriately interpreted.

LEDs are currently providing single-band sources of LWUV but are not readily available yet with emissions in gemmologically useful SWUV ranges. However, the LWUV bands just below the visible range and down to the Hg-discharge line at 365 nm are eminently suited to develop fluorescence economically and conveniently for certain gemmological identifications. LEDs generally do not develop single, almost monochromatic emissions like low pressure gas discharges, but emit a single broadened band, typically spanning as much as about 10 to 40 nm. However, these compact and convenient radiation sources are still very useful to confirm LWUV fluorescence of commonly responsive gem materials.

The proposal by Strong⁵ that a solution of cobalt and nickel sulphates would selectively filter out most of the interfering LWUV, especially the 365 nm emission, from the required SWUV emission, especially the 254 nm line, was not substantiated. The indicated concentrations of these salts removed some undesirable visible wavelengths, but unfortunately did little to diminish the level of the interfering LWUV emissions contaminating the SWUV range. There is apparently still no reliable absorption filter

to be able to isolate the desired SWUV radiation from interfering LWUV.

Acknowledgements

The initial impetus for this investigation was generated by Bear Williams (Stonegroup Labs) and Dr Don Hoover (retired from USGS), of Missouri, USA. The subsequent assistance, discussions and criticisms from Dr Hoover and from Bear Williams and the permission from Dr Hoover to reproduce the excitation-fluorescence spectrophotometric diagrams of chromiferous materials compiled by Hoover and Theisen at the USGS, are very greatly appreciated.

References

- (1) Hoover, D.B., and Theisen, A.F., 1993. Fluorescence excitation-emission spectra of chromium bearing gems: an explanation for the effectiveness of the crossed filter method. *Australian Gemmologist*, **18**(6), 182–7
- (2) Hoover, D. and Williams, B., 2005. Crossed Filters Revisited. *Journal of Gemmology*, **29**(7–8), 473–81
- (3) Williams, B., 2007. Technology update-ultraviolet light. *The Guide*, January/February 2007, p.8–11, 16
- (4) Gleason, S., 1972. *Ultraviolet Guide to Minerals*. UltraViolet Products, San Gabriel, CA
- (5) Strong J., 1938. *Modern Physical Laboratory Practice*. Blackie & Son Ltd., London
- (6) Bäckström, H.L.J., 1933. Ein Lichtfilter für das mittlere Ultraviolett. *Naturwissenschaften*, **21**(13), 251

The Author

Grant Pearson

Melbourne, Australia
email: grantpearson@optusnet.com.au

Gem-A Photographic Competition

The 2012 Competition is now open!

All Gem-A members are invited to participate. Once again there are four categories in which an image may be submitted:

1 **Natural**

Digital photograph (including photomicrography) with minimal post-production work (may include basic cropping, contrast and minor hue/saturation adjustments).

2 **Treated**

Digital photograph (including photomicrography) with significant post-production work (such as background manipulation, HDR, and contrast masking).

3 **Synthetic**

Computer-rendered 3D models of gemstones, crystals, crystal structures, images from microtomography, etc.

4 **Melange**

This category includes any gem-related image that doesn't fit in the above and may include such things as photos of a spectrum, a scanning electron microscope image, mining, cutting, etc.

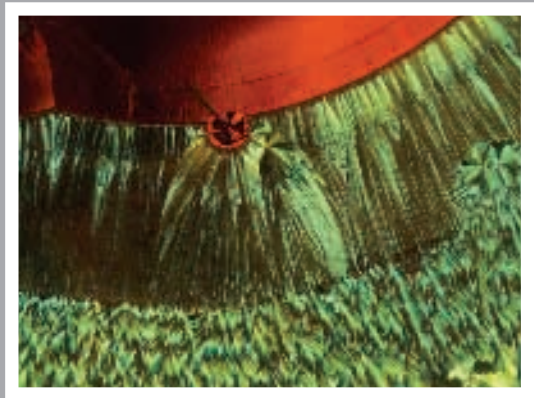
Winning entries will be announced at the Gem-A Conference 2012 and feature in *Gems & Jewellery*.

To enter

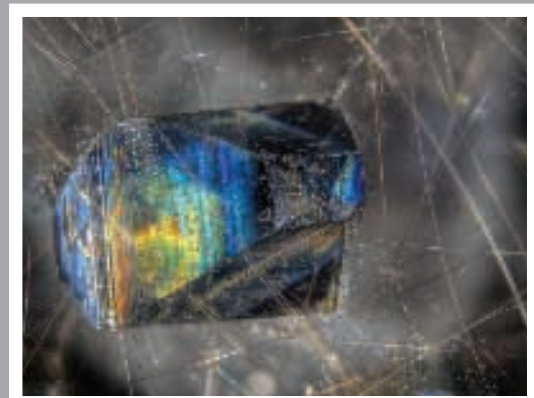
Please send a low resolution version of your photo to editor@gem-a.com. Entry forms and full details of the competition, including copyright information and Rules of Entry, can be accessed at www.gem-a.com/membership/photographic-competition.aspx or call Amandine on +44 (0)20 7404 3334.

Closing date: 29 June 2012

2011 Photographic Competition winners



Overall winner and winner of Natural category:
Fibrous hematite and goethite aggregates in quartz from Minas Gerais. © Michael Hügi.



Winner of Treated category:
Blue anatase crystal and rutile fibres in quartz from Minas Gerais. © Michael Hügi.



Winner of Melange category:
Cut cultured pearls in round slices. © Keiko Kon and Gem Science Academy of Gemology, Tokyo.



Gem-A

THE GEMMOLOGICAL ASSOCIATION
OF GREAT BRITAIN

UK registered charity no. 1109555

Abstracts

Diamonds

G.I.A.'s symmetry grading boundaries for round brilliant cut diamonds.

R.H. GEURTS, I.M. REINITZ, T. BLODGETT and A.M. GILBERTSON. *Gems & Gemology*, **47**(4), 2011, 286-95.

Basic measuring concepts are explained for symmetry parameters used in grading round brilliants. The ten symmetry parameters defined are: out-of-round; table off-centre; culet off-centre; table/culet alignment; crown height variation; crown angle variation; pavilion depth variation; pavilion angle variation; girdle thickness variation; and table size variation. Several thousand diamonds assessed over ten years provided the basis for the recommended limits of the symmetry grades Excellent, Very Good and Good. Assessments of combinations of these parameters are discussed in the context of a constant need for visual monitoring. R.R.H.

GIA Symposium 2011.

Gems & Gemology, **47**(2), 2011, 105-36.

Topics covered in the presentations include: irradiated diamonds from Zimbabwe; radio-coloration of diamond; treated diamond identification; colour treatment of diamond; the unknown sources of some alluvial diamonds; and the relationship of diamond sources to cratons, particularly in Canada.

There were poster sessions concerning shapes of fancy-cut diamonds; hydrogen-rich diamonds from Zimbabwe; coloured diamonds from Argyle, W. Australia; optical properties, structural defects, spectra and photoluminescence studies of diamonds; colour zoning; colour origin determination; black diamonds from Brazil; Yakutian diamonds; rough diamond descriptions for use in exploration; and ultra-deep diamond cleaning technology. R.R.H.

Gem News International.

B.M. LAURS. *Gems & Gemology*, **47**(3), 2011, 234-53.

Two type Ib diamonds showing a colour change from greenish brown under a daylight equivalent light to orangy brown under incandescent light are described. Their grades include the effects of their fluorescence properties and there is some detailed discussion of the causes. R.R.H.

Lab notes.

T.M. MOSES and S.F. McCLURE (Eds). *Gems & Gemology*, **46**(4), 2010, 298-307.

A type IIa HPHT-treated diamond with a hexagonal graphite inclusion typical of the treatment is illustrated. A 'tie' growth pattern in a coloured diamond revealed by examination in a DTC DiamondView indicates a natural stone and the similar but different pattern of a synthetic diamond is shown for comparison. Very thin coatings on fancy pink diamonds were detected from anomalous peaks in the visible spectrum near 505 and 540 nm. R.R.H.

Lab notes.

T.M. MOSES and S.F. McCLURE (Eds). *Gems & Gemology*, **47**(1), 2011, 49-55.

Stones described include: a 28.65 ct orange diamond with IR and UV-Vis spectra which indicated treatment at HPHT; a 38.59 ct type IIa diamond graded F colour is the largest seen so far in the GIA laboratory that has been HPHT-treated; some pure type IaB diamonds display a blue thermoluminescence when they warm up after exposure to a laser at liquid nitrogen temperatures. R.R.H.

Lab notes.

T.M. MOSES and S.F. McCLURE (Eds). *Gems & Gemology*, **47**(3), 2011, 222-32.

A 0.85 ct diamond was found to contain dark brown bands and strong plastic deformation, judged to be of

natural colour and graded Fancy black. A 1.29 ct pear-shaped diamond was found to have had its blackness enhanced by coating. A 1.05 ct pink diamond had a coating that had not been detected from its visible-range absorption spectrum but which was apparent under the microscope. Two type IIa diamonds graded D and E colours had unusually pronounced 'tatami' strain patterns. Four diamonds in the J-M colour range had been subjected to HPHT treatment and their colour grades changed to E-F. HPHT treatment had also been used to remove a brown tint and improve the pink colour of a 21.73 ct marquise brilliant. A diamond with brown stains on a cleavage and associated green fluorescence indicated a complex history. R.R.H.

Lab notes.

T.M. MOSES and S.F. McCLURE (Eds). *Gems & Gemology*, **47**(4), 2011, 308-15.

Unusual 0.81 ct diamond graded Fancy Vivid Purple, with green fluorescence. Grey-to-blue-to-violet 0.85 ct heart-shaped diamond with unusually dark tone, graded Fancy black, showed strong absorption features in mid IR (near 3107 cm^{-1}) attributed to H. HPHT treated diamond with fluorescence pattern of a HPHT-grown synthetic Type IIb diamond with D colour and IF clarity, greenish blue fluorescence to both long- and short-wave ultraviolet and then bright blue phosphorescence for several minutes. R.R.H.

Rio Tinto's Argyle Pink Diamonds Tender Update.

E. SANDERS and C. SANDERS. *Australian Gemmologist*, **24**(4), 2010, 80-4.

An update to the 1997 summary published in the *Australian Gemmologist* which chronicles the annual Argyle Pink Diamonds Tender since its inception

Abstracts (continued)

in 1985. New information includes: an overview of the unique Argyle Pink Diamonds' colour grading system; the girdle laser inscription instituted in late 2004 for diamonds over 0.20 ct and later in 2009, stones over 0.15 ct; notable diamonds since 2000, as well as a chart showing each year's offerings since 1985.

E.A.S.

Gems and Minerals

Research on gem feldspar from the Shigatse region of Tibet.

A. ABDURIYIM and 11 other authors. *Gems & Gemology*, **47**(2), 2011, 167–80.

Andesine was collected from Zha Lin and Yu Lin Gu about 55 km SE of Shigatse, Tibet. The samples are up to 2 cm across and most are red, some having blue-green or patchy red areas. They contain twin lamellae, turbid clouds, channels and some tiny copper grains or platelets. Glass residues are present on the surfaces and in cavities in some of the samples, but spectral and chemical analysis failed to establish the origin of the residue. Microprobe and LA-ICP-MS analyses were made of the samples and the latter indicated distinctly high amounts of silver in the rims of those from Yu Lin Gu. Powder X-ray diffraction results indicate that the andesines from Zha Lin and Yu Lin Gu had not been treated at high temperature; this conclusion is supported by argon isotope studies. It was noted that no andesines were collected that had adhering rock (volcanic) matrix, and in the Yu Lin Gu area, andesines were not found at depths of more than a few cm.

R.R.H.

Ivory carving in Germany.

M. CAMPBELL PEDERSEN. *Gems & Jewellery*, **19**(4), 2010, 20–2.

An outline of a unique German museum specializing in ivory and the history of carving. Based in Erbach, the museum's exhibits span over 300 years of historic ivory use, and the accompanying photographs within the article show some of these carved items (including the iconic Erbach Ivory Rose). The museum is a working example of the carving craft, in all its forms.

A.S.F.

Brownish red zircon from Muling, China.

T. CHEN, H. AI, M. YANG, S. ZHENG and Y. LIU. *Gems & Gemology*, **47**(1), 2011, 36–41.

Zircon occurs in alluvium derived from alkali basalt and is associated with other minerals of gem quality such as sapphire, spinel and garnet. RIs of >1.81 and SGs between 4.57–4.69 were determined, and apatite, metamict zircon, magnetite and dark ovoid glass inclusions were recorded. EPMA and LA-ICP-MS analyses indicate the presence of REE with up to 2440 ppm Th and 871 ppm U, which results are consistent with absorption peaks in the UV-Vis-NIR spectra. Raman spectra are recorded and samples subjected to heat treatment changed colours to lighter hues.

R.R.H.

And now composite chalcedony.

G. CHOUDHARY. *Gems & Jewellery*, **19**(4), 2010, 28–30.

As part of a series of articles published in various gemmological texts, Choudhary discusses a new composite stone consisting of chalcedony held in resins. A detailed table is provided with identifying features and results that cover observational and advanced laboratory techniques. Although readily identified as a composite, the analytical methods to identify the component parts give an insight into production techniques.

A.S.F.

Greenish yellow zoisite.

G. CHOUDHARY. *Australian Gemmologist*, **24**(4), 2010, 90–1.

An 8.33 ct faceted greenish yellow gemstone, at first glance resembling tourmaline, quickly reveals it is otherwise when striking strong trichroism is observed: yellow, blue and purplish pink. Standard gemmological testing indicates the specimen is zoisite; confirmed by FTIR spectral patterns and qualitative EDXRF analysis (major elements: Al, Si, Ca and Sr, with traces of V and Fe).

E.A.S.

Serpentine crystal with purple-red transmission.

G. CHOUDHARY. *Australian Gemmologist*, **24**(7), 2011, 164–6.

Having been sold as alexandrite, a bluish-green crystal showing purplish-red coloration in transmitted light is found to be a member of the serpentine

family. The tabular monoclinic crystal was revealed with EDXRF analysis to contain Mg, Si, Cr, Fe and Ni. These results and those of FTIR spectroscopy were both consistent with those of serpentine. The cause of the purplish red transmission remains unknown, but this and several other specimens mined in Andhra, Pradesh, Southern India, have recently been seen by the Gem Testing Laboratory of Jaipur — all represented as alexandrite in the marketplace.

E.A.S.

A chatoyant malachite.

G. CHOUDHARY. *Australian Gemmologist*, **24**(2), 2010, 44–5.

A 9.57 ct green cat's-eye cabochon was confirmed to be malachite by standard gemmological testing along with FTIR spectroscopy and EDXRF. The eye was exhibited as a broad band, reminiscent of lower-grade cat's-eye quartz. This appears to be the first published report of chatoyant malachite, though an Internet search did turn up offerings of such material, predominantly as rough or tumbled specimens or as beads.

E.A.S.

Mariupolite from the Oktyabrsky Massif (SE Ukraine) — a less well known rock in the gemstone trade.

M. DUMAŃSKA-SŁOWIK, P. BARANOV, W. HEFLIK, L. NATKANIEC-NOWAK, S. SHEVCHENKO and L.I. TSOTSKO. *Gemmologie. Z. Dt. Gemmol. Ges.*, **60**(1/2), 2011, 37–48. 16 photographs, 1 map, 1 geology map, bibl. [English with a German abstract.] Mariupolite is a nepheline syenite rock from the south eastern Ukraine. A diversity of colours and texture is caused by variable mineral composition, the main constituents being albite, nepheline and aegirine. Those materials containing sodalite are suitable for jewellery components, clocks, vases, ashtrays and for the production of facing stones both for indoor and outdoor use.

E.S.

Topaz crystals from various geological settings.

M. DUMAŃSKA-SŁOWIK, J. FIJAŁ and L. NATKANIEC-NOWAK. *Gemmologie. Z. Dt. Gemmol. Ges.*, **60**(3/4), 2011, 87–104. 16 photographs, 7 graphs, 6 tables, bibl. [English with German abstract.]

This paper deals with topaz crystals

Abstracts (continued)

from various geological settings, such as rhyolites, pegmatites, greisens and hydrothermal veins. Topaz crystals have various mineral and fluid inclusions, but have a fairly constant composition although they have different mineral associations. The major difference found in the samples is the F/OH ratio. Topaz from Ouro Preto, Brazil, has the highest content of the hydroxyl groups. The lowest amount of the hydroxyl groups and the highest fluorine content were found in topaz from the Thomas range in the U.S.A. Crystals from Volodarsk-Volynsky exhibit the most ordered lattice, while those from Ouro Preto have the most defects in their structure. E.S.

GIA Symposium 2011.

Gems & Gemology, 47(2), 2011, 107-53.

Topics covered in the presentations include: the geological conditions for formation of ruby, emerald and alexandrite; pegmatites; opals from Ethiopia; origin determination; Australian opal nomenclature; lavender jadeite from Myanmar, Guatemala and Japan; natural colour tanzanite; durability of treated ruby and sapphire; archaeogemmology of peridot; natural and treated nephrite in China; the use of photoluminescence spectra in determining growth media and colour origins in cultured pearls; review of the range of testing methods used to distinguish natural and cultured pearls and their treatments.

There were poster sessions concerning blue and pink sapphires from Muling, N.E. China; a review of gems in southern Brazil; ruby from Liberia; petrogenesis of the Stewart pegmatite, Pala, CA; ruby overgrowths on painite from Mogok, Myanmar; gemstones from Mexico; tourmaline from the Pederneira pegmatite, Minas Gerais; blue cristobalite (described as opal) from Rio Grande do Sul; world production figures for coloured gems compiled by the U.S. Geological Survey; tourmalines from Madagascar; use of discriminant analysis for identifying coloured stone sources and for distinguishing HPHT-treated from untreated diamonds; review of the range of quartz varieties and some notable gems tested in the Jaipur laboratory; exotically coloured Chinese freshwater cultured pearls; non-nacreous pearls from the giant clam; roundness and lustre

variations in cultured pearls and their relations to grafting methods in *Pinctada margaritifera*; experiments to test ancient treatment techniques on gems; Oregon sunstones compared from two deposits; changes in colour of various sapphires by electron beam irradiation; experiments on the effects on sapphires of heating them with Be; the spectra of some gem tourmalines; and some new artificially asteriated gemstones. R.R.H.

Black Beauty.

K. GREGORY. *Gems & Jewellery*, 19(4), 2010, 34-6.

Kerry Gregory's experiences of testing a faceted checkerboard style black opaque stone set into a pendant. Although not conclusively identified, the processes and reasoning involved show how cut and setting can affect and limit the choice of tests available. A full table of possible gem materials is provided, along with explanations of how certain materials were discounted. A.S.F.

Jaded.

K. GREGORY, *Gems & Jewellery*, 20(1), 2011, 15-17.

Reviewing a talk at the South-West Branch by Edward Johnson on Jadeite, this article looks at the possible alternatives to jadeite (tabulated), and highlights some precautionary tales. A.S.F.

Three-dimensional X-ray radiography.

T. HAINSWANG. *Gems & Jewellery*, 20(1), 2011, 11-14.

Micro X-ray tomography is a new technique that allows pearls and other gem materials to be represented in three dimensions in sufficiently high quality to allow detailed analysis. Whilst not suitable or cost effective for everyday use, a more viable alternative system has been designed that allows 3D films to be produced for analysis of inclusions/fillers, and in particular allow the nature of pearls to be determined. With the advent of cultured pearls using smaller pearls as bead nuclei, this technology will become more important, and is currently in use on all pearls sent to the GEMLAB (Liechtenstein) laboratory. A.S.F.

Explaining the flame structure of non-nacreous pearls.

H. HÄNNI. *Australian Gemmologist*, 24(4),

2010, 85-8.

Through conventional microscopy and scanning electron microscopy (SEM), the flame structure of porcellaneous pearls is revealed and the appearance of the optical phenomenon is explained. Since the same structures are present in the shells of the molluscs from which the pearls originate (including *Melo*, *Tridacna*, *Strombus gigas*), such shells may be sacrificed for analytical work. At magnification of 500x, *Tridacna* shell reveals a crisscross structure of fibrous aragonite lamellae which alternately reflect and absorb light, producing spectral colours due to interference when found at a thickness of 500 nm. Other species exhibit different patterns of the same dull and bright effect, depending on how the fibrous aragonite bundles of ultra-fine fibres, laths or lamellae are arranged. E.A.S.

Neues aus China: Ming Perlen.

H. HÄNNI. *Gemmologie. Z. Dt. Gemmol. Ges.*, 60(3/4), 2011, 105-10. 7

photographs, bibl. [German with English abstract.]

These cultured pearls are similar to the Japanese cultured pearls 'Kasumiga-ura'. They are freshwater, beaded and gonad grown. These new Ming pearls are round, often larger than 15 mm, and are white or pastel-coloured due to their producing shell which is a hybrid of *Hyriopsis schlegeli* and *Hyriopsis cumingii*. E.S.

Das Farbenspektrum der Quarze.

U. HENN and R.SCHULTZ-GÜTTLER.

Gemmologie. Z. Dt. Gemmol. Ges., 60(3/4), 2011, 63-86. 17 photographs, 1 table, 8 graphs, 2 flow-sheets, bibl. [German with English abstract.]

Macro-crystalline quartz can be classified into several groups. Iron-bearing quartz is represented by amethyst which can be thermally modified to yellow or green. Prasiolite changes from blue to violet by irradiation and thermal treatment. Light amethyst can be thermally improved to lilac.

Aluminium-bearing quartz appears yellow (citrine) or brown (smoky quartz) or black (morion) which can be changed into greenish-yellow lemon quartz by heat treatment. Water-containing quartz can be modified to green by irradiation. Rose quartz is formed by adding dumortierite

Abstracts (continued)

or produced by substitution of silicon by phosphorus.

Both iron-bearing and aluminium-bearing quartz can appear as multi-coloured stones. This article shows colour and colour modification as well as the absorption spectra and other testing methods such as pleochroism, twinning and IR-spectra. E.S.

Spinel from Ywathit, Kayah State, Myanmar.

U.T. HLAING, W. ATICHAT, and C. SUTTHIRAT. *Australian Gemmologist*, **24**(3), 2010, 61-3.

A description of the spinels found in alluvial deposits in the area of Bawlake Township, southeast of Ywathit in the eastern part of Myanmar. These apparently originated from the Pawn Chaung Series mountain range, north of Ywathit between the Salween River and Pawn Chaung. These mountains consist of schist and a fine-grained sugary white-grey marble. Chemical analysis of the spinels was conducted using Electron Probe Micro-Analyser (EPMA) and results are presented in chart form. A photograph illustrates the gems alongside a red and black *Abrus precatorius* seed. Also known as wild liquorice (English) and Ywe gale or Ywe nge (Burmese), these seeds are of a uniform 0.5 cm size and 0.5 ct weight and have been used locally as a unit of measurement for precious stones and metals. E.A.S.

A microstructural study of pietersite from Namibia and China.

K. HU and P.J. HEANEY. *Gems & Gemology*, **47**(4), 2011, 280-6.

Pietersite specimens from the two main sources, Kuruman, Namibia, and Xichuan, Henan Province, China, are mixed rocks largely blue-grey, golden and white (Namibian) or red brown and white (Chinese). They consist of major quartz or chalcedony, less calcite, and fibrous crocidolite (magnesian riebeckite) or chlorite embedded in (but not replaced by) the quartz; the latter structure gives rise to the rather contorted chatoyancy of the specimens. Gemmological properties of stones from the two localities are similar although the Namibian pietersite tends to be more fluorescent and have a higher SG, and in thin section, crocidolite

in the Chinese samples is seen to be intensely coated with hematite. R.R.H.

Aquamarine from the Thuong Xuan District, Thanh Hoa Province, Vietnam.

L.T-T. HUONG, W. HOFMEISTER, T. HÄGER, N.N. KHOI, N.T. NHUNG, W. ATICHAT and V. PISUTHA-ARNOND. *Gems & Gemology*, **47**(1), 2011, 42-8.

Aquamarines from eluvial deposits derived from pegmatites intruding granites of Paleogene age are light to medium blue, elongate crystals up to 4.5 cm long. They contain biotite and hematite crystal inclusions and ubiquitous two-phase inclusions in channels. Their Fe and Cs contents are high compared with other aquamarines, and Raman and IR spectra indicate the presence of type I H₂O and CO₂ in the channels. R.R.H.

Synthetischer Smaragd – Topas – Dublette.

J. HYRSL and U. HENN. *Gemmologie. Z. Dt. Gemmol. Ges.*, **60**(3/4), 2011, 111-12. 3 photographs. [German with English abstract.]

This interesting doublet comes from India. The upper part is a synthetic emerald, the lower a colourless topaz. E.S.

Scottish agates.

B. JACKSON. *Gems & Jewellery*, **20**(1), 2011, 3-9.

An in-depth look at agates, which have been used as artefacts for over 9000 years. Through the use of photographs showing different formations of banding and other structural features, the controversy over the genesis of agates and the difficulties in forming a single explanation as to the structural mechanisms is explored. A.S.F.

UV-Vis-NIR reflectance spectroscopy of natural-color saltwater cultured pearls from *Pinctada margaritifera*.

S. KARAMELAS, E. FRITSCH, J.-P. GAUTHIER and T. HAINSWANG. *Gems & Gemology*, **47**(1), 2011, 31-5.

UV-Vis-NIR spectra of a range of colours of these pearls from shells grown in the Pacific Ocean revealed nine visible-range absorption features. One of these at 405 nm is attributed to uroporphyrin, but

the attributions of the remainder are the subject of further work. R.R.H.

Infrared spectroscopy of natural vs. synthetic amethyst: an update.

S. KARAMELAS, E. FRITSCH, T. ZORBA and K.M. PARASKEVOPOULOS. *Gems & Gemology*, **47**(3), 2011, 196-201.

When traditional gemmological techniques are inadequate to enable distinction between natural and synthetic amethyst, detection and study of the 3595 cm⁻¹ absorption band at high resolution in the IR spectrum could lead to a reliable decision. But this criterion should be used along with other properties discussed; it is not valid for amethysts with large near-colourless zones. R.R.H.

A study of the gems in a ciborium from Einsiedeln Abbey.

S. KARAMELAS, M. WÖRLE, K. HUNGER, H. LANZ, D. BERSANI and S. GÜBELIN. *Gems & Gemology*, **46**(4), 2010, 292-6.

This late sixteenth century treasure from a Benedictine abbey contains ten pinkish red stones (almandine), four orange (grossular) and three pale blue (sapphire) stones, identified by means of microscopy, EDXRF and Raman spectroscopy. Respectively they had been labelled ruby, hyacinth and sapphire by Fr. Tonassini around 1798. Their features and styles of cut are consistent with an origin in Sri Lanka. R.R.H.

Ruby and sapphire from the Tan Huong – Truc Lau area, Yen Bai Province, northern Vietnam.

N.N. KHOI, C. SUTTHIRAT, D.A. TUAN, N.V. NAM, N.T.M. THUYET and N.T. NHUNG. *Gems & Gemology*, **47**(3), 2011, 182-95.

Rubies and pink sapphires are recovered from gneisses, amphibolites and marbles in the Red River Shear Zone, NW of Hanoi, and from eluvial and alluvial deposits nearby. Associated gem minerals included spinel, garnet and trapiche-like sapphire. Most rubies are cabochon quality but there are many good quality stones and they tend to come from the secondary deposits. Stones from this area are compared with those from older mines about 15 km away in the Khoan Thong-An Phu area and their inclusions, identified using microprobe analyses and Raman spectra, are abundant, including

Abstracts (continued)

rutile, ilmenite, zircon, apatite, spinel, diaspore and calcite. The deposits yield many star stones and corundum crystals with spinel overgrowths are not uncommon. R.R.H.

A historic turquoise jewelry set containing fossilized dentine (odontolite) and glass.

M.S. KRZEMNICKI, F. HERZOG and W. ZHOU. *Gems & Gemology*, 47(4), 2011, 296-301.

Six mid-nineteenth century brooches set with diamonds and pale blue cabochons were examined using microscopy, and Raman and EDXRF spectroscopy. Most of the pale blue stones proved to be odontolite (fluorapatite), but some were turquoise and some artificial glass. Features seen on some of the odontolite surfaces include micropores, weak banding and curved bands showing intersections (cf. elephant ivory). R.R.H.

Gem News International.

B.M. LAURS (ed.). *Gems & Gemology*, 46(4), 2010, 309-31.

Stones described include: clear yellow amber with pyrite and other mineral inclusions; Tibetan andesine at its alleged source; aquamarine from Vietnam and Madagascar; heliodor probably from Cambodia; diopside from Pakistan; the 'Carolina Emperor', an emerald from Hiddenite, N. Carolina, and the largest cut emerald from N. America; emerald in matrix from Bahia, Brazil; 19th century AD jewellery containing red garnets from Romania; natural pearls in *Pinctada radiata* shells in the waters off Bahrain; updates on sapphire mining in Pakistan, Afghanistan and Madagascar, and the rediscovery of sapphires in the Auvergne, Massif Centrale, France; a 16.17 ct green stone was identified as spodumene and while being examined under a fibre optic light became bright orange, displaying thermoluminescence, returning to green on cooling; four faceted oval greenish blue stones resembled Paraíba tourmaline but their compositions fall in the liddicoatite field, not the elbaite field of Paraíba stones. R.R.H.

Gem News International.

B.M. LAURS (ed.). *Gems & Gemology*, 47(1), 2011, 56-73.

Stones mentioned include Vietnamese

spinel with a range of colours; a new find of green grossular in Tanzania; blue quartz cabochons coloured by trolleite and lazulite inclusions from Minas Gerais; quartz with spectral interference colours caused by twinning along internal minor rhombohedral directions; yellow scapolite from Tamil Nadu, India; scapolite also from Afghanistan, colourless and blue and fluorescing yellow; yellow-brown pargasite from Tanzania; spectacular blue and green tourmalines from Mt. Marie, Paris, Maine; and the rare gems cavansite and zektzerite. R.R.H.

Gem News International.

B.M. LAURS (ed.). *Gems & Gemology*, 47(3), 2011, 234-53.

A recent import from Afghanistan, gem-quality afghanite (a member of the cancrinite group of feldspathoid minerals, its identity confirmed by microprobe analysis) is pale to medium blue resembling aquamarine and is probably from the Sar-e-Sang region of Badakshan. The regional context of aquamarine deposits on the west side of Thanh Hoa Province in northern Vietnam is described. Iridescent ammonites from southern Madagascar have been known for more than ten years and are now being fashioned into cabochons and some are sold as 'Madammolite'. Fine blue chalcedony and an intense red-brown sard or carnelian are described from Peru, and there is an update on emerald mining in Afghanistan. A new deposit of colour-change garnets in southern Tanzania has been found; their compositions are comparable with those from Bekily, Madagascar. Iridescent amphibole from Mauritania closely resembles the variety 'Nummite' from Greenland although the Mauritanian colours are blue- to yellow-green rather than golden. Other stones mentioned include blue opal from Sinaloa, Mexico (to be marketed as 'Lightning Blue Opal'); pallasite pendants fashioned from the Esquel meteorite, a rare type of stony iron meteorite; cat's-eye quartz in which the colour and chatoyant effect are provided by pink tourmaline needles; green cat's-eye spodumene from Araçuaí, Minas Gerais; and variscite from Peru. Chinese freshwater cultured pearls are described with off-round (baroque) beads which were produced from an alleged hybrid of *Hyriopsis cumingii* and

Hyriopsis schlegelii whose shell has an unusual shape and intense iridescence. An oval black cabochon sold as a star sapphire was eventually considered to be a corundum-glass-corundum triplet. R.R.H.

Gem News International.

B.M. LAURS (ed.). *Gems & Gemology*, 47(4), 2011, 316-34.

Stones and topics covered include: small gem-quality golden yellow chondrodites from Tanzania; blue dolomite with three-phase inclusions from the Muzo emerald mine in Colombia; orange and purple zoned fluorite cut and polished as small slabs for silver pendants from Namibia; two sections on opal: common opal from Laverton, W. Australia — red (fire opal), yellow and pale blue, all near-transparent and faceted; a hydrophane opal cabochon, probably from Ethiopia, with one end a white body colour with predominant blue and green iridescent colours, and the other end a brown body colour with much redder iridescence; three sections on quartz: a red cat's-eye quartz cabochon whose minute slender inclusions were identified as cinnabar; a marquise-shaped cabochon of colourless quartz with included elongate prisms of emerald; a skull carved in quartz by Harold van Pelt which has a network of silver grey submetallic inclusions identified as izoklakeite, a lead-antimony sulphide with some copper; colour-change titanite (sphene) from the Pakistan-Afghanistan border area containing vanadium but no chromium; blue spinel from Vietnam; pinkish orange to red spinel from Mogok, Myanmar, which shows a trapiche structure, best viewed in transmitted light. Imitations described include: black 'pearls' sculpted from calcite and showing a cat's-eye effect; and four large synthetic quartzes variously described as amethyst, citrine and two aquamarines. Experimental sugar-acid treatment of Ethiopian opal is also described to make future possible detection easier. R.R.H.

Gemmological News.

C.C. MILISENDA and K. SCHOLLENBRUCH. *Gemmologie. Z. Dt. Gemmol. Ges.*, 60(1/2), 2011, 3-8. 10 photographs.

The authors report on two intense dark blue sapphires (5.42 ct and 4.78 ct)

Abstracts (continued)

from a new occurrence in Gabon, Western Central Africa. The stones show a distinct colour and growth zoning accompanied by rutile silk. Some pink-red to red rubies weighing between 1.79 and 3.58 ct from the Macenta region in southeast Guinea, West Africa, were examined. The stones showed lamellae, cracks, boehmite tubes and rutile silk similar to stones found in East Africa. Some grey-yellow to green-yellow star sapphires weighing 3.65, 4.39 and 7.98 ct were submitted as untreated stones from Burma, but showed numerous round and flat bubble inclusions caused by a filler of glass which contained lead. Some faceted danburites from Tanzania revealed fibrous mineral inclusions which would allow danburite cat's-eyes to be cut from the rough. Further details given concerned transparent mint-coloured cupro-adamite from Mexico, transparent faceted red roselite from the Bou Azzer mining complex in Morocco, a faceted translucent blue-green grandidierite from Madagascar, an epistilbite from the Nasik and Khandivali quarries in India, and a 0.27 ct creedite from Mexico (the name deriving from an occurrence near Creede in Colorado, U.S.A.). Also mentioned is a colourless, faceted pear-shaped chiolite weighing 0.70 ct from the cryolite deposit Ivigtut in Greenland (the name derives from the Greek meaning 'snowstone').

E.S.

Schleifwürdige Titanite und Apatite aus der Eifel.

C.C. MILISENDA, M. WILD and H.-J. KOLZEM. *Gemmologie. Z. Dt. Gemmol. Ges.*, **60**(1/2), 2011, 49–52. 7 photographs, 1 graph, bibl. [German with English abstract.]

The Eifel is a volcanic zone in western Germany producing many minerals. Those of gem quality include peridot, sanidine and hauyne. The article describes pink apatite and orange-brown to reddish-orange titanite (sphene) recovered from a pumice quarry near Laacher Lake. E.S.

Lab notes.

T.M. MOSES and S.F. McCLURE. *Gems & Gemology*, **46**(4), 2010, 298–307.

A rare green pearl of 6.72 ct is natural, of saltwater origin and considered to have grown in the black-lipped oyster from Baja California *Pinctada mazatlanica*. An intense blue triangular step-cut stone was found to be a mixture of sugilite and the amphibole richterite. R.R.H.

Lab notes.

T.M. MOSES and S.F. McCLURE (Eds). *Gems & Gemology*, **47**(1), 2011, 49–55.

Three cabochons of similar green were identified as jadeite, omphacite and hydrogrossular; sapphires from a new deposit near the lapis lazuli mines in Afghanistan contain unusually high amounts of beryllium and tungsten and some of the blue stones have yellow cores displaying a star structure in transmitted light. R.R.H.

Lab notes.

T.M. MOSES and S.F. McCLURE (Eds). *Gems & Gemology*, **47**(3), 2011, 222–33.

An orange clinohumite weighing 84.23 ct and cut as a pear-shaped brilliant contains two-phase inclusions, colour banding and twin planes. A natural sapphire coloured by iron and a synthetic sapphire coloured by cobalt had remarkably similar colours of green. A beryllium-diffused pink sapphire was detected from analyses of orange colour bands in the absence of any Be near the girdle — which is the usual location for search for this treatment. In contrast high Be contents (up to 33 ppm) were found in natural blue sapphires (one of which was unheated) and it was noted that these positively correlated with transition metals and light rare-earth elements. Cultured pearls from *Pteria sterna* proved to have plastic beads. A large conch pearl of about 100 ct has a very fine flame structure and is overall pink, of natural colour. R.R.H.

Lab notes.

T.M. MOSES and S.F. McCLURE (Eds). *Gems & Gemology*, **47**(4), 2011, 308–15.

Clarity-enhanced opal on artificial matrix. Ethiopian black opal with a dark body colour attributed to the natural presence of black manganese oxides. Coated bead-cultured freshwater pearls, unusually large white baroque, with thin nacre and pearlescent coating. Review of tenebrescent zircon, i.e. one that can change colour when exposed to sunlight and return to its original colour when left in the dark, and although rare, comments are made on lack of reporting in gemmological literature. R.R.H.

Microstructures observed in Andamooka matrix opal.

G. PEARSON. *Australian Gemmologist*, **24**(2),

2010, 32–7.

Contrary to statements in literature which incorrectly indicate that much of Australian opal is porous, Andamooka matrix opal is the only significantly porous opal found in Australia. Microscopic evidence suggests that this porosity, which enables the opal to be stained black, may be due to residual interstices and voids between pseudomorphed microcrystals. The use of stained opal specimens in this study facilitated the observation of microstructures, including pseudomorphed euhedral crystals resembling calcite. This and other structures were consistent with opal having pseudomorphed pre-existing components such as massive polycrystalline limestone, possibly initially arising from biogenic calcareous marine debris such as accumulating beds of Cretaceous foraminifera shells. Oolitic structures from Andamooka were also examined and the observations suggested their fossiliferous origin rather than the alternative mechanical origin of oolitic sands. E.A.S.

Demantoid and topazolite from Antetetzambato, northern Madagascar: review and new data.

F. PEZZOTTA, I. ADAMO and V. DIELLA. *Gems & Gemology*, **47**(1), 2011, 2–14.

Microprobe and LA-ICP-MS analyses, UV-Vis-NIR and FTIR spectroscopy confirm recently published data on the Antetetzambato andradites. They are near end-member andradite in composition with low Cr and V, the colours presumably being caused by Fe, although finding any link of the green or golden brown colours examined to chemistry proved elusive. Fractures with partially healed 'fingerprint' inclusions are present along with wollastonite crystals and diopside clusters, identified using Raman spectra. The contents of light rare earth elements found using LA-ICP-MS are consistent with a skarn origin for the stones. R.R.H.

Dyed purple hydrophane opal.

N. RENFRO and S.F. McCLURE. *Gems & Gemology*, **47**(4), 2011, 260–70.

Purple opal specimens with play of colour are shown to have been dyed by means of microscopic examination and spectral analyses of the acetone solution after the opal had been immersed. The

Abstracts (continued)

gemmological properties of the opal are consistent with an origin in Wollo, Ethiopia, although it was said by the merchant/donor to come from Mexico. Inclusions also consistent with an Ethiopian origin are quartz with even rhombohedral and short prism faces, and dark brown to black radial patches; also inclusions of a zeolite, possibly chabazite, were found. The authors' experiments on dyeing Ethiopian hydrophane opals are reported. R.R.H.

The Chinese red feldspar controversy: chronology of research through July 2009.

G.R. ROSSMAN. *Gems & Gemology*, **47**(1), 2011, 16–30.

Active research on red feldspar variously suggested as originating in Democratic Republic of Congo, 'China', Tibet, Inner Mongolia and Mexico is chronicled. Spectra in the UV-Vis-NIR range indicate similarities of this feldspar with Oregon sunstone but EPMA analyses indicate a clear distinction with both the sunstone and suggested Mexican feldspars being more calcic. Argon release experiments were conducted to test for heat treatment and argon isotopes along with Ca, Sr, Ba, Zn and Pb isotopes were measured to test source correlation. In 2008 experiments, Cu was found to diffuse easily into plagioclase above 1200°C, experiments prompted by the presence of high levels of Cu in glassy residues on the surfaces and in cracks in rough andesine specimens. The provisional conclusion was that there was a strong case for at least some of the stones to be copper-diffused andesine from Inner Mongolia; however further research is needed. R.R.H.

Triphylite from Brazil — a rare colour-change gemstone.

K. SCHMETZER and E. EREL. *Australian Gemmologist*, **24**(5), 2011, 104–5.

Triphylite is a collector's stone which is rarely described in gemmological literature. Three faceted Brazilian specimens display yellow green or greenish yellow in daylight changing to yellowish orange or brownish orange in incandescent light — both conditions varied depending on viewing angle due to distinct trichroism. Refractive indices of α 1.690, β 1.691, γ 1.696 and a Fe:Mn

ratio of 2.08 were consistent with the triphylite-lithiophilite series in which the refractive indices increase with increasing Fe and decreasing Mn contents. Numerous absorption bands were present in the non-polarized spectrum, with maxima assigned to either Mn²⁺ or Fe²⁺. Colorimetric parameters were also recorded. E.A.S.

Alexandrites from the Novello alexandrite-emerald deposit, Masvingo District, Zimbabwe.

K. SCHMETZER, S. STÖCKLMAYER, V. STÖCKLMAYER and A.K. MALSY. *Australian Gemmologist*, **24**(6), 2011, 133–47.

The Zimbabwean Novello locality, which is similar geologically to the famous Ural Mountain deposit in Russia, has produced mineral specimens and a limited amount of facet-quality rough. Comparisons to the Russian material are drawn via an in-depth discussion of the crystallographic and gemmological features of Novello alexandrites, as well as an overview of the geology of the deposit and gem genesis. Both deposits are dominated by cyclic twins (trillings), while single crystals and contact twins are rare. Unlike most Russian alexandrites, the Novello gems have a higher Cr and Fe content and show strong colour-zoning. Though they have comparable colour-change, the Zimbabwean material is highly fractured and included; rarely of faceting quality. E.A.S.

Identification of extraterrestrial peridot by trace elements.

A.H. SHEN, J.I. KOIVULA and J.E. SHIGLEY. *Gems & Gemology*, **47**(3), 2011, 208–13.

Since their RI and SG properties overlapped, 26 peridot samples from the Esquel meteorite, a stony-iron (pallasite) meteorite, were analysed using LA-ICP-MS and compared with analyses of peridots selected from major terrestrial sources. The elements found to be useful in identifying a peridot as terrestrial or extra-terrestrial are Li, V, Mn, Co, Ni and Zn, and two-element plots such as V vs. Li, Ni vs. Mn and Zn vs. Co show clearly separate fields. R.R.H.

Neue künstlich geritzte Sternsteine und ihre natürlichen Gegenstücke.

M.P. STEINBACH. *Gemmologie. Z. Dt. Gemmol. Ges.*, **60**(1/2), 2011, 25–36. 21

photographs, bibl. [German with English abstract.]

Asterism in stones is usually created by minute, orientated inclusions forming 4-, 6-, 8-, 12-, 18- and even 24-rayed stars. As well as the well-known stones with 4- and 6-rayed stars, the article mentions a few new and rare varieties. About ten years ago, gems with scratched stars appeared on the market. The scratches were made by 'artists' in Sri Lanka and included garnet, chrysoberyl, rutile, sinhalite, cassiterite, scheelite or samarskite, tourmaline (schorl) and sphalerite. Newly described are scratched stars on pyrite, iolite, green garnet, chromian diopside, green tourmaline and sapphire, as well as twin stars and doublets imitating iolite and tourmaline. There are about 40 different star stones known plus the diverse trapiche varieties. E.S.

Mookaite — a Western Australian ornamental rock.

S. STÖCKLMAYER and V. STÖCKLMAYER. *Australian Gemmologist*, **24**(3), 2010, 56–60.

A description of the geological setting, mining practices, mineralogical properties and causation of colour is presented and is accompanied by photographs of petrographic thin sections and of mookaite's unique appearance following fashioning. Mookaite is a trade name for a porcellanite composed predominantly of massive ultrafine silica and coloured by iron oxide granules. This ornamental material is popular because it takes a high polish, is fine grained, is hard with no directional weakness and has an attractive mottled coloration. Due to the rock's variable mineralogy and composition, its gemmological properties also vary. Deposits are found in the former Mooka Pastoral Station located approximately 170 km east of Carnarvon and have been worked since the 1960s. E.A.S.

Yellow scapolite from Ihosy, Madagascar.

M. SUPERCHI, F. PEZZOTTA, E. GAMBINI and E. CASTAMAN. *Gems & Gemology*, **46**(4), 2010, 274–9.

Yellow scapolite has been recovered from veins in skarn rocks about 35 km south of Ihosy in southern Madagascar since the late 1990s. Twenty one representative samples have been studied

Abstracts (continued)

yielding RIs of 1.552–1.581 and SGs of 2.68–2.72, both ranges consistent with compositions rich in meionite (the Ca member of the meionite-marialite series). EPMA analyses confirmed the Me content between 60 and 70%. The fluorescence behaviour of yellow under long wave and purplish red under short wave ultraviolet differs from that of most gem scapolites, being however similar to rare crystals from Switzerland. The influence of a small component of silvialite in the composition is discussed. There are some channel inclusions in the samples and rare crystals of garnet, mica and pyroxene, identified using Raman spectroscopy. R.R.H.

Instruments and Techniques

GIA Symposium 2011.

Gems & Gemology, 47(2), 2011, 123–58.

Topics covered in the presentations include: the range of effects of different light sources on the buying, grading and selling of gemstones; understanding luminescence in gems; applications of fluorescence in gemmology; and a review of the application and limits of advanced techniques used to investigate gems.

There were poster sessions on using a concrete mixer to sort limited quantities of gem-bearing gravels; IR and UV-Vis spectroscopy of emeralds; extreme conoscopy; Raman spectroscopy of garnets; chemical analysis and photoluminescence techniques applied to pearls; 3D mapping of diamond surfaces and inclusions; symmetry assessment of cut diamonds; instrumental colour measurement and grading of faceted gemstones; automated real-time spectral analysis of gems; laser-induced breakdown spectroscopy (LIBS) linked to pattern-recognition software to determine provenance of gemstones; provenance of rubies and sapphires; and colour science and standards for the gem trade. R.R.H.

Determining garnet composition from magnetic susceptibility and other properties.

D.B. HOOVER. *Gems & Gemology*, 47(4), 2011, 272–85.

The apparatus to measure the magnetic susceptibility of a gem is briefly described, and its advantage as

a non-destructive gem testing method additional to RI, SG and other methods is discussed. The method is applied to 28 well characterized garnets from the GIA collections selected to cover the full range of compositions and RI values. The aim was to provide reliable data to enable gemmologists to estimate the end-member proportions in gem garnets being tested, and this can be done on the basis of the magnetic susceptibility versus RI or versus SG diagrams which record the 28 analysed garnets. The problems associated with multiple end members in the garnet group are discussed, but the usefulness of this additional technique in arriving at a reliable test result is clear. R.R.H.

Identifizierungshilfe zur Unterscheidung zwischen natürlichen und synthetischen (HPHT) gelben, gelb-braunen und rötlich-braunen Diamanten.

M. SEUBERT. *Gemmologie. Z. Dt. Gemmol. Ges.*, 60(1/2), 2011, 53–5. 4 photographs. [German with English abstract.]

A blue-violet laser pointer (wavelength 405) can be helpful in distinguishing between natural and synthetic yellow, yellow-brown and reddish-brown diamonds. The strong energy of the laser pointer causes luminescence patterns which make the growth structure of synthetic diamond visible. This method should not be used as a reliable identification feature, but may be useful as an easy, portable and economic first step in the identification process. E.S.

The radioactive decay pattern of blue topaz treated by neutron irradiation.

J. ZHANG, T. LU, M. WANG and H. CHEN. *Gems & Gemology*, 47(4), 2011, 302–7.

A study of 15 neutron-irradiated blue topaz samples was conducted using high-purity germanium digital gamma ray spectroscopy. The specific activities in Bq/g of ¹³⁴Cs, ¹⁸²Ta, ⁴⁶Sc and ¹⁶⁰Tb, which were the radionuclides detected in this set of samples, were measured, and the times they took to decay to the exemption level of 74 Bq/g were determined. Most of the samples were relatively safe at the time of the first measurement, 95 days after irradiation, but if a radionuclide such as ¹⁸²Ta is present in unusually high quantities, the stone may require to be

quarantined for longer than the two or three years it normally takes to reach the exemption level. Measurements were on Chinese topaz and the results should not be assumed relevant to topaz from other localities without further checks. R.R.H.

Synthetics and Simulants

Update on Mexifire synthetic fire opal.

R. BHANDARI and G. CHOUDHARY. *Gems & Gemology*, 46(4), 2010, 287–90.

Current production of synthetic fire opal marketed as ‘Mexifire’ has different properties from those reported in 2008. RI is 1.47 (c.f. 1.38–1.41), SG is 2.19 (c.f. 1.63–1.77) and the FTIR spectrum shows more transmittance at longer wavelengths. The RI and SG values now overlap those of natural fire opals but the presence of scattered fine pin-point inclusions is said to help in identifying the synthetics. R.R.H.

Gem News International.

B.M. LAURS. *Gems & Gemology*, 46(4), 2010, 309–31.

Stones mentioned include: copal and plastic beads; green glass with crystal inclusions; a quartz-synthetic ruby composite sold as natural ruby; and cubic zirconias and glass replica stones assembled to imitate Louis XV’s Golden Fleece jewel of 1749. R.R.H.

Gem News International.

B.M. LAURS. *Gems & Gemology*, 47(1), 2011, 56–73.

Stones mentioned include: doublets of lace agate and reconstituted turquoise are being sold as ‘Coral Sea agate’; dendritic agate doublets and inlays; a trapiche emerald imitation which had been assembled from cut crystal(s) and patchy black adhesive; imitation nephrite consisting of decorated probable polyester resin and containing steel discs only revealed when the ‘boulder’ was broken; a non-nacreous pearl imitation made of shell with a deliberately engraved pattern; and a lead-glass-filled trapiche ruby.

R.R.H.

Lab notes.

T.M. MOSES and S.F. MCCLURE. *Gems & Gemology*, 46(4), 2010, 298–307.

Abstracts (continued)

An intense purplish-pink round brilliant was identified as a treated HPHT-grown synthetic diamond rather than a treated natural stone. Among HPHT-grown synthetic diamonds tested were a 4.09 ct yellow-orange stone, a blue 0.30 ct stone with silicon vacancy defects and melee-size yellow brilliants. Purple and greenish blue cabochons manufactured from turquoise, metal flakes and plastic appeared to contain metal veining and resemble some natural materials. A doublet with both components synthetic, one ruby and the other spinel, was identified. R.R.H.

Lab notes.

T.M. MOSES and S.F. McCLURE (Eds). *Gems & Gemology*, **47**(1), 2011, 49–55.

A black submetallic round brilliant was identified using Raman spectroscopy as an intergrowth of synthetic moissanite and crystalline silicon. A cabochon that initially looked like moonstone was identified as a synthetic star spinel with a blue metallic coating on the base. R.R.H.

Lab notes.

T.M. MOSES and S.F. McCLURE (Eds). *Gems & Gemology*, **47**(3), 2011, 222–33.

The features of 16 faceted CVD synthetic diamonds are described; all are type IIa and have a weak to moderate green fluorescence under SWUV radiation. Two pink diamonds graded Fancy Vivid purplish pink and Fancy Deep purple-pink were found to have quite different structures when seen with DiamondView equipment — one grown in HPHT conditions and the other formed by CVD. The HPHT diamond showed much more uneven colour zoning than the CVD diamond. R.R.H.

Synthetic gem materials in the 2000s: a decade in review.

N. RENFRO, J.I. KOIVULA, W. WANG and G. ROSKIN. *Gems & Gemology*, **46**(4), 2010, 260–73.

Synthetic versions of diamond (particularly gem-quality CVD diamond),

ruby, sapphire, emerald, aquamarine, red beryl, alexandrite, jadeite, quartz, opal and the unexpected examples of synthetic apatite and topaz are reviewed. Comments are made of the current status of methods of identification of these synthetic stones and the ever-present possibility of confusing them with heat-treated natural stones. R.R.H.

Characterisation of a new synthetic fancy yellow diamond.

V. ROLANDI, A. BRAJKOVIC, A. GIORGIONI, A. MALOSSI and R. SCOTTI. *Gemmologie. Z. Dt. Gemmol. Ges.*, **60**(1/2), 2011, 9–24. 14 photographs, 1 table, 8 graphs, bibl. [In German and English.]

The stones examined were HPHT grown with BARS equipment, modifying the geometry of the high-pressure growth cell and treated post growth by annealing and high temperatures. These new attractive synthetic intense bright yellow diamonds are being sold by the Italian firm Malossi Gemcreate (Milan) and marketed as ‘Malossi synthetic fancy yellow diamonds’. They have a homogeneous colour distribution and very good clarity grades. They can be distinguished from natural diamonds by some distinctive gemmological and spectroscopic properties such as evenly distributed green fluorescence to both long and short wave ultraviolet radiation, infrared features typical of type 1aA diamonds, a general increasing absorption from the visible towards the ultraviolet, characteristic UV-Vis and PL spectroscopic features, green cathodoluminescence and paramagnetic properties. Nine faceted and one rough synthetic diamond were examined. E.S.

High quality synthetic yellow orange diamond emerges in China.

S. SHONGHUA, L. TAIJIN, S. MEIDONG, S. JUN and S. JINGJING. *Australian Gemmologist*, **24**(4), 2010, 168–70.

Several Chinese universities and companies now have the ability to produce large HPHT yellow diamonds,

some of which are of high quality and high clarity. This report describes a faceted 1.57 ct orange yellow synthetic diamond of relatively good clarity whose internal scene was comprised of tiny pinpoint inclusions and a pattern of internal graining in the form of a rectangle; metallic inclusions were absent. FTIR, Raman, Vis-NIR and EDXRF analysis were performed, and along with a DiamondView luminescence image of a green cross-shaped fluorescence, the diamond was confirmed as a type Ib synthetic — the first such large, high quality gem that the NGTC lab had encountered in the Chinese gem market. E.A.S.

Exploring the origin and nature of luminescent regions in CVD synthetic diamond.

B. WILLEMS, A. TALLAIRE and J. BARJON. *Gems & Gemology*, **47**(3), 2011, 202–7.

In the DiamondView instrument, blue to blue-green luminescent zones may be seen in CVD synthetic diamond when the growth run has been interrupted and resumed, a well-known practice in the production of gem-quality CVD synthetics. DiamondView, photoluminescence (PL) and cathodoluminescence (CL) imaging were applied to study the origin and nature of these luminescent regions in two samples of high-purity single-crystal CVD synthetic diamond. DiamondView and PL measurements showed a correlation with silicon-related centres. In addition, CL analysis confirmed the presence of boron. Both silicon and boron showed preferential incorporation at the interface between CVD layers, where a higher uptake of impurities lead to the observed luminescence. Although the growth interruptions cannot be detected with the naked eye, the growth history can be determined accurately using luminescence imaging and spectroscopy techniques. Authors' abstract

Abstractors

A.S. Fellows – A.S.F.

R.R. Harding – R.R.H.

E.A. Skalwold – E.A.S.

E. Stern – E.S.

Book reviews

The Diamond Compendium

DEE DEE CUNNINGHAM, 2011. Robert Hale, London. pp 888. Over 200 colour photos plus 150 figures and charts. Hardback, ISBN-13 9780719804113. £150.00.

The first thing I do when I look at a diamond textbook is to check the entry on the Grand Condé. This fancy pink pear-shape weighs 9.01 ct; one would think that this fact would be relatively easy to verify, given that the stone has been sitting on public display in the Musée de Condé in Chantilly for over a century. However, for some reason, many texts state that the diamond weighs 50ct! Perhaps the name 'Grand Condé' misleads authors into thinking that the stone must be bigger than it really is? If a book quotes the correct mass, I usually take it as an indication that the author has taken the trouble to do some proper research. I was therefore pleased to discover that the *Compendium* states the correct figure in Chapter 16 and, suitably reassured, I settled down for some serious reading: at nearly nine hundred pages, the *Compendium* certainly packs a punch.

In hindsight, it is just as well that I started off by delving into the middle, as the opening pages in Chapter 1, 'Diamond origin and geological occurrence', are unfortunately amongst the least readable in the book. At this point, one of the *Compendium's* two major flaws becomes apparent: diamond is not only the cornerstone of a multi-billion-dollar jewellery industry, but also a supermaterial. The books and journals devoted to diamond could fill a library – something which cannot be said of any other gemstone. Whereas monographs on other gems (such as Hoover's *Topaz*) can be quite satisfying and accessible,

to attempt to write a compendium of knowledge on the topic of diamonds is a mammoth challenge, and it is never entirely clear what kind of audience the author is trying to reach. Retailers or consumers wishing to know more about diamonds will find some chapters impenetrable, whereas those with a more scientific background will find the same chapters inadequate when compared to dedicated academic texts such as Wilks & Wilks' *Properties and Applications of Diamond*. The end result is a slightly awkward compromise of a book. Chapter 1 also showcases the *Compendium's* second major flaw: in the author's enthusiastic attempt to compile the authoritative source of diamond-related knowledge, contentious statements are often presented as if they were undisputed fact. Unlike many coloured stones, diamond does not crystallize in accessible locations, but formed deep within the Earth under conditions that are still imperfectly understood. However, this is not the impression one gets from reading the *Compendium*. One unfortunate example is when carbonado is described as originating from meteorite impacts. Firstly, published research papers appear to suggest that the origins of carbonado are still controversial. Secondly, the author muddies the waters further by apparently confusing impact synthesis (the process that is thought to transform terrestrial carbon into microcrystals of lonsdaleite thanks to the heat and pressure of impact) with true extraterrestrial origin (where the meteorite itself contains non-terrestrial polycrystalline diamond that existed prior to impact).

Chapter 2, 'Geographical occurrence of diamond and diamond-bearing rocks',

provides profiles of the world's diamond-producing countries. The diamond world is fast-changing and the author wisely admits that the chapter should be seen only as a snapshot at the time of writing (the situation in Zimbabwe, for example, has already been overtaken by events).

Chapter 3, on crystallography, is adequate, though readers who have a qualification in gemmology from Gem-A will compare it unfavourably to Wood's excellent *Crystals and Light*.

Chapters 4, 5 and 6 are very good. They cover the exploitation of primary and secondary deposits and diamond processing and recovery. Interesting historical background on obsolete techniques is accompanied by useful information on modern technology that is seldom found outside specialist geology texts.

Chapter 7, 'Diamond Properties' is useful although once again the author takes selected academic research, in this case Sunagawa's work on the morphology of Type II diamonds, and uncritically presents it as gospel. Although Sunagawa may not have been challenged academically to date, the article itself seems rather speculative upon close examination. It is rejected by some diamantaires for the simple reason that flat octahedral faces are practically never seen on Type II stones — surely it is a stretch to assume that they have all been etched or broken off? After all, the *Compendium* itself acknowledges that manipulating growth conditions can lead to synthetics crystallizing as cubes rather than octahedra, so one might wonder why the author is reluctant to admit similar possibilities for natural stones.

The author is to be congratulated

Book reviews (continued)

on Chapter 8, on colour. It is a solid introduction into a highly specialized and vitally important topic that is inadequately covered in most gemmology textbooks. There are occasional slip-ups, such as when the author claims that orange can be modified by green, which is not possible as 'warm' and 'cool' colours don't mix. Perhaps this is why the *Compendium* states that there are 270 colour possibilities, whereas I calculate that the GIA recognizes a total of 101 colour grading terms for fancy diamonds (including black, 'white' and grey). In addition, it is asserted that gamma irradiation makes diamonds radioactive, which is untrue for gamma rays with energies of less than several megaelectronvolts.

Chapter 9, 'Manufacturing' is probably the best summary available on the topic, although it is already slightly dated: diamond technology is currently developing at an incredible pace. For example, there is no mention of the use of diamond-impregnated grinding wheels for bruting (so-called 'Russian bruting machines'), which are currently making great inroads into the industry. The text also somewhat underplays the key roles of laser technology and computerized planning in modern manufacturing. The section describing international polishing centres could also use an update, with barely a mention of the effects of resource nationalism and the consequent establishment of polishing centres ('beneficiation') in Southern Africa. The author's tendency to rely uncritically on previous texts rears its head again when the *Compendium* states that cutting thicker girdles and crowns is a good way of improving depth-of-colour in fancy-coloured stones. This is an oversimplification; modern computer technology is now being used to design faceting patterns and angles that increase path length through the use of total internal reflection. Counter-intuitively, this can sometimes provide ways of increasing a stone's saturation by re-cutting it to shallower proportions.

Chapter 10, on cutting styles, is a good summary but for the unaccountable omission of the Asscher-cut, which helped to revitalize the popularity of emerald-cuts in the twentieth century. Amusingly, the author speculates that the baguette-

cut owes its name to the French word 'baguette', meaning ring. Although it is true that baguette-cuts have no relationship to loaves of bread, the etymology of the term is almost certainly better-explained by the fact that 'baguette' in French simply means 'rod/stick'! It is also unfortunate that the *Compendium's* preferred line-drawing for heart-shapes includes impossible facets that cannot exist in real life.

Chapters 11, 12, 13 and 14, on the 'four Cs', are the strongest in the book: in these sections, the author is solidly within her comfort zone, displaying clear evidence of GIA training. Modern techniques are outlined and there is genuine strength in the detail, such as an explanation of the technique of 'wet grading' which helps to showcase the fact that the *Compendium* has truly been carefully constructed from the ground up rather than cobbled together from existing books. The only unfortunate omission is that the comparative tables contrasting various rather similar grading schemes do not mention the Russian grading system — the only maverick among diamond laboratory standards.

Chapter 15, on the global diamond market, is unfortunately somewhat shaky. In addition to being very out-of-date (De Beers' former sorting house on 2 Charterhouse Street was vacated and demolished years ago, and the author's quoted figure of 400 diamond-sorters in London is a distant memory), there are also factual errors. For example, not all of the world's bourses are affiliated with WFDB, and the account of De Beers' sorting activities contains numerous mistakes (although the author could perhaps be forgiven for failing to unearth the finer details of this proprietary process, which will in any case be of little relevance to readers given that every diamond company has its own assortment, machinery and procedures). However, the most misleading error is the claim that Sightholders are faced with a coercive, "like it or lump it" dilemma at every Sight. In fact, Sightholders can reject a portion of their Box — so-called 'buy-backs' — or refuse the Box in its entirety. They can and do exercise these rights freely, notably during the economic crisis in late 2008 that nearly crippled the entire diamond-mining industry. The author would have gained a better understanding

had she referred to the diamond trade journals, or if she had simply downloaded a copy of the current Sightholder Contract from the company's website.

Chapter 16, 'Famous diamonds', is excellent. The list of largest gem-quality uncut diamonds shows signs of careful archival research: it is obviously more comprehensive than most of the existing lists, and includes several stones from Jagersfontein which others appear to have missed. Previous authors such as Bruton and Balfour have mentioned some additional 500-plus-carat stones in passing, and there are reports of a 602 ct rough discovered in 1993 in the Santo Antônio do Bonito river (Minas Gerais, Brazil) but this list restricts itself to 'gem-quality' items, which perhaps explains why such stones are not listed — although the author certainly appears to have given the rather murky-looking 620 ct Sefadu the benefit of the doubt! It is sheer bad luck that the 550 ct Letšeng Star was discovered on 19 August 2011, obviously too late for publication. In fact, the only other notable omissions from the list appear to be the Wynn and the Star of Stanley Ho, diamonds owned by competing casino moguls. The former is said to have weighed 581 ct when discovered in Brazil in 2002, and the latter is said to have weighed 570 ct when discovered in Angola around 2003 (it is now the world's largest D-flawless cushion-cut, on display in a casino in Macau).

The author has taken the Mouawad Collection's ownership at face value, although few people who work in 'haute joaillerie' seem to genuinely believe that Mr Mouawad has built up this fabulous private collection of famous diamonds on his own account: it is widely rumoured that they have long since been re-sold to private clients. With the exception of the Excelsior I, the gems are, in fact, conspicuous by their absence from the Robert Mouawad Private Museum in Beirut, and I have been unable to verify the author's report of the stones being exhibited in Mouawad boutiques in recent times.

Chapters 17, 18, 19 and 20 (diamond identification, simulants, treatments and synthetics respectively) are all excellent and very comprehensive, along the same lines as the 'Four Cs' chapters.

Book reviews (continued)

Conclusion

In spite of some of the above comments, the *Compendium* is a worthy piece of work. It supplants Bruton's *Diamonds* as today's leading general diamond textbook (although it is admittedly rather less enticing and readable) and it deserves to take its place on every gemmologist's bookshelf along with that other indispensable 900-page behemoth, O'Donoghue's *Gems: their sources, descriptions and Identification*. Like both of these tomes, the *Compendium* deserves to have a long shelf life and go through multiple

editions. Its flaws are usually minor — the occasional slightly wonky diagram, a persistent habit of mis-spelling surnames, an inconsistent approach to the inclusion of 'inline' references in the text — but, at its best, the *Compendium* manages to not only present a reasonably up-to-date summary of existing knowledge that is unavailable elsewhere, but also to add fascinating insights and background colour.

Michael Hing

(Michael Hing is a Fellow of Gem-A, and works as a diamond valuer in London.)

Gem-A Shop



Don't miss the monthly **SPECIAL OFFERS**
on books and instruments from the
Gem-A Shop

Log on to the Gem-A website at www.gem-a.com to discover what is on offer each month.

Proceedings of the Gemmological Association of Great Britain and Notices

Gem-A Graduation Ceremony and Presentation of Awards

On Monday 7 November the Graduation Ceremony and Presentation of Awards was held at Goldsmiths' Hall in the City of London. Professor Andy Rankin, President of the Gemmological Association, presided. James Riley, Chairman of the Gem-A Board, welcomed those present and introduced Jeffrey Monnickendam of Monnickendam Diamonds, a past Gem-A Council member, who presented the awards and gave the address.

Following the presentations to the graduates, Alan Hodgkinson was presented with an Honorary Lifetime Membership in recognition of his tremendous contribution to gemmology over fifty years. Alan is internationally recognized for his gem identification techniques using traditional gem testing equipment and for his book *Visual Optics*. Having been President of the Scottish Branch of Gem-A for many years, Alan is now Honorary President of the Scottish Gemmological Association formed in 2008.

The ceremony was followed by a reception for graduates and guests.



Graduates gather on the magnificent staircase at Goldsmiths' Hall following the ceremony. Photo courtesy of Photoshot.

Proceedings of the Gemmological Association of Great Britain and Notices

Gem-A Conference 2011

Record numbers attended the 2011 Gem-A Conference, held on Sunday 6 November at the Hotel Russell, Bloomsbury. Speakers included Steve Bennett, Brian Cook, Branko Deljanin, Alan Hart, Brian Jackson and Gary Roskin. Adolf Peretti was unable to attend due to flooding in Bangkok, but Willy Bieri kindly stepped in at the last minute to present his lecture.

During the breaks delegates had the opportunity to browse through the latest books and instruments from Gem-A Instruments and to view displays and demonstrations.

The day concluded with a dinner held at The Russell followed by a disco.

Conference Events

A programme of events and workshops was arranged to coincide with the Conference. These started on Saturday 5 November with two half-day seminars held by Branko Deljanin entitled 'Basic gemmology and diamond identification'.

On Monday 7 November two half-day seminars were held — 'Optical phenomena' with Brian Jackson and 'Snap decisions: photographing gems under less than ideal conditions' with Gary Roskin. The Graduation Ceremony and Presentation of Awards was held in the evening at Goldsmiths' Hall (see report opposite).

On Tuesday 10 November Alan Hart led a tour of the Mineral Gallery at the Natural History Museum, South Kensington, including the opportunity to view the Museum's new acquisitions. This was followed in the afternoon by a guided tour of the Crown Jewels at the Tower of London with David Thomas. The final event was Gem Discovery Club with guest speaker Dominic Mok

Conference Sponsors and Supporters:

The Association is most grateful to the following for their support:

MAJOR SPONSORS

Marcus McCallum FGA, London
www.marcusmccallum.com

SPONSORS

T.H. March, Insurance Brokers
www.thmarch.co.uk

Asian Gemmological Institute and Laboratory (AGIL)
w: www.agil.com.hk

The Goldsmiths' Company Assay Office
www.thegoldsmiths.co.uk/assay-office

SUPPORTERS

Apsara
www.apsara.co.uk

Brink's Global Services
www.brinksglobal.com

British Jewellers' Association
www.bja.org.uk

Gemfields
www.gemfields.co.uk

We would also like to thank **dg3 Diversified Global Graphics Group** for sponsoring the leaflets and delegate badges for the conference. Visit their website at www.dg3.com

who gave a presentation entitled 'Fei Cui: jadeite jade identification, from eye to high-tech'.

A full report of the Conference and events is to be published in the Winter 2011/2012 issue of *Gems & Jewellery*.



Gem-A Awards

Gem-A Examinations were held worldwide in January and June 2011. In the Examinations in Gemmology 293 students qualified in the Diploma Examination, including nine with Distinction and 44 with Merit. In the Foundation in Gemmology Examination 389 qualified. In the Gem Diamond Examination 81 qualified, including 11 with Distinction and seven with Merit.

The **Tully Medal** is awarded to the candidate who submits the best set of answers in the Gemmology Diploma examination which, in the opinion of the Examiners, are of sufficiently high standard. **Robin Hansen of** Warminster, Wiltshire, was awarded the **Tully Medal** as well as the **Christie's Prize for Gemmology** for the best candidate of the year in the Diploma Examination, and the **Anderson Bank Prize** for the best set of theory papers in the Diploma in Gemmology examination.

The **Read Practical Prize** for excellence in the Diploma Practical Examination was sponsored for 2011 by DeeDee Cunningham of Toronto, Canada. The Read Practical Prize was awarded to **Xianzhi Zhang** of Wuhan, China.

In the **Foundation Certificate in Gemmology** examination, the **Anderson Medal** for the candidate who submitted the best set of answers which, in the opinion of the Examiners, were of sufficiently high standard, and the **Hirsh Foundation Award** for the best candidate of the year, were awarded to **Dr Simon Gowry** of Wolverhampton.

In the **Gem Diamond Diploma** examination, the **Bruton Medal** for the best set of theory answer papers of the year was awarded to **Julia Anna Griffith** of Southampton

The **Deeks Diamond Prize** for the best candidate of the year, was awarded to **Julia Gowans-Poli** of London.

The **Dominic Mok Diamond Practical Prize** for excellence in the Diamond Practical Examination, is sponsored by Dominic Mok from AGIL, Hong Kong. The Dominic Mok Diamond Practical Prize was awarded to **David Lawrie** of Solihull.

The names of the successful candidates are listed below.

Examinations in Gemmology

Gemmology Diploma

Qualified with Distinction

Antonucci, Andrea, Stockholm, Sweden
 Di Cui, Beijing, P.R. China
 Diamond, Marcia Jane, London
 Hansen, Robin, Mere, Warminster, Wiltshire
 Huang Rong, Ling Shui County, Hainan, P.R. China
 Lacosta, Patricia, London
 Mogridge, Emma Denise, Totnes, Devon
 Tingting Ma, Shanghai, P.R. China
 Weng Xiao Fan, Fu Zhou City, Fujian, P.R. China

Qualified with Merit

Callandreau, Alexandra Bokobsa, Paris, France
 Chao Liu, Beijing, P.R. China
 Chayathorn, Chanruangvanich, Bangkok, Thailand
 Gao, Yu Jie, Henan, P.R. China
 Guo Huimin, Wuhan, P.R. China
 He Yiting, Jiangsu, P.R. China
 Hsu Shu-Lin, Taipei, Taiwan, R.O. China
 Hu Zhengying, Shanghai, P.R. China

In-Nang Cheong, Taipei, Taiwan, R.O. China
 Jain, Sanjay, Bangalore, Karnataka, India
 Jamieson, Pauline, Edinburgh, Midlothian
 Jiao Yongling, Beijing, P.R. China
 Lei Yuanyuan, Changsha City, Hunan, P.R. China
 Mailly, Caroline, Versailles, France
 Min Zhou, Beijing, P.R. China
 Möhler, Anja, London
 Papaux, David J.H., Geneva, Switzerland
 Pei Yu, Beijing, P.R. China
 Qiao Xiong, Honghu, Hubei, P.R. China
 Raj, Amrit, Jaipur, India
 Reynaud, Lucy, Singapore
 Reynolds, Eva, Cheltenham, Gloucestershire
 Ruiwei Ma, Guilin, Guangxi, P.R. China
 Shao Xinyuan, Wuhan, P.R. China
 Sheridan, Meghan E., Upper Montclair, New Jersey, U.S.A.
 Shevchenko, Olga, Montreal, Quebec, Canada
 Siyuan Bi, Guilin, Guangxi, P.R. China

Proceedings of the Gemmological Association of Great Britain and Notices

- Su Shi Zhen, Shandong, P.R. China
 Sujie Ai, Guilin, Guangxi, P.R. China
 Tang Pik Yin, Kowloon, Hong Kong
 Tianyin Xu, Beijing, P.R. China
 Vazzana, Franck, Cosnes-et-Romain, France
 Wang Jing, Shanghai, P.R. China
 Xu Ying, Shanghai, P.R. China
 Yan Shen, Guilin, Guangxi, P.R. China
 Yifan Li, Beijing, P.R. China
 Yiru Shi, Beijing, P.R. China
 Yu-Han Chen, Taipei, Taiwan, R.O. China
 Zdeb, Robert, Epping, Essex
 Zhang Di, Beijing, P.R. China
 Zhang Dongfang, Beijing, P.R. China
 Zhang Shengnan, Beijing, P.R. China
 Zhao Lu, Shanghai, P.R. China
 Zheng Yan, Beijing, P.R. China
- Qualified*
- Aiming Cao, Beijing, P.R. China
 Akerlund, Sophia, Lidingö, Sweden
 Akintayo, Olusegun James, London
 Allen, Amanda, Northampton
 Al-Saif, Manar, Stavanger, Norway
 An Yue, Beijing, P.R. China
 Andoniaina Harijaona, Rabetaliana, Antananarivo,
 Madagascar
 Andriamanohisoa Axhel, Robert, Antananarivo,
 Madagascar
 Andriamboavonjy, Rasamuel, Antananarivo, Madagascar
 Athavale, Seema Ashish, Mumbai, India
 Bane, Jonathan William, Sheffield, South Yorkshire
 Barnett, Myles, Unley Park, South Australia, Australia
 Beer, Jasmin, Birmingham, West Midlands
 Bell, Nicola, Newton Abbott, Devon
 Bernau, Eric, La Ciotat, France
 Bing Sun, Wuhan, P.R. China
 Burgoni, Eva Maria, Carnoux-en-Provence, France
 Butini, Enrico, Rome, Italy
 Butini, Flavio, Rome, Italy
 Caihuan Liao, Guilin, Guangxi, P.R. China
 Cao Hanxiao, Henan, P.R. China
 Chan Lim Chi, Ap Lei Chau, Hong Kong
 Chan Pei Pei, Betty, Quarry Bay, Hong Kong
 Chan Yuen Ping, Aberdeen, Hong Kong
 Chandrasiri, Hemali Iresha Kumari, Kegalle, Sri Lanka
 Chang Jing, Zhangjiakou City, Hebei, P.R. China
 Chaoguang He, Wuhan, P.R. China
 Charpentier, Frédéric, Fresnes, France
 Chen Jiankang, Guangzhou, Guangdong, P.R. China
 Chen Qian-Zheng, Beijing, P.R. China
 Cheng Lin Lv, Beijing, P.R. China
 Chengxuan Li, Beijing, P.R. China
 Cheung Siu Lui, Sharon, Tsuen Wan, Hong Kong
 Choi Wing Cheong, Chai Wan, Hong Kong
 Chunxia Chen, Shanghai, P.R. China
 Chunzhong Huang, Guilin, Guangxi, P.R. China
 Chuxin Song, Guilin, Guangxi, P.R. China
 Costanzo, Alessandra, Galway, Ireland
 Cui Dongmei, Taiyuan City, Shanxi, P.R. China
 Daijun Sun, Beijing, P.R. China
 de Gaspé Beaubien, Isabelle, Montreal, Quebec, Canada
 Deutschl, Norbert, Montreal, Quebec, Canada
 Di Gregorio, Giuseppe, Spadafora, Italy
 Elliott, Paul, Woodville, South Australia, Australia
 Elmetto, Pamela, London
 Feng Yan, Guangzhou, P.R. China
 Ferré, Iohan, Vingrau, France
 Fitchko, Dorian Nicholas, Montreal, Quebec, Canada
 Fong Tik Kwan, Tseung Kwan O, Hong Kong
 Franks, Elliot, Worthing, West Sussex
 Gan Yanchao, Guangzhou, Guangdong, P.R. China
 Gao Shijia, Beijing, P.R. China
 Gaonkar, Mahesh, Mumbai, India
 Georgsen, Cecilia Andrén, Lund, Sweden
 Gilson, Karen Margaret, Wanstead, London
 Gross, Robyn Elizabeth, Mont-Royal, Quebec, Canada
 Gu Jialu, Shanghai, P.R. China
 Guo Fang Yu, Beijing, P.R. China
 Guo Yongquan, Xiamen City, P.R. China
 Hao, Yudi, Bayannaoer City, Inner Mongolia, P.R. China
 Hardy, Sarah, Stockton-on-Tees, County Durham
 Herzog, Franz A., Oltingen, Switzerland
 Hu Yuanfeng, Shanghai, P.R. China
 Huang Xi, Shanghai, P.R. China
 Huang Yuan, Beijing, P.R. China
 Huijie Huang, Beijing, P.R. China
 Hu Jiesheng, Shanghai, P.R. China
 Hunt, Glynis, Andover, Hampshire
 Hutchinson, Fiona, Albourne, West Sussex
 Ikeuchi, Mototeru, Tokyo, Japan
 Imberti, Daufresne, Antananarivo, Madagascar
 Ivancic, Ivan, Colombo, Sri Lanka
 Jacquier, Nathalie, Genthod, Switzerland
 Jia Song, Guilin, Guangxi, P.R. China
 Jiang Baoxin, Shanghai, P.R. China
 Jianmei Ouyang, Beijing, P.R. China
 Jiawen Li, Beijing, P.R. China
 Jing Chen, Urumqi, Xinjiang, P.R. China
 Jing Zhang, Wuhan, P.R. China
 Johnson, Louise, Edinburgh, Midlothian
 Johnston, Meredith, Marcoola, Queensland, Australia

Proceedings of the Gemmological Association of Great Britain and Notices

- Jokinen, Tiina, Tampere, Finland
 Jun Lu, Beijing, P.R. China
 Karimzadeh, Leyla, London
 Kaye, Charlotte Jane, Hungerford, Berkshire
 Kirkham, Sally Louise, Birmingham, West Midlands
 Knudsen, Christine, Oslo, Norway
 Knutsen, Annmari Ellila, Oslo, Norway
 Kun Wang, Guilin, Guangxi, P.R. China
 Lahtinen, Tiina Marjaana, Oitti, Finland
 Lai Hsin Ya, Feng Yuan City, Taiwan, R.O.C.
 Lai Nga Ting, Eltham, London
 Lee, Alix, Rognes, France
 Lee, Sealim, London
 Lee Lai Chun, Loletta, Hong Kong
 Li Bin, Guangzhou, Guangdong, P.R. China
 Li Hangeng, Beijing, P.R. China
 Li Li, Guilin, Guangxi, P.R. China
 Li Shanshan, Wulumuqi City, Xinjiang, P.R. China
 Li Shuang, Beijing, P.R. China
 Liang Siqiao, Mile County, Yunnan, P.R. China
 Liang Xiaoyang, Wuhan, P.R. China
 Liao Mengyuan, Guangxi, P.R. China
 Lili Zhang, Wuhan, P.R. China
 Lin Jing, Xiamen City, Fujian, P.R. China
 Linlin Zhang, Guilin, Guangxi, P.R. China
 Liu Saihua, Yueyang, Hunan, P.R. China
 Liuyi Li, Guilin, Guangxi, P.R. China
 Liyuan Gan, Guilin, Guangxi, P.R. China
 Loosvelt, Bart, Kortrijk, Belgium
 Lowther, Joan, London
 Lu Gao, Beijing, P.R. China
 Lulu Mo, Guilin, Guangxi, P.R. China
 Ma March Yu, Chongqing, P.R. China
 Mane, Sandesh Narayan, Mumbai, India
 Maneekrajangsaeng, Marisa, Bangkok, Thailand
 Matsuura, Miho, Yokohama, Japan
 Mayer, Helen, London
 Mayer, Melanie, St Helens, Jersey, Channel Islands
 Ménard, Georges-Etienne, Saint-Hyacinthe, Quebec, Canada
 Meng, Caizhen, Nanning City, Guangxi, P.R. China
 Mengying Luo, Wuhan, P.R. China
 Minassian Bardehshahi, Odett, Mykonos, Greece
 Misme, Eric, Lyon, France
 Mitchell, Anne Susan, Harpenden, Hertfordshire
 Mkogian, Elen, Stavroupoli, Thessalonika, Greece
 Modi, Upaasna, London
 Neurauter, Amy Lynn, New York, U.S.A.
 Nguyen, Michel, Saintry-sur-Seine, France
 Odén, Naime Marielle Angelica, Brunflo, Sweden
 O'Reilly, Erin M.M., Montreal, Quebec, Canada
 Owen, Cheryl Mae, Erdington, West Midlands
 Palliyaguruge, Lalake Sanjeewa, Battaramulla, Sri Lanka
 Papalekakou, Despoina, Korydallos, Greece
 Parkes, Matthew A., Dublin, Ireland
 Parry, Tessa Pryce, Wantage, Oxfordshire
 Patenaude, Lizanne, Westmount, Quebec, Canada
 Pei Ying Hsiao, Zhongli, Taiwan
 Peng Cunzhen, Wuhan, P.R. China
 Poon Pak Kei, Hong Kong
 Qi Weihong, Birmingham, West Midlands
 Qian Gan, Guilin, Guangxi, P.R. China
 Quentin, Dartois, Vence, France
 Ranatunga, Galla Ge Deershika, Meetiyagoda, Sri Lanka
 Ratnayake, Dayanthi, Colombo, Sri Lanka
 Regala, Benjamin, Aiea, Hawaii, U.S.A.
 Ren Xiaoxue, Wu Lan Cha Bu City, Inner Mongolia, P.R. China
 Richbourg, Carole, Los Altos, California, U.S.A.
 Rie, Okayasu, Antananarivo, Madagascar
 Roach, Fay, Norwich, Norfolk
 Rufa Feng, Guilin, Guangxi, P.R. China
 Sai Qin, Wuhan, P.R. China
 Sakakibara, Kenichi, Oita, Japan
 Sequino, Francesco, Naples, Italy
 Shan Xinying, Beijing, P.R. China
 Shang Guoqiang, Wuhan, P.R. China
 Shang Mei, Wuhan, Hubei, P.R. China
 Shen Lida, Xiamen City, P.R. China
 Sheno, Anita, Longhope, Gloucestershire
 Shih-Ying Wu, Taipei, Taiwan, R.O. China
 Shuang Zhou, Beijing, P.R. China
 Shuihan Yi, Birmingham, West Midlands
 Shuxuan Xiao, Beijing, P.R. China
 Sibley, Christopher, St Albans, Hertfordshire
 Smither, Susannah, London
 Song Wenyan, Zengcheng City, Guangdong, P.R. China
 Sun Hongmeng, Xingping City, Shaanxi, P.R. China
 Sy, Dicken, Kowloon, Hong Kong
 Tew, Timothy David, Atlanta, Georgia, U.S.A.
 Thomas, Craig Arthur, Santon, Gauteng, South Africa
 Tims, Ashley, Indooroopilly, Queensland, Australia
 Ting Huang, Guilin, Guangxi, P.R. China
 Toure, Abdoul, Toamasina, Madagascar
 Tsang Hing Cheung, Hong Kong
 Valentini, Francesca, London
 Varhadpande, Milind Arun, Mumbai, India
 Verwijk, Moira, Toronto, Ontario, Canada
 Von Allmen, Andrea, Munsingen, Switzerland
 Vorilhon, Alix, Antananarivo, Madagascar
 Voulgaridis, Konstantinos, London
 Wang Jinlan, Guilin City, Guangxi, P.R. China

Proceedings of the Gemmological Association of Great Britain and Notices

Wang Ming Ying, Beijing, P.R. China
 Wang Mingtian, Zhongshan, Guangdong, P.R. China
 Wang Yuyan, Henan, P.R. China
 Wang Zhen, Beijing, P.R. China
 Wang Zi, Beijing, P.R. China
 Ward, Sarah, Leeds, West Yorkshire
 Welsh, Simon Ian, Exeter, Devon
 Wenhua Liang, Guilin, Guangxi, P.R. China
 Weyers, Stefanus Salomon, Brandhof Bloemfontein,
 South Africa
 Whiting, Marielle, Salisbury, Wiltshire
 Willmott, Karra Jane, Croydon
 Wilson, Maria Dorothea, Stretton-on-Dunsmore,
 Warwickshire,
 Windeyer, Patricia Annette, Brisbane, Queensland,
 Australia
 Wingate, Simon, Tiverton, Devon
 Wolff, Ella S., Silver Lonnen, Tyne and Wear
 Wong Wing Suet, Kowloon, Hong Kong
 Woodcock, Olga Faye, Basingstoke, Hampshire
 Wu Chung-Kang, Yung He City, Taipei, Taiwan, R.O.C.
 Wu Yi, Beihai City, Guangxi, P.R. China
 Wu Zhi Yuan, Beijing, P.R. China
 Xiangbo Yang, Beijing, P.R. China
 Xiaoan Chen, Guilin, Guangxi, P.R. China
 Xiaofei Chen, Wuhan, P.R. China
 Xiaowen Huang, Guilin, Guangxi, P.R. China
 Xiong Ranran, Xiangfan City, Hubei, P.R. China
 Ranran Xu Yanyan, Shanghai, P.R. China
 Xue Tian, Beijing, P.R. China
 Xue Yuan, Zhengzhou, Henan, P.R. China
 Yamaguchi, Nao, Osaka, Japan
 Yang Xi, Beijing, P.R. China
 Yanming Feng, Wuhan, P.R. China
 Yanran Xu, Beijing, P.R. China
 Yat, Richard, New Territories, Hong Kong
 Ye Ma, Beijing, P.R. China
 Yi'an Jiang, Guilin, Guangxi, P.R. China
 Yishun Huang, Guilin, Guangxi, P.R. China
 Yu Miao, Chengdu City, Sichuan, P.R. China
 Yu Jinping, Beijing, P.R. China
 Yu Zhang, Beijing, P.R. China
 Yu Zheng, Wuhan, P.R. China
 Yue Yin, Guilin, Guangxi, P.R. China
 Yuet Chai, New Territories, Hong Kong
 Yujiao Chen, Beijing, P.R. China
 Zang Xiaoliang, Wuhan, P.R. China
 Zhang Jingwen, Central, Hong Kong
 Zhang Li, Wuhan, Hubei, P.R. China
 Zhang Qian, Beijing, P.R. China
 Zhang Xianzhi, Wuhan, Hubei, P.R. China

Zhang Yiwen, Beijing, P.R. China
 Zhao Mei Tao, Beijing, P.R. China
 Zhao Yang, Xuchang City, Henan, P.R. China
 Zhao Zhuanghua, Beijing, P.R. China
 Zhenghuan Huang, Guilin, Guangxi, P.R. China
 Zhongjing Kang, Beijing, P.R. China
 Zhou Qi, Zhuji City, Zhejiang, P.R. China
 Zhu Lin, Beijing, P.R. China
 Zhu Ning, Beijing, P.R. China
 Zhu Xiao Li, Yun Cheng City, Shan Xi, P.R. China

Foundation Certificate in Gemmology

Qualified

Abraham, Helen Louise, Weybridge, Surrey
 Ai Sujie, Zhongxiang City, Hubei, P.R. China
 Aissaoui, Mehdi, Laxou, France
 Alsvold-Torndahl, Rebecca, Skanor, Sweden
 Andersson, Helene, Lannavaara, Sweden
 Andre, Sandrine, London
 Aponsu, Malimage, Moratuwa, Sri Lanka
 Au Siu Tong, Kowloon, Hong Kong
 Au Sui Keung, New Territories, Hong Kong
 Au Tsz Wai, New Territories, Hong Kong
 Avendano, Edson, Montreal, Quebec, Canada
 Bai Dan, Guangzhou City, P.R. China
 Bailey, Kathryn, Aberdeen
 Barrows, Michael James, Kidderminster, Worcestershire
 Benistand, Angelique, Grenoble, France
 Bertenshaw, Emma, Luz-Lagos, Algarve, Portugal
 Bi Siyuan, Jiyuan City, Henan, P.R. China
 Boisserand, Anne, Frejus, France
 Bombardier, Valerie, Candiac, Quebec, Canada
 Boylan, Penny, London
 Bragg, Caitlin, London
 Branchard, Jean-Yves, Kamaryut Township, Yangon,
 Myanmar
 Brasseur, Agnes, Le Tholonet, France
 Brianceau, Boris, Saint-Julien des Landes, France
 Buckley, Amanda, North Shore, Auckland, New
 Zealand
 Buono, Pascal, Mont Royal, Quebec, Canada
 Burlando, Elisabetta, Genova, Italy
 Cancé, Gregory, Montreal, Quebec, Quebec, Canada
 Caussin, Karine, Drumettaz Claraford, France
 Chai Yuet, New Territories, Hong Kong
 Chamayou, Isabelle, Saint Raphael, France
 Chan Hei Yiu, Hong Kong
 Chan Shuk Lam, Kowloon, Hong Kong
 Chan Wai Ling, New Territories, Hong Kong
 Chan Yin Ki Cubie, Hong Kong
 Charpentier, Frederic, Fresnes, France

Proceedings of the Gemmological Association of Great Britain and Notices

- Chau Lan Yee, Sheung Wan, Hong Kong
 Chayathorn, Chanruangvanich, Yannawa, Bangkok, Thailand
 Che Yandong, Calfeng City, Inner Mongolia, P.R. China
 Chen Chunxia, Shanghai, P.R. China
 Chen Ju-Yu, Taipei, Taiwan, R.O. China
 Chen Mengna, Rong County, Guangxi, P.R. China
 Chen Xiao, Teda of Tian Jin, P.R. China
 Chen Xiaolan, Yulin, P.R. China
 Chen Xueping, Shanghai, P.R. China
 Chen Yin, Shanghai, P.R. China
 Chen Yu-Han, Taipei, Taiwan, R.O. China
 Cheng Ping Shing, Kowloon, Hong Kong
 Cheon Ji Youn, Yeonsu-Gu, Incheon, South Korea
 Cheong In-Nang, Taipei, Taiwan, R.O. China
 Cheung Chak Ting, Christine, Kowloon, Hong Kong
 Cheung Chau, North Point, Hong Kong
 Cheung Mei, Karen, New Territories, Hong Kong
 Cheung Siu Lui, Sharon, New Territories, Hong Kong
 Chin Cheung, Beijing, P.R. China
 Cho Mi Hyun, Jung-Gu, South Korea
 Choi Shin A., Namyangju-Si, Kyunggi-Do, South Korea
 Chow Po Ling, Hong Kong
 Chu Hoi Ting, New Territories, Hong Kong
 Chu Pik Wa, Shek Lei Est, Hong Kong
 Chu Wai Hung, Kowloon, Hong Kong
 Chu Yung-Huan, Taichung, Taiwan, R.O. China
 Chung Pui Shan, Rosemary, Pok Fu Lam, Hong Kong
 Chung Wing Lam, Apleichau, Hong Kong
 Clausen, Tobias, Lannavaara, Sweden
 Corton, Annabelle Rachael, Dubai, U.A.E.
 Da Silva, Andre Fortunato, St Helier, Jersey, Channel Islands
 Dai Hin Kwan, New Territories, Hong Kong
 Dartois, Quentin, Vence, France
 Daufresne, Marie, Antananarivo, Madagascar
 David, Elysabeth, Bonn, Germany
 Davis, Valerie, Stone, Staffordshire
 Day, Kroy, Jimboomba, Queensland, Australia
 De Haller, Antoine, Geneva, Switzerland
 De Zoysa Jayatileke, Liyana Gracelyn, Colombo, Sri Lanka
 Di Geso, Alessandra, Kirkland, Quebec, Canada
 Dignet, Lydie, Les Pennes Mirabeau, France
 Doderer, Stephanie, Asnieres-sur-Seine, France
 Drouin, Claude, Loughborough, Leicestershire
 Dryland, Davina, Burton-upon-Trent, Staffordshire
 Duan, Qi, Harbin, P.R. China
 Eastmond, Fiona, Isleworth, Middlesex
 Elett, Birgit, Ebmatingen, Switzerland
 Ellis, Mairghread, Cousland, Midlothian
 Faure, Florian, Versailles, France
 Felanis, Kostas, Ioannina, Greece
 Feng Rufa, Xi'an City, Shanxi, P.R. China
 Feng Wei, Ghuangzhou City, P.R. China
 Ferré, Iohan, Vingrau, France
 Fitchko, Dorian Nicholas, Montreal, Quebec, Canada
 Fitzner, Manuela, Malmo, Sweden
 Forsner, Christina, Sodra Sandby, Sweden
 Franks, Elliot, Worthing, West Sussex
 Franses, Daniel, London
 Fremy, Pierre, Bois Colombes, France
 Fu Ziou, Haifu Garden, Kaiping City, P.R. China
 Gan Qian, Nanning City, Guangxi, P.R. China
 Gao Liyuan, Jingning County, Gansu, P.R. China
 Genet, Julie, Cagnes-sur-Mer, France
 Gericke, Chanel, Nottingham
 Gervais, Veronique, Brossard, Quebec, Canada
 Glover, Katie, London
 Goshanth, Namasivayam, Sabaragamuwa, Sri Lanka
 Goustiakov, Elodie, Boulogne Billancourt, France
 Gowry, Simon, Wolverhampton, Staffordshire
 Griffith, Julia, Southampton, Hampshire
 Gross, Robyn Elizabeth, Mont-Royal, Quebec, Canada
 Guilin Liu, Guangzhou City, P.R. China
 Hallsten, Caroline, Runhallen, Sweden
 Hameed, Aveen, Leicester
 Hammerstein, Quirine, Geneva, Switzerland
 Han Eun Sun, Guro-Gu, Seoul, South Korea
 Hasan, Aysha, London
 He Jie, Guangzhou City, P.R. China
 Heywood, Charlotte, Saxmundham, Suffolk
 Ho Hsuan Yi, Taipei, Taiwan, R.O. China
 Ho Wing Sze, London
 Hong Junbin, Shanghai, P.R. China
 Hou Jian, Shanghai, P.R. China
 Hsu Shu-Lin, Taipei, Taiwan, R.O. China
 Hsu Wei-Che, Taipei, Taiwan, R.O. China
 Htoi Kai, Yangon, Myanmar
 Hu Yuanfeng, Shanghai, P.R. China
 Hu Zhengying, Shanghai, P.R. China
 Huang Chiao-Ying, Richmond, Surrey
 Huang Chunzhong, Guangxi, P.R. China
 Huang Mulin, Changde, Hunan, P.R. China
 Huang Ting, Jingjiang, Jiangsu, P.R. China
 Huang Xi, Shanghai, P.R. China
 Huang Xiaowen, Nanning City, Guangxi, P.R. China
 Huang Yishun, Guilin City, Guangxi, P.R. China
 Huang Zhenghuan, Guangxi, P.R. China
 Hubbard, Amy, Aldershot, Hampshire
 Hughes, Beata, Sutton Coldfield, West Midlands
 Hui Ka Yeung, Kenny, Kowloon, Hong Kong

Proceedings of the Gemmological Association of Great Britain and Notices

- Hunter, Sam, London
 Imre, Alexandra, London
 Jackson, Christopher, Bradford, West Yorkshire
 Jacques, Cecile, Toulon, France
 Jang Jung Hye, Gyeonggi-Do, South Korea
 Jangsawang, Nongnuch, Bangkok, Thailand
 Janse, Leonardus, Zutphen, The Netherlands
 Jardel, Alice, Beausoleil, France
 Jeandidier, Nathalie, Asnieres-sur-Seine, France
 Jeffrey, Kip, Atterton, Nuneaton, Warwickshire
 Jeffries, Scott, Newport, Gwent
 Jen Chih-Yuan, Taipei, Taiwan, R.O. China
 Jiang Xue, Urumqi, Xinjiang, P.R. China
 Jiang Yi'An, Hechi City, Guangxi, P.R. China
 Jin Hua Jie, Hangzhou City, P.R. China
 Jo Ji Hee, Seoul, South Korea
 Johann, Deru, Villejuif, France
 Johansson, Sandra, Kungsbacke, Sweden
 Jonsall, Lisa, Edsbyn, Sweden
 Jonsson, Elin, Limhamn, Sweden
 Joo, Soo Kyung, Naju-Si, Jeollanam-Do, South Korea
 Kalenda, Mujinga, Ladywood, Birmingham, West Midlands
 Kanda, Sonia, Farnham Royal, Buckinghamshire
 Kang Chung-Jui, Tainan, Taiwan, R.O. China
 Keatwitoo, Weerachat, Bangkok, Thailand
 Ki Hyo Gab, Songpa-Gu, Seoul, South Korea
 Kim Sol Hee, Buk-Gu, Ulsan, South Korea
 Klints, Robins, Hounslow, Middlesex
 Knifeld, Stephanie Ann, Bournemouth, Dorset
 Knochenhauer, Cecilia, Vastra Gotalands Lan, Sweden
 Knudsen, Christine, Oslo, Norway
 Kong, Helen, Toronto, Ontario, Canada
 Konishi, Mika, Kanagawa Pref., Kawasaki City, Japan
 Kourbouzou, Maria, Athens, Greece
 Kozhisseril Abdul Haque, Edgbaston, Birmingham, West Midlands
 Lacosta, Patricia, London
 Lai May Wah, Kennedy Town, Hong Kong
 Lally, Joanne Claire, Southampton, Hampshire
 Lam Man Ngor, Cherrie, Hong Kong
 Lam Pui Kwan, Kowloon, Hong Kong
 Lam Pui Pik, Kowloon, Hong Kong
 Lambert, Amelie, London
 Laszlo, Linda, Budapest, Hungary
 Lau, Ingrid, Hong Kong
 Lau Yin Ling Lecky, New Territories, Hong Kong
 Laureau, Corinne, La Madeleine-de-Nonancourt, France
 Lavoie, Martine, Montreal, Quebec, Canada
 Law, Yuk Fung, New Territories, Hong Kong
 Lee Chang-Hsin, Taipei, Taiwan, R.O. China
 Lee Hae Ji, Seo-Gu, Dajeon, South Korea
 Lee Hye Ran, Gwangjin-Gu, Seoul, South Korea
 Lee Jae Hyun, Chungcheongbuk-do, South Korea
 Lei Ying, Beijing, P.R. China
 Leong Chio Meng, Wai Un Fa Un, Macau, P.R. China
 Lesouef, Julie, London
 Leung, Elsa, Mid Levels, Hong Kong
 Li, Lida, Birmingham, West Midlands
 Li Chenxi, Tan'an City, Shandong, P.R. China
 Li Hui, Chi Fen City, Inner Mongolia, P.R. China
 Li Liuyi, Baise City, Guangxi, P.R. China
 Li Li, Guigang City, Guangxi, P.R. China
 Li Qi, Qionghai City, Hainan, P.R. China
 Li Yuan, Beijing, P.R. China
 Liang, Wenhua, Nanning City, Guangxi, P.R. China
 Lin Guangkai, Beihai City, Guangxi, P.R. China
 Lindelow, Susanna, Malmö, Sweden
 Lindvall, Lisa, Nacka, Sweden
 Liu Feng, Guangzhou City, P.R. China
 Liu Lu, Shenzhen City, P.R. China
 Liu Si Tong, Beijing City, P.R. China
 Liu Ye, Shanghai, P.R. China
 Liu Yunting, Deyang City, Sichuan, P.R. China
 Liu Yunzhong, Beijing, P.R. China
 Lo Che Hong Chris, Kowloon, Hong Kong
 Lopez, Gisele, Pomérols, France
 Loumagne, Antoine, Fragnes, France
 Love, Mary, Alabama, U.S.A.
 Lubunga, Justin, Clamart, France
 Lv Yandi, Wu Xi Shi, Jiangsu Sheng, P.R. China
 Ma Sui Hung, Kowloon, Hong Kong
 Ma Ruiwei, Quzhou City, Zhejiang, P.R. China
 Ma Shui Chu, Kowloon, Hong Kong
 Ma Tingting, Shanghai, P.R. China
 Ma Yutong, Beijing, P.R. China
 McCallum, Neil Keith, Martinborough, New Zealand
 Mack, Darling, Dollard-des-Ormeaux, Quebec, Canada
 MacMillan, Margaret-Anne, Grangemouth, Stirlingshire
 Mak Kwan Ting, Kowloon Tong, Hong Kong
 Mak Yee Ki, Tuen Mun, Hong Kong
 Mak Yee Man, New Territories, Hong Kong
 Mallett, Alex, Cubert, Cornwall
 Man Lai Wa, New Territories, Hong Kong
 Maneekrajangsaeng, Marisa, Bangkok, Thailand
 Marier, Valerie, Acton Vale, Quebec, Canada
 Martin-Gutierrez, Francesca, London
 Mas, Anais, Vitrolles, France
 Matsumoto, Mami, Nara-City, Nara Pref., Japan
 Meissirel, Mathilde, Canterbury, Kent
 Miranda, Tânia, Geneva, Switzerland
 Mitchell, Anne Susan, Harpenden, Hertfordshire

Proceedings of the Gemmological Association of Great Britain and Notices

- Mitchell, Shirley D., Windsor, Berkshire
 Mo Lulu, Guangxi, P.R. China
 Mo Xiangzhi, Hepu County, Guangxi, P.R. China
 Mok Khomkrit, Kowloon, Hong Kong
 Mok Yan Yan, Kowloon, Hong Kong
 Molina, Jose, Malaga, Spain
 Mui Mei Kuen, New Territories, Hong Kong
 Nadeeva, Katerina, London
 Napawongsuwan, Nilwan, Lopburi, Thailand
 Negus, Patricia, Moor, County Durham
 Ng So Ching, New Territories, Hong Kong
 Ngan Ian Nei, Jenny, Pak Lei San Chun, Macau, P.R. China
 Nguyen, Michel, Saintry-sur-Seine, France
 Niala, Josephine, Nairobi, Kenya
 Nie Ting, Zhong Xue, P.R. China
 Nilsson, Paul Graham, Triton, Auckland, New Zealand
 Odén, Naime Marielle Angelica, Brunflo, Sweden
 Okayasu, Rie, Antananarivo, Madagascar
 Olausson, Hasse, Hunnebostrand, Sweden
 Oqvist, Elin, Örebro, Sweden
 O'Sullivan, Lauren, Glenside, Pennsylvania, U.S.A.
 Pallot, Emily Elise, St Johns, Jersey, Channel Islands
 Palmieri, Angelo, New York, U.S.A.
 Palmieri, Donald A., New York, U.S.A.
 Pan Shenchao, Shanghai, P.R. China
 Papaux, David, Geneva, Switzerland
 Park Jong Min, Dalseo-Gu, Daegu, South Korea
 Park Sang Hyun, Seo-Gu, Daejeon, South Korea
 Park Seo Kyeong, Cheonan-Si, Chungcheongnam-do, South Korea
 Patel, Hiren, London
 Payne, Alison, London
 Pentelow, Irene, Shrewsbury, Shropshire
 Permingeat, Fabrice, Arzon, France
 Phillips, Jane, Hendra, Queensland, Australia
 Pino, Loredana, Chiavari, Italy
 Poisson, Francis, Montreal, Quebec, Canada
 Porter, Rex, Hartley Whitney, Hook, Hampshire
 Qin Yu Song, Jilin, P.R. China
 Raj, Amrit, Jaipur, India
 Rao Jinghui, Xiamen City, Fujian, P.R. China
 Rapti, Spyridoula, Glyfada, Greece
 Raybaut, Eric, Montreal, Quebec, Canada
 Reynolds, Eva, Cleve Hill, Cheltenham, Gloucestershire
 Roberts, Barry, Beckenham, Kent
 Roberts, Deborah, Holloway, London
 Roden, Rhiannon, Derby
 Rothstein, Michaela, Lindingö, Sweden
 Russell, Lucy, Kidderminster, Worcestershire
 Rutherford, Rhys, Gloucester, Gloucestershire
 Sandin, Emilia, Lannavaara, Sweden
 Santarsiere, Miguel Angel, Folkestone, Kent
 Scott, Vicki, Hollywell, Queensland, Australia
 Sena, Aree, London
 Sepper, Mariliis, London
 Shen Lingyun, Shanghai, P.R. China
 Shen Yan, Shanghai, P.R. China
 Shepherd, Steve, Greenbank, Queensland, Australia
 Shi Miao, Beijing, P.R. China
 Simpson, Christopher, Weybridge, Surrey
 Smith, Billy, Colchester, Essex
 Sombatworapat, Supatra, Bangkok, Thailand
 Song Chuxin, Luoyang City, Henan, P.R. China
 Song Wen, Tianjin City, P.R. China
 Sorensen, René, Viborg, Denmark
 Springe, Karl, Lannavaara, Sweden
 Stevens, Sophie, Kingston-upon-Thames, Surrey,
 Su Shi, Xuan Wu, Beijing, P.R. China
 Sun Hsiang-Han, Taichung, Taiwan, R.O. China
 Sundqvist, Sonja, Hägersten, Sweden
 Surensoy, Zubeyde, London
 Suzuki, Yuri, Fulham, Fulham, London
 Swe, Thet Htar, Yangon, Myanmar
 Tan Xiaoyan, Shanghai, P.R. China
 Tan Zhuting, Birmingham, West Midlands
 Tanaka, Atsuko, Tokyo, Japan
 Tang Wenguan, Nanning City, Guangxi, P.R. China
 Tao Jiangli, Wuhu, Anhui, P.R. China
 Thongthai, Natheethong, Bangplee, Samutprakarn, Thailand
 Tin Yin, Vicki, Kowloon, Hong Kong
 Torretta, Janice, Glen Spey, New York, U.S.A.
 Triantafillidis, Antonia, Montreal, Quebec, Canada
 Tsai Ta-Wei, Taiwan, R.O. China
 Tsang Yuk Lung, Billie, New Territories, Hong Kong
 Tse Man Fung, New Territories, Hong Kong
 Tse Ping, New Territories, Hong Kong
 Tseng De-Luen, Taipei, Taiwan, R.O. China
 Tun, Danny, Yangon, Myanmar
 Tyler, Linda, Wokingham, Berkshire
 Ullmer-Schindler, Jacquelyn, Englewood, Ohio, U.S.A.
 Vahman, Sarira, Westmount, Quebec, Canada
 Van Der Wolf, Nicole, Dublin, Republic of Ireland
 Van Lenten, Andrea, Red Bank, New Jersey, U.S.A.
 Verwijk, Moira, Toronto, Ontario, Canada
 Visvanathan, Sokkalingam, Singapore
 Wang Jia, Jinzhou, P.R. China
 Wang Qingbo, Shanghai, P.R. China
 Wang Weiwei, Shanghai, P.R. China
 Wang Xiaojuan, Beijing, P.R. China
 Wang Yan, Beijing, P.R. China

Proceedings of the Gemmological Association of Great Britain and Notices

Wang Yue, Guangzhou City, P.R. China
 Wang Zhexin, Zhoushan City, Zhejiang, P.R. China
 Warner, Simon, Amersham, Buckinghamshire
 Warren, Rebecca, Kenilworth, Warwickshire
 Weber, Thorsten, Steinmaur, Switzerland
 Wengrowe, Lauren, London
 Westwood, Timothy, Putney Heath, London
 Will, Diana, Howth, County Dublin, Republic of Ireland
 Wong, Jackson, Kowloon, Hong Kong
 Wong, Sabina, Richmond, British Columbia, Canada
 Wong Gwin Hang, New Territories, Hong Kong
 Wong Man Ho, Hunghom, Hong Kong
 Wong Ting, Kowloon, Hong Kong
 Wong Yi Sai, Kowloon, Hong Kong
 Wong Yuk Man, Janice, Kowloon, Hong Kong
 Woodrow, Gillian, Wokingham, Berkshire
 Woods, Georgina, London
 Wu Fei, Takapuna, Auckland, New Zealand
 Wu Huijuan, Anlu City, Hubei, P.R. China
 Wu Shih-Ying, Taipei, Taiwan, R.O. China
 Wu Tianyi, Beijing, P.R. China
 Wu Xiaoting, Shandong, P.R. China
 Wyndham, Jessica, Stanmore, Middlesex
 Xu Chun, Zhejiang, P.R. China
 Xu Jingzhe, Colombo, Sri Lanka
 Xu Lixin, Beijing, P.R. China
 Xu Yang, Tianjin City, P.R. China
 Xu Yanyan, Shanghai, P.R. China

Yang Yufei, Pan Yu, Guangzhou City, P.R. China
 Yeh Wen-Ting, Taipei, Taiwan, R.O. China
 Yeung Sin Yee, New Territories, Hong Kong
 Yevno, Nahir, Västra Frölunda, Sweden
 Yin Yue, Xinyang City, Henan, P.R. China
 Young, Olivia, London
 Yu Ho Fai, New Territories, Hong Kong
 Yu Qingyuan, Guangzhou, P.R. China
 Yuan Miao, Hangzhou, P.R. China
 Yuen Lung Hon, New Territories, Hong Kong
 Yuen Shui Ping, Central, Hong Kong
 Yukiko, Horie, Tokyo, Japan
 Zavala, Diana, Round Rock, Texas, U.S.A.
 Zhang Congcong, Shandong, P.R. China
 Zhang Jian, Beijing, P.R. China
 Zhang Rui Jia, Kunming, P.R. China
 Zhang Yiqun, Beijing, P.R. China
 Zhang Yunting, Qingdao, Shandong, P.R. China
 Zhao Lu, Shanghai, P.R. China
 Zheng Kexiu, Zhejiang, P.R. China
 Zheng Xin, Shan Tou, Jin Xin Hua Yuan, P.R. China
 Zheng Yifei, Shanghai, P.R. China
 Zhou Haohao, Beijing, P.R. China
 Zhou Mei, Guangxi, P.R. China
 Zhou Yuping, Shanwei City, P.R. China
 Zhu Lin, Wanzhuang, Langfang, Hebei, P.R. China
 Zuo Youjing, Nanjing City, Guangxi, P.R. China

Gem Diamond Diploma examination

Qualified with Distinction

Dennis, Louise, Halesowen, West Midlands
 Gowans-Poli, Julie, London
 Griffith, Julia Anna, Southampton, Hampshire
 Lacosta, Patricia, London
 Liao Caihuan, Nanning City, Guanxi, P.R. China
 Logan, Peter M., Coventry, Warwickshire
 Ludlam, Louise Helen, Birmingham, West Midlands
 Ning Liu, Beijing, P.R. China
 Tao Jiangli, Anhui, P.R. China
 Westley, Penny, Hagley, Worcestershire
 Wong Shing Shun, Philip, Guangzhou City, Guangdong, P.R. China

Qualified with Merit

Han Xi, Beijing, P.R. China
 McKeown, Julia, Oldbury, West Midlands
 Man Yee Kong, Tuen Mun, Hong Kong
 Petropoulou, Eleni, Athens, Greece

Roberts, Barry, Beckenham, Kent
 Samartseva, Julia, Bracknell, Berkshire
 Sandoval-Williams, Cuauhtemoc, Fribourg, Switzerland

Qualified

Beale, Sioned Ann, Lapworth, Warwickshire
 Byrne, David Mark, Cradley Heath, West Midlands
 Chen Weiguang, Zhujiang Newtown, Guangzhou, P.R. China
 Chen Jun, Yujiashan, Hubei, P.R. China
 Chetwin, Sheridan Lesley, Morecambe, Lancashire
 Cheung Ching Chi, Hong Kong
 Choi Tsz Ling, Kowloon, Hong Kong
 Chow Chiu Hung, Chris, Kowloon, Hong Kong
 Choy Ka Mei, Quarry Bay, Hong Kong
 Criaco, Leo, London
 Di Sera, Susanna, Rome, Italy
 Dulay, Sundeep, Leamington Spa, Warwickshire
 Feng Leyuan, Guangzhou, P.R. China

Proceedings of the Gemmological Association of Great Britain and Notices

Goshanth, Namasivayam Pillai, Kandy, Sri Lanka
Hui Ka Ching, New Territories, Hong Kong
Junjie Lu, Beijing, P.R. China
Knudsen, Christine, Oslo, Norway
Ko Yuen Yuk, Hong Kong
Kum-Yun Tai, Fiona, London
Lau Pui Ting, Yau Tong, Hong Kong
Lee Chak Man, Kowloon, Hong Kong
Lemeshko, Nathalie, London
Leung Ching Yee, Kowloon, Hong Kong
Leung Sin Ming, New Territories, Hong Kong
Li Huanhuan, Yujiashan, Hubei, P.R. China
Li Jin, Yujiashan, Hubei, P.R. China
Liang Yuanyuan, Hong Kong
Liu Haodan, Beijing, P.R. China
Lok Chi Keung, Chai Wan, Hong Kong
Manasse, Daniele, Rome, Italy
Mkogian, Elen, Thessaloniki, Greece
Ng Siu Kwai, New Territories, Hong Kong
O'Cock, Sabrina Alice Palmer, London
Petropoulou, Alexia, Nea Symni, Athens, Greece
Pui Fan Yu, Kowloon, Hong Kong
Rimmer, Heather Elizabeth, Lichfield, Staffordshire
Roditi, David Hubert, London
Rufeng Liu, Beijing, P.R. China
Sallie, James Norman, Boughton, Northamptonshire
Shao Xinyuan, Yujiashan, Hubei, P.R. China
Shi Su, Beijing, P.R. China
Sze Pui Gee, Peggy, Kowloon, Hong Kong
Tan Zhuting, Birmingham, West Midlands
Tao Cheung Sin, New Territories, Hong Kong
Tong Wai Yin, Aberdeen, Hong Kong
Tsui Ka Kin, Kenneth, New Territories, Hong Kong
Visvanathan, Sokkalingam, Singapore
Vodyanova-Hitzi, Elena, Athens, Greece
Wang Wenjun, Zhujiang Newtown, Guangzhou, P.R. China
Weiyang Feng, Beijing, P.R. China
Wen Wen, Beijing, P.R. China
Wetherall, Alan, Hitchin, Hertfordshire
Wong Hoi Lam, Colleen, New Territories, Hong Kong
Xiaojun Zhou, Beijing, P.R. China
Xue Yanan, Yujiashan, Hubei, P.R. China
Xueying Wu, Beijing, P.R. China
Yau Chun Fai, Chai Wan, Hong Kong
Ying Wai Kwong, Richard Alexander, Ap Lei Chau, Hong Kong
Yu Ho Fai, New Territories, Hong Kong
Zhao Huiyun, Beijing, P.R. China
Zhao Yangyang, Beijing, P.R. China
Zheng Xin, Beijing, P.R. China
Zhu Lin, Beijing, P.R. China

Membership

During 2011, the Council approved the election to Membership of the following:

Fellowship and Diamond Membership (FGA DGA)

Chai Yuet, New Territories, Hong Kong
Chan Lim Chi, Ap Lei Chau, Hong Kong
Cheung Yuk King, New Territories, Hong Kong
Choi Wing Cheong, Chai Wan, Hong Kong
Fong Tik Kwan, Tseung Kwan O, Hong Kong
Harris, Jennifer, Auckland, New Zealand
Lee Wai Kwok, Simon, New Territories, Hong Kong
Mai Zhi Qiang, Guangzhou, P.R. China
Owen, Cheryl, Birmingham, West Midlands
Reynolds, Eva, Cheltenham, Gloucestershire
Wong Wing Suet, Kowloon, Hong Kong
Yin Ying Ngan, Betty, Kowloon, Hong Kong

Fellowship (FGA)

Allen, Amanda, Northampton
Andren Georgsen, Cecilia, Lund, Sweden
Bane, Jonathan, Sheffield, South Yorkshire

Butini, Enrico, Rome, Italy
Butini, Flavio, Rome, Italy
Chayathorn, Chanruangvanich, Bangkok, Thailand
Chen Binhui, Guangzhou, P.R. China
Chui Wing Chung, Kowloon, Hong Kong
Cooper, Amy, Las Vegas, Nevada, U.S.A.
Costanzo, Alessandra, Ragoon, Galway, Ireland
Cox, Rebecca Jane, York
Crockett, Sheri, Santa Cruz, California, U.S.A.
Dartois, Quentin, Vence, France
De Gaspé Beaubien, Isabelle, Montreal, Quebec, Canada
Dennis, Louise, Halesowen, West Midlands
Deutschl, Norbert, Montreal, Quebec, Canada
Fitchko, Dorian Nicholas, Montreal, Quebec, Canada
Franks, Elliot, Worthing, West Sussex
Gauci, Karen Elizabeth, Burnaby, British Columbia, Canada
Gross, Robyn, Mont Royal, Quebec, Canada
Gu Jialu, Shanghai, P.R. China
Hansen, Robin, Warminster, Wiltshire

Proceedings of the Gemmological Association of Great Britain and Notices

Herzog, Franz Adrian, Oltingen, Switzerland
Ivancic, Ivan, Colombo, Sri Lanka
Jacquier, Nathalie, Genthod, Switzerland
Jain, Sanjay, Karnataka, India
Johnston, Meredith, Marcoola, Queensland, Australia
Jokinen, Tiina, Tampere, Finland
Jones, L. Bruce, Rathdrum, Idaho, U.S.A.
Karimzadeh, Leyla, London
Kim Sang Ki, Seoul, Korea
Kirkham, Sally, Birmingham, West Midlands
Klinski, Frank, Niebüll, Germany
Lahtinen, Tiina, Oitti, Finland
Lai Nga Ting, London,
Lawson, Charles, Brisbane, Queensland, Australia
Lee, Alix, Rognes, France
Lee, Sealim, London
Lemaire, Alisson, Drummondville, Quebec, Canada
Li Liufen, Guangzhou, P.R. China
Maclean, Victoria, London
Maneekrajangsaeng, Marisa, Bangkok, Thailand
Mayer, Melanie, St Lawrence, Jersey, Channel Islands
Mayer, Helen, London
Menard, Georges-Etienne, Saint Hyacinthe, Quebec,
Canada
Minassian Bardehshahi, Odett, Mykonos, Greece
Mitchell, Anne Susan, Harpenden, Hertfordshire
Mogridge, Emma Denise, Birmingham, West Midlands
Neurauter, Amy, New York, U.S.A.
Nguyen, Michel, Saintry-sur-Seine, France
Palliyaguruge, Lalaka, Battaramulla, Sri Lanka
Parkes, Matthew, Dublin, Ireland
Patenaude, Lizanne, Westmount, Quebec, Canada
Perosino, Lorenzo, Novi Ligure, Italy
Regala, Benjamin, Aiea, Hawaii, U.S.A.
Reynaud, Lucy, Singapore
Richbourg, Carole, Los Altos, California, U.S.A.
Rocchiero, Loredana, Genova, Italy
Sawas, Jeremy, Montreal, Quebec, Canada
Shenoi, Anita, Longhope, Gloucestershire
Sheridan, Meghan, Upper Montclair, New Jersey, U.S.A.
Shevchenko, Olga, Montreal, Quebec, Canada
Sibley, Christopher, St. Albans, Hertfordshire
Tai Ai-Hwa, London
Tong Siu-Kuen, Ma On Shan, Hong Kong
Valentini, Francesca, London
Verma, Dheeraj, Palwal, India
Voulgaridis, Konstantinos, London
Ward, Sarah, Leeds, West Yorkshire
Weyers, Stefanus Salomon, Bloemfontein, South Africa
Wilson, Maria Dorothea, Warwickshire
Windeyer, Patricia Annette, Brisbane, Queensland,
Australia

Woodcock, Olga Faye, Basingstoke, Hampshire
Wu Chung-Kang, Taipei, Taiwan, R.O. China
Yat, Richard, New Territories, Hong Kong
Yueping Luo, Beijing, P.R. China
Zdeb, Robert, Epping, Essex

Diamond Membership (DGA)

Chetwin, Sheridan, Morecambe, Lancashire
Dulay, Sundeep, Leamington Spa, Warwickshire
Gong, Sheng Wei, Guangzhou, Guangdong, P.R. China
Griffith, Julia, Southampton, Hampshire
Namasivayam, Goshanth, Kegalle, Sri Lanka
Roberts, Barry, Beckenham, Kent
Roche, Patrick, Ballydehob, West Cork, Ireland
Sallie, James, Boughton, Northamptonshire
Samartseva, Julia, Bracknell, Berkshire
Spenser, Sarah, London
Starkey, Imogen M.S., Shanklin, Isle of Wight
Stephenson, Elizabeth, Poole, Dorset
Tai Kum-Yun, Fiona, London
Tan Zhuting,, Birmingham, West Midlands
Ying Wai Kwong, Richard Alexander, Ap Lei Chau, Hong
Kong

Associate Members

Adrem, Hanna, Saltsjobaden, Sweden
Afemikhe, Eunice, Morden, Surrey
Al-Yawer, Najwa, London
Bealey, Philip, Ilfracombe, Devon
Bhargav, Deepak Prakash, Birmingham, West Midlands
Bishop, Carole, Marlborough, Wiltshire
Braun-Goldinger, Bettina, Küsnacht, Switzerland
Burman, Marc, London
Daya Zakir, Djunivia Hamdini, Bogor, Indonesia
De Basilio, Adolfo, Madrid, Spain
Dixon, Katie-Jean, Auckland, New Zealand
Emmerton, Peter Gordon, Lindfield, West Sussex
Fazlali-Zadeh, Sonia, London
Federico Becker, Giovanna, New York, U.S.A.
Fleming, Ellen, London
Hartogsohn, Ira, Copenhagen, Denmark
Helps, Mark, Chislehurst, Kent
Hillcoat, Cathryn, Wheathampstead, Hertfordshire
Hodges, Jayne, Canvey Island, Essex
Hyder, Saarah, Dewsbury, West Yorkshire
Isherwood, Nicholas John, Burgess Hill, West Sussex
Kaplan Gross, Frieda, London
Kim, Jinchang, Seoul, R.O. Korea
Lobenstein, Meir, London
Ma Tingting, Shanghai, P.R. China
Manley, Deborah Jane, Bridgwater, Somerset
Mastrolorenzo, Maurizio, Paris, France
Matthews, Kate Louise, Auchenblae, Aberdeenshire

Gifts and Donations to the Association

The Association is most grateful to the following for their gifts and donations for research and teaching purposes:

Bear Essentials, Missouri, U.S.A., for diffused andesine teaching samples.

Brian D. Cooksey FGA DGA, Elizabeth Cannon Antiques, Colchester, Essex, for two faceted tourmalines.

Deryck Fitzsimmons, Borehamwood, Hertfordshire, for a selection of jeremejevite crystals.

Adrienne H. Grahame-Ballin FGA, Drummore, Scotland, for three agate and tourmaline pendants.

Dr Roger Harding FGA, Devizes, Wiltshire, for a selection of gemmological books and mineral samples.

Dr Donald Hoover FGA, Springfield, Missouri, U.S.A., for topaz crystals and selenite crystals from Lake Milton, Ohio

Jochen Knigge, Brasil Opal, Lampertheim, Germany, for a Brazilian opal and a DVD entitled *The Precious Opals of Pedro Segundo*.

Marcia Lanyon FGA, London, for a selection of gemstones.

Susanne Lesley FGA RJ Dip, Maidenhead, Berkshire, for a selection of gemmological testing equipment.

Cora Patel, Bolton, Lancashire, for a large faceted amethyst displaying textbook 'tiger stripe' inclusions

Martin P Steinbach, Idar-Oberstein, Germany, for two pieces of trapiche 'Cerasite' (a trapiche variety of altered cordierite) from Japan, a trapiche sapphire, a piece of sapphire in matrix from the Urals, Russia, a star sapphire from Thailand displaying a 12-rayed star, a foil backed paste star stone and a piece of haüynite in matrix.

Henry Gerald Stonley FGA, Aylesbury, Buckinghamshire, for a large selection of cut gemstones.

David Weinberg, Bangkok, Thailand, for a selection of zircon sample stones, plus stones of similar appearance.

Diana Lesley Wenham FGA DGA, Harrow, Middlesex, for a selection of back issues of *The Journal of Gemmology*.

Jason Williams FGA DGA, G.F. Williams, London, for a selection of gemstones including amethyst, cameo, CZ, emerald, ruby, sapphire, smoky quartz and blue topaz.

Gladys Yao for a selection of cut gemstones.

Monetary donations were gratefully received from:

Petra Bardehle FGA, Holzhausen, Germany

Philip Bealey, Ilfracombe, Devon

Anthony James Boyce FGA, Doncaster, South Yorkshire

Vincenzo De Michele, Milan, Italy

James C. Finlayson FGA, Stoke on Trent, Staffordshire

Meryan Holman FGA, London

Kiyokatsu Koike FGA, Toride, Japan

Torbjorn Lindwall FGA DGA, Lannavaara, Sweden

John Mason FGA, Harrogate, North Yorkshire

Veronica Wetten FGA, Hounslow, Middlesex

Christine Woodward FGA DGA, Chiswick, London

Maury, Christophe, New Malden, Surrey

Mazza-Newmann, Deborah, Rochester, Kent

Mok, Barend, Halifax, West Yorkshire

Molina, Jose, Malaga, Spain

Morgan, Lorisa, Holywell, Flintshire

Moses, June, London

Mumford, Nicola, London

Murphy, Heather, Bolton, Lancashire

Nielsen, David, London

O'Faolain, Stephen, Sandymount, Co. Dublin, Ireland

Pattani, Arun, Harrow, Middlesex

Philp, Alexander W.L., Banchory, Aberdeenshire

Portch, Amanda, Wolli Creek, New South Wales, Australia

Regala, Benjamin, Aiea, Hawaii, U.S.A.

Sandecki, Anne Marie, Parsippany, New Jersey, U.S.A.

Shah, Arvind, London

Shaikh, Hanif, London

Shen, Mei, Taipei, Taiwan, R.O. China

Sliti, Sondos, Dubai, U.A.E.

Steinbach, Martin, Idar-Oberstein, Germany

Street, Neil, Wilton, Connecticut, U.S.A.

Tatlow, Emily Louise, Guildford, Surrey

Thilakarathne, Kanishka Lalith, Kandy, Sri Lanka

Toufexis, Mario, London

Valasmo, Hannu, Vantaa, Finland

Van Der Westhuizen, Victor, Kingston upon Thames, Surrey

Way Hnin, Newcastle upon Tyne, Tyne and Wear

Windeyer, Patricia Annette, Brisbane, Queensland, Australia

Winterflood, Letitia, London

Wong, Flora, Hong Kong

Proceedings of the Gemmological Association of Great Britain and Notices

Wood, Nina, London
Youenes, Gina, Cambridge

Gold Corporate Membership

Alisha Gems, Rochdale, Lancashire
Chevenix Jewellery, Woodbridge, Suffolk
Just Gems, Aberdeen
Nexus Agencies Ltd, Birmingham, West Midlands
Percy Davies & Son Ltd, Gerrards Cross, Buckinghamshire
Rudell & Co. Ltd, Wolverhampton, Staffordshire
Shri Nadika Jewellery, Ilford, Essex

Corporate Membership

Bassange, London
Bonhams, London
IP Diamonds Ltd, London
IMK Ltd, London
Kuropatna Brothers, London
Ramesh Jewellers, London
Simvinell Ltd, London

Transfers

Fellowship to Fellowship and Diamond Membership (FGA DGA)

Byrne, David, Cradley Heath, West Midlands
Dennis, Louise, Halesowen, West Midlands
Gowans-Poli, Julie, London
McKeown, Julia, Oldbury, West Midlands
O'Cock, Sabrina, London
Visvanathan, Sokkalingam, Singapore
Westley, Penny, Worcestershire
Wetherall, Alan, Hitchin, Hertfordshire

Diamond Membership to Fellowship and Diamond Membership (FGA DGA)

Diamond, Marcia, London
LaCosta, Patricia, London
Poon Pak Kei, New Territories, Hong Kong

Associate Membership to Fellowship (FGA)

Antonucci, Andrea, Stockholm, Sweden
Elliott, Paul, Woodville, South Australia, Australia
Hardy, Sarah, Stockton-on-Tees, County Durham
Hunt, Glynis, Andover, Hampshire
Hutchinson, Fiona, Albourne, West Sussex
Ikeuchi, Mototeru, Tokyo, Japan
Jamieson, Pauline, Edinburgh, Midlothian
Johnson, Helen, Edinburgh, Midlothian
Kaye, Charlotte, Hungerford, Berkshire
Knutsen, Annmari, Oslo, Norway
Loosvelt, Bart, Kortrijk, Belgium
Ma Tingting, Shanghai, P.R. China
Matsura, Miho, Yokohama, Japan

Ratnayake, Dayanthi, Colombo, Sri Lanka
Sakakibara, Kenichi, Oita, Japan
Tew, Timothy David, Atlanta, Georgia, U.S.A.
Verwijk, Moira, Toronto, Ontario, Canada
Yamaguchi, Nao, Osaka, Japan

Associate Membership to Diamond Membership (DGA)

Lemeshko, Nathalie, London
Manasse, Daniel, Rome, Italy
Roditi, David, London

Annual General Meeting

The Annual General Meeting was held on Thursday 7 July 2011 at the Imperial Hotel, London WC1. The meeting was chaired by James Riley the Chairman of the Council. The Annual Report and Accounts were approved. Brian Jackson, Cally Oldershaw and Steve Jordan (who had been appointed by the Council since the 2010 Annual General Meeting) were re-elected to serve on the Council. Alan Collins retired from the Council in rotation and did not seek re-election. Gwyn Green was re-elected and Kerry Gregory and Elizabeth Gleave elected to serve on the Membership Liaison Committee. Hazlems Fenton were re-appointed as auditors for the year.

Subscriptions 2012

The membership subscriptions for 2012 remain at £90 for UK members and £95 for those in Europe and overseas.

Obituary

Brian R. Dunn FGA (D.1978), Staplehurst, Kent, died suddenly in December 2011. Brian, a former chairman of the NAG Valuations Committee, ran a number of seminars for Gem-A members on the valuation of antique and modern jewellery.

James (Jim) Gemmell FGA (D.1992), Kelloe, Co. Durham, died on 10 April 2011 aged 86. A skilled faceter, Jim was instrumental in setting up the UK Facet Cutters Guild (UKFCG) in 1994 and served as chairman of the Guild for nine years.

Helen Muller FGA (Tully Medal 1974) died on 4 January 2012. Helen was an expert on jet and published three books on the subject.

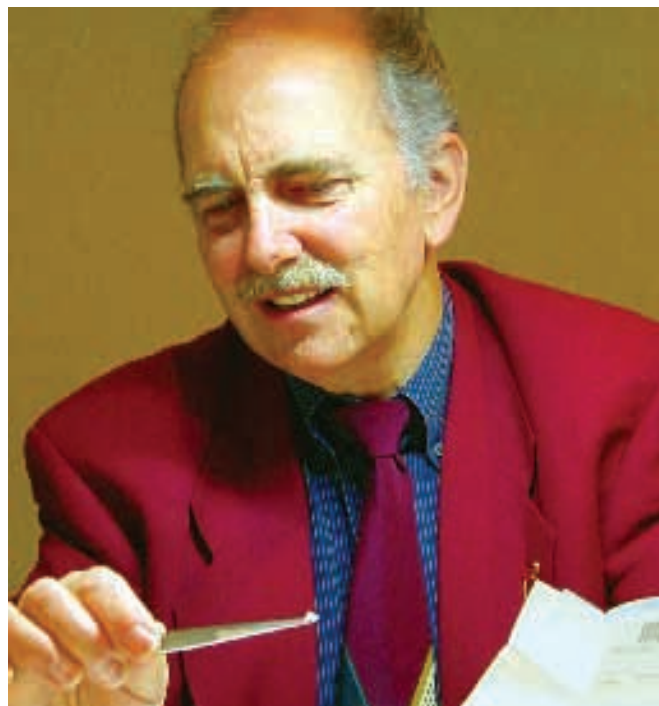
Edward H. Wain FGA (D.1964), Kings Lynn, Norfolk, died in 2011.

George Bosshart, MSc, SFIT, GG, CSEJ
1943–2012

George Bosshart, who died on 14 January aged 68, was one of the most stimulating and internationally respected gemmologists of the last thirty years. His main interest was diamonds, especially green diamonds, but his talent for incisive and well-researched investigation was applied also to emeralds, rubies, sapphires and a range of other coloured gem species.

George was born on 8 May 1943 in Rüti, canton of Zürich, Switzerland, the son of Georg Albert and Martha Magdalena Bosshart; his younger brother Robert was born the following year. His early education was in Rüti and with Robert he had a very active and 'sporty' childhood. He graduated from the cantonal college in Wetzikon in 1963 with languages and natural sciences as main subjects and then attended an air defence training school, qualifying as a radar operator. This phase of his life may well have sown the seed of his ambition to become a Swissair pilot but such a career was not to be — ruled out by injuries sustained in a near-fatal automobile accident.

He recovered, and instead directed his energy into earth science studies at the Swiss Federal Institute of Technology (Eidgenössische-Technische Hochschule (ETH)) in Zürich with the aim, as he put it, of an "uncommon future occupation involving language skills and travelling". He graduated in 1969 with a Master's degree in earth sciences and was employed first in ore prospecting using geophysics in Canada. However, a position in mineralogical analysis at the aluminium producer ALCAN in Quebec soon proved more attractive and he spent three years in their R and D division. It was during this time that his interest in gems started to grow and he studied in Los Angeles at the GIA, qualifying as a GG. By 1974 he was looking at ways of furthering his career and a project of the Swiss Watch and Jewellery Associations tempted him most. This was to set up a gem testing laboratory for the Swiss Foundation for Research of Gemstones (SSEF) in Zürich. This he established with the motto 'Reliability, rigour, integrity', and during his sixteen years there, he pioneered analytical techniques for



advanced gemstone testing, authored articles on gem identification in several languages, and, with his new colleague Dr Henry Hänni, introduced a service which offered opinions on the geographical origins of rubies, sapphires and emeralds on the basis of analyses of stones that they themselves had collected or sourced. After he left in 1990, it gave George much satisfaction to see the SSEF lab under its subsequent directors Drs Hänni and Krzemnicki grow and prosper. During his time at SSEF, he proposed and in 1988 was granted permission to record infrared and cryogenic, high-resolution ultraviolet to visible absorption spectra of the historic 'Dresden Green' diamond to establish its fundamental properties and also to improve the criteria for distinguishing natural green from artificially-induced green diamonds (i.e. artificially irradiated stones). The innocuous-looking words "... proposed ... granted ..." used above, gloss over a saga about which George could speak for a whole evening, one in which the Dresden authorities needed convincing about the security of the stone, introduction of analytical equipment to the Vaults, and reassurance about

Proceedings of the Gemmological Association of Great Britain and Notices

measuring procedures not changing the diamond's colour. In addition, there was a dispute with GIA gemmologists which eventually led to each team's work being published separately. Indeed green diamonds continue to contain some mysteries and George's most recent publication on the topic was in 2008.

In 1990 George was appointed Chief Gemmologist of the Gübelin Gemmological Laboratory in Lucerne, a move prompted by the opportunity for more far-reaching visits to gem market centres and gem mining locations. First assignments took him to Kunming, Tokyo and Riyadh. Later he visited East African countries and many if not most of the countries in the Far East — of which treks in 1993 to Mogok and 1997 to the jadeite mines in upper Burma were the most challenging. Since 1995 the Gübelin Gem Lab has regularly offered external testing weeks to the gem trade and auction houses in Bangkok, Hong Kong and New York, services which helped their global recognition. George disliked the growing numbers of artificially treated and synthetic gems that came onto the market in the 80s and 90s but in 1999, with his typical realism, he became involved in researching detection of type IIa diamonds which had been decolourized by high pressure high temperature techniques in Russian and American laboratories.

In 2004 George took early retirement to concentrate on enlarging and improving the analytical database for blue-green to yellow-green diamonds, whether naturally or artificially irradiated. This 'Green Diamond Research Project' involved working with colleagues in the SSEF and Gübelin laboratories, with museums, and with colleagues in Paris, and highlights an important thread throughout his career that led to many publications and presentations at international meetings. In such research, he was a reliable co-worker, but the extent of his determination to complete everything he had committed himself to meant that meeting deadlines was at times quite tense.

The gem trade, gemmology and gem testing have, over the last forty years, seen a growing number of new stone localities, new synthetics and innovative treatments, and George has played a full part in their detection, description and disclosure. His first paper in *The Journal of Gemmology* in 1978 was a description of stabilized cubic zirconias, and this remains a first-class example to gemmology students of how to carry

out and report on such an investigation. Since then he has graced the *Journal* pages with his work on the Dresden Green diamond, major papers on Colombian emeralds, freshwater pearl cultivation in Vietnam, and colour-change stones, to name but a few of the topics he addressed. In 1994 he accepted an invitation to join the *Journal's* board of Associate Editors and his critical, fair and balanced assessment of a submitted manuscript was always something to look forward to for the editor. He also served in the same way on the board of the *Australian Gemmologist*.

George was a Swiss delegate to the International Gemmological Conference and was on the organizing committee for their meeting in Interlaken in 2011. There he presented a paper on colour causes and stability in spodumene. His significant presence on the international stage did not mean that he neglected the national scene. George was strongly patriotic and was a member of the Swiss Mineralogical and Petrographic Society, the Geological Society of Zürich, and the Swiss Chamber of Technical and Scientific Forensic Experts.

In 1973 George met his future wife Anna Verena Geser in New York. They married on 22 April 1977, settled in Horgen, and in 1980 moved into their own home overlooking Lake Zürich and the Alps. George and Anne always enjoyed entertaining friends, and after George took early retirement they almost had an open house — some called it a gemmological hotel but with limited rooms! Anne worked at Gübelin in New York and Lucerne and became head of staff at Meister in Zürich, and shared a love of gems and jewels with George. This found expression in later years when she accompanied George on some of his more demanding treks in the Far East to see gems in their natural settings.

Despite suffering from cancer for many years, George was grateful he survived the accident when he was twenty and went on to experience a colourful world with many natural treasures, human and otherwise, and felt that he was particularly blessed with the companionship of a loving partner.

Roger Harding

This brief summary has drawn on notes provided by George himself, his wife Anne and his long-standing friend Karl Schmetzer.

A word of thanks . . .

Since the 1940s the status of the *Journal* has been built up by a succession of editors noted for their gemmological knowledge and integrity. By the 1970s the pace of scientific advancement in the discipline had started to accelerate, and by the time that Alan Jobbins relinquished the editorial chair in 1994 it made sense to formally seek some support for the editor from those in more specialist areas of expertise. Thus was established a band of Assistant and Associate Editors with a wide range of skills very relevant to today's gemmology. To them I owe a great deal, not only for their technical expertise in assessing manuscripts, but also for their constructive comments, common sense and wise counsel.

Some members of this band also contributed Abstracts — a technical and writing skill which I fear at the present moment is declining but which in the future I hope will revive as one antidote to the information deluge we have to contend with — and to them and the other abstractors who have so succinctly conveyed the essences of material published elsewhere, I offer my thanks.

Although gems have a very pervasive social impact, this cannot be said about the associated science, and to stimulate any appreciation about gemmology's practical, legal or intellectual benefits and values, it must be presented in an attractive way. The success of Mary Burland's efforts in this

respect is brought home most vividly when *Journal* issues through the years are laid side by side, and the changes in size, style and impact are apparent. I thank her for her dedication to the task, for her ability to overcome the unforeseen and for her tolerance of my shortcomings.

In turn, both of us have relied upon staff at the Gem-A office, and I would like to thank them all for their consistent willingness over many years to help in matters concerning publications, an attitude which makes all the difference when outside the office and working from home.

. . . and a word of welcome!

Being out of the office does however have its disadvantages, and over time, the lack of close personal contact with many aspects which affect the gem trade in such places as Hatton Garden does affect how well one can assess material submitted for publication. I am very pleased that someone who is in the thick of gemmological activity and who has knowledge and access to many of the advanced techniques now being used to examine gems, has agreed to be the next editor. In this, the last issue of the *Journal* that I will be editing, my very best wishes go to Elise Skalwold and I wish her, the *Journal* and the Association a most successful future.

Roger Harding

NEW: Gem-A Blended Learning Gemmology Courses

Enrolling now
for October 2012



Starting in October 2012, Gem-A's new blended learning gemmology courses combine the advantages of online education with on-site tuition. The courses start with a distance preparation section that can be studied anywhere in the world. This leads to on-site face-to-face seminars and practical tutorials at Gem-A's London headquarters. This intensive fast-paced learning method covers both the Foundation and Diploma parts of Gem-A's famous gemmology course. The on-site portion of this course consists of daytime tuition and study sessions, held three days a week for five months.

Gemmology Foundation and Diploma Blended Learning Course

(Access to a computer with an internet connection is essential)

Start dates:	Online – 1 October 2012 Daytime, on-site – 29 January to June 2013
On-site class days:	Tuesday, Wednesday and Thursday
Course fees:	£6,950

Full details at www.gem-a.com/education.aspx or call **+44 (0)20 7404 3334** email education@gem-a.com



Gem-A

THE GEMMOLOGICAL ASSOCIATION
OF GREAT BRITAIN

The Gemmological Association of Great Britain
27 Greville Street (Saffron Hill entrance), London EC1N 8TN
tel: +44 (0)20 7404 3334 fax: +44 (0)20 7404 8843
email: information@gem-a.com
UK Registered Charity No. 1109555

Contents

- | | | | |
|------------|---|------------|--|
| 129 | Measurement and interpretation of growth patterns in chrysoberyl, including alexandrite
<i>K. Schmetzer</i> | 224 | Abstracts |
| 145 | A Russian Maxixe beryl?
<i>L.O. Andersson</i> | 233 | Book Reviews |
| 151 | Chemical and growth zoning in trapiche tourmaline from Zambia – a re-evaluation
<i>K. Schmetzer, H.-J. Bernhardt and T. Hainschwang</i> | 236 | Proceedings of The Gemmological Association of Great Britain and Notices |
| 174 | Untreated yellowish orange sapphire exhibiting its natural colour
<i>J.M. Duroc-Danner</i> | | |
| 179 | Alexandrite and colour-change chrysoberyl from the Lake Manyara alexandrite-emerald deposit in northern Tanzania
<i>K. Schmetzer and A.-K. Malsy</i> | | |
| 211 | Review of ultraviolet sources for gem fluorescence and testing
<i>G. Pearson</i> | | |

Cover Picture: Slices of trapiche tourmaline from Zambia cut perpendicular to the *c*-axis. In the centre of the slice, upper left, the dark arms of the fixed three-rayed star separate three pyramidal growth sectors. The slice, lower right, cut from the same tourmaline, has a rim with six prismatic growth sectors which are separated from each other and from the pyramidal growth sectors of the centre by less transparent boundaries. View parallel to the *c*-axis, size of the samples about 13 × 12 mm. Photos by T. Hainschwang. (See Chemical and growth zoning in trapiche tourmaline from Zambia – a re-evaluation by K. Schmetzer, H.-J. Bernhardt and T. Hainschwang, pages 151–173.)

The Gemmological Association of Great Britain

27 Greville Street, London EC1N 8TN, UK

T: +44 (0)20 7404 3334 **F:** +44 (0)20 7404 8843

E: information@gem-a.com **W:** www.gem-a.com

